Isolation and characterization of human monoclonal antibodies blocking Plasmodium falciparum transmission

Axelle Amen

THÈSE

Pour obtenir le grade de

DOCTEUR DE L'UNIVERSITÉ GRENOBLE ALPES

École doctorale : CSV- Chimie et Sciences du Vivant
Spécialité : Virologie - Microbiologie - Immunologie
Unité de recherche : Institut de Biologie Structurale

Isolement et caractérisation d'anticorps monoclonaux humains bloquant la transmission de Plasmodium falciparum

Isolation and characterization of human monoclonal antibodies blocking Plasmodium falciparum transmission

Présentée par :

Axelle AMEN

Direction de thèse :

Pascal POIGNARD PROFESSEUR DES UNIVERSITES - PRATICIEN HOSPITALIER, Université Grenoble Alpes	Directeur de thèse

Rapporteurs :

Rogerio AMINO
CHERCHEUR HDR, Institut Pasteur - Paris
Dorian MCILROY
MAITRE DE CONFERENCE HDR, Université de Nantes

Thèse soutenue publiquement le **16 décembre 2022**, devant le jury composé de :

Pascal POIGNARD PROFESSEUR DES UNIVERSITES - PRATICIEN HOSPITALIER, Université Grenoble Alpes	Directeur de thèse
Rogerio AMINO CHERCHEUR HDR, Institut Pasteur - Paris	Rapporteur
Dorian MCILROY MAITRE DE CONFERENCE HDR, Université de Nantes	Rapporteur
Isabelle TARDIEUX DIRECTRICE DE RECHERCHE, CNRS délégation Alpes	Présidente
Mireia PELEGRIN DIRECTRICE DE RECHERCHE, CNRS délégation Occitanie Est	Examinatrice
Bertrand HUARD PROFESSEUR DES UNIVERSITES, Université Grenoble Alpes	Examinateur

Invités :

Robert SAUERWEIN
PROFESSEUR DES UNIVERSITES, Radboud University

ACKNOWLEDGMENTS

To my jury members:

To my referees ("rapporteurs"), Drs. Amino and McIlroy, for their expert and careful review of my manuscript, guaranteeing the scientific quality of this work.

To my examiners ("examinateurs"), Dr Pelegrin, Dr Tardieux and Pr Huard, for allowing me to benefit from their scientific expertise in immunology and parasitology during this PhD defense.

Finally, to Pr Sauerwein, a specialist in transmission blocking antibodies, for participating on this jury as a guest of honor, but especially for having allowed this fruitful collaboration between our two research teams.

A mon directeur de thèse :

A Pascal, pour la confiance que tu m'as toujours accordé pour mener à bien ce projet ambitieux alors que je n'étais qu'une toute jeune interne en pharmacie, peu habituée à la recherche fondamentale. Merci pour cette opportunité incroyable que tu m'as offerte de travailler sur un sujet aussi passionnant, qui je l'espère, continuera à vivre même après cette thèse de sciences. Merci de m'avoir transmis ta passion de la recherche et ta curiosité scientifique !

Plus important encore, je te souhaite le meilleur à côté du boulot, avec de belles journées en montagne, probablement en rando dans le Vercors !

To our collaborators :

To the Malaria Vaccine Initiative for fundings that made this PhD project possible, and to R. King and R. Mac Gill for sharing their wise scientific feedback monthly, which allowed the project to progress.

To M. Jore and his team, for his essential and extensive expertise in parasitology, and more specifically on Transmission Blocking Antibodies. Special thanks to A. Fabra-Garcia and R. de Jong who performed tests to determine mAbs functionality and the targeted proteins at the gametocyte surface.

To the TropIQ team who performed SIFA and SMFA experiments, and especially to Judith Bolscher for her kindness and availability.

To J-P. Julien and his team, and notably R. Yoo, for their interest in the characterisation of the epitope targeted by B1E11K and their efficacy when it came to doing experiments.

To W. Stone team for performing protein microarray for determination of B1E11K antigen.
To K. Miura and his team for performing their Growth Inihibition Assay with B1E11K monoclonal antibody.
A M. Pezet et P. Battiston- Montagne pour avoir rendus les tris nécessaires au bon déroulement de la thèse possibles. Merci pour votre pédagogie, votre patience et votre bienveillance. J'espère que nous nous recroiserons autour de séminaires de cytométrie !
A Y. Couté pour les expériences de spectrométrie de masse, et à P. Verdié pour sa réactivité pour la synthèse des peptides.
To all the collaborators that I could have forgotten, for having made this project possible.

A mes collègues du CHU Grenoble Alpes :
Au Pr Pelloux, au Dr Robert, et aux biologistes du service de parasitologie pour avoir permis l'accès aux échantillons nécessaires aux mises au points.
Aux biologistes du service de virologie du CHU de Grenoble pour leur accueil durant ces cinq années de thèse de sciences.
A mes nouvelles collègues du service d'immunologie du CHU de Grenoble pour leur accueil, et avec qui je suis ravie de commencer une nouvelle aventure !

A mes collègues de l'Institut de Biologie Structurale :
A Nicole Thielens, pour ton implication dans les premières relectures de mon manuscrit et ta très grande pédagogie. Mille mercis.
A Isabelle, pour m'avoir supporté et soutenue pendant les deux dernières années de ma thèse. Merci pour ton optimisme inébranlable qui aura toujours su me faire voir le verre à moitié plein ! Merci pour toutes les choses que tu m'a apprises au laboratoire, et pour ton aide précieuse sur plusieurs manipes déterminantes !
A Sebastian, pour m'avoir aidé dans mes premiers pas de doctorante, en m'apprenant la plupart des basiques du laboratoires, de la cytométrie à GraphPad en passant par les mots fleuris en espagnol.
A Laurence et Marlyse, pour les coups de main, la bienveillance et les conseils avisés partagés autour d'un carré de chocolat (noir !)
A Aless, pour m'avoir aidé avec la production des anticorps monoclonaux, avec ta rigueur habituelle et tes codes couleurs !
A mes compères de paillasse (« heureusement que vous êtes là ! ») qui se sont succédés pour supporter mes ronchonneries. Mention spéciale à Jean-Mi, pour le sarcasme et les fous rires

(souvent combinés) qui m'aura accompagné dans cette dernière longue ligne droite. A Romina, Audrey et Benjamin, sans qui cette longue aventure n'aurait pas été la même.
A Jean-Baptiste Reiser pour son expertise pour les expériences de BLI.
A la team Fender, et surtout Solène pour nos sessions rédaction à l'EMBL.

A mes proches :
Cette fois ci les remerciements seront plus succincts que pour la thèse de pharmacie, mais ils viennent toujours du cœur !

A mes amis :
Qui m'ont toujours soutenus dans cette longue épopée, de près ou de loin : Laura (mon petit caillot préféré), Marioune, Béren, Auré, Laura L, Lolo et Lélé, Alex, Klara, Emelyne, Capsou, Clairette M, Anaëlle, Tristan et Maud, Caro, Antho, Simon, Claire, Léa, Théo, Aurélie, Anthony, Alex et Maurane et les copains de la team resto-canyon !

A ma famille :
Enfin, un immense merci à mes parents, mon frère, mes grands-parents (et tout le reste de la famille !) et aussi à ma belle-famille, pour les ultimes encouragements pour cette deuxième soutenance de thèse en moins d'un an ! Promis, les thèses c'est fini, pas de troisième petite dernière !
A Quentin, puissions-nous vivre longtemps heureux comme Carl et Ellie.

PREAMBLE

The implementation of the sorting techniques for MBCs isolation followed by RT-PCR was my primary mission as a PhD student. Indeed, the Poignard team was only created two years ago, when I began my PhD. This part of the pipeline had never been done in Grenoble before, but was instead performed through collaborations with the Scripps Institute. Obtaining a functional pipeline was the first major result of my thesis work, then the application to the isolation and characterisation of TRAbs, a project designed in collaboration with several teams, as detailed in introduction, part 7. The results obtained during this PhD are the subject of a publication in progress.

Beyond my thesis project, development of the cell sorting and downstream RT-PCR experiments allowed the sorting of a panel of mAbs neutralising the BK virus, but also mAbs neutralising *Pseudomonas aeruginosa*. These projects are also the subject of publications in preparation.

In parallel with my PhD, I also made my PharmD in P. Poignard's team. My thesis was entitled « Stratégies vaccinales anti-SARS-CoV-2, évaluation de l'immunogénicité de deux candidats vaccinaux » (Anti-SARS-CoV-2 vaccine strategy: immunogenicity evaluation of two vaccine candidates). I took part in two projects of SARS-CoV-2 vaccine design and immunogenicity evaluation, in collaboration with two teams from the Institute of Structural Biology from Grenoble: the team of P. Fender and of W. Weissenhorn. These projects led to the publication of two different articles (1) (2), briefly summarised and presented at the end of the manuscript. Participating in these two projects enabled me to improve my understanding of the role of antigen conformation and vectorisation methods in the induction of a strong, functional humoral immune response by vaccination. Thus, these projects brought me knowledge complementary to my PhD work on vaccinology techniques and humoral responses.

ABBREVIATIONS

Ab(s): Antibody / Antibodies

ADCC: Ab-dependent Cellular Cytotoxicity

BCR: B Cell Receptor

BLI : BioLayer Interferometry

CDR: Complementary Determining Region

DNA: DeoxyriboNucleic Acid

DP: Double Positive cells: cells positive for the gametes staining signal and for memory B cell staining signal (complexes of gametes and B cells.) in flow

ELISA: Enzyme Linked ImmunoSorbent Assay

EC50: half maximal effective concentration

Fab: Fragment antigen-binding

FACS: Flurorescence-Activated Cell Sorting

FBS: Fetal Bovine Serum

Fc: Crystallisable Fraction

GE: Gametocyte extract

Gy: Gray

HC: Heavy chain

HEK: Human Embryotic Kidney

HLA: Human Leucocyte Antigen

IPP: Immuno-PreciPitation

IgG: Immunoglobulin G

IMDM: Iscove's Modified Dulbecco's Medium

IMGT: IMmunoGenetics database

ITC: IsoThermal Calorimetry

kC: Kappa chain

KO: Knock-Out

kon: association rate constant

koff: dissociation rate constant

KD: dissociation constant

LC: Light chain

lC: lambda chain

mAb(s): Monoclonal antibody / Monoclonal antibodies

MBC: Memory B Cell

MFI: Mean Fluorescence Intensity

MHC: Major Histocompatibility Complex

MS: Mass - Spectrometry

NB: Not binding

NBC: Naïve B cell

NGS: New Generation Sequencing

NHP: Non-Human Primate

nsEM: negative stain Electron Microscopy

OD: Optical Density

PBMC: Peripheral Blood Mononuclear Cells

PBS: Phosphate Buffer Saline

PCR: Polymerase Chain Reaction

Pf: Plasmodium falciparum

RBC: Red Blood Cell

RNA: RiboNucleic Acid

RT-PCR: Reverse Transcription Polymerase Chain Reaction

SIFA: Surface ImmunoFluorescent Assay

SMFA: Standard Membrane Feeding Assay

SMH: Somatic HyperMutations

TF: ThermoFisher

TRA: Transmission Reducing Activity

TRAb(s): Transmission Reducing Antibody / Transmission Reducing Antibodies

VH: Variable domain of the Heavy chain

VL: Variable domain of the Light chain

WB: Western-Blot

WHO : World Health Organisation

w/o: without

WT: Wild-type

TABLE OF CONTENT

LIST OF FIGURES

LIST OF TABLES

LIST OF ANNEXES

LIST OF SUPPLEMENTARY DATA

INTRODUCTION

1. Malaria, a parasitic disease caused by plasmodial parasites

1.1 General overview

Malaria is a human disease caused by infection with apicomplexan parasites belonging to the genus Plasmodium. Plasmodium species that naturally infect humans and cause malaria are: *Plasmodium falciparum (Pf), Plasmodium ovale, Plasmodium vivax, Plasmodium malariae and Plasmodium knowlesi.* They are transmitted via a vector: the female *Anopheles* mosquito. This thesis will only focus on *Pf* and not the other species of Plasmodium as it is the most lethal and prevalent species on the African continent. Of note, there are over 200 species of Plasmodium but most do not infect humans.

Malaria is characterised by a wide range of symptoms which include: shaking chills, hyperthermia, headache, nausea, vomiting, abdominal pain or diarrhea. *Plasmodium falciparum* can also induce severe cases of malaria, causing in particular neurological symptoms that can lead to death. Children under five years old and pregnant women are the most at-risk to declare severe malaria. *Plasmodium falciparum* can be found in various areas (Africa, South-East Asia, South America and Oceania.), especially tropical ones (3)(4).

Although simple prophylactic solutions exist to avoid infection, such as wearing covering clothing or using mosquito nets as detailed in part 1.4, their use requires a daily implication which can be hard to achieve in high-transmission areas. Repellents can also be used to avoid mosquito bites, but they can become toxic when used chronically. In case of infection, various chemical drugs are available but chemoresistances are rising worldwide, even to front-line treatments such as artemisinin (5).

An effective vaccine could reduce the use of these treatments and yet despite decades of intense research, only one vaccine has been recommended for use by the World Health Organisation (WHO) in October 2021 with only moderate efficacy and a complex dose regimen (6).

1.2 Malaria epidemiology:

According to the WHO 2020 malaria report, about 229 million malaria cases occurred in 2019, in 87 endemic countries (7). Ninety five percent of the cases were reported in the WHO African Region with five countries accounting for 51% of total cases: Nigeria, the Democratic Republic of the Congo, Uganda, Mozambique and Niger. The WHO South-East Asia region accounted for 3% of the total malaria cases.

While the number of cases is globally decreasing compared to the 2000s, the malaria-induced mortality remains unfortunately very high, with about 405 000 deaths in 2019. Young children and pregnant women are one of the most at-risk populations, and children under 5 years account for 67% of the total death toll. In countries with a very high prevalence, such as Central Africa, it has been estimated that 40% of pregnant women are exposed to malaria, resulting in a high prevalence of low birthweight babies.

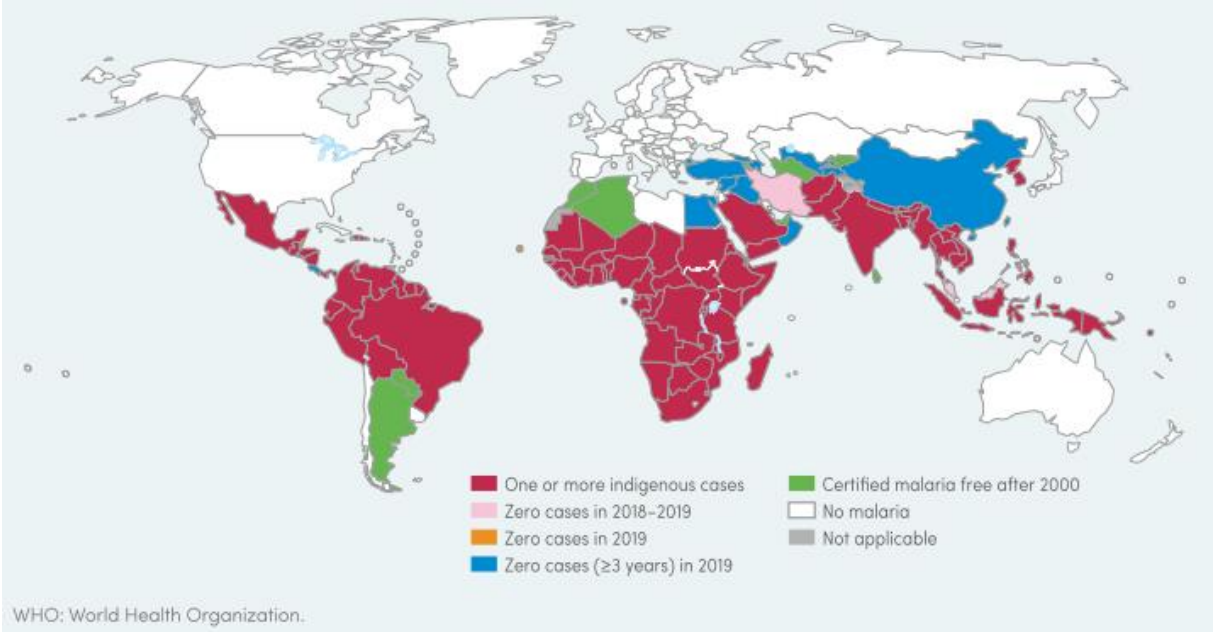

Figure 1: Worldwide distribution of malaria cases as in 2019.

To tackle this concerning situation, ambitious goals to free the world from malaria have been settled by the WHO and reported in the "Global Technical Strategy for Malaria" in 2015 and updated in 2021 (8). For 2030, the main objectives of the report are as follows: a 90% worldwide decrease in malaria mortality and incidence rate in comparison with 2015, an elimination of malaria in 35 countries that were endemic in 2015 and, the absence of malaria re-establishment in all countries presently considered as malaria-free.

1.3 *Plasmodium falciparum* lifecycle and physiopathology

Although malaria has plagued humanity for thousands of years, with almost no area in the world ever exempt of it, the pathogen responsible for this disease was only discovered in 1880 by Alphonse Laveran, and its transmission stage was only described in 1897 by Ronald Ross (9).

Plasmodium falciparum has a complex lifecycle involving two types of hosts: humans and mosquitoes, and can reside in several localisations among these hosts, as represented in figure 2.

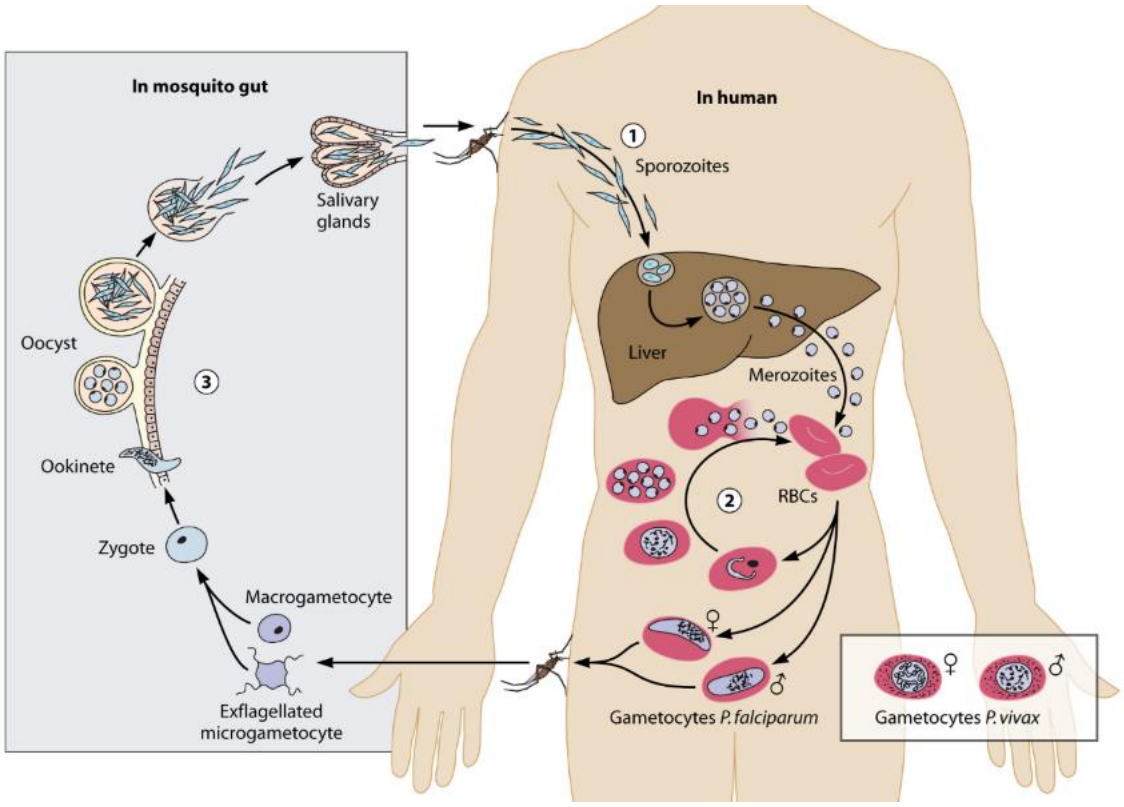

Figure 2: *Plasmodium falciparum* lifecycle, from Bousema et al (10)

Plasmodium falciparum-infected mosquitoes belong to the *Anopheles spp* family, which are found in tropical areas. Female *Anopheles* mosquitoes use human blood as a source of proteins for the development of their eggs. Human infection begin with an infected mosquito bite that releases parasitic sporozoites into the skin (Figure 2, ①). The sporozoites rapidly migrate to the bloodstream and then reach the liver. Inside hepatocytes, sporozoites are enclosed by a parasitophorous vacuole and develop into schizonts, which then transform and multiply into merozoites, ultimately causing the death of the host cell (Figure 2, ②). Merozoite-filled

vesicles, called merosomes, bud from the hepatocytes and reach the blood stream, where parasites can infect red blood cells (RBCs). Once inside RBCs, parasites export hundreds of proteins to the host cell cytoplasm and cell surface, allowing an exchange of nutrients necessary for the preparation of intraerythrocytic reproduction. Protein export also modifies the external architecture of RBCs increasing cell adherence to endothelium or to other non-infected RBCs, leading to RBCs sequestration in capillaries, and finally microvascular obstruction and organ failure. This phenomenon of sequestration also occurs in the placenta of pregnant women, and is responsible for miscarriages and premature or low birth weight children.

During the intraerythrocytic reproduction step, which correspond to successive mitoses and is thus also called “asexual reproduction”, merozoites transform successively into rings, trophozoites and schizonts. Parasites rupture RBCs and infect others, increasing the parasitic load. The haemolysis that is induced is responsible for the paroxysmal symptoms of malaria such as fever and anaemia. In parallel to asexual reproduction, and depending on environmental conditions such as the level of infected RBCs (4), a minority of the parasites are redirected to sexual reproduction through a developmental switch towards the production of male and female sexual progeny or gametocytes. During eleven days, inside the bone marrow, these parasites undergo several steps of development, from stage I to stage V gametocyte, as indicated figure 3 (11).

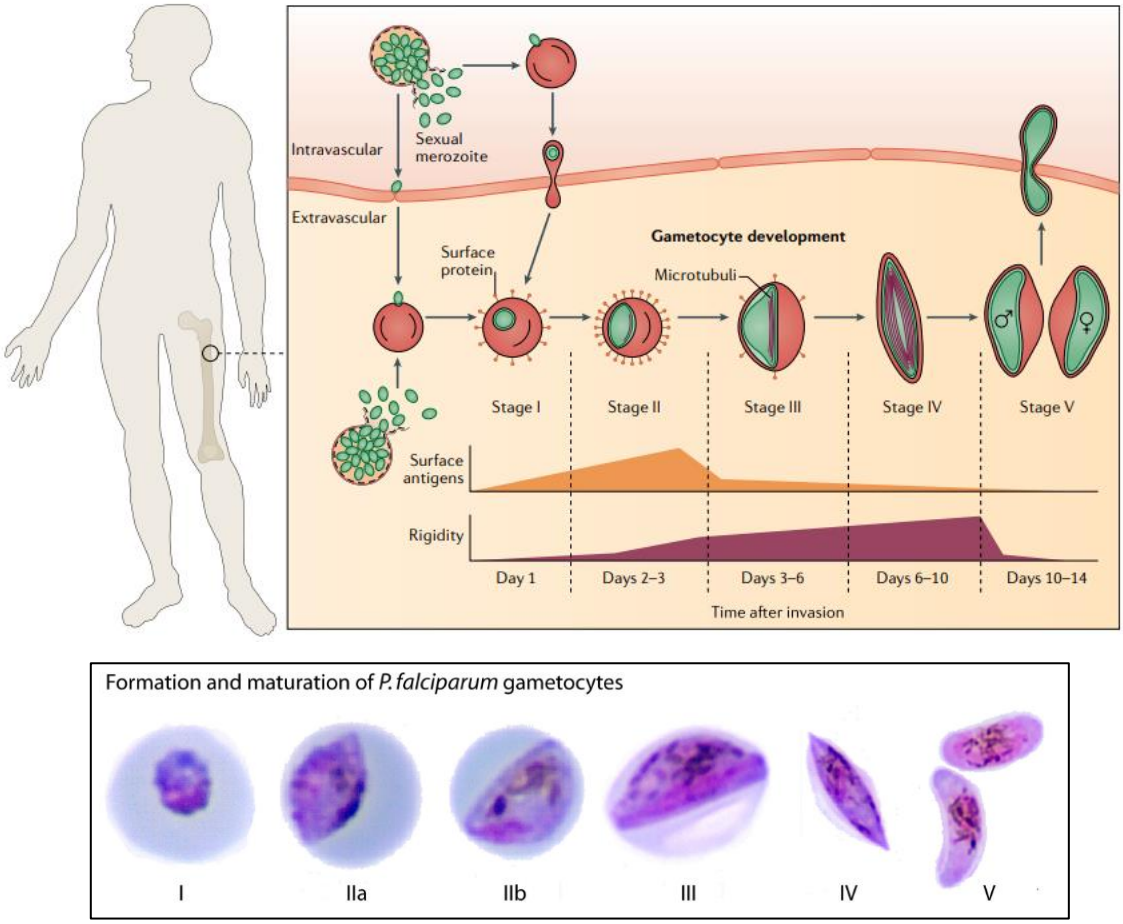

Figure 3: Gametocyte development steps, from Venugopal et al (12), and gametocytes photographs, from Bousema et al (10)

Stage I and stage II are morphologically similar to asexual parasites, with the late stage II being the first stage that can be distinguished from the latter. Stage III and stage IV gametocytes adopt a spindle shape that further evolves in a crescent shape with close contact between the parasitic and the RBCs' membranes (13)

Once at their final developmental step, male and female gametocytes are released inside the blood stream and reach skin capillaries. Gametocytes are then eventually ingested by *Anopheles* mosquitoes as they drink blood. *Anopheles* is the definitive host, in which the sexual replication occurs. Once inside the mosquito gut, the change in conditions (temperature decrease, pH increase, exposure to xanthurenic acid…), makes the gametocytes rapidly egress from the RBC, forming male and female gametes (14) (15). Male gametes evolve into eight microgametes and female gametes into one macrogamete. The fusion of micro- and macrogametes creates ookinetes that are able to migrate through the epithelium of the mosquito midgut and reach the basal lamina in the abluminal side of the midgut. Once mature, oocysts transform into sporozoites and reach the mosquito's salivary glands. These sporozoites will then be released into the human's body during another blood meal, starting a new cycle.

1.4 Malaria prevention and treatment

To diminish the incidence of a vector borne disease, two types of primary prevention tools are classically used: host vaccination and vector control measures. Vaccination will be discussed further in chapter 3.

Because the malaria is mosquito-borne, the use of insecticide-treated nets and indoor residual spraying are the methods of choice to prevent transmission (16). Personal protective measures can be used too, such as the use of covering clothing, or repellents (based on DEET, icaridin or citriodiol). *Anopheles* tend to bite as soon as the sun goes down but fear the cold, thus sleeping in an air-conditioned room is also recommended. These methods are somehow costly, require a daily involvement and high levels of compliance that can be hard to achieve in endemic regions. However, they are particularly suitable for tourists who only stay for a short period of time in at-risk areas. Apart from methods that simply prevent mosquito bites, another solution can be the elimination of the mosquitoes through larviciding. Indeed, *Anopheles* have a reproductive lifecycle that involves the development of their larvae in stagnating water. Thus, drying swaps or the spraying of insecticide in those areas are efficient ways to decrease *Pf* transmission. Overall, vector control is highly effective at reducing malaria transmission and a crucial component of the malaria control and elimination strategies that are part of the WHO Global Technical Strategy for Malaria recommendations (8).

At an individual level malaria can be also prevented through prophylactic chemical treatments. Those are offered to people living in non-endemic countries when travelling to highly infested areas for more than a week. In France, people are offered either chloroquine + proguanil, atovaquone + proguanil, mefloquine or doxycycline, depending on where they travel to and on contraindications. Some anti-malaria drugs can also be used as a cure. For uncomplicated cases, treatment is commonly based on an artemisinin combination therapy (artemether + lumefantrine, artenimol + piperaquine or atovaquone + proguanil). For complicated cases, treatment is based on perfusions of artesunate or quinolone. However, treatment efficacy is being jeopardized with the increase of anti-malarial drugs resistances (17). Resistances are also seen against active ingredients in repellents (18). In addition, molecules used in repellents (notably pyrethroids) are not only toxic to mosquitoes but also to other types of invertebrates such as bees, threatening ecosystems. Furthermore, while pyrethroids are not toxic to mammals at low doses, studies have looked at the potential link between chronic pyrethroids exposure and developmental disorders in children (19).

All these observations strongly underline the need for an effective and widely available vaccine to spare the use of repellents and anti-malarial drugs, while decreasing cases and mortality.

2. Humoral immune response to *Plasmodium falciparum* infection

Pf infection induces both humoral and cellular immune responses in patients, that are essential in limiting the replication of *Pf* and its clinical consequences. Cellular immune responses will not be detailed, as they are not the focus of this thesis. In particular, T cells play an important role in protection against malaria, but their mechanisms of action in this have not yet been fully understood. Existing knowledge on the role of T cells in malaria have been reviewed in detail by Kurup et al (20). According to Perlmann et al (21), "it is a reasonable generalisation to say that T cells are required for the induction and maintenance of malaria immunity while humoral Abs are important for the control of parasite loads in acute infection". Beyond the cell-mediated immune response, many studies have also shown involvement of complement in the anti-*Pf* response and are reviewed by Reiss et al (22) and Inklaar et al (23), but again, details of this immune mechanism are also beyond the scope of this thesis.

Studies have shown that people living in highly endemic countries develop, upon infection, Abs against the parasite, potentially targeting each stage of its lifecycle. For example, it has been determined that 54% of the Burkina Faso population developed Abs directed against the *Pf* circumsporozoite protein (CSP, expressed at the pre-eythrocytic stage), 65% against the *Pf* GLURP protein (asexual stage) and 22 to 28% against the Pfs48/45 and Pfs230 proteins (sexual stage) (24). Of note, the characteristics of the sexual stage antigens and the corresponding Ab response will be further detailed below, it being the focus of this thesis project.

The key role of Abs in protecting against malaria disease was determined early on. In experiments carried out in the 1960s, immunoglobulins from the serum of chronically infected adults living in endemic areas were passively transferred to young children suffering from an acute malaria crisis, resulting in a rapid decrease in parasitaemia and improvement of their clinical condition, compared to children who were either not treated or received gamma globulins from malaria-naïve donors (25). This experiment thus demonstrated that the anti-*Pf* Abs acquired by several years of exposure have a protective effect. However, if natural humoral immunity against *Pf* confers protection against severe disease or death, it appears that it cannot

prevent reinfection (26). The immune response naturally developed with exposure to Pf is not sterilising.

Accordingly, in parallel with the acquisition of humoral immune response, the incidence of acute infections decreases with time of exposure. Children between 6 months and 5 years of age are the most at risk to develop symptoms, having lost the protection conferred by maternal Abs and having not yet developed their own anti-malaria responses (see figure 4). The speed of acquisition of malaria immunity is directly correlated with the rates of parasite transmission in the area (27). In areas of low malaria prevalence or seasonal transmission, even adults are likely to report severe forms of the disease, as they don't develop strong enough Ab responses to *Pf*. In addition, this slowly acquired immunity tends to vanish rapidly, and people that left endemic countries for some years can undergo serious malaria crisis when returning to these areas.

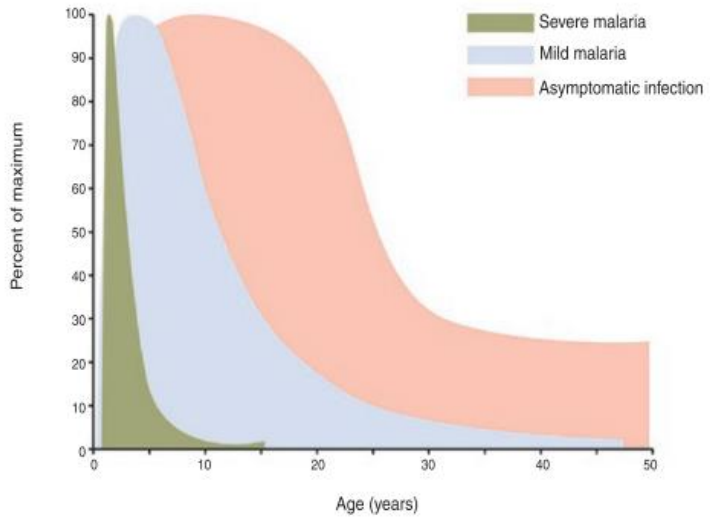

Figure 4: Acquisition of immunity in general population is correlated to decrease of severe cases. From Langhorne et al (28)**.**

The absence of development of sterilising immunity upon *Pf* infection results in chronic, low and asymptomatic carriage of parasites by a portion of the population, contributing to the persistence of a reservoir (29). For example, it has been shown that in Burkina Faso, even during the dry season, 15.5% of individuals are asymptomatic but infectious and capable of transmitting the parasite to mosquitoes (30). While eventually promoting the development of protective Ab responses, the chronic carriage of the parasite also appears to alter immune responses, with notably an expansion of the number of atypical memory B cells in *Pf* chronically infected individuals (31) (32). Atypical memory B cells have a decreased ability to be stimulated though their BCR complex and thus have limited capacity to proliferate, secrete

cytokines, or produce Abs. It has been estimated that more than 50% of the population living in endemic areas harbour such atypical cells, whereas only 3 to 6% of a healthy population does so (33). This alteration of B cell responses may explain in part the slow acquisition of protective Abs observed in malaria.

To date, the most studied target of protective Abs is PfCSP. The following is found at the sporozoite surface and enables their development when inside the mosquito, it is also necessary for sporozoite entry into the liver cells (34). Studies demonstrated that anti-PfCSP Abs can have a protective activity (35) (36) (37). Even if the detailed protection mechanism is not yet fully understood, anti-PfCSP Abs may hinder parasite mobility in the skin, cell traversal abilities and liver infection. More precisely, PfCSP contains an immunodominant central domain, rich in NANP amino acid repeats, which is the target of the majority of protective Abs. As an important aim of vaccines against malaria is to induce protective Abs, PfCSP has entered the composition of many pre-erythrocytic vaccines (38), as detailed in part 3.

3. The special case of antibodies able to reduce *Pf* transmission (TRAbs)

As mentioned previously, people living in endemic areas develop Abs targeting sexual stage parasites. In a study from Drakeley et al (39) on 1- 4 years Gambian children, 42% of gametocytes carriers had Abs against live gametes. Similarly, a study from Saheed et al (40) also on Gambian children showed that 34% had Abs reactive against late-stage gametocyte and that this recognition increased with age, but was not correlated to recognition of asexual stage parasites. Importantly, among Abs targeting the sexual stage it has been demonstrated that some have the ability to block/reduce the transmission of Pf.

3.1 Measuring Transmission Reducing Activity

As defined by Takashima et al (41), transmission reducing antibodies (TRAbs) are directed against antigens expressed at the sexual stage of the malaria parasite (either gametocyte or gamete) or at the zygote and ookinetes stages, and that are able to reduce the number of oocysts in mosquito vectors fed with gametocytes. In the same way, Abs can even have a Transmission Blocking Activity, when no oocyst could develop.

The concept of Abs that can reduce the transmission of Plasmodium spp. emerged from experiments performed in the 70s, involving chicken immunisation with irradiated blood from

birds infected with *Plasmodium gallinaceum*, containing sexual forms of the parasite. When fed on these immunised chickens, mosquitoes developed less oocysts than those fed on unimmunised chickens. The observation suggested that immunised chickens developed an immune response against gametocytes that reduced parasite development inside the mosquito vector (42) Thus, although gametocytes are intra-erythrocytic, the results suggested that they may express proteins at the surface of the RBCs that elicit functional immune responses in naturally exposed individuals.

Since these pioneering experiments, the determination of a serum (or mAb) transmission blocking/reducing activity has been standardized using an in vitro test, the SMFA (for Standard Membrane Feeding Assay), now considered as the "gold-standard". SMFA is schematized in figure 5. Briefly, laboratory-reared *Anopheles* mosquitoes are fed with a mixture designed to mimic their blood meal during a real infection, which is composed of the following:

- the serum (or mAb) to be tested, at the desired concentration,
- a determined amount of gametocytes
- blood at 37°C (originating from malaria-naive blood bank donors). Of note, SFMA can be performed with or without the complement, as certain TRAbs need complement to be active (43).

One week after the blood meal, mosquitoes are dissected for determination of the number of oocysts contained in their salivary gland, and compared to mosquitoes fed with a control serum (or control mAb). If the tested serum (or mAb) was able to decrease oocysts number by more than 80%, it is considered as having a Transmission Reducing Activity (TRA). Of note, Transmission Blocking Activity (TBA) is defined as the ratio between the proportion of mosquitoes with any oocyst in the test group over the proportion of mosquitoes with any oocysts in the control group. According to Miura et al (44), "the TBA readout is thought to be the best predictor of vaccine efficacy under field conditions, as a single oocyst can still generate a large number of infectious sporozoites".

Depending on the parasite strain used, the readout can be either manual or semi-automated. With wild-type (WT) strains (most often NF54), the number of oocysts is determined by dissection and microscopic counting, while with NF54-HT-GFP-Luc strains (a transgenic parasite strain with a luciferase reporter gene), oocysts density is detected via luminescence, avoiding the tedious dissection step (45). However, SMFA remains in any case a labour-intensive technique, as it requires analysing at least 20 mosquitoes per serum (or mAb sample) to obtain robust results due to the high variability of the experiment (46).

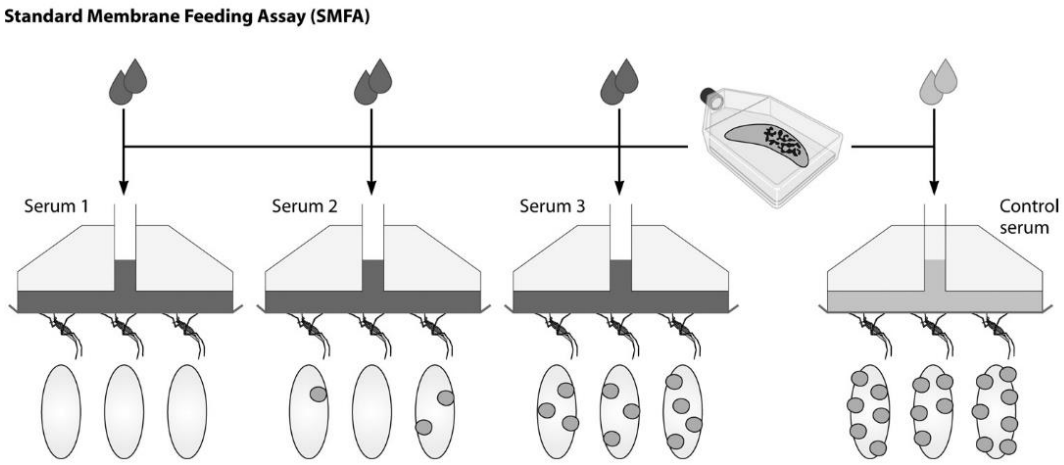

Figure 5: Principle of the Standard Membrane Feeding Assay, from Bousema and Drakeley (10)**.** *Here, three different sera are tested for TRA, and oocysts number on the midgut are compared to those obtained with the control serum. In this example, serum 1 possess a TBA (transmission blocking activity), totally inhibiting oocyst formation, when sera 2 and 3 have a TRA (the latter being less functional than serum 2).*

Alternative techniques can be performed to determine serum TRA, such as DMFA (direct membrane feeding assay). As explained by Bousema et al (10), in this assay " blood samples from naturally infected gametocytes carriers are fed to mosquitoes in the presence of autologous plasma and control serum". If DMFA tests have the advantage to be closer to real-life settings (multiple parasite strains infecting an individual, physiological gametocytes densities and locally caught and reared mosquitoes) and thus being adapted to epidemiological studies, they are not suitable to determine in vitro TRA for monoclonal antibodies. For this application, SMFA is preferred.

Beyond the TRA defined by a decrease in oocyst levels in the mosquito, it is important to note that gametocyte-targeting Abs can increase gametocyte clearance, both during sequestration in the bone marrow or during release into the bloodstream. They will consequently have an impact on the number of parasites absorbed during the mosquito blood meal, thus indirectly helping to reduce transmission. However, these mechanisms are much less documented than TRA and are beyond the scope of this thesis. Similarly, Abs that target the parasite at the asexual stage also have an indirect activity, by decreasing the number of gametocytes that can be formed (47).

3.2 Main antigens targeted by TRAbs

Among individuals whose sera have high TRA levels, studying the characteristics of their immune response brings interesting clues to which are the targeted antigens and which are the characteristics of the Abs elicited. As reviewed by Stone et al (48), the results of 16 different epidemiological studies showed that the presence of anti-Pfs230 and anti-Pfs48/45 Abs was correlated to serum TRA. In addition, Stone et al (49) studied people living in seasonal-transmission areas (Burkina Faso, Cameroon and Gambia) or returning from these areas following a long stay, whose sera induced TRA levels above 90%. Interestingly, 3.3 % of the studied population developed such serological features. Acquisition of TRA was correlated to the time of gametocyte exposure and again to both Pfs230 and Pfs48/45 titers. Therefore, Pfs230 and Pfs48/45 are the most studied and well described TRAbs inducing antigens. They make-up the composition of numerous vaccines that aim to reduce *Pf* transmission, as described in part 5.2.

Beyond Pfs230 and Pfs48/45, *Pf* possess thousands of other antigens that are specifically expressed at the sexual stages (50). Among them, several have been identified as also capable of inducing TRAbs, the main being listed in table 1. Antigens expressed at the sexual stage can be classified into two categories: either those expressed at the gametocyte stage, and therefore visible to the human immune system during infection, or those expressed in the mosquito's intestine, which are then not visible (51). However, immunisation experiments have shown that antigens solely expressed inside the mosquito’s gut are also capable of inducing TRA responses when injected in humans. As they are not subject to selection pressure by the immune system, the diversity of this type of antigen is limited in comparison to antigens expressed during the other stages (52). Of note, the difference with antigen expression is sometimes not as clear, as degradation of late gametocytes may present antigens that were intracellular and dedicated to gametes, zygotes ookinetes or oocysts development in the immune system (53).

Stage of expression	Antigen name	Main characteristics
Gametocytes Gametes	Pfs48/45	51.6 kDa protein composed of three domains with up to six conserved cysteines in each domain. Overall, Pfs48/45 is relatively conserved among strains. *Pf* males KO for Pfs48/45 are unable to fertilize female gametes. (42) (43)
	Pfs230	In complex with Pfs48/45. 360 kDa protein composed of 14 domains. Pfs230 is cleaved and secreted during gametes egress from RBC, and become a 230 kDa protein (44) . *Pf* parasites KO for Pfs230 produce less oocysts (45) (46).
Female gametocytes and gametes	Pfs 47	31 kDa protein and is composed of three 6 cystein domains. Pfs47 allows fertilisation and parasite binding to mosquito midgut. (47) (48)
Gametocytes	Pfs11.1	2400 kDa disordered protein, with many glutamate-rich repeats. Cleaved during gametocyte, egress from RBC. Its role in parasite development has to be clarified, but mAb targeting Pfs2400 has a TRA. (49)
Activated male gametes	HAP2 /GCS1	102 kDa protein Pfs HAP2 KO male gametes are unable to fertilize female gametes. (50) (51)
Gametes Zygote Ookinetes	Pfs25	25 kDa protein composed of four EGF-like domains with 22 cysteins (52). Important for ookinete survival in the mosquito midgut, assist with penetration of the mosquito epithelium and aid in maturation of ookinetes into oocyts. (53)
	Pfs28	Partially redundant to Pfs 25 (54). Considered as a Pfs25-like protein.
***Anopheles* midgut**	AnAPN1	113,5 kDa protein **Not localized on the parasite but inside the mosquito gut, necessary for parasite attachment.** (55) (56)(57)

Table 1: Localisation, principal characteristics and putative function of the main antigens able to induce Transmission Reducing Antibodies. known to date.

Not all putative antigens able to induce TRAbs are listed, and more information can be found in Bousema et al (8).

Stone et al (48) hypothesised that "many more new TRAbs targets have to be discovered, and that they may belong to proteins families already described for asexual parasites, such as STEVOR proteins or subsets of the variant RIFIN antigen". To test this hypothesis, Stone et al (54) depleted six sera from these individuals from their Abs targeting Pfs48/45 and Pfs230

recombinant proteins (Pfs48/45-10C and Pfs230CMB, proteins constitution is detailed in figure 11), they observed that sera still retained TRA. The depleted sera were then tested for binding in a surface immuno-fluorescence Assay (SIFA) against WT and Pfs48/45 KO parasites. It has been demonstrated by Eksi et al (55) that the Pfs48/45 KO also downregulates the Pfs230 retention at the gamete surface. Sera were still able to fix Pfs 48/45 KO parasites, highlighting the presence of Abs binding to other antigens. This was confirmed when running the samples in a microarray test composed of 315 putative target proteins, mainly expressed at the gametocyte stage (228/315). Sixteen proteins were found to fix Abs, suggesting that many new TRA antigens remain to be characterise.

4. Immune escape strategies of *Plasmodium falciparum*

There is no consensus to date as to why there is no sterilising immunity to *Pf*, or why protective immunity takes so long to develop. However, clues may come from the parasite lifecycle and its constitution, beyond the defective host immune response (56). According to D. Burton (57), *Pf* belongs to the "evasion strong pathogens, which had evolved a multitude of mechanisms that result in the elicitation of suboptimal Ab responses with respect to long-term protection against circulating forms of the pathogen."

4.1 Complexity of the *Plasmodium falciparum* lifecycle

The first explanation may come from the parasite lifecycle itself, as the parasite cycle in humans involves very diverse localisations that are difficult to access for either cellular or humoral immunity. Human infection starts with the inoculation of sporozoites in the skin, and the skin being a relatively immune-tolerant area, the injection of sporozoites does not elicit a strong immune response. These injected sporozoites correspond to an initial low antigenic load: a mosquito bite contains only 10 to 100 parasites (58), and a single sporozoite reaching the liver is sufficient to induce an infection. Thus, sporozoites disappear from the blood stream in less than thirty minutes, making it difficult for the immune response to control the first step of infection. In other words, "the complexity of the parasite life cycle rather than the inability of the human immune system to induce memory B cells expressing protective Abs against CSP may be associated with the lack of sterilising immunity", according to Triller et al (59).
Following the sporozoite entry into the liver, most of the parasite's development inside its human host is intracellular, making it poorly accessible for recognition by Abs. As mentioned above, the presence of extracellular parasite in the bloodstream is very brief, and only a few minutes are needed for merozoite to (re)infect a RBC (60). Finally, although some studies have demonstrated that recognition of immature gametocytes by Abs of chronically infected malaria patients is possible (61), early sexual stages of *Pf* gametocytes development take place in the bone marrow, making the gametocytes less accessible to mature immune cells. Gametocytes are released into the blood stream several days after the onset of symptoms due to RBC lysis, this being a potential strategy to evade toxic levels of human cytokines released during febrile paroxysms (10).

4.2 Complexity of Plasmodium falciparum proteins

Due to its very large genome that comprises more than 5000 genes (62) *Pf* harbours numerous different antigens at each stage of its cycle, some of them being stage-specific, as indicated in figure 6 (63). In comparison, some viruses only possess a dozen of genes, and only one well-defined antigen is the main target of protective Abs (i.e the spike glycoprotein of the SARS-CoV-2). To date, there is no clear correlation between efficacy and immunogenicity for *Pf* protection (64).

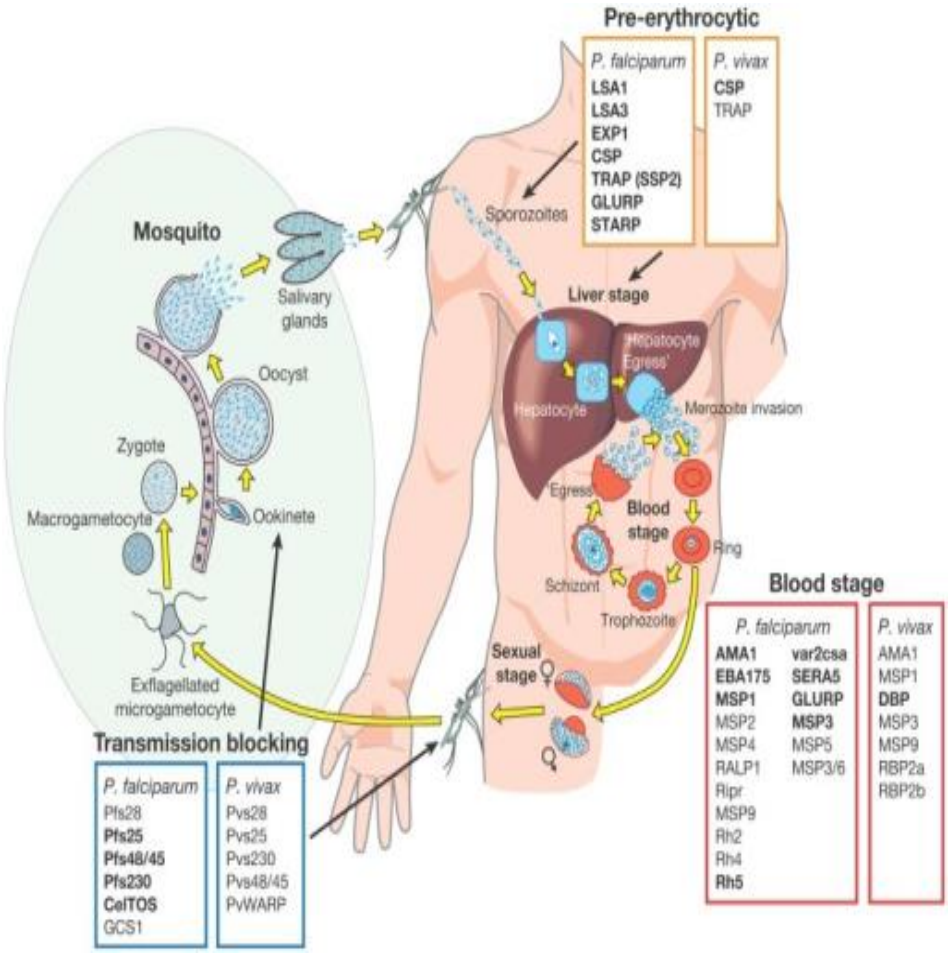

Figure 6: Plasmodium falciparum lifecycle with potential antigenic vaccine candidates, from Barry et al (65)**.**

Listed proteins are antigens of interest for vaccine design, highlighting the diversity of Pf protein expression at each stage of the parasite lifecycle. The pre-erythrocytic proteins listed above are responsible for liver infection. Blood-stage proteins allow erythrocyte entry and re-infection. Finally, proteins listed at the transmission stage allow parasite replication. In bold are vaccine antigens currently evaluated in pre-clinical trials or that have entered at least a phase 1 clinical trial.

In addition to genetic complexity, *Pf* present a very high genetic diversity implying that a person is generally infected by different *Pf* genotypes at the same time. During a blood meal, roughly a dozen of parasites are absorbed by the mosquito, which will generate, following sexual reproduction, newly and genetically unique parasites, representing a permanent challenge for the immune system of people living in endemic countries. The antigenic diversity of *Pf* is exacerbated for some proteins, for which there are genes coding for slightly different antigenic variations. It is for example the case for the PfEMP-1 protein, which is encoded by 60 *var* genes. Each individual parasite expresses a single var gene at a time, maintaining all other members of the family in a transcriptionally silent state (66). This makes the diversity of this pathogen staggering, even on the scale of an individual infection.

Plasmodium falciparum also express several proteins with redundant functions, such as proteins of the PfEBA (erythrocyte binding antigens) or PfRHs (reticulocyte binding) families. This implies that even if some blocking Abs arise against one of the proteins of this family, other proteins are expressed that have the same functionality (67). This redundant-protein expression system enables the parasite to efficiently bypass Ab blockage and at the same time offers an opportunity for rapid selection and dissemination of variants of the parasite.

The antigens themselves harbour an unusual composition, as many of them contain numerous repeats, notably rendering the structure of the protein disordered (68). These repeats do have several extraordinary properties, as explained by Kemp et al (69):

- they can reach very high levels in some antigens,
- they also tend to vary in number following immune pressure, and participate to the antigenic diversity of *Pf* strains,
- they tend to represent the immunodominant part of the protein, thus acting like an "antigenic smokescreen" that will induce non-effective low-affinity Abs.

Kemp et al consequently distinguished two types of repeats: some that only confer immune-escape properties to the antigen, and some harbouring a very conserved sequence, that have an essential function in the parasite lifecycle, such as in RESA (ring-infected erythrocyte surface antigen).

As the PfCSP contains numerous NANP and NVDP repeats in its central immunodominant domain, it is a good model to understand the involvement of repeated motifs on *Pf*. It was shown by Pholcharee et al (70) that mice immunisation with a recombinant 9-NANP-repeats CSP protein conferred a humoral protective immune response in more animals than immunisation with a 25-repeats. Regarding those results, a hypothesis was made that the repeat-rich

constitution of the Pf CSP may favour high-avidity Ab-antigen contacts, inducing the premature exit of MBCs from the germinal centre without them performing many somatic mutations. In the same way, a mutated cell that fails to interact with the trigger epitope with sufficient affinity may react with a cross-reacting one and undergo further proliferation. Similarly, Langowski et al (71) showed that when testing different virus like particle (VLP) designs for new vaccine candidates, the one containing only five NANP repeats was the most efficient for induction of protective Abs in mice and monkeys, compared to the one containing 20 NANP repeats.

This thesis will discuss in detail the glutamic acid rich repeat units found in numerous *Pf* proteins (RESA, Pfs230, Pf11.1 …). If these repeats confer negative charges to the proteins and render them partially disordered (72), they are also particularly immunogenic and "tend to be decoy epitopes that drives the host humoral immunity away from functional domains", as explained by Hou et al (73).

5. Approaches for malaria vaccines

As explained in the introduction, the number of malaria cases is still high and situations where prevention measures are lenient (civil wars, COVID-19 pandemic) generate epidemic bursts that are difficult to control. Having an effective vaccine would therefore make it possible to stop contaminations once and for all. Despites hopes of the scientific community (74) and global organisations (75) to have a malaria vaccine available between 2020 and 2030, to date only one vaccine, the RTS,S/AS01 , has been authorized by the World Health Organisation on October 2021 for at-risk children. As we will see in the next paragraph, its efficacy is moderate. If phase 3 clinical trial showed a four-year efficacy of 36% (76), efficacy 7 years after the immunisation of children with a prime-boost regimen was only 4.4% (77), emphasising the need for new, more effective vaccines.

There are various limitations that may explain why there is currently only one moderately effective vaccine licensed for malaria control. One of the main levers is economic: as malaria is a disease that almost exclusively affects developing countries, there is insufficient funding for research (78). The other limitations are more of a technical and scientific nature. Indeed, the use of the whole pathogen as an immunogen is first difficult to envisage on a large scale, as the culture conditions for this parasite are very restrictive (RBC cultures, etc.). This implies that a careful choice and an appropriate design of the immunogen(s) is needed for them to be used for the induction of effective Abs. This step is a technical challenge due to the composition of *Pf* proteins (numerous disulfide bridges, repeated motifs and disorganized domains...) which make it difficult to produce them with a conformation close to the one found in the parasite, either as a whole protein or as domains, as we will see in the TBVs section.

To speed-up malaria vaccine discovery, the Malaria Vaccine Roadmap set two goals to be reached by 2030: the development of vaccines with a protective efficacy of at least 75% against clinical malaria and the development of transmission blocking vaccines (79). Thus, several malaria vaccines are currently being developed to target one of the three main stages of the parasite's cycle, as indicated in figure 7.

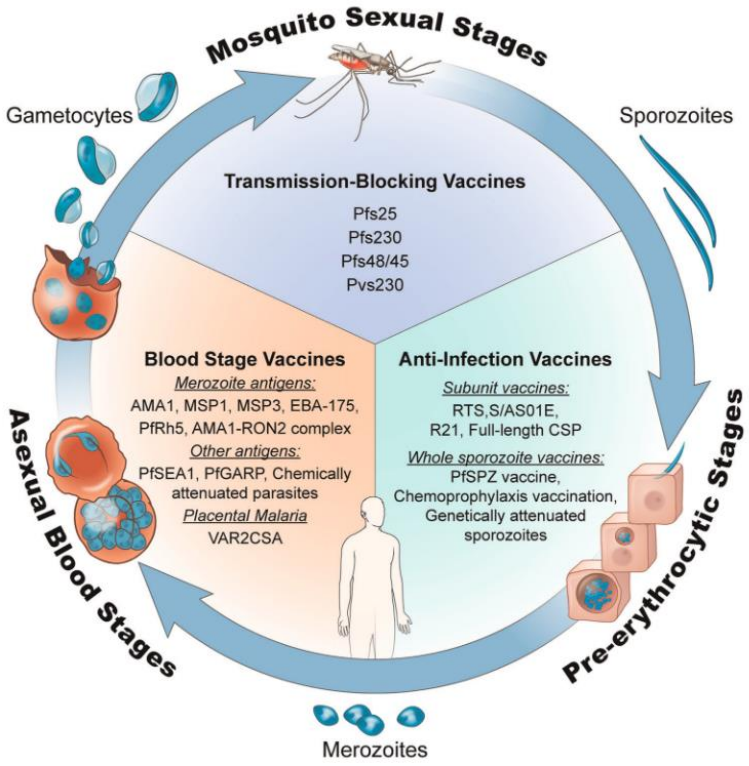

Figure 7: Malaria vaccine candidates in clinical development as in 2020, from Duffy et al (80)

Malaria vaccines can be divided into two categories, depending on whether they are effective on symptoms or not. Vaccines targeting the pre-eythrocytic phase aim to prevent hepatocyte infection by sporozoites, indirectly avoiding clinical symptoms. So do vaccines targeting the intra-erythrocytic asexual replication phase, hindering parasite infection and multiplication inside red blood cells, directly avoiding clinical symptoms.

In contrast, vaccines targeting the sexual replication phase aim to block the downstream transmission of the parasite, but do not have any impact on the appearance of symptoms. These vaccines are the subject of my thesis.

5.1 Vaccines to prevent malaria disease

5.1.1 Testing malaria vaccine efficacy

Phase 1 clinical trials are performed in a small fraction of human volunteers. Indeed, malaria is curable when treated early, allowing for parasite challenge experiments, also called controlled human malaria infection (CHMI) (81) (82). In these tests, a previously vaccinated volunteer is infected with *Pf*, either through a mosquito bite or by direct sporozoite intra-venous injection. If not blocked by the immune system, the infection develops quickly and parasites are detectable in blood following the rupture of the hepatocytes (approximately one week after the sporozoite injection). At this point, a drug is administered to the volunteer to prevent the appearance of severe symptoms. This technique enables the determination of vaccine efficacy by comparing the parasite load (parasitemia, PCR) between vaccinated and control individuals. A vaccine is considered as efficient when able to avoid parasite liberation from hepatocytes. Of note, CHMI can also be performed on *Pf* transmission area, which gives additional information about the effect of pre-immunity on vaccine efficacy.

Real-world vaccine efficacy tests are also feasible. In such a setting, infected mosquito bites are numerous, and injected parasites originate from a large diversity of strains (compared to CMHI performed on volunteers with homologous or heterologous Pf strain). Such tests require a larger population of volunteers, longer study periods and are also more expensive. In this configuration, vaccine efficacy can be determined either against clinical malaria (fever and parasitemia) or against severe malaria.

5.1.2 Pre-erythrocytic vaccines (PEV)

Pre-erythrocytic vaccines were the first malaria vaccines investigated and several strategies for immunisation have been deployed, by using either the whole parasite or part of it as an immunogen.

The use of whole sporozoites as immunogens is a vaccination method that has been investigated since the 60s. In the famous experiment from Nussenzweig et al (83), mice were immunised with irradiated sporozoites, and challenged 2 weeks following immunisation. Sixty-three percent of the immunised animals developed protective immunity against parasitemia,

and most of the animals remained protected following a second challenge 3 years after the first immunisation. Experiments were then performed in humans with irradiated *Anopheles* mosquitoes carrying sporozoites. Hundreds of mosquito bites were used for weekly sporozoite inoculations to volunteers, during several months (with periods of time varying greatly depending on the volunteer) (84). Once challenged with a variable number of non-irradiated mosquitoes, some volunteers did not develop parasitemia. Although difficult to reproduce, these experiments provided evidence that sterilising immunity could be induced against Plasmodium falciparum in humans.

Based on the injection of the whole pathogen, two vaccines types have been designed: injection of non-infectious sporozoites (either irradiated or genetically attenuated live parasites), or injection of live non-attenuated parasites with concurrent anti-malarial drug administration. The latter strategy is also called chemoprophylaxis vaccination, CVac.

Developed by Sanaria Inc, the PfSPZ vaccine is the most advanced irradiated sporozoite - based vaccine. The phase I clinical trial was conducted following two steps: first by immunisation of malaria-naive volunteers, then by immunisation of adults living in a high transmission area (NCT02627456) (85). Following a round of three injections (at a dosage of 1.8 × 106 sporozoites) separated by an 8 week interval, vaccine efficacy (VE) was determined 5 weeks after having completed the injection procedure. VE was estimated at 100% following CMHI on volunteers, while it was evaluated at 52% in real-life settings. Those encouraging results motivated further investigations. Unfortunately, phase II clinical trials performed on children aged 5 to 12 months did not demonstrate VE 6 months after the last injection (NCT02687373) (86).

Based on a different strategy than the PfSPZ vaccine, the GAP3KO one is actually under investigation in clinical trial (NCT03168854). Genetically modified parasites depleted for their virulence genes are administrated through mosquito bites (87).One week following effective immunisation, no parasite could be detected in the blood of the ten volunteers, showing that GAP3KO has a low risk of breakthrough infections.

Finally, based on the administration of live parasites, the PfSPZ-CVac contains non-inactivated sporozoites, administered with either chloroquine or pyrimethamine to avoid infection (88). In a phase I clinical trial (NCT03083847), the vaccine had an efficacy of 100% when administered with the highest dosage (2x105 parasites), on six volunteers.

Of note, for whole-parasites vaccines, the number of sporozoites injected is extremely high compared to the number of parasites injected by the mosquito during natural infection. Whole

pathogen immunisation is a strategy that successfully induces sterilising immunity in CHMI experiments performed on malaria-naïve individuals, thus providing an interesting proof-of-concept. However, its large-scale deployment seems difficult because of the high logistical constraints. Indeed, it implies labour-intensive cultivation of the parasite in specific laboratories, and in the case of irradiated parasite, the -80°C vaccine transportation and intra-venous administration.

To overcome the obstacles encountered with whole-pathogen vaccines, others have been developed, such as protein-based ones, especially PfCSP-based ones, of which RTS,S/AS01 is the most advanced. Besides the repeat-rich central domain, the PfCSP contains an N-terminal domain which is conserved among the different strains of Pf and a highly polymorphic C-terminal domain, as schematised in the figure 8. Only the central part and the C-terminal parts of PfCSP are included in the composition of RTS,S/AS01. The selection of the C-terminal rather than the N-terminal domain was motivated by the presence of T cell epitopes in the C-terminal domain. The truncated PfCSP is produced and fused to a recombinant HbS protein, found at the surface of hepatitis B virus. HbS is used in numerous hepatitis B vaccines, but also possesses VLP self-assembly properties. This VLP vaccine is adjuvanted with AS03, a liposomal adjuvant.

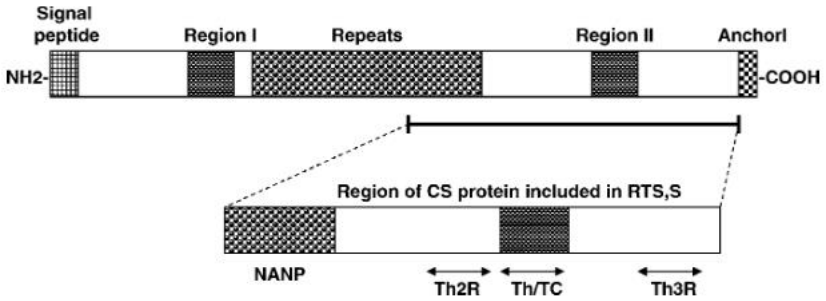

Figure 8: Schematic composition of the Pf CSP and the region of the protein included in the RTS,S/AS01 vaccine, from Casares et al (89)**.**

Arrows indicate T helper cell epitopes localisation.

Unfortunately, when tested in humans, the RTS,S/AS01 vaccine showed only poor efficacy, as mentioned in the introduction. Indeed, in infants aged 6-12 weeks, four doses conferred only a 30% protection against severe malaria lasting no more than four years (90). Some studies raised the question of the immunogen design, highlighting that in some individuals, the most potent Abs were able to bind the repeats in the central region, but also

epitopes in the N-terminal region, that are not present in the RTS,S/AS01 vaccine (91). The C-terminal part being highly polymorphic, further research has shown a mismatch between the strain used for the design of the CSP used in the RTS,S/AS01 and the strains currently circulating in South and Central Africa, which could also be an explanation for the poor clinical efficacy observed in the field (92).

In response to the poor performance of the RTS,S/AS01 a new version of the latter was built, that harbours more truncated CSP and less AgHbS at the VLP surface: the R21, adjuvanted with Matrix M instead of AS01. One year after the first immunisation, the R21 efficacy was 77% (93) but it will be necessary to confirm whether these results are maintained over time. Nevertheless, as the R21 is composed of the central and C-terminal domains, it still does not address the limitations mentioned above, which will only be solved with the design of new vaccine candidates.

Another antigen than PfCSP was tested in clinical trials. Pf CelTOS (cell traversal protein for ookinetes and sporozoites) is a protein necessary for Pf entry to the liver (94) that has been used as a vaccine candidate because it induced sterile immunity in mice (95). A vaccine based on this antigen has been evaluated in a phase I clinical trial by the American Army but no results have been disclosed to date.

Beyond the selection of new pre-erythrocytic antigens in the composition of vaccines, new platforms are being developed that would allow antigen presentation on the surface of other various types of VLPs (96) (97) (98), rendering the antigens more immunogenic (NCT01540474).

Notably, following the advent of the mRNA anti-COVID-19 vaccine, this vaccine strategy is being tested for malaria. Lipid nanoparticles encapsulating mRNA coding for fragments of the PfCSP protein were used for immunisation in mice. The chosen fragments were 1, 4 and 38 copies of the NPDP/NVDP and NANP motifs, shown to be the target of functional Abs (this aspect being discussed in details below). The candidate induced sterile protection against P.berghei infection (99), and more results may be expected in the near future.

As mentioned earlier, following the injection of the parasite into the human host, the second stage consists of its intrahepatic multiplication, protected from the recognition by Abs. Thus, platforms inducing strong T cell responses via presentation of the antigen through MHC I molecules may be the most efficient in inducing an effective immune response. In a phase I clinical trial (NCT01364883), a vaccine harbouring ME-TRAP antigens has been evaluated in malaria naïve individuals with CMHI experiments. ME-TRAP is a fusion protein composed of 20 epitopes (mainly CD8 ones) fused to the TRAP (thrombospondin related adhesion protein) antigen. The vaccine is based on a heterologous prime-boost regimen with viral vectors (ChAD63 or MVA) and has demonstrated its ability to induce high T cell activation levels (100). The vaccine had a 21% sterile efficacy and delayed parasitemia in 36% of the vaccines. Unfortunately, phase IIb clinical trial (NCT01635647) performed in 5-17 months infants living in Burkina Faso showed only moderate T cell responses and no significant efficacy was observed against clinical malaria (101). Of note, to improve the protection conferred by both vaccines, researchers tried to co-administer the RTS,S/AS01 with the ChAd63-MVA vaccine (NCT0225264). Unfortunately, following CHMI, vaccine efficacy against parasitaemia was found to be lower in the groups receiving both vaccines compared to those who only received the RTS,S/AS01 (102).

5.1.3 Blood stage vaccines

Blood stage vaccines can be distinguished depending on the targeted stage: either free parasites on the merozoite stage, or RBCs infected by merozoites (iRBC). Most anti-merozoite vaccines aim to elicit Abs that bind to proteins involved in the process of RBC entry thus leading to RBC invasion blockage. For such a vaccine, it is very important to select antigens that are well conserved between strains and sufficiently susceptible to Ab neutralisation in the minute or so between schizont egress and RBC re-invasion in a way that significantly impacts the in vivo parasite multiplication rate. Among those proteins, AMA-1 (103) and RH5 are the two most studied vaccine candidates (104). Being responsible for the parasite sequestration inside the placenta, the VARC2CSA variant of the PfEMP1 protein is also an antigen of interest for the development of a vaccine against placental malaria. Of note, investigations are underway to discover potential new antigenic targets, which would ideally have a synergistic effect to the already known vaccine candidates (105) .

The most advanced anti-merozoite vaccine is the RH5.1 (106), which is comprised of the full-length RH5 protein, adjuvanted with AS01. In a phase I/IIa clinical trial in malaria-naive volunteers, the vaccine was highly immunogenic but only resulted in a 1-day delay until threshold parasitemia levels were reached following CHMI in comparison to the unvaccinated control group (107) . More results are expected from a phase I clinical trial enrolling Tanzanian children and adults. One of the challenges faced in the development of a blood stage vaccine is the induction of an effective response against the different types of merozoite strains, which harbour a vast number of polymorphic proteins. To circumvent this problem, researchers designed a vaccine containing four versions of the AMA-1 protein, that proved to efficiently reduce RBC invasion (108).

Based on the use of VARC2CSA as an antigen, the PAMVAC and PRIMVAC vaccines were tested in Phase I clinical trials. If they prove to be immunogenic and well tolerated, their efficacy still has to be determined in further trials (109) (110).

More anecdotally and similar to the whole pathogen pre-erythrocytic vaccines, infected RBCs were tested as a vaccine in phase I clinical trial (ACTRN12614000228684). Although the vaccine proved to be well tolerated and able to induce T cell responses, Ab levels were really low. Moreover, feasibility of this type of vaccination on a large scale is still a problem (111)

5.2 Vaccines to prevent transmission of *Plasmodium falciparum*

As schematised in figure 9, transmission blocking vaccines (TBVs) aim to induce TRAbs, to block parasite dissemination. There are currently no commercialized TBVs, and the most advanced have only reached phase I clinical trials. Such vaccine candidates do not have an impact on the RBC stage and consequently do not prevent patients from declaring symptoms. Instead, they are active at a population scale, in case of high vaccine coverage, by decreasing the parasite carriage by the mosquitoes and therefore their infectivity. Although this type of vaccine is not able to prevent symptom from appearing, it holds many promises and may be able to prevent the spread of emerging drug-resistant parasites. TBVs are also called "altruistic vaccines", and might only be effective if there is a high adherence to vaccination by the local population (112) (113). Of note, since transmission of the parasite occurs within an approximate radius of 1 km from a larval site, the high level of vaccination of distant communities could have a strong local impact (114).

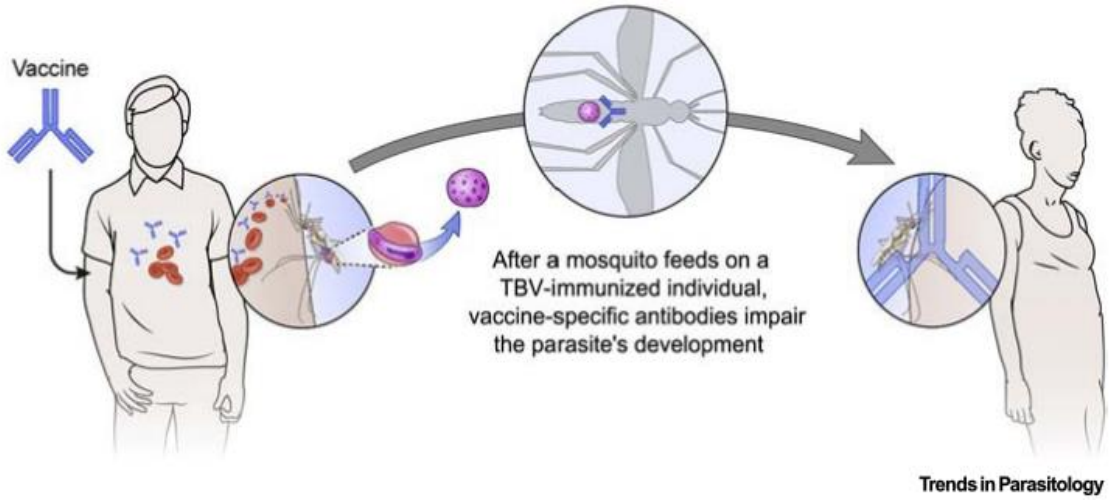

Figure 9: Transmission Blocking Vaccines mechanism of action, from Coelho et al (112). *TBVs aim to induce TRAbs which block the reproduction of the parasite inside the mosquito's gut, avoiding new contaminations.*

Compared to vaccines aiming to protect against the malaria disease, TBV ones have several advantages. First, the proteins expressed at the surface of the parasite at this stage are among the most conserved ones as indicated figure 10, harbouring a low polymorphism (115). As mentioned before, this could be explained by the lower immune pressure applied to the sexual stage antigens compared to the other stages, especially for antigens expressed only inside the

mosquito as it is the case for Pfs25 (116). Thus, compared to asexual-stage antigens, Ab responses induced by TBV may confer a broader cross-protection in endemic settings.

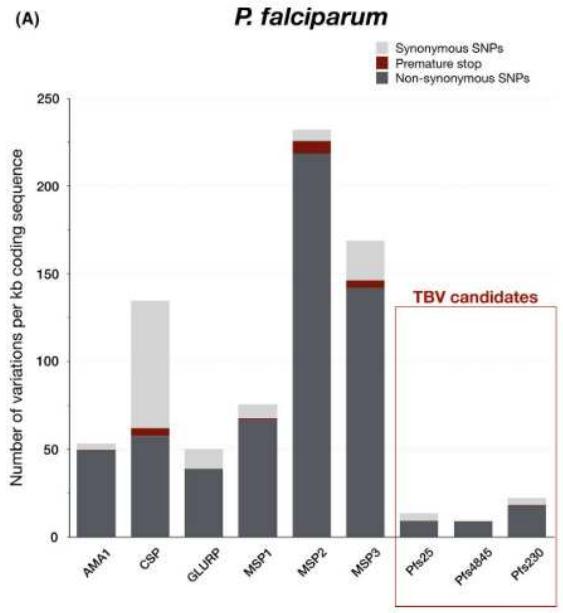

Figure 10: Polymorphism among different vaccine candidates, from De Jong et al (117)**.**

The non-synonymous SNP density of three major TBVs antigens: Pfs 25, Pfs48/45 and Pfs230 is significantly lower compared to antigens from other stages. Of note, Pfs230 is the one with the highest polymorphism among the three.

Second, similarly to reinfection in an endemic setting, if TBV vaccination is done with antigens present on gametocytes, the MBCs previously induced by vaccination will be activated by their encounter with the antigen and will return to perform maturation rounds. As gametocytes persist for a long time in the human host, they may be the target of these matured MBCs or their Abs. This natural boosting mechanism may make it possible to avoid frequent vaccine administrations, which could be particularly interesting in developing countries (118).

Finally, at this step of the parasite lifecycle, the gametocyte load is relatively low compared to the erythrocytic stage, which in contrast generates a very high asexual parasite load (48). Therefore, TBVs may not have to induce Ab levels as high as they do for erythrocyte stage vaccines, to be effective. Conversely, although the levels of induced Abs should be potentially lower than those for the erythrocytic stage, the induced Abs should be sufficiently resistant to degradation in the protease-rich stomach of the mosquito.

The first TBV antigen to be successfully expressed as a recombinant truncated protein for immunisation purposes was Pfs25 in the early 90s, and it was recognized by conformational Abs (119). Indeed, one of the main obstacles encountered when producing TBVs has been to produce the multi-domain cysteine-rich proteins, to which Pfs25 but also Pfs48/45 and Pfs230 belong, as properly folded recombinant proteins. The different constructions produced for these three proteins are schematised in figure 11. Later, Pfs25 was successfully synthetised as a full-length, properly-conformed protein, used in different Pf25 vaccines (120).

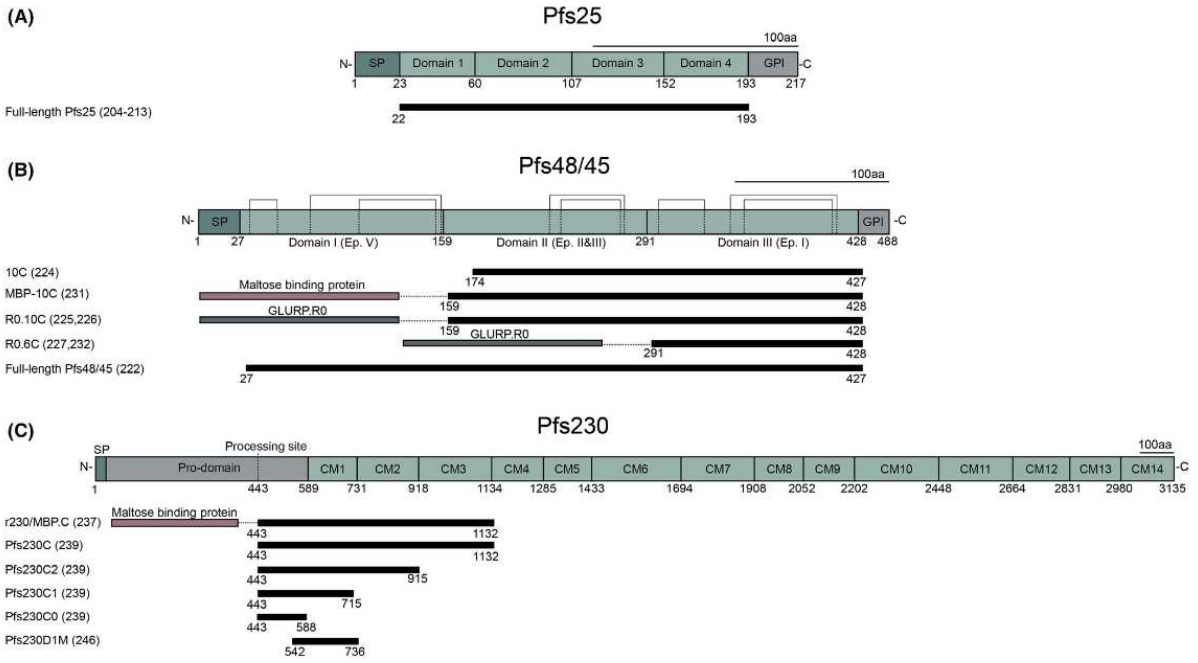

Figure 11: Schematic representation of the native three main TBV antigens, and their corresponding recombinant versions, from de Jong et al (117)**.**

As mentioned before, Pfs48/45 and Pfs230 were early on identified as also being capable of inducing TRA. New expression systems have consequently been set-up, notably to accommodate production with disulphide bridges and without N-glycosylation as *Pf*, contrary to the other eucaryotes, are not able to perform N-glycosylation. A solution was found by Outchkourov et al (121) for Pfs48/45 production, by driving the expression of Pfs48/45 to the periplasmic space of *E. coli*, where oxidases present in the periplasmic space were able to form disulfide bridges, allowing for the proper antigen post-translational modifications. Alternative solutions came from the fusion of the 6C domain (aka epitope III, targeted by the most potent TRAb described to date) to a fragment of the GLURP protein (expressed at asexual stage), leading to the R0-6C protein, that demonstrated high production yield under GMP conditions

(122). This immunogen is actually being tested in phase 1 clinical trial (table 2). Of note, Pfs48/45 has only been produced as a full-length protein by Lennartz et al (123) in 2018.
This is not the case for Pfs230, which is larger than Pfs25 and Pfs4845, and has so far always been produced as domains. As for Pfs48/45, different expression systems were tested to allow domain production in the right conformation, the first being in *E. coli* (124) (125), then also in wheat germ cell-free system (126), Nicotiana benthamiana (127) or baculovirus (128).
Importantly, the production of truncated proteins to be used as immunogens involves a selection of the protein parts considered to be immunogenic, and for Pfs230, the selected domains only span the first three N-terminal domains. If these latter were targets of TRAbs, it would not be possible to exclude that the remaining domains are not.

Of note, to get around this conformation problem, some teams have also tried immunisation with linear epitopes. This strategy was used for example with Pf 11.1, a megadalton protein implicated in parasite erythrocyte rupture during gametogenesis, whose size made its production as full-length unrealistic. Scherf et al (129) selected a nonamer repeated motif for mice immunisation. If the peptides would've been able to induce T cell responses (no information about the induced TRA was available), such strategies would raise the question of the choice of the linear epitope for immunisation.

In spite of these technical limitations, several TBVs candidates have advanced to clinical steps (130) (131), and the main ones are summarized in table 2. To increase immunogenicity, some vaccine candidates were designed using platforms allowing presentation of a network of antigens on their surface, at the surface of a virus-like particle or a nanoparticle (using EPA). Indeed, according to Healy et al (132), Pfs25 and Pfs230 recombinant antigens have shown poor immunogenicity as monomers. This multimerisation enables a crosslinking of B receptors on the surface of lymphocytes, inducing a more important humoral response than with monomeric soluble recombinant proteins.
Despite promising pre-clinical results when tested in animals, the only vaccine which successfully induced TRA was the Pfs230D1M-EPA, which is now under phase II evaluation. This highlights the difficulty of transposing the results obtained in pre-clinical trial in animals to humans.

	Vaccine name / Adjuvant / Administration regimen	Clinical trial	Results
Gene carrying vaccine	Prime: ChAd63 coding for Pfs25-IMX313 Boost: MVA coding for Pfs25-IMX313 *IMX313 is a complement inhibitor C4b-binding protein used to form heptamers, with the antigen fused to it.*	Phase I *NCT02532049* Tested on 26 healthy adult volunteers.	The vaccines were immunogenic, but did not induce TRA (133) (131).
Protein-based vaccines	- Pfs230D1M-EPA/ Allhydrogel or AS01 - Pfs25-EPA/ Allhydrogel or AS01 - Combination of both vaccines *EPA : exoprotein A from Pseudomonas aeruginosa and is used as a carrier for conjugated vaccines.*	Phase I *-NCT02334462* Five individuals per arm (healthy adult volunteers or individual living in Mali).	Vaccination with the Pfs25 vaccine alone did not induce TRAbs. **Vaccination with Pfs230D1M vaccine alone induced TRA in 4 out of 5 volunteers.** Combination with Pfs 25 did not increase activity over Pfs230 D1M alone (134)
	Pfs230D1M-EPA/ AS01	**Phase II** **-***NCT03917654* Tested on 1449 individuals living in Mali (children and adults).	Results are expected in the near future.
	R0.6C/ Matrix M *R0.6C is a fusion protein comprising the domain III of the Pfs48/45 and a domain of the GLURP antigen.*	Phase I *NCT04862416* Tested on 32 healthy adult volunteers.	Initiated on July 2021 (135). Investigators are the Radboud University and Novavax. Results are expected in the near future.
Virus-like particle	Pfs25 VLP-FhCMB/ Allhydrogel *Chimeric non-enveloped virus-like particle comprising Pfs25 fused to the Alfalfa mosaic virus coat protein.*	Phase I *NCT02013687* Tested on 44 healthy adult volunteers.	Weak TRA induced by vaccination (136).

Table 2: TBVs in clinical development, as in October 2022.

In blue are vaccine adjuvants.

Poor performances of TBVs currently in clinical trials highlight the need for new vaccine formulations, new antigen conformations or even the use of new antigenic proteins. A good

example of this new TBV generation may be the use of a heterologous prime-boost vaccination regimen, where the simian adenovirus 63 (ChAd63) or the modified vaccinia Ankara virus (MVA) viruses are vectors used to carry genes coding for several antigens: AgAPN1, Pfs230-C1, Pfs 25 and Pfs48/45 (137).

Finally, to obtain more effective malaria vaccines, the development of multi-stage malaria vaccines may be more promising than TBVs alone.

6. Monoclonal antibodies instruct rational malaria vaccine design

As mentioned previously, more efficient malaria vaccines have to be developed to date. To this aim, new antigen conformations, or even new antigens can be used in vaccine formulation. The selection and the rational design of these antigens can be guided by "reverse vaccinology 2.0 techniques ".

6.1 Reverse vaccinology 2.0

The initial so-called reverse vaccinology strategy was based on the identification through gene sequencing of proteins as potential immunogens for vaccine development (138) (139). This strategy successfully led to the development of several vaccines such as the one against meningitidis (140). Developed in the early 2000s, "reverse vaccinology 2.0" strategies aim to isolate mAbs with a functional activity of interest, notably correlating with protection against a disease, in order to define, through structural approaches, epitopes to be incorporated in immunogens and to elicit corresponding protective Abs through rational vaccine design approaches (141) (142).

In practice, as shown in figure 12, sera from vaccinated or infected individuals are screened for a functional activity that is usually determined based on correlates of protection against the disease of interest. Peripheral Blood Mononuclear Cells (PBMCs) of individuals having a high functional activity (for example convalescent donors following an infectious disease) are then harvested and used for Ab isolation from specific B cells that are selected through various methods, as described below. The advent of immunoglobulin gene amplification techniques from single B cells has made possible such approach. High throughput methods now eventually allow for the screening of thousands of mAbs for a particular functional activity or the binding

to a particular antigen or epitope of interest that may have been previously determined. The strategy therefore yields a panel of mAbs with a particular functional activity of interest, potentially targeting a particular antigen/epitope that can be further characterised. The large number of mAbs obtained through novel high throughput methods eventually gives insight in the corresponding B cell repertoires.

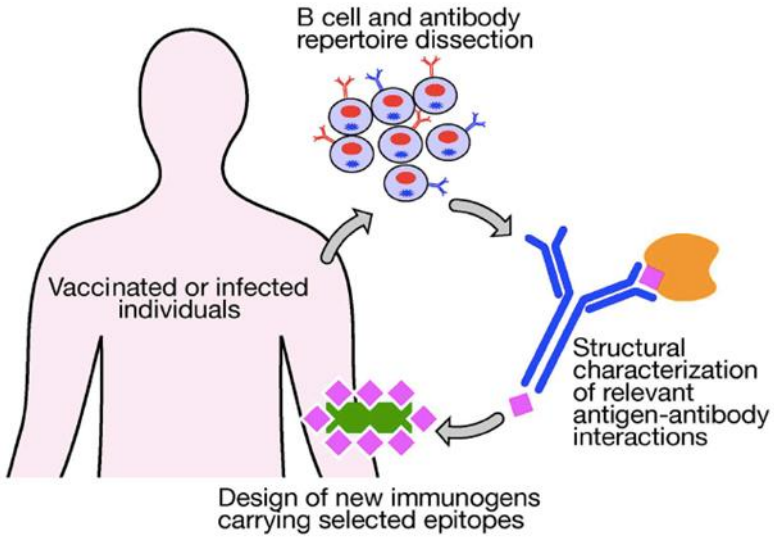

Figure 12: Principle of the reverse vaccinology 2.0, from Finco and Rappuoli (143).

Advances in structural biology techniques have also been crucial for the development of reverse vaccinology. The fine characterisation of interactions between functional Abs and their epitopes by crystallography or cryo-EM techniques gives a clear understanding of the epitope and the mode of recognition of Abs with the desired functional activity, potentially highlighting their mechanism of action, and therefore of the desired properties of Abs to be elicited through vaccination.

Rational immunogen design can be then used to elicit such Abs through vaccination. Of note, iterative vaccination and Ab isolation can then potentially lead to the design of antigen modifications to optimize immunogenicity and the improve the elicitation of Abs with the desired properties. Structural biology and rational vaccine design have, for example, enabled the stabilisation of the respiratory syncytial virus fusion protein in the prefusion conformation, leading to an improved immunogenicity (144). Information gained from such stabilisation techniques was ultimately used for the design of anti-SARS-CoV-2 vaccines (145). Very recently, structure guided immunogen design was used in the TBV field, to improve the stability

and the biophysical properties of Pfs48/45-6C (aka R0-6C). Immune responses induced by mice immunisation showed ten to hundred times enhanced TRA (146).

In the malaria vaccine field, the use of reverse vaccinology 2.0 approaches may hopefully accelerate rational vaccine design and development (147). These strategies are currently applied to pre-erythrocytic vaccines, via the study of monoclonal antibodies developed by individuals living in endemic areas (59) or volunteers who received the PfSPZ vaccine (148). Of note, as some pre-erythrocytic vaccines are based on the injection of the whole pathogen, either attenuated by irradiation or alive in association with a chemoprophylaxis, the immune response developed is very close to the one induced by natural infection. In these individuals, researchers studied Ab responses to the PfCSP protein, which is the main target of the protective antibodies, in order to better understand the nature of protective epitopes and gain relevant information for the design of improved PfCSP vaccines. Finally, in addition to helping rational design of vaccines, the mAbs identified by these studies can be used for passive immunization trials in humans, as detailed in 6.3.

6.2 Method for monoclonal antibody isolation

Various methods have been used over the years to generate mAbs, in particular for clinical use in humans (figure 13): humanisation of murine monoclonal antibodies obtained from hybridomas (A); selection of Abs from phage display libraries of human Ab fragments (B); and more recently immunisation of transgenic mice carrying human immunoglobulin loci followed by hybridoma generation or cloning from single B cells (C); and cloning from single B cells from individuals following infection or immunization (D) (149) (150).

Monoclonal antibodies obtained using high-throughput singe B cell sorting and screening and directed against various infectious diseases have been reviewed by Corti and Lanzavecchia (151).

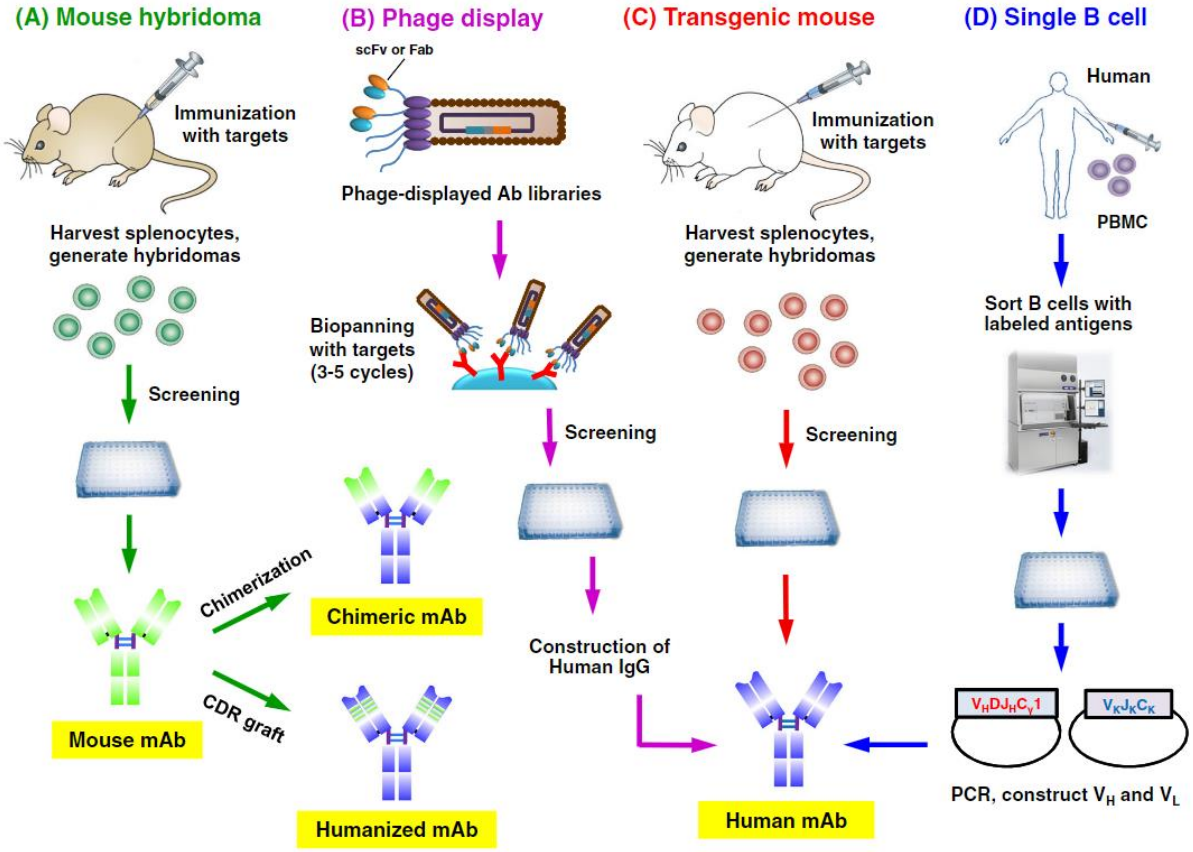

Figure 13: Four main techniques for monoclonal antibodies obtention, from the oldest to the most modern, from Lu et al (152)

6.3 Passive immunotherapy: using mAbs for prevention of malaria disease and transmission

Faster to develop than vaccines, mAbs are a rapidly expanding therapeutic class, particularly in the field of infectious diseases (153) (152) and could thus be used for neglected tropical diseases such as malaria. When administered to patients, they confer immediate passive immunity. Because the protection persists for several months, immunotherapies could thus be administered at the beginning of the rainy season, decreasing the number of infected people. Compared to anti-malarial drugs that may induce serious side-effects, mAbs, especially when humanized or fully human, are well tolerated. They can also be used in areas where drugs are becoming less effective due to the emergence of resistance. Compared to malarial vaccines, they provide a reliable level of Abs, regardless of the host immune status (pre-exposed, immunocompromised …) (154)

MAbs able to block parasite entry into the liver are good immunotherapy candidates, as they may prevent symptoms from appearing. To date, two anti- Pf CSP mAbs have been tested in clinical trials: CIS43LS and L9LS, and both have showed very high efficacy against sporozoite infection. CSI43LS binds to an epitope containing NPDP at the junction between N-terminal and repeat region and with less affinity to NVDP containing peptides in the same region (155). When administered in volunteers, none of them developed parasitaemia (156). Similarly, L9LS mAb, which binds to minor repeats NVDP but also cross-react with NANP major repeats (157) , protected 88% of the volunteers against sporozoite infection (158). Finally, in order to limit the risk of parasite escape, other mAbs targeting other antigens among the Pf CSP could be incorporated in an immunotherapy cocktail design.

Contrary to anti-Pfs CSP mAbs, the use of TRAbs in passive immunotherapy is less obvious, as they have no direct impact on the appearance of symptoms. However, monoclonal TRAbs can be useful when administered in combination with Abs against sporozoites or merozoites, to limit local transmission for a season. This kind of cocktail immunotherapy can be particularly effective in the case of a malaria outbreak in an area where the parasite has been previously cleared. In this sense, a study from Sherrard-Smith et al (159) showed that the injection of an anti-CSP Ab (mAb 3D11) combined with an anti-Pfs25 Ab (mAb 4B7) in mice was more efficient than the injection of one of the mAbs alone in reducing prevalence and density of sporozoite inside mosquitoes fed from the passively immunized mice.

Interestingly, recent work from van der Boor (160) demonstrated the safety and tolerability of TB31F, the humanised version of mAb 85RF45.1, in a phase 1 clinical trial. The TRA of the serum of all participants was above 80%, regardless of the dose. Moreover, with the 10 mg/ml dosage, the researchers estimated that the serum retained 80% TRA for approximately 160 days. Interestingly, de Jong et al (161) demonstrated that the 85RF45.1 mAb targets a very conserved epitope on Pfs48/45 and retains high TRA levels with different *Pf* strains. TB31F having the same binding properties than 85RF45.1 with an increased half-life (162), it is likely that this mAb can be used on large geographical areas, encompassing different *Pf* strains.

Because of lack of availability and costs, access to chemical antimalarial treatments is already difficult for people living in endemic areas. As immunotherapy treatments are much more expensive, require cold chain with respect to their storage and often need intravenous administration, they do not appear as a realistic solution for endemic population to date compared to vaccination. Malarial immunotherapies may find their use with people from high-income countries, travelling to endemic areas (military members, tourists).

6.4 Monoclonal antibodies with transmission blocking activity

To date, several monoclonal TRAbs (mTRAbs) have been obtained, and the principal are summarized in table 3. The majority of these mTRAbs were isolated following animal injection, mainly using recombinant proteins or vaccine candidates, but also sometimes gametes for immunisation. Only few mTRAbs were isolated following human immunisation, such as LMIV230-01 mAb obtained *via* immunisation with 230D1M and 2530 and 2544 mAbs, both obtained *via* immunisation with Pfs25-VLP.

Actually, the most potent TRAb is TB31F as already mentioned above. TB31F is directed against Pfs48/45 with an IC_{80} (Ab concentration that gives 80% TRA) of 1 µg/ml (162). In comparison, the most potent anti-Pfs25 mAb, 2544, had an IC80 of 16 mg/ml (116) and the most potent anti-Pfs230, LMIV230-01, an IC80 of 60 mg/ml (163).

Target	Name	Epitope	Source / technique
Pfs230 *Pfs230 Abs described to date are complement dependent !*	63F2A2.2a (164) (165)	Unknown	Mouse immunised with gametocytes / Hybridoma
	P5E2-2F7-2B4 (166)	Unknown	Mouse immunised with gametocytes / Hybridoma
	LMIV230-01 (167)	Conserved epitope on domain 1	Human malaria naïve donors after immunisation with 230D1M
Pfs48/45	85RF45.5 (168)	Epitope V	Rat immunised with gametocytes / Hybridoma
	85RF45.1 (168) (162)	**Epitope I**	**Rat immunised with gametocytes / Hybridoma**
	32F3 (169)	Epitope I	Mouse immunised with macrogametes / Hybridoma
	TB31F (162)	Epitope I	Humanized rat Ab (from 85RF45.1)
Pfs 25	**4B7** (170)	**Site 1a/ EGF3**	**Mouse immunised with recombinant vaccinia virus expressing Pfs25 and boosted with gametes / Hybridoma**
	32F81 (171) (169)	LDTSNPVKT peptide on EGF 3	Mouse immunised with gametes / Hybridoma
	1245 (172)	**Site 2, EGF1-4**	**Transgenic mouse (Kymice) immunised with Pfs25-VLP**
	1269 (172)	Site 1a/b, EGF3	Transgenic mouse (Kymice) immunised with Pfs25-VLP
	2530 (116)	**Site 3, mainly on EGF 2**	**Human malaria naïve donors after immunisation with Pfs25-VLP**
	2544 (116)	Site 1, EGF1/3/4	Human malaria naïve donors after immunisation with Pfs25-VLP
Pf11.1 (Pfs 2400)	mAb1A1 (173)	Nonamer repeat $[PEE(L/V)VEEV(I/V)]_2$	Mouse immunised with gametocytes / Hybridoma
Pfs 47	IB2 (174)	Central region of domain 2	Mouse immunised with full-length Pfs47
	BM2 (174)	Central region of domain 2	Mouse immunised with full-length Pfs47

Table 3: Principal mAbs isolated for each main TBV antigen, adapted from de Jong et al (117) **and Julien et al** (148)**.**

Information about IC80 can be found in the corresponding articles. In bold are the Abs for which a structure has been obtained. In light blue-gray are highlighted human or humanized mAbs.

Although the information provided by those studies enable a precise characterisation of the epitope that induced TRA, it must be kept in mind that because many of them are based on the injection of recombinant proteins, they only partially reflect naturally immune response induced during *Pf* infection, in animals as well.

This is for example the case of the Pfs25 antigen. First experiments performed on mice immunised with gametocytes determined Pfs25 as a suitable TBV candidate, able to induce TRAbs (170) (171) (169). Of note, the most potent mAb produced with this method was the 4B7, having an IC80 of 29µg/ml. As previously mentioned, researchers successfully developed a Pfs25-VLP production method, were Pfs25 retained a conformation close to the native one (175,176) . This construction was used for immunisation of humanized mice (Kymice, producing human mAbs) (172). A crystal structure was obtained for six mAbs and revealed two non- overlapping epitopes able to induce TRAbs. MAbs targeting the two different epitopes had a synergistic activity, but Abs targeting epitope 1 had a notably higher activity, in particular the 1269 mAb (IC80 = 63µg/ml). These encouraging results motivated the phase I clinical trial mentioned in 5.2, where healthy volunteers were immunised with Pfs25-VLP. This time, the obtained mAbs targeted a greater diversity of epitopes. Among them, the 2544 mAb had the highest TRA ever described for an anti-Pfs25 Ab with an IC80 at 16µg/ml (116). It targeted an epitope spanning through the EGF 1, 3 and 4 domains that was not described following mice immunisation. Thus, even if humanized mice are a useful model, the immune response they develop is far from the one induced in humans. Those studies also showed that the conformation of Pfs25 is not rigid, suggesting that giving the antigen a preferential conformation, may be able to induce highly functional Abs, such as 2544.

This example once again illustrates the usefulness of having access to human mAbs to inform vaccine design, here TBVs.

7. PhD project: isolation and characterisation of human mAbs blocking *Plasmodium falciparum* transmission

The discovery of new antigenic targets for TRAbs could lead to the development of novel TBVs to help eradicate malaria. The main purpose of my Ph.D. thesis project was to identify such new antigens using a reverse vaccinology 2.0 approach, through the isolation, from selected donors, of mAbs with strong TRA. Indeed, as mentioned before, recent work by Stone et al (54) has showed the existence of yet undescribed TRA-associated proteins. Therefore, we designed an innovative pipeline for TRAb isolation and production, using memory B cells (MBCs) from patients chronically infected by *Plasmodium falciparum*.

Two methods have been commonly used to isolate human mAbs from MBCs as detailed above. The first method consists in using protein baits to isolate specific MBCs from selected individuals, such as convalescent donors following an infectious disease or chronically infected donors. The second approach is based on the high-throughput activation and screening of MBCs from similar subjects. Both methods have proven their efficacy, notably in the HIV vaccine research field to isolate broadly neutralizing Abs. In the first case, labelled gp120 envelope glycoproteins, the target of HIV neutralization, were used as a bait to isolate the neutralizing Abs (177). In the second case, supernatants from a very large number of activated MBCs were screened for neutralization of a small panel of HIV isolates leading to the isolation of broadly neutralizing Abs (178). More recently, as already mentioned, the first strategy was successfully used in the malaria field to isolate mAbs from volunteers vaccinated with the Pf SPZ vaccine (155); recombinant full-length biotinylated Pf CSP being used as a bait to select specific MBCs. The second method has allowed the isolation of mAbs directed against other viruses than HIV such as SARS-CoV-2 (179) and the BK virus (180).

The first part of my PhD was dedicated to the implementation and adaptation of the two single cell-based methods described above to isolate monoclonal antibodies with TRA from selected individuals. In our case the antigen of interest were not known, so we could not use a recombinant protein as a bait. Therefore, as a first approach, we opted for isolating MBCs based on their ability to bind to the whole parasite, here in the form of live gametes. We reasoned that these would indicate specificity for gamete surface proteins, some of which may be involved in TRA. A similar approach has been used before to isolate HIV neutralizing Abs using cells expressing gp120 on their surface (181). As a second method we chose to activate MBCs in a

high throughput format and screen Ig-containing supernatants for binding to gamete proteins in an ELISA format. A direct screen for functional activity, here TRA, was not possible due to the high concentration and amount of Ab required for SMFA and the difficulty to perform SMFA in a high-throughput manner. In both methods, following the first selection, mAbs were produced and tested further for binding to gametes in SIFA and for functional activity in SFMA.

The second part of my work was dedicated to the characterization of the mAbs isolated with the approaches above, in particular of the B1E11K Ab as detailed below.

The work presented in this PhD thesis originates from a collaborative project designed with Path-Malaria Vaccine Initiative in Washington DC (Rick King and Randall MacGill), as well as with two teams based in Nijmegen (Netherlands) and specialized in the biology of *Plasmodium falciparum* and more precisely in the study of the sexual stage of the parasite: the team of R. Sauerwein from the Radboud University, and TropIQ Health Sciences (https://tropiq.nl). The team of J - P Julien, University of Toronto (Canada), later joined the project to bring its expertise for structural determination.

MATERIAL AND METHODS

1. MEMORY B CELL SORT AND DOWNSTREAM MONOCLONAL ANTIBODY PRODUCTION AND CHARACTERISATION

As schematised below, the first part of the workflow implies different sorting protocols, followed by a common monoclonal Ab production protocol.

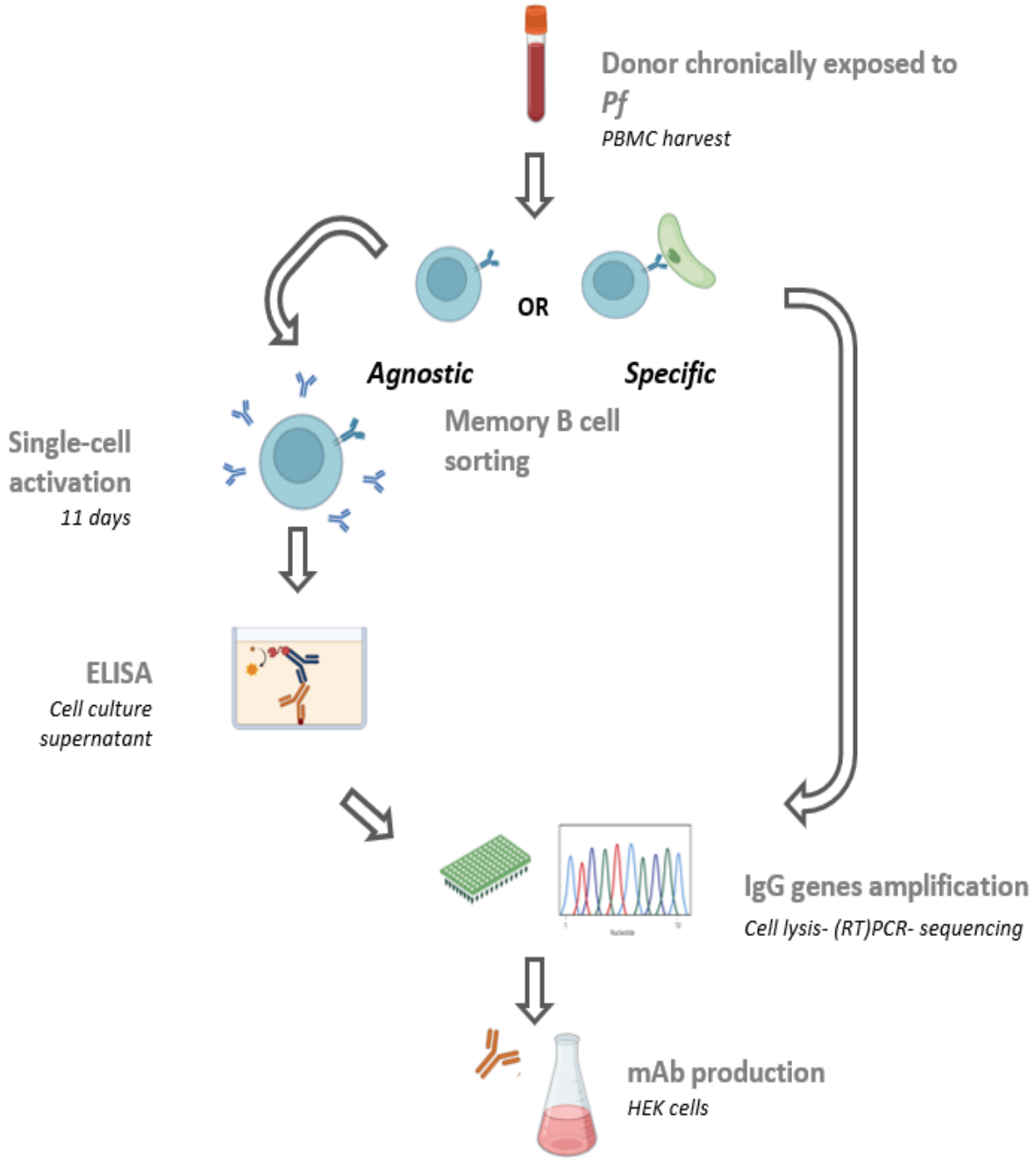

Figure 14: Experiments workflow, part I: from donor selection to mAb production and characterisation.

1.1 Donor selection

1.1.1 Donor selection for the MBC-gamete complexes sorting approach

Of note: For ease of reading, ThermoFisher reagents will be abbreviated "TF".

PBMCs sampling:

To spare precious samples from Radboud University, blood sample leftovers harvested following malaria diagnosis at CHUGA were retrieved. PBMCs were separated from total blood using Lymphoprep (Eurobio #CMSMSL01) Ficoll density gradient centrifugation for 30 min at 1110 g without braking. RBC lysis buffer (Eurobio#CMSLYS0007) was added to the cell pellet for 5 min, then discarded following 5 min centrifugation at 350 g. Cells were then counted and diluted in 1 ml conservation media (90% FBS, 10% dimethylsufoxide). Tubes were then placed in an appropriate freezing container (TF#5100-0001) for 48h at -80°C, then moved into liquid nitrogen for long-term storage.
Following consultation of the appropriate ethics committee (CHUGA Direction de la Recherche Clinique et de l'Innovation), collection of the patient's non-opposition of was not necessary, as these samples were left-over from the care and were used anonymously only for set-up purposes. We would like to deeply acknowledge the CHUGA parasitology unit for giving us access to these samples.

Serum ELISA on gametocyte extract (GE) and recombinant proteins:

Sera were screened for their reactivity in ELISA against gametocyte extract or recombinant Pfs48/45 (R06C) or Pfs230 (Pfs230 C1).

Prior to the coating step, gametocyte extract was prepared using -80°C stored gametocytes. The lysis solution (composed of 50µl of 1% sodium deoxycholate; 20 mM Tris; 150 mM NaCl and 1 µl of 100 mM phenylmethylsulfonyl fluoride) was added to a 15x 10^6 gametocyte pellet tube. Manual mixing was made using an 1,5ml Eppendorf tube pestle (TF #NC9907525) for 15 min. The mix was then resuspended in 200µl of phosphate buffer saline (PBS), prior to a 5 min centrifugation (15000 g). The supernatant was then harvested and total protein amounts were determined using the Bradford technique (TF# 23227).

PBS composition: 0.137M NaCl; 2.5mM KCl; 0.01M Na2HPO4(2H2O); 1.7mM KH2PO4. pH 7.4

Gametocyte total protein extracts were coated in 96 well plates (Maxisorp NUNC Immunoplate #442404) at 0.5 µg/ml (dilution in PBS, 50 µl each well) and stored overnight at 4 °C.
Plates were washed three times with 100 µl of washing buffer (PBS-Tween 0,05%) and then blocked with 100 µl of PBS-BSA 3% for 1 hour. Sera dilutions were dispensed on the well for a 1-hour incubation step. Following washing, a phosphatase-coupled goat anti-human IgG (Jackson Immuno #109 056 098) diluted at 1/5000 was added and incubated for 1 hour. Plates were then washed and 50 µl of para-nitrophenylphosphate (Interchim #UP 664791) were added. The reaction was measured at 405 nm using a TECAN Spark 10M plate reader. Wells were considered positive for IgG detection if OD sample > average (OD background) + (3 x SD (OD background)).

Pfs48/45 6C and Pf 230 D1 ELISA were performed similarly, coating the plate with 0.5 µg/ml of the proteins.

1.1.2 Donor used in the agnostic MBC sorting

PBMCs sampling:

Donor A PBMCs samples were provided by our collaborators from Radboud. Sampling was made under ethics statements as described in PMID: 29422648 (54).

SMFA and gamete SIFA experiments:

These experiments were performed by Stone and al and are described in a previous article (54). Total purified IgGs and serum fractions depleted in anti-Pfs230 and/or anti-Pfs48/45 antibodies were tested for TRA in SMFA, and for Wild-type and KO gametes recognition in SIFA.
Of note, similar SIFA and SMFA protocols were used in our study for mAbs characterisation and are detailed in Material and Methods, part 1.5.2 and 1.6 respectively.

Donor A and the characteristic of his serum are described in detail below in Results, chapter 1.2.2 and in supplementary data 1 and 2.

1.2 Memory B cell sorting and lysis

1.2.1 Plate preparation for sorting

Plates were prepared one day ahead of sorting: either as direct cell lysis plates, that are then stored at 80°C or cell culture plates that are then incubated at 37° C.

1.2.1.1 Sorting of gamete-specific MBCs

For direct cell lysis, 96-well PCR plates (Biorad # HSP9641) were prepared at 4 °C using the following mix: 0.5 µl of RNASE out (TF#10154652), 5 µl of buffer (TF#18090050), 1.25 µl of dithiothreitol (TF#707265ML), 0.05 µl of NP40 (Sigma-Aldrich #18890) and 13.2 µl of H_20 (quantities for one well).

1.2.1.2 Agnostic sorting of MBCs

Prior to agnostic MBCs sort using precious samples, the most appropriate cell culture conditions for maximal MBC activation and IgG secretion were previously determined using non-precious samples. To this aim, a sandwich ELISA for determination of IgG levels in cell culture supernatant was designed.

The ELISA protocol is similar to the one described in 1.1.1. A goat anti-human IgG Fc (TF#31125) was coated overnight at 4 °C, at 2µg/ml on 384-well ELISA plates (TF #10192781). Washing steps, plates blocking, secondary Ab, PNPP adding and plates reading were performed as described in part 1.1.1

For B cell culture, 384-well cell culture plates (Corning #CLS3570-50EA) were prepared with the appropriate MBC stimulation media one day before cell sorting experiments, to allow the feeder cells sedimentation at the bottom of the wells. Iscove's Modified Dulbecco's Medium (IMDM) (Gibco #12440061) was complemented with 1% penicillin-streptomycin (TF #10378016) and supplemented with 20% FBS (Gibco #16170-078). A cytokine cocktail was added to stimulate MBCs activation, with IL21 (Preprotech #200-21) at 100 ng/ml and IL2 (Preprotech#200-02) at 51 ng/ml. Fibroblasts expressing CD40L ("L cells", generated by the laboratory of J Banchereau (182) and kindly provided by L Chaperot, EFS Grenoble) and 5000

were added in each well as feeder cells. Fibroblast were previously irradiated at 50 Gy to avoid their proliferation.

1.2.2 Thawing protocol for PBMCs

Cryopreserved PBMCs were thawed by short incubation in a 37 °C warm bath. Once the ice pellet was almost totally unfrozen, PBMCs were gently transferred in a 50 ml tube containing 7.5 ml of warm IMDM medium (complemented with 20% FBS, 1% Penicillin-Streptomycin) and 15 µl of benzonase (Merck #70664). PBMCs were centrifuged at 335 g for 10 minutes, the supernatant was discarded, and the cells resuspended in 5 ml of IMDM for cell counting.

1.2.3 Flow cytometry:

More information about the fluorochromes used can be found in annex 1.

1.2.3.1 Sorting of MBC-gamete complexes

When PBMCs were to be sorted using gametes, B cells were purified using the Miltenyi Pan B cell isolation kit (Miltenyi #130-101-638). Then, cells and gametes were stained separately during a 1 hour incubation step, protected from light, at 4 °C. Cells were stained with anti-CD19 and anti-CD20 for B lymphocyte selection and with anti-IgA, anti-IgD and anti-IgM for negative selection of IgG+ cells according to working concentrations specified in supplementary data .... An Aqua live/dead stain (TF #L34957) was used for selection of the live lymphocytes. Depending on the experiment, gametes were stained with either SYTO 61 (TF #S11343), a nucleic stain, or an anti-Pfs47-Dylight 650 coupled Ab produced by our Radboud collaborators. Both cells and gametes were separately washed with “Miltenyi buffer” (pH 7.2, 2 mM EDTA and 0.5% BSA). When using SYTO61, a minimum of 6 washes was necessary to get rid of the stain, that otherwise do not specifically mark primary cells during joint incubation. Gametes and B cells were then incubated together at a 1:6 ratio. Incubation was performed at 4°C under intermittent agitation for 1 hour. Complexes of MBCs and gametes were sorted into the prepared 96-well plates (either Biorad #HSP9641 for direct cell lysis or Greiner #655180 for short-term cell culture), using a FACSAria III (BD Biosciences) with the Diva software (9.0 version). Gating strategy is detailed in Results 1.1.2. Experimental results were analysed using the Flowjo software (10.6.1 version).

1.2.3.2 Agnostic sorting of MBCs

The following Miltenyi REA Abs were used to stain PBMCs before sorting by flow cytometry, following working concentration specified in annex 1: anti-CD3 (#130-114-519), anti-CD19 (#130-113-649), anti-CD20 (#130-113-649), anti-IgM (#130-113-476), anti-IgD (#130-110-643) and anti-IgA (#130-113-476). A Thermofisher live/dead stain was also used (#L34957). Cells were incubated with labelled Abs for 30 min, at 4°C, protected from light, before a washing step. Cells were then passed through a single-cell staining cap into a polystyrene tube (Corning #352235) to avoid clump formation during sorting. Cells were sorted using a FACS Aria III into the prepared 384-well cell culture plates, each well containing 50 µl of the activation media. Gating strategy is detailed in Results 1.2.2.

After 11 days of culture, 35 µl of supernatant was harvested using a pipetting robot (Eppendorf #5073) for transfer to 384-well storage plates and shipment to Radboud University. The slow robotic aspiration allowed MBCs to remain at the bottom of the well for downstream molecular biology experiments. Using the mRNA TurboCapture kit for 384 wells (Qiagen #72271) and according to manufacturer specifications, MBCs were lysed and their mRNA purified. Lysates were stored at -80 °C, waiting for gametocyte extract (GE) ELISA results.
Lysates from wells of interest according to GE ELISA results were transferred in 96-well RT-PCR plates (Biorad #HSP9641) to perform RT-PCR with the purified mRNA. The mix used for each well is as described in 1.3.1.

1.3 Amplification of IgG variable domain genes: multiplex nested RT-PCR

Of note, IgG supernatant screening following agnostic sort was performed using gametocyte or gamete extract ELISA and SIFA experiments by TropIQ. Gamet(ocyt)es ELISA protocol has been described in part 1 and SIFA experiments are described in part 4 of Material and Methods.

1.3.1 RT-PCR

The RT-PCR was performed using for each well: 0.5 µl of Superscriptase IV (TF #18090050), 1 µl of desoxyribonucleotide triphosphate (dNTP) (TF #11853933), 0.8µl of buffer (TF #18090050), 3.75 µl of random hexamer (#10580091) and 1.45 µl of H20. The total 7.5 µl was

then added to the cell lysis plate. The following thermocycler PCR program was then used: 10 min at 42 °C, 10 min at 25 °C, 60 min at 50 °C, 5 min at 94 °C.

1.3.2 Multiplex nested PCR

In case of need, the reader may refer to annex 2 and 3, which provide information about the structure of an Immunoglobulin and the V,D,J recombination mechanism.

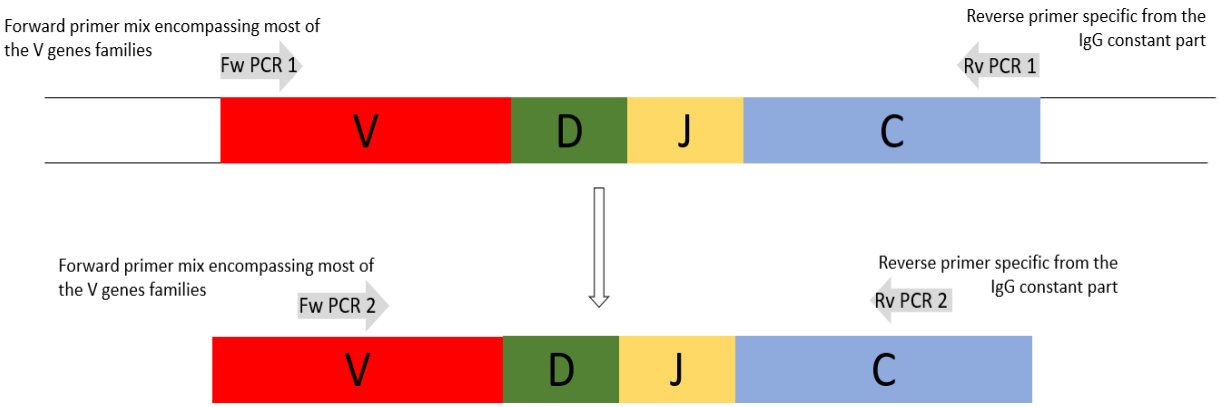

Figure 15: Scheme of the nested PCR used to amplify HC genes from IgG.

To amplify the variable part of IgG genes from the obtained cDNA, nested multiplexed PCRs derived from Tiller et al (183) (see figure 15) were separately performed for amplification of heavy, lamda or kappa genes. Each forward primer set corresponds to a mix of primer that encompasses most of the Variable gene families. Reverse primers are specific from the IgG constant part. Information about the primers used can be found in annex 4 and 5. The following reagents were added in each well: 12.5 µl of Master Mix (Qiagen #203445), 0.5 µl of primers forward master Mix, 0.5 µl of reverse primer (using the primer set corresponding to either PCR1 or PCR2 reaction) and 9 µl of H20. Thus, from one RT-PCR plate, three PCR 1 plates (for heavy, kappa and lambda amplification) and three PCR-2 plates are obtained.

The following Thermocycler PCR program was then used:

- 5 min at 94 °C
- 30 sec at 94 °C
- 30 sec at 58 °C
- 1min at 72 °C

} x 50 cycles

- 1 min at 72 °C

PCR products were run on a 94-well 2% agarose gel (Invitrogen #10063143). Well contents with successful gene amplification were sent to sequencing using Genewiz® Sanger sequencing services. The obtained sequences were analysed using the IMGT (ImMunoGeneTics) database (184), to retrieve the heavy and light genes families used by the MBC to produce its corresponding Ig.

1.3.3 IgG variable domain gene cloning

Once the gene family is known, family-specific primers were used for cloning (see annex 6). The sequences of those primers overlapped with the chain expression vector of one extremity and with the family gene-specific constant part of the other.
The cloning PCR was performed using the following mix:

PCR 1 product	2 µl	
Forward primer	2.5 µl at 10 µM	
Reverse primer	2.5 µl at 10 µM	
Master Mix	25 µl	Fisher scientific # F532S
H_20	18 µl	
Total reaction volume	50 µl	

The following PCR program was then applied:

- 1min at 98 °C
- 30 sec at 98 °C
- 30 sec at lower primer Tm
- 40 sec at 72 °C

x 40 cycles

- 5 min at 72 °C

PCR products were run on a homemade 1.5% agarose gel and purified with the Qiaquick gel extraction kit (Qiagen #28706). Using the mix described below, the obtained PCR products were inserted either inside a previously linearised (using XhoI and NheI) HC dephosphorylated vector, kC (BsiWI and AgeI) vector, or lC (XhoI and AgeI) vector, coding for respectively IgG1 heavy, kappa or lambda chain constant part.

lC, kC or HC open vector	50 ng	
PCR product (insert)	15 ng	
Master Mix	2.5 µl	NEB #M5510AA
Total reaction volume	10 µl	

Ligation was performed at 50 °C during 30 min. Competent bacteria (DH5α) were transformed with 2.5 µl of the ligation product, plated on Luria-Bertani (LB) agar + ampicilin plates and grown at 37 °C overnight. Colonies were picked up for an overnight culture in 5 ml LB broth. Cultures were centrifugated at 6000 g for 15 min, then plasmidic DNA was extracted from bacteria with the Miniprep Qiagen kit (#27106). Plasmidic DNA was then sent for sequencing (Genewiz®) to verify matching with the PCR2 sequencing results.
To obtain suitable DNA amount for HEK 293 F cells transfection, another round of DNA amplification was performed and the DNA extraction was performed using the Midiprep Qiagen kit (#12643).

1.4 Monoclonal antibody production

For transient mAb expression, Human Embryonic Kidney (HEK) 293F cells were transfected with both plasmids (coding for heavy and light chains). Typically, 25 µg of both plasmids were transfected using 4 ml of OptiMEM (TF #11058021) and 100 µl of 293 Fectin (TF#12347500) to 100 ml Freestyle culture medium (Gibco #12338018) of HEK293 cells at 1,2x106 cells/ml. After 3 days of culture, HEK293 F cells were centrifugated at 800 g for 15 min to harvest cell culture supernatant containing the produced monoclonal antibody. Protein A – Sepharose column (Sigma #ge17-1279-03) was used for mAb purification. Once the supernatant was deposited on the column, it was rinsed with 10 ml of PBS-NaCl 0.5M, then mAbs were eluted using 9 ml of glycine 0.1M pH2.5 followed by a neutralisation step with 1 ml Tris pH 9.0. This step was repeated with 4.5 ml of glycine 0.1M pH2.5 and 0.5 ml Tris pH 9.0 to get maximum elution yield. Amicon ULTRA concentrators (Merck #UFC803096) were used for downstream mAb concentration.

1.5 Study of mAb binding properties

Gametocyte extract and recombinant Pfs48/45 and Pfs230 ELISA were also performed to determine the mAbs reactivity to sexual stage parasites and main antigenic targets. Protocols used were the same as described in part 1.1 for serum testing.

1.5.1 Gametocyte extract Western-Blot

Gametocyte extract Western blot were performed by our collaborators from Radboud University.

P. falciparum NF54 gametocyte extract was prepared as described above. The extract was mixed with NuPAGE™ LDS sample buffer (TF # NP0008) and heated for 15 minutes at 56 °C. A 25mM dithiothreitol solution was added for the sample's reduction. The equivalent of 0.5 million lysed gametocytes were deposited per lane. A NuPAGE™ 4-12% Bis-Tris 2D-well gel (TF#NP0326BOX) was used for proteins migration and separation. Using the Trans-Blot Turbo system (Bio-Rad #1704150) samples were then transferred to a 0.22 µm nitrocellulose membrane (Bio-Rad #1620150). The blots were cut into strips, blocked with 5% skimmed milk in PBS and incubated with 5 µg/ml of the monoclonal antibody to be tested. Strips were incubated with the secondary anti-human IgG-HRP antibody (Pierce#31412), diluted 1/5000 in PBS-Tween 0.05%. Clarity Western ECL substrate (Bio-Rad #1705060) was used for chemiluminescence development and strips were imaged with the ImageQuant LAS4000 equipment (GE Healthcare).

1.5.2 Gamete SIFA

Gametes SIFA were performed by our collaborators from TropIQ.
To perform gametes SIFA, either WT or Pfs48/45 KO Pf strains can be used. Pfs48/45 KO also downregulates Pfs230 retention at the gametes surface. Wild-type or Pfs48/45 KO gametes were obtained following gametocytes activation in FBS for 1 h at room temperature. Cells that included gametes were washed with PBS and incubated with mAbs dilutions in SIFA buffers for 1 hour at 4 °C in sterile V bottom plates (VWR#736-0223). After incubation, wells were washed three times with SIFA buffer (0.5% FBS in PBS and 0.05% NaN3) and secondary antibody Alexa Fluor® 488 Goat Anti-Mouse IgG (H+L) (Invitrogen#A11001), diluted at 1/200, was added for a 1hour incubation step on ice. Following a washing step, gametes were resuspended in 4% PFA and transferred in 384-well clear bottom black plates. Four images per well were taken using the IX PICOD instrument (Molecular Devices).

1.5.3 MAb poly-reactivity testing in ELISA

The ELISA protocol was the similar as the one described in section 1.1.1. The coating antigens were diluted to 1 µg/ml. Antigens used were: ssDNA (Sigma #D8899-5MG), disialoganglioside GD1α (Sigma #G2392-1MG), lipopolysaccharide (Sigma #L2630-10MG), transferrin (Sigma #T3309-100MG), apotransferrin (Sigma #T1147-100MG), hemocyanin (Sigma #H7017-20MG), insulin (Sigma #I2643-25MG), cardiolipin (Sigma #C0563-10MG), albumin and histone (Sigma #H9250-100MG). The secondary Ab used was a phosphatase-coupled goat anti-human IgG (Jackson immuno #109 056 098). O.D were read at 405 nm, one hour after the addition of PNPP, and compared to the O.D obtained using 4E10, a polyreactive anti-HIV mAb (positive control).

1.5.4 Endotoxin detection

Endotoxin detection levels were performed using the Pierce Chromogenic Endotoxin Quant Kit (TF#A395525), following manufacturer's specifications.

1.6 SMFA

1.6.1 SMFA protocol at TropIQ

NF54-HT-GFP-Luc SMFAs were made by our collaborators at TropIQ.
SMFA experiments were performed using P. falciparum NF54-HT-GFP-Luc gametocytes with luminescence-based readout, following a protocol set-up by Vos et al (184), as described in the introduction. All the procedure was run at 37 °C. Briefly, 180 µl of RBCs were added to 300 µl of gametocyte culture, centrifugated for 20 sec at 10 000 g and the supernatant was discarded. Gametocyte pellets were resuspended in 200 µl of a mix containing 20% FBS and 80% human serum type A (not decomplemented). Three hundred µl of this mix were immediately injected into an individual membrane covered minifeeder, where 50 female A. stephensi mosquitoes were allowed to feed for 10 minutes.

1.6.2 SMFA protocol at Radboud

SMFAs with manual counting were made by our collaborators from Radboud University.
SMFA experiments were performed using *P. falciparum* NF54 wildtype gametocytes with oocyst count readout by our collaborators at Radboud University, following a protocol set-up by Ponnudurai et al (185) , also described in the introduction of this thesis. Briefly, blood meals containing cultured *P. falciparum* gametocytes were fed to *A. stephensi* mosquitoes (Nijmegen colony). Experiments were conducted with or without active complement. For each condition, 20 fully-fed mosquitoes were analysed. Reported Ab concentrations are concentrations in the total blood meal volume. Transmission reducing activity (TRA) was calculated as the reduction in oocysts compared to a negative control.

2. B1E11K EPITOPE CHARACTERISATION

As schematised below, the experimental workflow comprised three main steps.

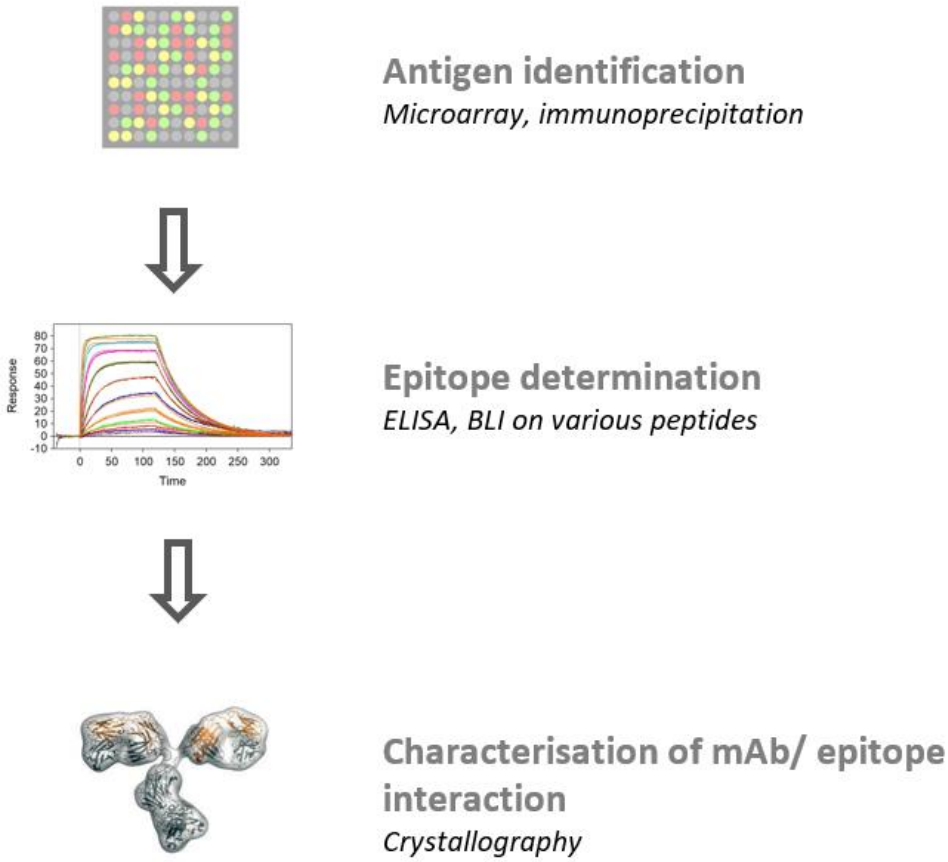

Figure 16: Experiment workflow, part II: Identification of poorly described or new antigens followed by fine characterisation of the targeted epitopes.

2.1 Identification of the antigen recognized by the B1E11K mAb

2.1.1 Protein microarray

The protein microarray has been designed and performed by Stone team.

Microarray design and protocol has been extensively detailed in Stone et al (54). Briefly, selection of the proteins to be printed on the array was mainly made according to proteomic analyses made by Lasonder et al (186) and Silvestrini et al (187). Microarray chips were rehydrated in blocking buffer while B1E11K was diluted in a 3 mg/ml E.Coli lysate solution in protein arraying buffer and incubated for 30 min. Blocking buffer was discarded before B1E11k overnight incubation at 4° C. Following five washes with TBS-Tween 0.05%, biotin-conjugated goat anti-human IgG (Jackson ImmunoResearch #109-065-098) diluted 1/200 in blocking buffer was added for incubation. After three washes, streptavidin-conjugated SureLight P-3 (ColumbiaBiosciences #D7-2212) was added. Chips were finally washed three times and air dried and scanned on a GenePix 4300A High-resolution Microarray Scanner (Molecular Devices). R and STATA 12 softwares were used for data treatment and analysis.

2.1.2 Immunoprecipitation

Mass Spectrometry analysis following immunoprecipitation was performed by Y.Couté.

To perform immuno-precipitation experiments, the mAb of interest (B1E11K) was coupled to tosyl-activated beads (Invitrogen #14203) following manufacturer specifications. The gametocyte extract was pre-cleared against non-decorated beads to get rid of aspecific binding of gametocyte proteins to beads. Hundred micrograms of Ab (at 666 µg/ml) were coupled to 5 mg of Dynabeads during a 18-hour incubation at 4 °C. Once decorated with mAb, beads were washed. The gametocyte extract was pre-cleared against non-decorated beads to get rid of potential aspecific binding of gametocyte proteins to beads. To initiate antigen-antibody interaction, 500 µg of whole proteins from gametocyte lysate were incubated with 50 µl of the decorated beads for 4 hours at 4 °C. Following several washes in PBS, the antigen was eluted using a 0.1 M glycine pH 2.5 solution, then neutralized with a 1 M Tris pH 9 solution.

This experiment was repeated with an Ab directed against HIV gp120 protein, in order to have a negative control.

Both elution fractions were then analysed using the Native PAGE 3-12% Bis-Tris Gel system (Invitrogen #BN1001BOX, molecular weight marker: page ruler plus, TF #26619). Samples

were prepared with a non-reducing Laemmli buffer (Invitrogen #B002) and run on the gel for 10 min at 100 V, then 4 h at 150 V. Silver staining was then applied to the gel according manufacturer's specifications (Invitrogen #LC06070). Positive bands compared to negative control were cut and sent for MS experiments.
The proteins sequences retrieved were then submitted for comparison to the Plasmodium falciparum (isolate NF54) taxonomy in the Uniprot database.

2.2 B1E11K epitope determination

2.2.1 Peptide synthesis:

Peptides were produced by the team of P Verdié, IBMM - SynBio3, Montpellier, France. Peptides were produced as powders to resolubilize in a phosphate-rich buffer (we chose PBS at pH 7.4).

2.2.2 ELISA with biotinylated peptides:

ELISA protocol was similar to the protocol already described in part 1.
Briefly, 96-well ELISA plates were coated overnight at 4° C with 0.5 µg/ml of streptavidin (TF # 434301). Plates were washed and then blocked for 1 hour. Following the wash, peptides diluted at 0.5 µg/ml were added to the plates for a 1 hour incubation, then washed again. Serially diluted mAbs were added to the plates. MAbs fixation was detected using phosphatase-coupled goat anti-human IgG (Jackson Immuno #109 056 098) and para-nitrophenylphosphate (Interchim #UP 664791). The enzymatic reaction was measured at 405 nm using a TECAN Spark 10M plate reader.
Half maximal effective concentration (EC50) was calculated from crude data (O.D) after normalisation using GraphPad Prism (version 9) "log agonist versus normalised response" function.

2.2.3 BioLayer Interferometry assay

BLI experiments were performed and analysed with the help of J-B Reiser.

All BLI experiments were done using an Octet Red96e Instrument (Satorius/FortéBio fromer Pall/FrotéBio) at 25°C and were recorded with the manufacturer software (Data Acquisition v11.1). Streptavidin biosensors (SA, Sartorius # 18-5019) were pre-wetted in 200 µl PBS pH 7.4 for 10 min, followed by equilibration in the analysis buffer (PBS-Tween 0.05% pH 7.4) for 120 s. Biotinylated peptides were diluted at 0.12 µg/ml in PBS pH 7.4 in Nunc F96 microwell plates (TF#237105) and immobilised on surfaces by dipping the biosensors for 15 sec, followed by an additional 120 sec equilibration step in analysis buffer. For kinetics analyses, Ab samples were serially diluted in analysis buffer at a concentration between 0.547 nM and 0.017 nM. Association phases were monitored in real time by dipping the functionalized biosensors in analyte solutions for 600 sec, and dissociation step monitored in analysis buffer for 1200 sec. To assess and monitor nonspecific binding of analytes, measurements were performed with biosensors treated in the same conditions but replacing the ligand solutions with analysis buffer. Kinetic data were processed using the manufacturer's software (Data analysis HT v11.1). Signals from zero-concentration samples were subtracted from the signals obtained for each functionalized biosensor and each analyte concentration. Resulting specific kinetics signals were then fitted using a global fit method and 1:1 Langmuir model and mass transport model for mAb and 1:1 Langmuir model for Fab.

2.2.4 Fab production (as performed by our team)

The plasmid used for Fab production was generated by mutagenesis to insert a stop codon inside the Ab heavy chain constant part, following the specifications of the Quickchange kit (Agilent #200523). The following primers were used, the stop codon being highlighted in bold:

Forward primer	CCAAATCTTGTGAC**TAA**ACTCACACATGCCCACC
Reverse primer	GGTGGGCATGTGTGAGT**TTA**GTCACAAGATTTGG

Briefly, following the PCR step, samples were treated twice with DpnI enzyme at 37 °C during 1 h. Ultracompetent XL-10 Gold bacteria were then transformed with the digested plasmid. Amplified DNA was purified using Miniprep and Midiprep kits (Qiagen #27106 and #12143), and sent for sequencing to verify stop codon insertion. HEK 293F cells were transfected with a kappa/heavy chain plasmid ratio of 1/4. Following three days of culture, the supernatant was

harvested and applied to a Kappaselect resin (Cytiva #17545812) for purification. Fab elution was performed twice with 5 ml of glycine 0.1 M (pH 2.5) and 500 µl of Tris 1 M (pH 9), followed by buffer exchange and concentration steps using AmiconUltra (Merck #36100101).

2.3 Fine characterisation of the B1E11K Fab and epitope interaction

The experiments presented in this section were performed by JP Julien's team. In their case, they synthesized the gene coding for B1E11K Fab de novo after codon optimisation.

2.3.1 B1E11K Fab expression and purification (as performed by J-P Julien's team)

The DNA sequences of V_K and V_H of the B1E11K Fab domain were cloned upstream of human Igκ and Igγ1-C_H1 domains respectively and inserted into a custom pcDNA3.4 expression vector. The plasmids were co-transfected into FreeStyle 293 F cells that were cultured in FreeStyle 293 Expression Media (Gibco #12338018). The recombinant Fab was purified *via* KappaSelect affinity chromatography (Cytiva #17545812) and cation exchange chromatography (MonoS, Cytiva).

2.3.2 Isothermal Titration Calorimetry

An Auto-ITC_{200} (Malvern) was used to conduct calorimetric experiments. The RESA *(P2)* peptide, RESA 10AA peptide, and recombinant B1E11K Fab were buffer-exchanged into Tris-buffered saline (20 mM Tris pH 7.0, and 150 mM NaCl). The B1E11K Fab was concentrated at 90 - 100 µM for experiments utilising the RESA P2 peptide and 60 µM for those utilising the RESA 10AA peptide. The RESA P2 peptide and RESA 10AA peptide were concentrated at 5 µM and 10 µM respectively. Peptide (syringe) was titrated into the cell (B1E11K Fab) at 25 °C using a protocol involving 20 injections each at a volume of 2.0 µL. The curves were fitted to a 2:1 or 1:1 binding model using the MIcroCal ITC Origin 7.0 Analysis Software.

2.3.3 Size-Exclusion Chromatography-Multi-Angle Light Scattering (SEC-MALS)

SEC-MALS experiments were performed at 4 °C using Superdex 200 Increase 10/300 GL (Cytiva #GE17-5175-01). RESA P2 peptide was incubated with B1E11K Fab at a 1:6 to 1:10 molar ratio for 30 minutes prior to loading onto the Superdex 200 column. The column was set up onto an Agilent Technologies 1260 Infinity II HPLC coupled with a MiniDawn Treos MALS detector (Wyatt), Quasielastic light scattering (QELS) detector (Wyatt), and Optilab T-reX refractive index (RI) detector (Wyatt). Data processing was performed using the ASTRA software (Wyatt).

2.3.4 Negative Stain Electron Microscopy (nsEM) and image processing

Fractions of the first peak of the SEC-MALS experiments containing the 2:1 B1E11K:RESA P2 complex were used to make nsEM grids. 50 µg/mL of the complex was deposited onto homemade carbon grids stained with 2% uranyl formate. Data was collected onto a Hitachi HT7800 microscope paired with an EMSIS Xarosa 20 Megapixel CMOS camera. Images were taken with the microscope operating at 120 kV at a magnification of 80000 X and pixel size of 1.83 Å. Particle picking, extractions, 2D classifications, and 3D reconstructions were done in cryoSPARC v2 (188).

2.3.5 X-Ray crystallography and structural determination

The RESA P2 peptide was incubated with B1E11K Fab at a 1:5 molar ratio for 30 minutes prior to loading onto the Superdex 200 column Increase 10/300 GL. Fractions containing the complex were pooled and concentrated at 8.6 mg/mL. A seed stock prepared from a previous crystallisation trial was used for seeding. The stock was derived from condition G9 of a JCSG Top96 screen (0.2M NH_4SO_4 25% [w/v] PEG4000, and 0.1M sodium acetate [pH 4.6]). The complex, reservoir solution, and seed stock were mixed at a 3:4:1 volumetric ratio using various reservoir conditions derived from the condition G9 of the JCSG Top96 screen. Crystals grew within 6 hours in a reservoir condition consisting of 0.1M NH_4SO_4 25% (w/v) PEG4000, and 0.1M sodium acetate (pH 5.2). Crystals were cryo-protected with 15% ethylene glycol (v/v) before being flash-frozen in liquid nitrogen.

Data collection was performed at the 23-ID-B beamline at the Argonne National Argonne National Laboratory Advanced Photon Source. Datasets were processed using DIALS 3.7 (189)Molecular replacement was performed using Phaser (190) followed by multiple rounds of refinement using phenix.refine (191)and coot (192) . Inter- and intra-molecular contacts were determined via Protein-Ligand Interaction Profiler (193) and manual inspection.

RESULTS

As explained before, the results presented in this PhD thesis were generated in a close collaboration with three other teams. TropIQ Health Sciences performed gamete SIFA using WT or Pfs48/45 K0 parasites and Standard Membrane Feeding Assays using the HT-GFP-Luc parasite strain. The team of Prof. Sauerwein from the Radboud University notably performed SMFA using WT strain and Western blot tests against gametocyte extract (GE). The team of J - P Julien, University of Toronto (Canada), performed biophysical and structural work on the B1E11K Fab.

1. ISOLATION OF TRANSMISSION BLOCKING HUMAN mABS TRHOUGH SPECIFIC MEMORY B CELL IDENTIFICATION

As explained above in Introduction, we designed 2 strategies to isolate mAbs able to reduce or block transmission of *Pf:* a first one based on direct sorting of gamete-specific MBCs and a second one based on the agnostic sorting of MBCs, followed by cell activation and high-throughput Ab screening. For the two strategies, samples originating from different individuals were used as detailed below.

1.1 Isolation of mAbs specific of gamete surface proteins via sorting of memory B cell-gamete complexes

Briefly, the isolation of B cell-gamete complexes via flow cytometry cell sorting required labelling of both MBCs and gametes using different fluorochromes, prior to a co-incubation and sorting. Indeed, following this approach, memory B cells specific of gamete surface antigens bind to live gametes to form complexes that get sorted as "single cells" in single wells thanks to a specific double fluorescence signal compared to unbound free MBCs. IgG variable domain genes are then amplified from the selected single B cells, cloned in expression vectors, and mAbs are produced. As explained below, mAbs isolated through this strategy were then tested to verify their reactivity against sexual stages antigens in ELISA and SIFA. The mAbs giving strong binding signals in these assays were further tested in SMFA.

1.1.1 Finding the proper conditions for gamete labelling

In order to use gametes as bait to isolate specific MBCs through cell sorting, we needed to find the right conditions for live gamete staining, prior to their incubation with B cells.

We first analysed gamete morphology and viability in flow-cytometry. As shown in figure 17, two gamete populations of different sizes can be distinguished. When stained with live/dead stain, one population appeared to contain mainly dead gametes (labelled gametes 1, containing 70.4% of dead cells) and the other mainly live gametes (gametes 2, containing 4.41%).

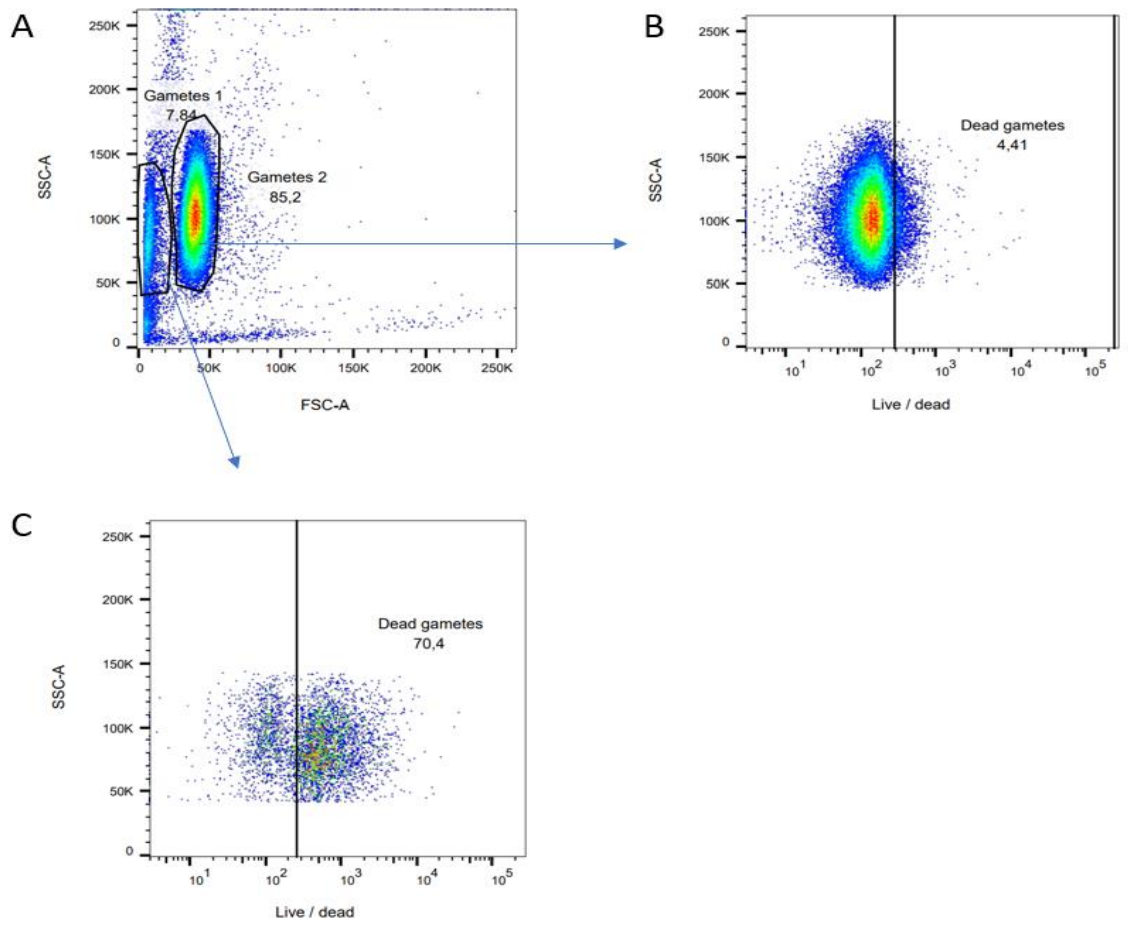

Figure 17: Gametes aspect in flow cytometry when stained with live/dead stain (Thermofisher #L34957).

Panel A shows gametes FSC-A and SSC-A characteristics. Panel B and C show live/ dead stain and SSC-A fluorescence intensity for gametes 2 or gametes 1 populations respectively.

For gamete labelling two alternatives were considered: either a nuclear marker (SYTO 61) or an anti-Pfs47 (a surface protein) coupled to the Dylight 650 fluorochrome. The use of a nucleic acid stain was theoretically preferred to avoid the risk of the anti-Pfs47 interfering through steric hindrance with access of MBCs' BCRs to some potentially close surface proteins. However, labelling with SYTO 61 gave different mean fluorescent intensities (MFI) depending on whether gametes were alive or not (figure 18 A), which was not useful for proper detection of gamete-MBC complexes. In contrast, the Dylight 650-conjugated anti-Pfs47 (figure 18 B) gave a consistent labelling of live and dead gametes.

Moreover, when testing the conditions for proper incubation of MBCs and gametes, it was found that enough SYTO 61, a nucleic acid stain, remained despite washes, and also stained MBCs. A solution was to perform at least six washes but this procedure was time-consuming and induced gametes loss at each centrifugation step.

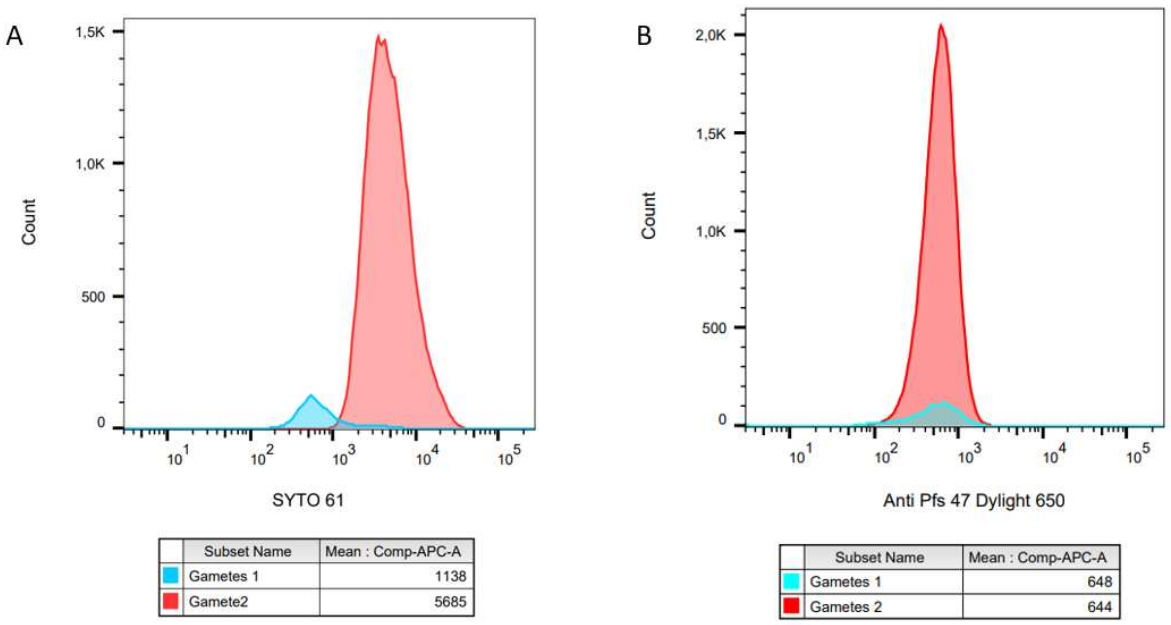

Figure 18: Flow cytometry analysis of gametes labelled with SYTO 61 (A) or anti-Pfs 47 Dylight 650 (B)

(In the tables are shown SYTO61 or anti-Pfs 47 Dylight 650 MFI for each population).

We therefore choose to label gametes with anti-Pfs47 Dylight for sorting of MBCs – gamete complexes.

1.1.2 Sorting of specific MBCs using a non-precious donor sample from CHUGA

As the number of samples from donors with TRAbs was very limited, we first decided to set up the protocol for MBC-gamete complex sorting using cells from a non-precious donor. Thus, we obtained PBMCs from an uncomplicated malaria case from the Grenoble hospital (CHUGA), using blood left over from diagnosis tests. Results presented below were obtained using cells from this non-precious donor.

Serum binding to sexual-stage parasites in ELISA:

We first verified that the selected CHUGA donor had mounted an Ab response to *Pf* sexual stage antigens upon infection. We performed an ELISA using gametocyte extract as well as recombinant Pfs48/45 and Pfs230 for coating. The results confirmed the presence of Abs

directed against the gametocyte extract and the recombinant proteins. The serum gave a signal at a 1/250 dilution equivalent as the one from a positive control serum from our collaborators:
- at a dilution of 1/800 for the gametocyte extract
- at a dilution of 1/400 for Pfs48/45
- at a dilution of 1/10000 for Pfs230.

The recognition of the gametocyte extract and surface proteins by the serum of the CHUGA donor, was thus weaker than the one of the positive control serums, which is considered as having particularly high titers. Nevertheless, the ELISA titers of the CHUGA donor were significant, validating the use of PBMCs from this donor in further experiments aiming at setting-up direct sorting with gametes. Of note, when this serum was further tested by our collaborators in SMFA, no TRA was detected, but this information was not available at the time.

Sorting of Memory B cells and gametes complexes:

Gametes and PBMCs were prepared following the procedure described in Material and Methods. Briefly, a vial containing 6.4 x 10^6 PBMCs was thawed, and mortality was determined manually under the microscope using a Malassez counting chamber. Only eight percent of the PBMCs were dead, demonstrating that the protocol used for sample preparation prior to liquid nitrogen preservation as well as the thawing step allowed for an optimal cell recovery.

Following thawing, PBMCs were incubated with a Miltenyi Pan B cell isolation kit Ab cocktail (Abs coupled to magnetic beads and directed against CD2, CD14, CD16, CD36, CD43 and CD235a) and passed through a magnetic column for non-B cell depletion, as indicated in Material and Methods. This step was performed to get rid of non-B cells to increase the probability of encounters between specific memory B cells and gametes. A total of 3.6 x 10^5 B cells were isolated for sorting, corresponding to 5.62% of total PBMCs, a percentage in agreement with physiological values (2.14 - 5.04% in adults (194)). Following purification, B cells were stained with a live/dead stain and fluorochrome-coupled Abs directed against CD19, CD20, IgM, IgD and IgA. To avoid potential steric hindrance issues during gametes and MBC's B cell receptor interactions, no anti-IgG was used. Gametes were separately stained with anti-Pfs47 Dylight 650. The detailed characteristics of the Abs and fluorochromes used can be found in the appendix of Material and Methods.

Following a washing step, cells and gametes were co-incubated during 75 min, at 4 °C under intermittent agitation. Gametes were incubated in excess compared to cells (6:1 ratio) to favour gamete-MBC encounter.

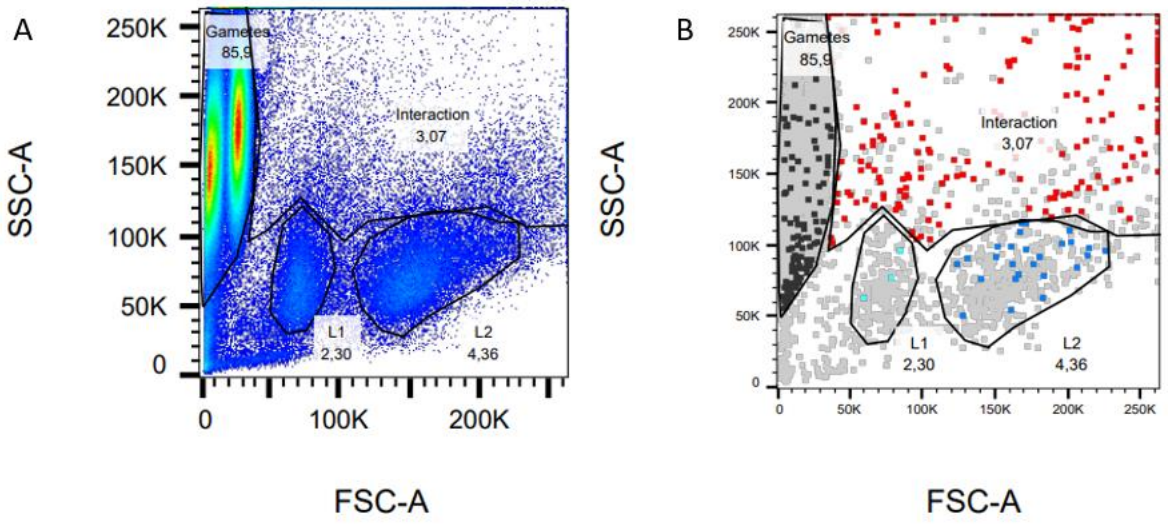

Figure 19: Memory B cell–gamete complexes localisation.

A: FSC-A/SSC-A cytogram. L1: dead lymphocytes. L2: live lymphocytes. B: coloured representation of double positive (DP) cells giving both MBC and gamete fluorescence signal in the interaction gate. Red: DP cells in the interaction area. Light and navy blue :DP cells in the lymphocyte gates. Black are DP cells in the gametes gate.

As shown in figure 19 A, three populations of different size were clearly visible in the FSC-A versus SSC-A plot corresponding to gametes, dead lymphocyte (L1) and live lymphocytes (L2). Two-parameter density plots in which each axis represents a particular marker were further used to identify cells of interest. Live IgG+ memory B cells were determined as CD19 and CD20 positive and IgD, IgM and IgA negative. MBC-gamete complexes were identified as cells giving fluorescence signals corresponding to both MBCs and gametes (double positive cells, DP) as shown as coloured spots in Figure 19 B. As no well-defined DP population was visible in the FSC-A versus SSC-A plot, we hypothesized that DP cells found inside the large so-called “interaction” area represented complexes, the FSC and SSC values corresponding to the size of one (or more) gametes bound to an MBC. These double positive cells in the “interaction” gate are highlighted in red in figure 19 B.

In total, 2882 MBCs were analysed, and among them, 402 (13.6%) gave a fluorescence signal for both MBCs and gametes located inside the “interaction” gate. This rather high percentage

could be due to non-specific binding of some MBCs to gametes. In addition, this patient was sampled during an acute malaria crisis, which may have boosted his immune system, increasing the number of gamete-specific B cells.

One hundred and eighty complexes giving a signal for both MBCs and gametes in the interaction window were subsequently sorted at one cell/well in three different plates (one plate containing a cell lysis buffer and two plates containing cell culture mediums, conditions tested are detailed in Chapter 1.1.3). Of note, more cells could have been sorted considering the number of double positive cells but the experiment was primarily designed for set-up purposes. The different steps and yields are summarized in figure 20.

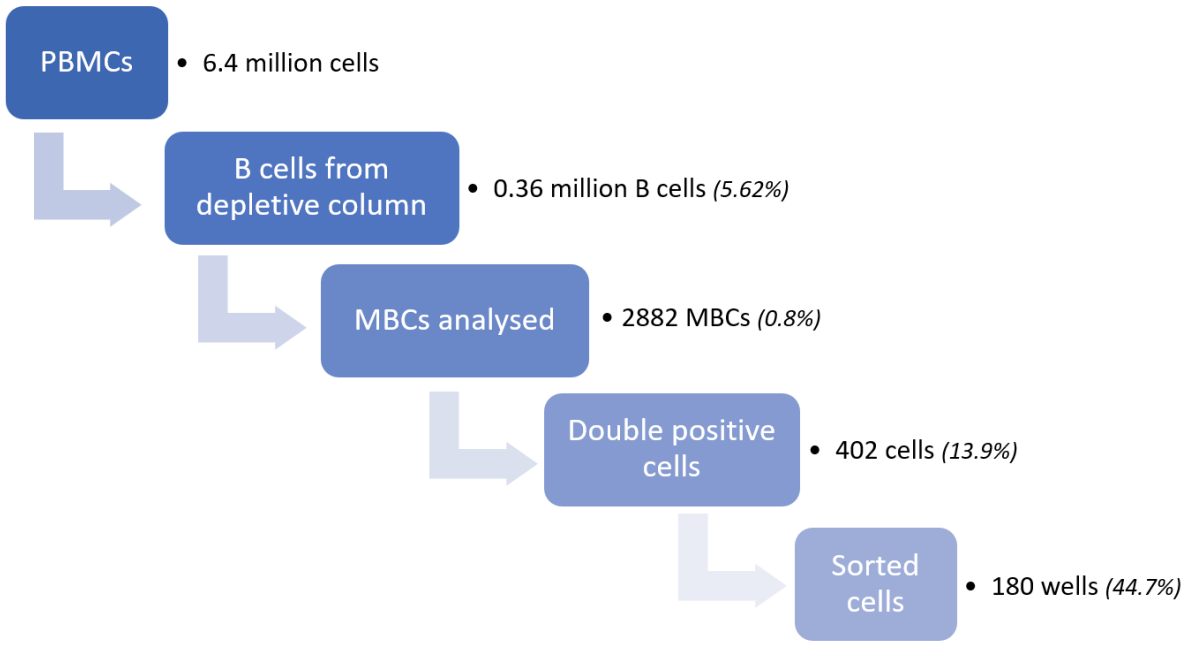

Figure 20: Yield of each sample preparation step, from the thawing of PBMCs to the sorting of putative specific MBCs.

Post-sort analysis of the fluorescence characteristics of B cell-gamete complexes:

Following sorting, to better characterise the memory B cell-gamete complexes identified, we further analysed their fluorescence patterns. When looking at the intensity of the anti-Pfs 47 staining, three populations were distinguishable, with putative complexes giving a low, intermediate or high anti-Pfs 47 Dylight intensity signal, suggesting that MBCs could have bound one, two or more gametes (figure 21A).

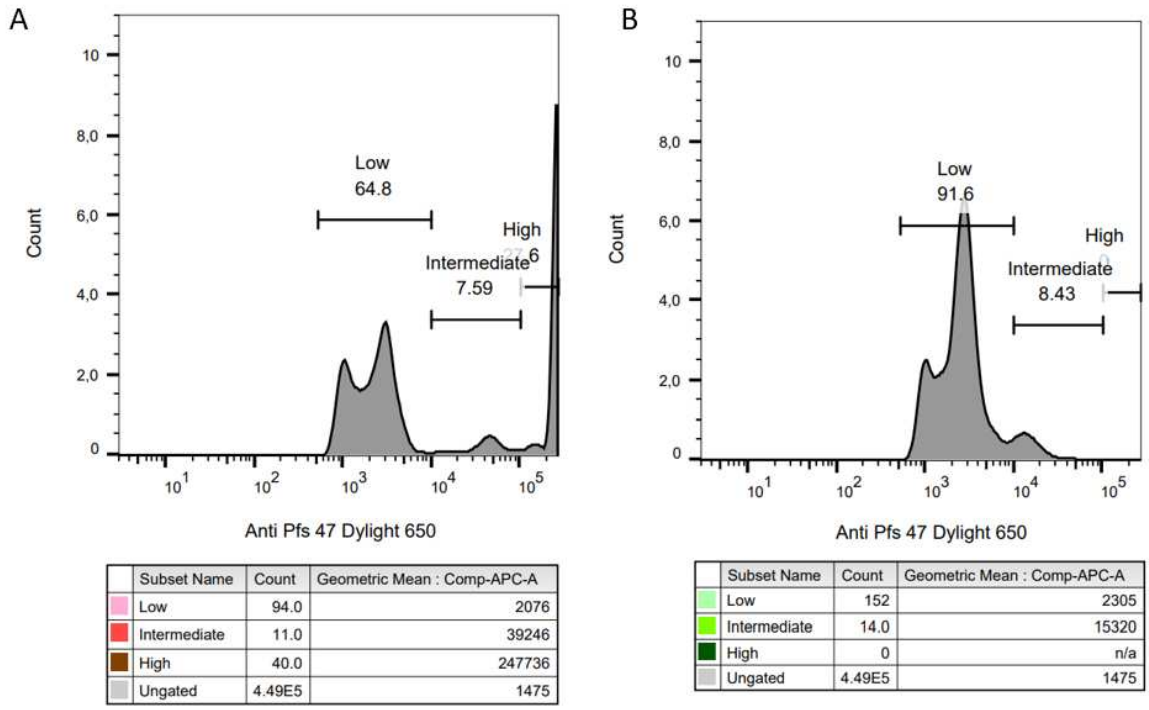

Subset Name	Count	Geometric Mean : Comp-APC-A
Low	94.0	2076
Intermediate	11.0	39246
High	40.0	247736
Ungated	4.49E5	1475

Subset Name	Count	Geometric Mean : Comp-APC-A
Low	152	2305
Intermediate	14.0	15320
High	0	n/a
Ungated	4.49E5	1475

Figure 21: Fluorescence intensity of anti-Pfs47 labelling on memory (panel A) or naïve (panel B) B cells-gametes complexes.

Fluorescence intensity was ranked as low, intermediate or high, for panel A or B respectively.

To better understand whether gamete binding was a phenomenon specific to memory B cells, the proportion and characteristics of naive B cells (NBCs) potentially bound to gametes in the "interaction" area was also studied. Live cells considered as naive B cells were those CD19 and CD20 positive and IgD, IgM and IgA positive. As shown in figure 21B some NBCs appeared to bind to gametes too but the anti-Pfs 47 signal intensity only varied from low to intermediate. This may suggest the absence of complexes between NBCs and multiple gametes, which could be due to a lack of specific binding. This hypothesis was supported by the calculation of the ratios of memory B cells and naïve ones found in the different lymphocyte populations and in the "interaction" gate. Whereas ratios of MBCs and NBCs were 0.24 and 0.39 in the L1 and L2 populations, respectively, the ratio was 2.07 in the interaction gate, suggesting an enrichment of MBCs in this area, which could be explained by a specific recognition of gametes by the latter.

Taken together, the results suggested that MBCs bound to gametes were potentially successfully sorted. In order to verify this hypothesis, amplification of IgG genes from the corresponding MBCs, production of the corresponding mAbs and testing for binding to sexual stage proteins in ELISA or SIFA had to be done.

1.1.3 Amplification of IgG variable domains genes following isolation of specific MBCs

Our usual protocol for Ig gene amplification following single B cell sorting, calls for the collection of sorted cells in a lysis buffer. Messenger RNAs from the lysed B cell were then retrotranscribed before PCR amplification of Ig genes. The yield of this latter PCR is somehow low, most likely due to the small quantity of mRNAs obtained from the lysis of single memory B cells. We thus hypothesized that a B cell activation step following sorting could increase Ig mRNAs quantities and in consequence improve PCR yield. Following sorting, we thus tested three different conditions, corresponding to three different collection plates. For the first one, cells were directly sorted in cell lysis buffer as usual. For the two others, cells were sorted in an MBC culture and activation medium (see Material and Methods 1.2.1.2) and kept in culture for 24h and 48h, respectively. Cell lysis, RT-PCR and PCR were then performed as detailed in Material and Methods. A multiplex nested PCR was further performed to amplify IgG genes variable regions corresponding to the kappa, lambda and heavy chains (figure 22). PCR products were run on a 2% agarose gel to visualize DNA amplification (figure 23).

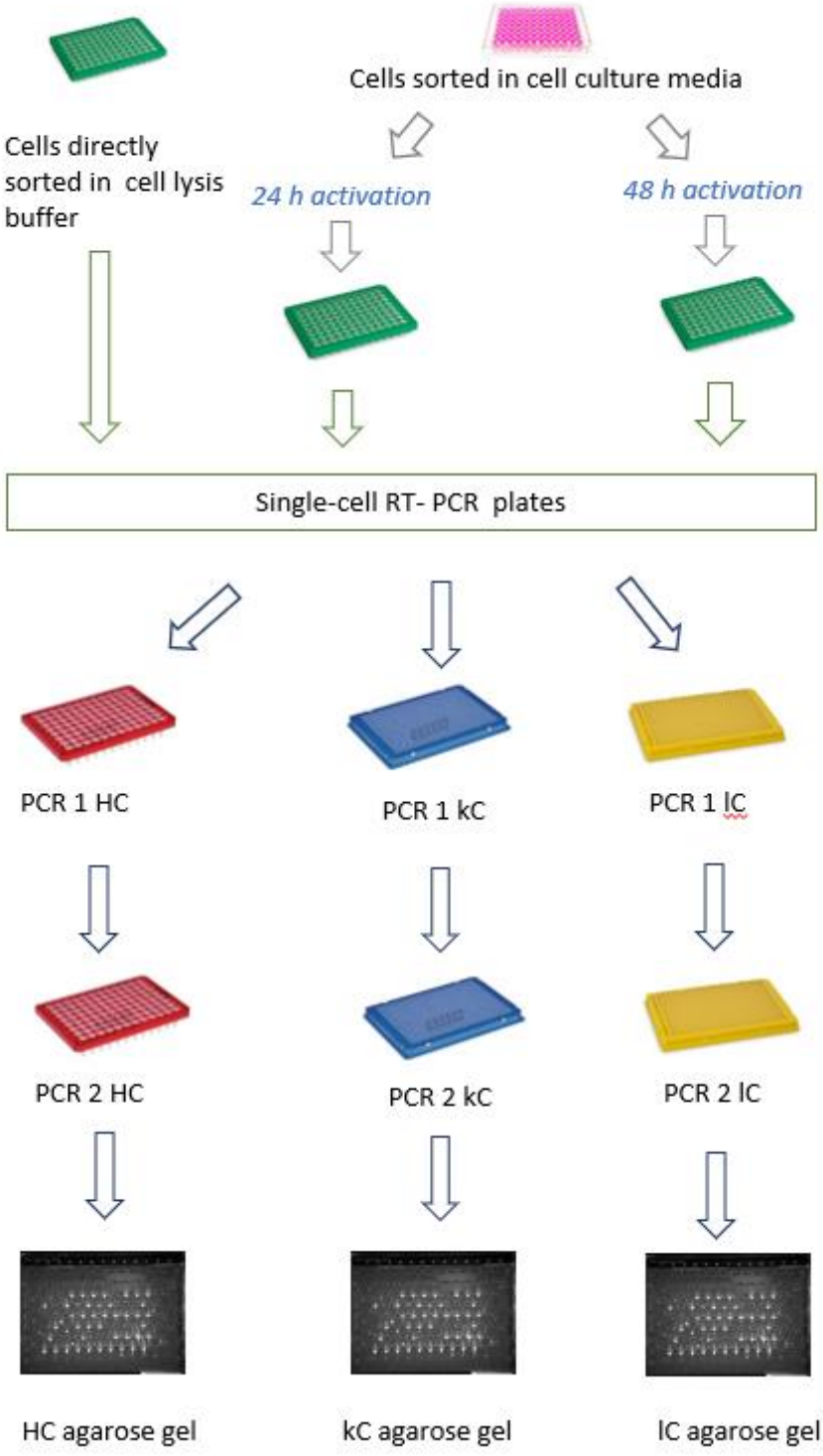

Figure 22: Differential plates processing after direct sorting: either immediate RT-PCR or RT-PCR performed after 24 h or 48 h, followed by heavy, lambda and kappa chain amplification using multiplex nested PCR.

Contents of wells showing a PCR amplification product potentially corresponding to an amplified Ig gene variable region were then sent to sequencing. The sequences obtained were analysed using the IMGT (International immunogenetics information system) database, in order

to verify whether the amplified sequence corresponded to an Ig gene, and to assign the corresponding gene families. Of note, the PCR products from the wells containing activated cells appeared different from the ones from the wells with cells that were lysed directly after sorting, the latter ones seemingly giving sharper bands.

		Plate type		
		Direct lysis	24 h activation	48 h activation
HC	Bands in agarose gel	25%	50%	78%
	↳ Wells matching an HC sequence	100%	0%	29.4%
kC	Bands in agarose gels	30%	11%	0%
	↳ Wells matching a kC sequence	72%	0%	0%
lC	Bands in agarose gels	23.3%	13.3%	8.3%
	↳ Wells matching a lC sequence	92.3%	0%	0%

Table 4: Percentages of well contents yielding bands in agarose gel following DNA amplification and percentages of these well contents matching an IgG sequence when analysed with IMGT.

Table 4 shows that for the plate where cells were directly collected in lysis buffer, an Ig sequence was indeed recovered from most wells considered from the gel as containing an amplified Ig variable region. Among those, 4 kC sequences and 10 lC sequences were found to be paired to a heavy chain, leading to 14 putative mAbs (23% of the total sorted wells). According to Tiller et al (183), typically paired HC and lC chain recovery rates vary between 30 to 60% and follow physiological light chain repartition, with roughly 40 % of Kappa chain and 60 % of Lambda chain. Compared to these reference percentages, our recovery rates were lower than expected.

On the base of this experiment, modifications were implemented for the composition of the cell lysis and RT mixes, the timing of the experiment and the storage conditions, leading to a significant increase in Ig gene amplification yields. HC recovery is now commonly above 50%, lC recovery above 30% and kC above 50%. *(Averages of recovery made on 480 wells for 2 different projects in the laboratory that have used the optimized protocol).*

In contrast to wells with cells lysed immediately after sorting, in wells corresponding to activated cells almost no PCR products corresponded to IgG sequences. The contamination likely came from the genomic DNA of the 5000 live irradiated feeder cells seeded at the bottom of each well.

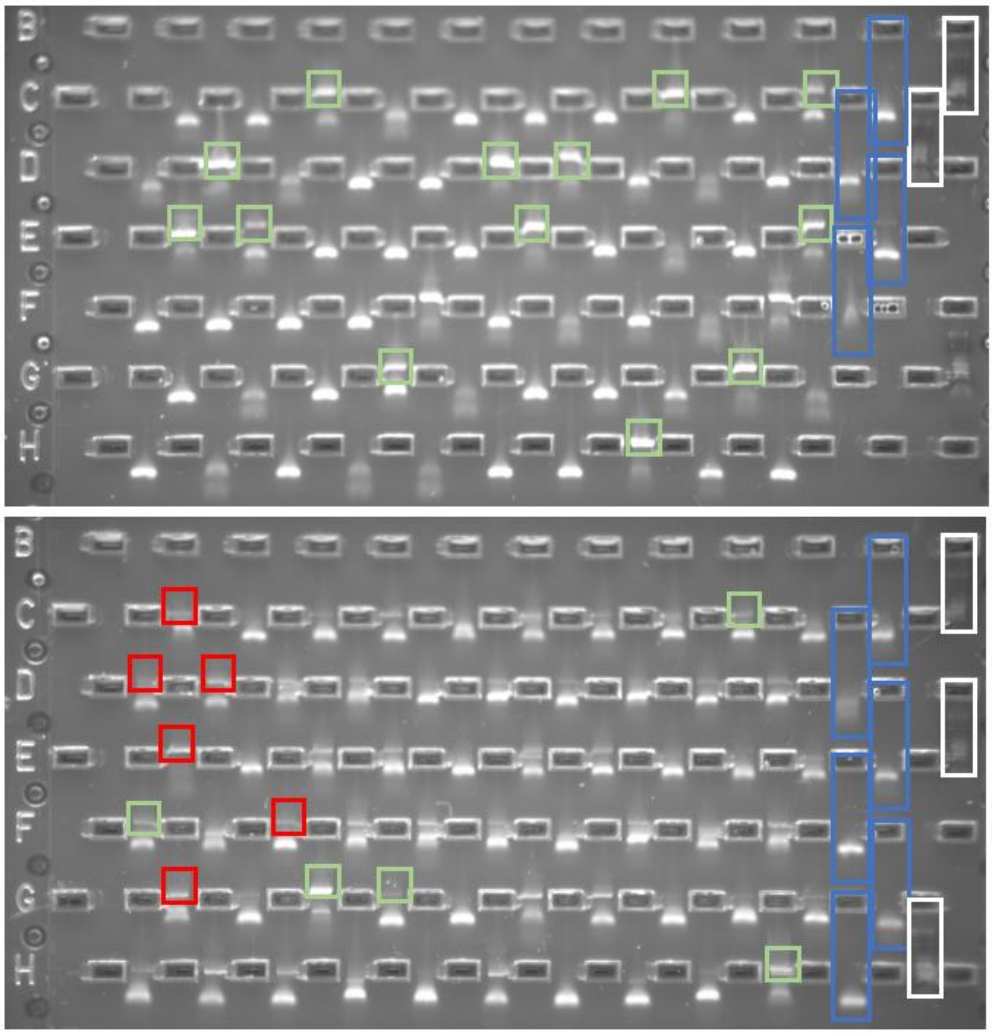

Figure 23: Example of HC PCR products migration on 2% agarose gels.

Upper gel corresponds to HC PCR products following direct lysis. Lower gel corresponds to HC PCR products following 48h activation. Well contents that gave IgG sequences are boxed in green and examples of smeary fibroblasts-contaminated wells (which do not correspond to an IgG sequence) in red. Control lanes (no PCR product) are boxed in blue and molecular weight (seqTF #SM133) lanes in white.

In conclusion, only the plate containing cells lysed immediately following sorting yielded Ig sequences and the short-term activation approach we attempted did not succeed in improving PCR yields.

Furthermore, wells for which sequences coding for both a heavy and a light chain were recovered were selected for production of mAbs. Briefly, amplified Ig variable region genes of heavy or light chains were cloned in corresponding expression vectors, which were further

cotransfected in HEK 293 F cells for mAb production. Following three days of culture, supernatants were harvested and mAbs were purified on protein A.
Out of the 14 putative mAbs, 9 were successfully produced. Among those, two shared the exact same sequence, and therefore only 8 different mAbs were finally recovered.

1.1.4 Reactivity of the mAbs isolated against *Plasmodium falciparum* sexual stage proteins

Once produced, the 8 mAbs were sent to our collaborators at TropIQ to test their ability to recognize sexual stage antigens in ELISA. Due to gamete unavailability at the time and technical constraints, ELISAs were not performed using gamete but rather gametocyte extract.

First, preliminary experiments were performed by TropIQ to compare the recognition of main *Pf* TRA antigens (Pfs48/45, Pfs230, Pfs25 and Pfs47) by mAbs in ELISA using gametocyte versus gamete extract (figure 24).

Comparison of main TRAbs targets detection in 384-well plates gamete versus gametocyte ELISA (set-up experiments) :

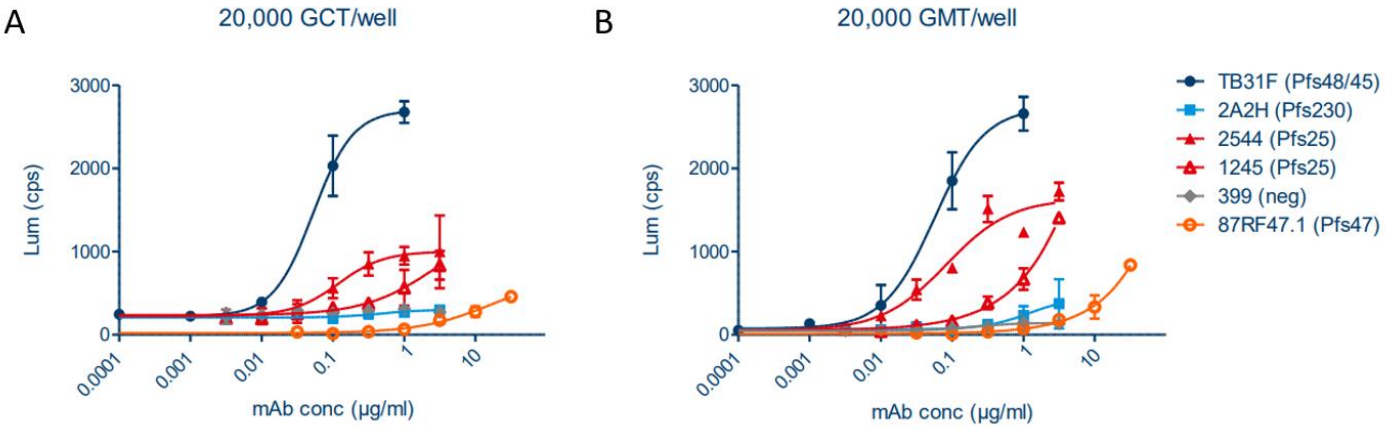

Figure 24: Detection of main Pf antigens by mAbs, in gametocyte extract ELISA (A) versus gamete extract ELISA (B).

TB31F is an anti-Pfs48/45 mAb, 2A2H is an anti-Pf230 mAb, 2544 and 1245 mAbs are anti-Pfs25 mAbs, 87RF47.1 is an anti-Pfs47 mAb, and 399 is an anti-CSP mAb (negative control).

Positive control mAbs were used to detect main TRAbs antigens. Of note, when performed by our collaborators from TropIQ, an alternative detection protocol as the one described in

Material and Method 1.1 was performed, and results were expressed in Luminescence units rather than O.D. Detection of Pfs48/45 and Pfs25 was high and similar in gametocyte and gamete ELISAs. Contrary to what could have been expected, Pfs230 detection was low, probably not due to a lack of expression, as Pfs230 is abundantly expressed at the surface of gametocyte and gametes, but to an experimental error with the Pfs230 mAb. Finally, Pfs47 being expressed at the surface of female gametes, the intensity of detection may be dependent of the quantity of female parasite in the experiment. Overall, main antigen detection between gametocyte and gamete experiments was fairly consistent.

Following these experiments, and considering that most of the antigens of interest appeared detectable between gametocyte and gamete extract, we assumed that mAbs produced from MBCs selected for their ability to bind gametes would also likely bound gametocyte extract.
The 8 mAbs panel was thus tested in gametocyte extract in ELISA and the E11 and F10 mAbs showed some level of reactivity, although the binding of E11 may likely not be specific as it was only detected at the highest concentration used (figure 25).

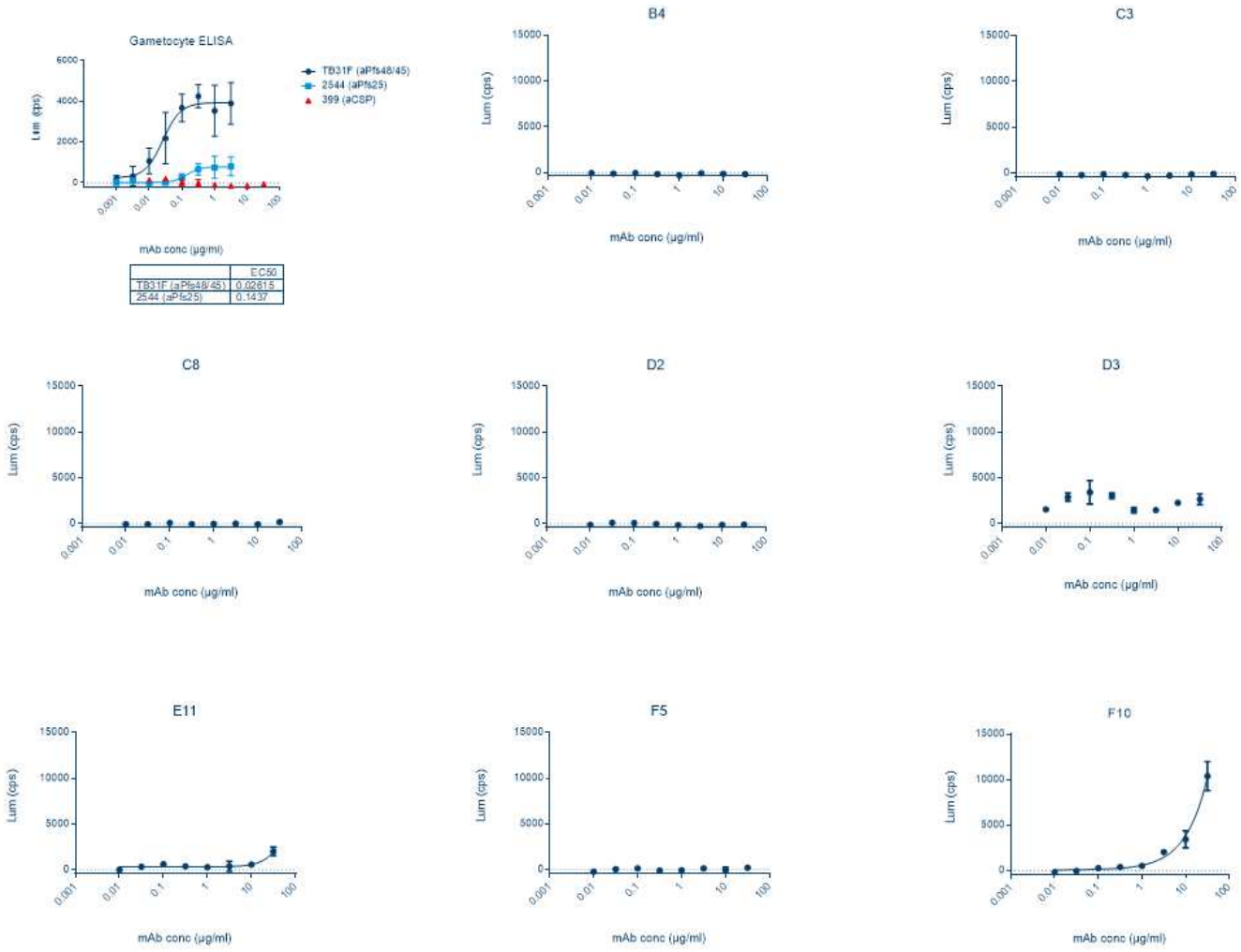

Figure 25: Monoclonal antibodies reactivity against gametocyte extract in ELISA.

TB31F is an anti-Pfs48/45 mAb, 2544 mAb is an anti-Pfs25 mAbs and 399 is an anti-CSP mAb (negative control). Name of each tested mAb is indicated at the top of the graph.

The mAbs were simultaneously tested in ELISA for their reactivity against Pfs48/45 and Pfs230. As full-length proteins were not available, recombinant protein fragments R06C and Pf230 C1 were used. As a reminder (see in introduction 5.2), R0C6 corresponds to a truncated Pfs48/45 (amino acid 159 to 428, domain II to III) fused to the N-terminal region of the glutamate rich protein GLURP. Pfs230 C1 corresponds to the amino acid sequence 443 to 715 of the Pfs230 protein. None of the mAbs showed significant reactivity against the recombinant Pfs48/45 or Pfs230 fragments. An absence of recognition in this assay can nevertheless not exclude binding to the native protein.

Because of its binding profile in GE ELISA, the F10 mAb was selected to undergo gamete SIFA.

When tested at 100 µg/ml, F10 mAb stained 11.7 % of the wild-type gametes and 19.6 % of the Pfs48/45 KO gametes. Of note, abrogating Pfs48/45 expression down-regulates Pfs230 expression. At a 5 µg/ml concentration, F10 mAb stained 10.7% of the wild-type gametes and 8.25% of KO gametes. Finally, at 1 µg/ml it stained 8.25% of WT gametes and 11.9 % of KO gametes. These numbers were close to background compared to those obtained for control Abs and we could not conclude that the F10 mAb could bind specifically to the surface of gametes.

1.1.5 Activity of the F10 mAb in SMFA

Although the SIFA did not confirm binding to the gametocyte surface, based on the GE ELISA results the F10 mAb was tested in SMFA. No transmission blocking activity was found, neither at 100 µg/ml nor at 500 µg/ml (data not shown).

1.1.6 Analysis of the sequences of the mAbs isolated following direct sorting

Analysis of the sequences of the 8 mAbs isolated (6 lambda and 2 kappa), did not reveal any particular trend. Only four different Heavy variable gene families (IGHV1, IGHV3, IGHV4 and IGHV5) were recovered, but the number of Abs was too low to conclude an enrichment. As already mentioned, two (B4 and C3) of the Abs were identical, suggesting either the isolation of two clonal MBCs or an intra-plate contamination. Interestingly, this mAb had a long CDR3s of 29 amino acids.

	Heavy Chain					Light Chain			
mAb	V gene	D gene	J gene	CDR3 length (AA)	V region identity %	V gene	J gene	CDR3 length (AA)	V region identity %
B4	IGHV3-7*01	IGHD2-21*02	IGHJ3*02	29	91.67	IGLV1-40*01	IGLJ2*01	12	94.79
B11	IGHV4-34*01	IGHD1-26*01	IGHJ4*02	10	85.26	IGKV4-1*01	IGKJ3*01	9	97.37
C3	IGHV3-7*01	IGHD2-21*02	IGHJ3*02	29	91.67	IGLV1-40*01	IGLJ2*01	12	95.14
D2	IGHV1-46*04	IGHD6-19*01	IGHJ4*03	19	69.79	IGLV1-47*01	IGLJ2*01	11	94.74
D3	IGHV1-3*01	IGHD3-10*01	IGHJ3*02	18	87.15	IGKV4-1*01	IGKJ4*01	9	92.04
E11	IGHV1-46*04	IGHD2-21*02	IGHJ1*01	16	88.46	IGLV4-69*01	IGLJ2*01	9	66.67
F5	IGHV3-49*04	IGHD3-10*01	IGHJ4*02	9	81.25	IGLV2-8*01	IGLJ2*01	9	94.79
F10	IGHV1-69*01	IGHD5-24*01	IGHJ4*02	14	89.58	IGLV3-21*03	IGLJ2*01	11	92.83
G9	IGHV5-51*01	IGHD3-16*01	IGHJ5*01	10	72.55	IGLV1-47*01	IGLJ1*01	11	70.18

Table 5: Sequence characteristics of the produced mAbs following direct sorting.

In the first column, mAbs are highlighted in yellow and blue for lambda or kappa Abs respectively. Gene usage, CDR3 length and V,D,J region identity are also indicated.

1.1.7 Summary of the isolation of mAbs via sorting of MBC-gametes complexes

In conclusion, the sorting of MBC-gamete complexes from the CHUGA donor resulted in the isolation of one mAb, F10, that appeared able to recognise proteins from a gametocyte extract in ELISA but bound only very weakly to the gamete surface in SIFA and did not display any TRA. The poor binding in SIFA seems contradictory with the fact that B cells were selected in this approach for binding to gamete surface antigens. One possible explanation may be that a B cell bearing an Ab binding with low affinity to a gamete surface antigen were selected thanks to the strong avidity effect potentially generated by the cell-cell interaction. The profile of the binding curve in GE ELISA suggests a fairly low affinity for the gamete antigen potentially recognised, and is compatible with this hypothesis. In addition, the protein recognized by F10 could be proportionally more abundant in the gametocyte extract than at the gamete cell surface, potentially explaining the detection of a signal in ELISA but not in SIFA. Alternatively, we cannot exclude that the F10 signal in ELISA may correspond to unspecific binding and more experiments are required to rule out this hypothesis.

Assuming that the F10 mAb was specific for a gamete antigen, the yield of the approach would still seem low. One explanation lies in the fact that only a small number of cells were sorted as this was a set-up experiment. In addition, it is possible that the relatively low fluorescence threshold used for selecting complexes to be sorted may have resulted in high proportions of MBCs unspecifically bound to gametes. Unfortunately, this latter hypothesis could not be

verified because the index sorting was not recorded for this experiment. This would otherwise may have allowed us to know the Pfs47 Daylight 650 fluorescence intensity for each sorted complex (notably in the case of F10) and indirectly the potential number of gametes attached to sorted memory B cells. If the hypothesis was to be verified the approach could then be improved by using a higher threshold and sorting only MBCs that have potentially fixed more than one gamete.

Finally, another potential explanation for the low amount of gamete specific Abs isolated is the fact that we used a donor with suboptimal serum titers against sexual stage antigens. Although Abs to Pfs230 and Pfs48/45 were clearly present in the donor serum, the corresponding B cells may have been present only at a low frequency and we may not have sorted enough specific B cells to isolate them.

In conclusion, in order to better understand how effective our B cell-gamete complex sorting approach is, the experiment would have to be repeated, using new sorting parameters and with donors with stronger Ab titers against gamete surface antigens.

.

1.2 Isolation of gamete surface protein-specific mAbs via agnostic memory B cell sorting followed by single B cell activation and cell supernatant screening

1.2.1 Finding proper conditions for the activation of single MBCs

As for the previous approach, we first used non-precious samples derived from care to set up conditions.

Activation of MBCs from a healthy individual:

IgG+ MBCs from a healthy individual (derived from care) were sorted at one cell per well to test different experimental conditions for MBC activation. Protocols were adapted from Huang et al (195) and Muir et al (196), using different cytokine cocktails, feeder cell types and FBS percentages. The most efficient conditions to activate B cells and stimulate IgG production were found to be using IMDM (1% penicillin - streptomycin and complemented with 20% FBS) and adding IL 21 (at 100 ng/ml) and IL 2 (51 ng/ml) as a cytokine cocktail (data not shown). Mouse fibroblasts expressing the CD40 ligand, irradiated at 50 Gy and seeded at a density of 5000 cells per well were used as "feeder cells".
Activation was done three times using those settings, with PBMCs from the same healthy donor (blood harvested at different times, leftover from healthcare), and results are shown in table 6.

	Average (n=3)
Activated wells	74%
Average IgG concentration in "activated wells" *95% confidence interval*	107 ng/ml *178.9 – 248.0 ng/ml*
Average maximal IgG concentration detected	306 ng/ml

Table 6: IgG secretion levels following activation of MBC originating from a healthy individual.

IgG levels were high in comparison to those obtained by Huang et al (195): when plating MBCs at a density of four cells per well (compared to one cell per well in our experiments), 76% of the wells contained more than 10 ng/ml of IgG.

The experiments helped determine if the IgG concentrations obtained in cell culture supernatants were high enough to directly test the functionality of the secreted IgGs in HT-SMFA, as this could have allowed the direct selection of mAbs with the functional activity of interest. Even though IgG levels were found to be too low for SMFA, they were high enough to test IgG binding to gametocyte extract ELISA and to gametes in SIFA.

Finally, positive control mAbs (TB31F, an anti Pfs48/45 mAb and 2544, an anti-Pfs25 mAb) were diluted in cell culture medium, then tested for their gamete recognition in SIFA to ensure that the cell culture media did not cause high background signals (data not shown, experiment performed by TropIQ).

Activation of MBCs from a donor with malaria:

As explained in introduction, chronic malaria infection may hinder the development of humoral responses. Thus, we feared that the response to activation of B cells from patients with malaria may be decreased compared to the one of malaria-naïve individuals. Therefore, we decided to test the response to the activation cocktail described above of MBCs from a *Pf*-infected individual.

As in part I, we verified the presence of Abs to *Pf* surface proteins in the donor serum using gametocyte extract or recombinant Pfs48/45 and Pfs230 ELISAs. At a 1/250 dilution, this serum gave a signal which was the same as a positive control serum from our collaborators:
- at a dilution of 1/1700 for the gametocyte extract
- at a dilution of 1/600 for Pfs48/45
- no reactivity was detected against Pfs230 for this donor.

	(n=1)
Activated wells	83%
Average IgG concentration in « activated wells »	143,4 ng/ml
Average maximal IgG concentration detected	492 ng/ml

Table 7: IgG secretion levels following activation of MBC originating from an malaria individual.

PBMCs from the donor were then activated as described above and the percentage of activated B cells and IgG concentrations were measured. These were comparable to those obtained before with of a healthy donor (table 7), which suggested that malaria infection did not reduce the memory B cell response to the cytokine cocktail, at least in this individual.

To evaluate the percentage of cells reactive against the sexual stage of *Pf* among all the agnostically sorted MBCs, supernatants were tested in ELISA for their binding to gametocyte extract. Thirteen wells were positive for gametocyte extract out of 1023 potentially activated wells (1232 wells screened). In total, the percentage of gamete-reactive wells was 1.27%. This percentage, suggested the possibility to obtain a significant number of MBCs reactive against gamet(ocyt)es when screening a greater number of cells. According to this percentage and to physiological reference values (194), for this donor a sample of 10 million PBMCs would contain approximately 254 MBCs reactive against gameto(cytes).
In conclusion, we implemented, based on the literature, an activation protocol for single MBCs giving a high percentage of activated cells and a concentration of secreted IgGs amenable to screening for binding to gamete surface antigens. Being infected with Pf did not appear to impact activation rates and IgG levels although this was only tested in a single individual with malaria. Based on those results, we decided to proceed with activation of cells from a donor with strong serum TRA in order to isolate TRAbs.

1.2.2 Activation of MBCs from an individual with high serum TRA: Donor A

Donor A serum binding and functional characteristics :

Donor A is a 69 year-old Dutch man who returned to the Netherlands after a prolonged stay in an endemic country. He was recruited in 1994 in a cohort of the Radboud university medical centre, because of malaria infection. PBMC samples were collected following ethical procedures as specified in Material and Methods.
Donor A is one of the 6 donors studied in detail in the work of Stone et al (54), mentioned in the introduction in 3.2. As a reminder, serum of these donors retained TRA when depleted of Abs directed against recombinant Pfs48/45 *(R0.10C: the region comprising amino acids 159 to 428 of Pfs48/45 fused to the N-terminal region of GLURP)* and Pfs230 *(Pfs230 CMB: the region*

comprising amino acid 444 to 730), which suggested the presence of TRAbs directed against antigens not previously described.
The results from Stone et al obtained for donor A are shown in supplementary data 1 and 2.

Activation of MBCs from Donor A:

In order to isolate MBCs, 2 PBMCs samples from donor A were thawed. Unfortunately, the cell viability was low (around 50% for one sample and 75% for the other sample), which led to cell clumps and cell loss. It should be noted that those samples were prepared in 1994 and underwent several journeys alternating periods of storage at -80°C and in liquid nitrogen, which may explain their relatively poor condition. Thawed PBMCs were then stained according to the protocol detailed in Material and Methods, using a live/dead stain, anti-CD3, -CD19, -CD20, and -CD27 Abs as well as anti-IgD, -IgA and -IgM Abs. As shown in figure 26, lymphocytes were selected depending on their FSC/SSC profile, and doublets were excluded. Only live cells negative for CD3, positive for CD19 and C20, negative for IgA, IgM and IgE and finally CD27 positive were selected, corresponding to IgG+ MBCs (figure 26F).
IgG+ MBCs were sorted from total PBMCs at one cell per well in 384-well plates in activation medium in the presence of feeder cells and cultured for 11 days. In total, 1465 MBCs were sorted (figure 27).

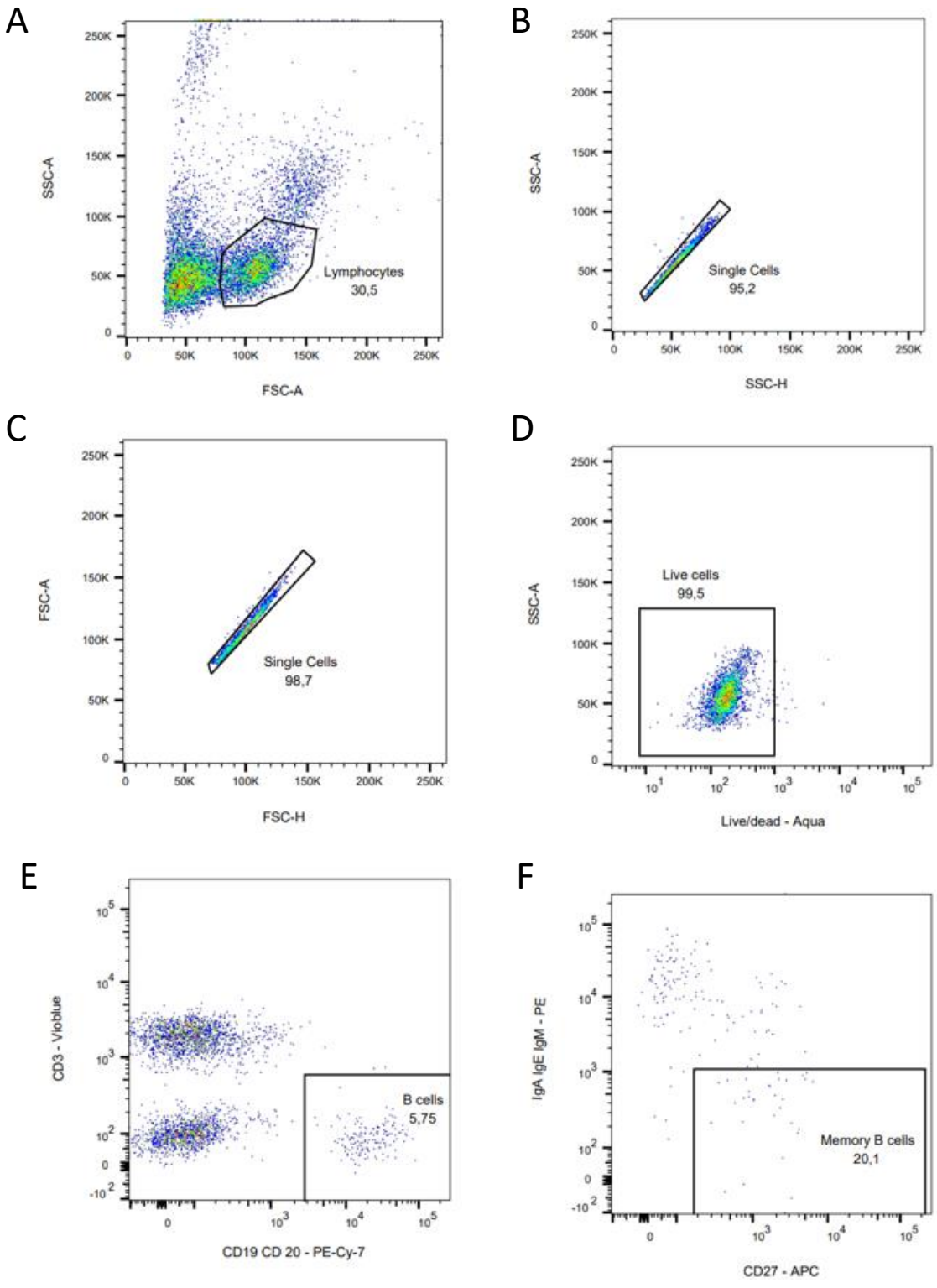

Figure 26 : Gating strategy for agnostic MBCs sorting

Lymphocytes were selected depending on their FSC/SCC profile (A). Doublets were excluded (B and C). Only live cells (D) negative for CD3, positive for CD19 and C20 (E), negative for IgA, IgM and IgE and finally CD27 positive were selected (F).

This low number of cells can be explained by the high mortality of cells following the thawing step and also by the application, during the sorting process, of a single cell “mask”. The "mask" parameter determines how the sorter processes "conflict" events (i.e. when two cells cannot be properly differentiated or separated before they fall into the well). By choosing the "single cell" mask, only the cells for which there was absolutely no risk of taking also a cell other than an MBC were sorted. In retrospect this stringency was not justified, as having other cells than MBCs in some wells would likely not have prevented the activation of the MBC. Thus, the use of the “single cell” mode may have led to the loss of a significant amounts of MBCs.

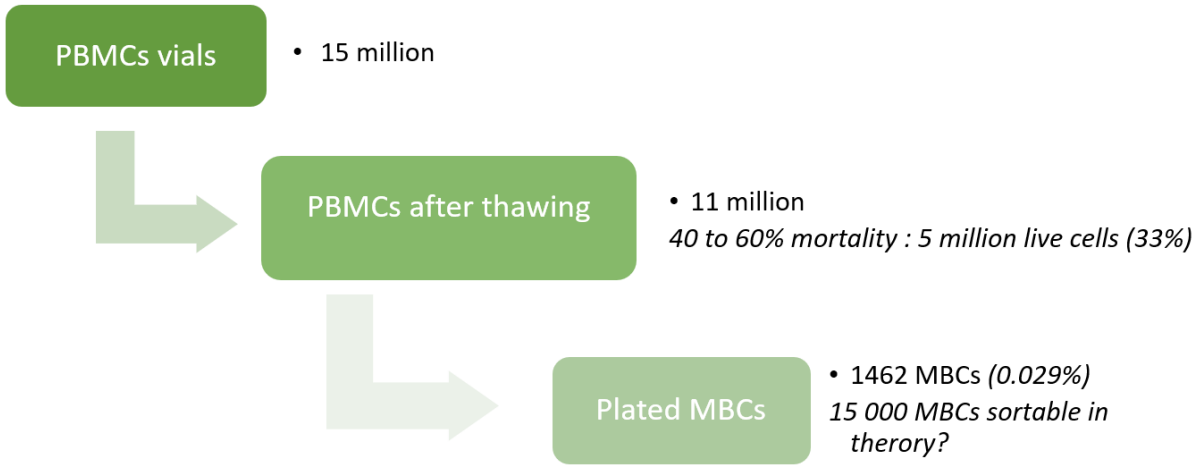

Figure 27: Yield of each sample preparation step, from PBMCs thawing to agnostic cell sorting.

Of note, among the 1462 sorted MBCs, approximately 75% were activated according to the 78.5% average activation rate described in 1.2.1, which finally correspond to theoretically 1096 MBCs with secreted IgGs in the supernatant. The volume of supernatant was too small to check the IgG concentrations in each well, and was instead used to perform gamet(ocyt)es ELISA and gametes SIFA.

1.2.3 Selection of cell culture supernatants reactive against gamet(ocyt)es proteins

Following 11 days of activation, cell culture supernatants were harvested and sent to our collaborators at TropIQ. As described in Material and Methods, harvest was performed with the help of a pipetting robot allowing for the precise and delicate IgG-containing supernatant aspiration while leaving the MBC at the bottom of the well to undergo cell lysis necessary for downstream IgG gene amplification. Plates containing lysed cells were stored at - 80 °C.

Cell culture supernatants were screened in a high-throughput 384-well ELISA for their reactivity against gamete extract. For wells containing a sufficient volume of the supernatant (an evaporation-dependent parameter), a screening *via* gametocyte-extract ELISA was also performed. One hundred thirty-six well contents showed a binding signal above background in gamete or gametocyte ELISA, representing 9.3% of the total sorted MBCs (or 12.4% of the activated MBCs). Each well result is listed in supplementary figure 3. These 136 supernatants were then tested in gamete SIFA, and 8 of them were confirmed as strongly positive, as shown in figure 28.

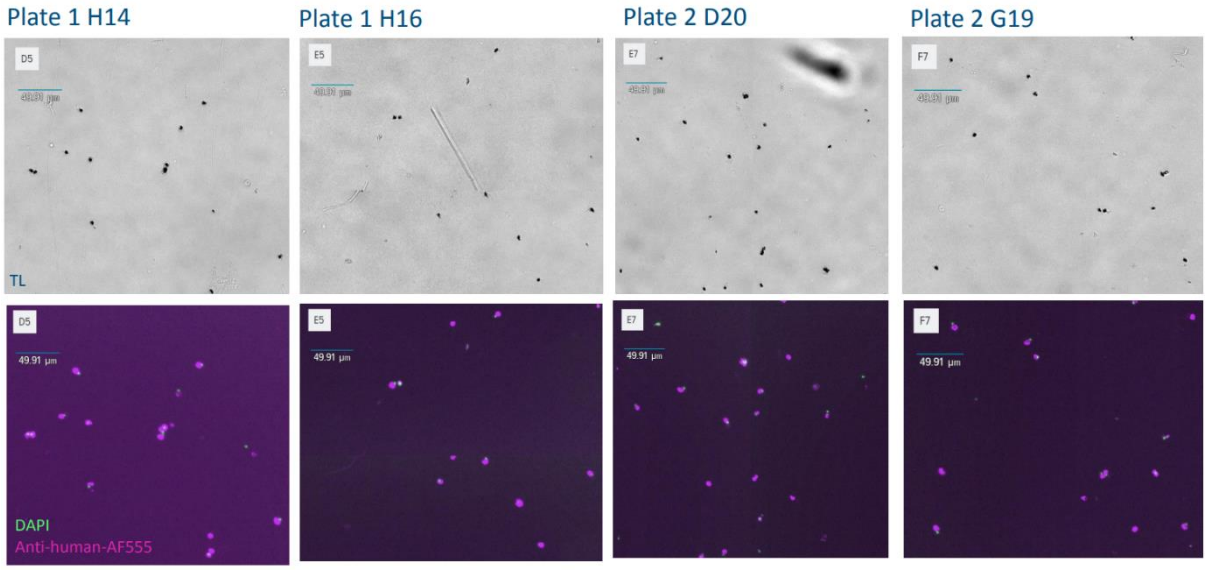

Figure 28: Cell culture supernatants positive in gamete SIFA following MBC activation

. Example of four different wells that were detected as clear "hits" by eye and by the software. Five microliters of cell culture supernatant were mixed with 5 µl of gamete suspension (containing approximatively 10000 gametes). Cells are stained with DAPI and IgG are detected with an anti-human-IgG-AF555 coupled Ab. An anti Pfs48/45 mAb was used as positive control and an anti-CSP mAb as a negative control.

The contents of the 136 wells selected as positive according to the gamet(ocyt)es ELISA results were then cherry-picked with the help of the pipetting robot and transferred to 96-well plates for IgG gene amplification.

1.2.4 Amplification of Ig genes from selected MBCs and mAb production

IgG gene variable domain amplification was performed for all 136 wells which were detected as positive in the gamet(ocyt)e extract ELISA, on two separated PCR plates. Results are presented in table 8:

		Plate 1	Plate 2
HC	Bands in agarose gel	36%	14%
	↳ Wells matching an HC sequence	100%	92.3%
kC	Bands in kC agarose gels	25%	14%
	↳ Wells matching an kC sequence	100%	100%
lC	Bands in lC agarose gels	23%	9%
	↳ Wells matching an lC sequence	100%	100%

Table 8: Percentages of well contents yielding bands in agarose gel following DNA amplification and percentage of these well contents giving an IgG sequence when analysed with IMGT.

IgG gene amplification yields were somehow lower in comparison to recovery rates usually obtained following direct lysis in our laboratory, as detailed in part 1.1.3. In contrast to direct cell lysis, cell sorting followed by activation implies long culture periods during which cells can die and genetic material can degrade, which can result in a lower PCR efficiency. This could theoretically be compensated by cell activation and increase of mRNA levels. Interestingly, in contrast to following short-term activation periods as described above in chapter 1.1.3, we noticed that after 11 days of culture almost all the amplified PCR products identified on the gel as having the right size corresponded to immunoglobulin sequences following analysis with the IMGT database. This difference could be explained by the death of the irradiated feeder cells during the 11 days of culture, resulting in a lower contamination level from their genomic DNA. However, RT-PCR efficiency was also likely greatly increased by adding a RNA purification step, performed with the mRNA TurboCapture kit (Qiagen #72271), especially designed for 384-well plates and low cell densities.

Finally, when compiling sequence data, both a light and heavy chain were recovered in 20 of the wells, corresponding to 26 putative mAbs (13 with kC and 13 with lC), with some Abs displaying positive sequences for both kC and lC. These well contents were selected for cloning experiments and downstream monoclonal antibody production. Fourteen mAbs (6 kappa and 8 lambda) were finally produced, corresponding to only 10% of the 136 well contents originally selected for Ig gene amplification. Possible explanations for this low yield are explored in discussion.

1.2.5 Reactivity of the isolated mAbs against *Plasmodium falciparum* sexual stage proteins

The 14 mAbs produced were then sent to our collaborators at TropIQ and Radboud to first study their ability to bind sexual stage antigens in gamete/gametocyte ELISA and in SIFA. Second, to determine the antigens recognized by the mAbs, Western blot analysis using gametocyte extract and ELISA with recombinant domains of Pfs48/45 and Pfs230 were performed.

Gamete Surface Immunofluorescence Assay:

Surface immunofluorescence assays were performed with both NF54 *Pf* WT and Pfs48/45 KO gametes as detailed in Material and Methods, in order to assess the ability of the mAbs to bind gamete surface antigens, eventually different from Pfs48/45 and Pfs230. MAbs were tested at three different concentrations (100, 5 and 1 µg/ml) and results are presented in table 9.

IgG supernatant tests			mAbs test						
			mAb	SIFA					
				% pos. GMT in WT SIFA			% pos. GMT in KO SIFA		
SIFA	GCT ELISA	GMT ELISA		100 µg/ml	5 µg/ml	1 µg/ml	100 µg/ml	5 µg/ml	1 µg/ml
NB	1190	2254	B1C5K	68.7	92.3	94.8	3.0	2.0	1.8
NB	1190	2254	B1C5L	77.5	82.7	92.5	7.2	1.6	1.0
NB	/	1691	B2C10L	66.5	58.6	68.9	3.1	4.0	4.6
Hit	/	553	B2E9L	76.2	75.3	82.3	11.3	9.9	9.7
NB	150	435	B1C8L	60.7	2.5	2.0	2.1	1.0	1.0
Hit	1395	173	B1D3L	3.0	2.0	2.0	6.4	1.1	0.7
Hit	1395	173	B1D3K	4.9	3.5	2.6	8.6	2.8	1.9
NB	/	440	B1F9K	1.5	1.9	2.0	1.0	0.8	0.9
NB	/	409	B1E7K	60.9	2.8	1.1	5.6	1.5	1.0
NB	434	678	B1C3L	2.8	1.0	1.1	3.5	1.7	1.5
NB	/	422	B2D10L	49.5	61.7	17.2	4.2	4.2	5.0
Hit	/	403	B2F7L	18.5	9.5	3.8	5.5	4.7	5.3
NB	150	435	B1C8K	10.5	1.0	0.8	3.8	0.6	1.3
NB	/	1290	B1E11K	27.8	30	19	18.8	18.8	19.9

Table 9: Summary of the produced mAbs reactivity when tested in gamete SIFA and comparison with the corresponding IgG supernatant (in blue, first column).

NB : Not binding. GCT: gametocyte. GMT: gamete. Clear positive hits in cell culture supernatant gamete SIFA detected by both the software and by eye are highlighted in yellow. Doubtful hits are in orange (not considered positive by eye but for which the software detected more than 10% of positive gametes). MAbs SIFA results are coloured depending on binding levels: red are the highest, green the lowest.

Seven out of the fourteen mAbs bound to more than 50% of gametes when tested at 100 µg/ml. Among those mAbs, four (B1C5K, B1C5L, B2C10L and B2E9L) recognised WT gametes with high scores (> 68%) at concentrations as low as 1 µg/ml. This recognition strongly decreased when using gametes KO for Pfs48/45 and thus with downregulated Pfs230, suggesting that these 4 mAbs were directed at one of these 2 antigens. The B2D10L mAb also had a similar recognition profile (disappearance of binding with KO gametes), but with lower percentages concerning binding to WT gametes compared to the 4 other mAbs.

Two other mAbs, B1C8L and B1E7K, strongly recognised gametes at 100 µg/ml, but the recognition greatly declined at lower concentrations and with Pfs48/45 KO gametocytes, suggesting a recognition of either Pfs48/45 and Pfs230, with a relatively low affinity.

Finally, the B1E11K had a different binding profile, recognising only a fraction (about a third) of the WT gametocytes at the 2 highest concentrations and still 19% at the lowest concentration. Recognition of the Pfs48/45 KO gametocytes was somehow lower than the one of the WT

gametes but the difference was not clearly significant, suggesting the potential recognition of antigens different from Pfs48/45 and Pfs230.

Interestingly, the B1C5 mAbs (B1C5K and B1C5L) showed similar binding properties, which suggest that their binding is in a large part mediated by the HC. Thus, no matter which LC is used (either kappa or lambda), the Ab can still bind its target and it is difficult to know which LC was originally paired with this HC. The two B1D3 mAbs had the same non-binding profile. Finally, the two B1C8 mAbs had different binding profiles suggesting that the presence of the lC is necessary for its binding and that the kC did not correspond to the originally paired LC.

Although the mAbs produced were selected from wells with IgG-containing supernatant binding in gamet(oocyt)e ELISA, seven of them gave no signal in mAb SIFA. This could be due to the ELISA detection threshold, which was chosen as relatively low to avoid missing interesting wells, and to the use of the game(tocy)te extract. Indeed, as explained before, this extract is made from whole parasites that are crushed and lysed, giving a mix of extra- and intracellular proteins (with notably many common to other stages of the parasite's development). Therefore, Abs bound to intracellular proteins may also have been selected. In contrast, in SIFA only the binding to surface antigens is detected. In this sense screening directly through SIFA could have been more effective but was precluded by technical difficulties.

Overall, 8 mAbs with a promising binding profile in SIFA were isolated and characterized further for their binding properties in gametocyte extract Western blot.

Western blot:

To identify the antigens recognized by the 8 mAbs with an interesting SIFA profile, Western blots were performed by our collaborators at Radboud University using gametocyte extract. Of note, the F10 mAb obtained with the direct sorting strategy was also selected for inclusion in the WB.

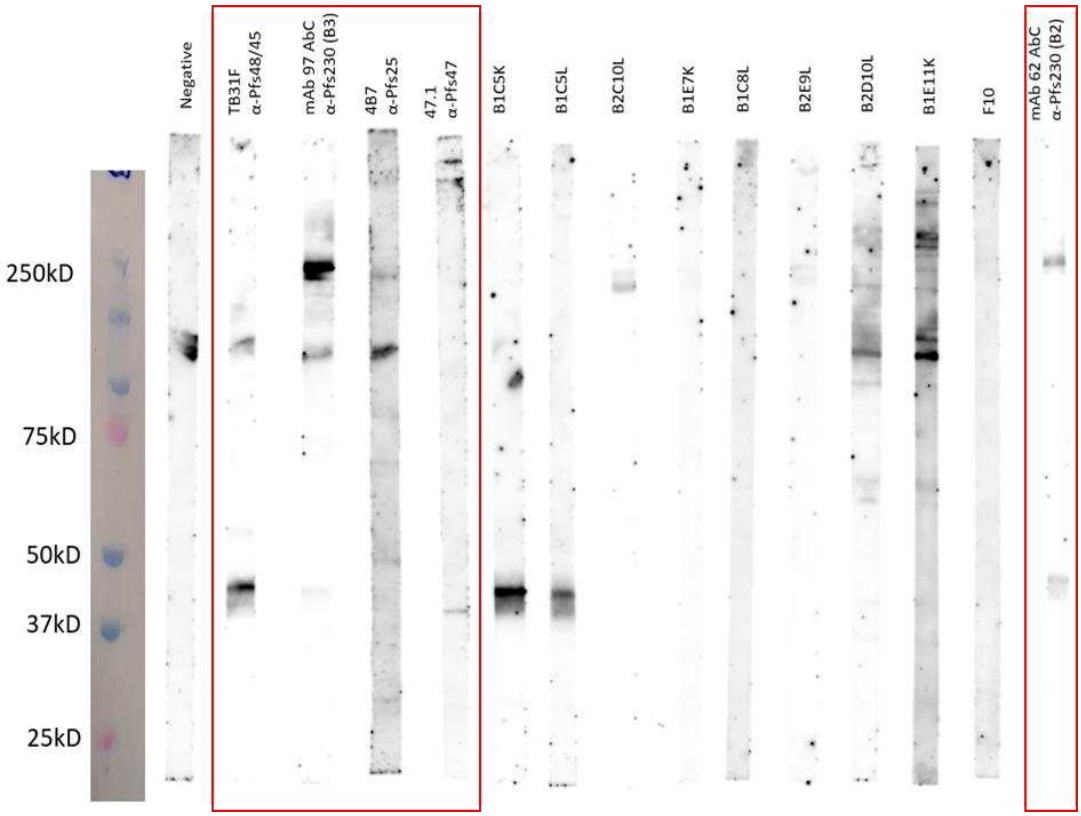

Figure 29: Western blots results obtained with mAbs that showed binding in SIFA.

Western blot analysis was made on reduced gametocyte lysate and mAbs were tested at 5 µg/ml, as described in Material and Methods. Positive control lanes are boxed in red and were TB31F (anti-Pfs48/45 mAb), 97AbC and 62AbC (anti-Pfs230 mAbs),4B7 (anti-Pfs25 mAb), 47.1 (anti-Pfs47 mAb). Of note, F10 mAbs, originating from the direct cell sorting was also included in this Western blot screening.

As shown in figure 29, the B1C5K and B1C5L mAbs recognised a band with a molecular weight corresponding to the one of Pfs48/45, in a similar manner as a control mAb specific of Pfs48/45 (TB31F). Abs B2C10L and B2E9L recognized a band corresponding to the molecular weight of Pfs230, in a similar manner than anti-Pfs230 mAbs (97AbC and 62 AbC). B1E11K and B2D10L appeared to bind to gametocyte extract proteins of different sizes, with two bands

of higher intensity. One of the two bands was around 130-140 kDa, corresponding to an unidentified protein, and the other band was slightly higher than the bands revealed by the two anti-Pfs230 controls. Finally, B1E7K and B1C8L showed no clear binding to any protein from the gametocyte extract in the WB.

Recognition of recombinant truncated Pfs48/45 and Pfs230 in ELISA:

To complete the information provided by the Western blots, ELISA was performed to test the recognition of the recombinant Pfs48/45 R06C and Pfs230 (Pfs230 C1) proteins.

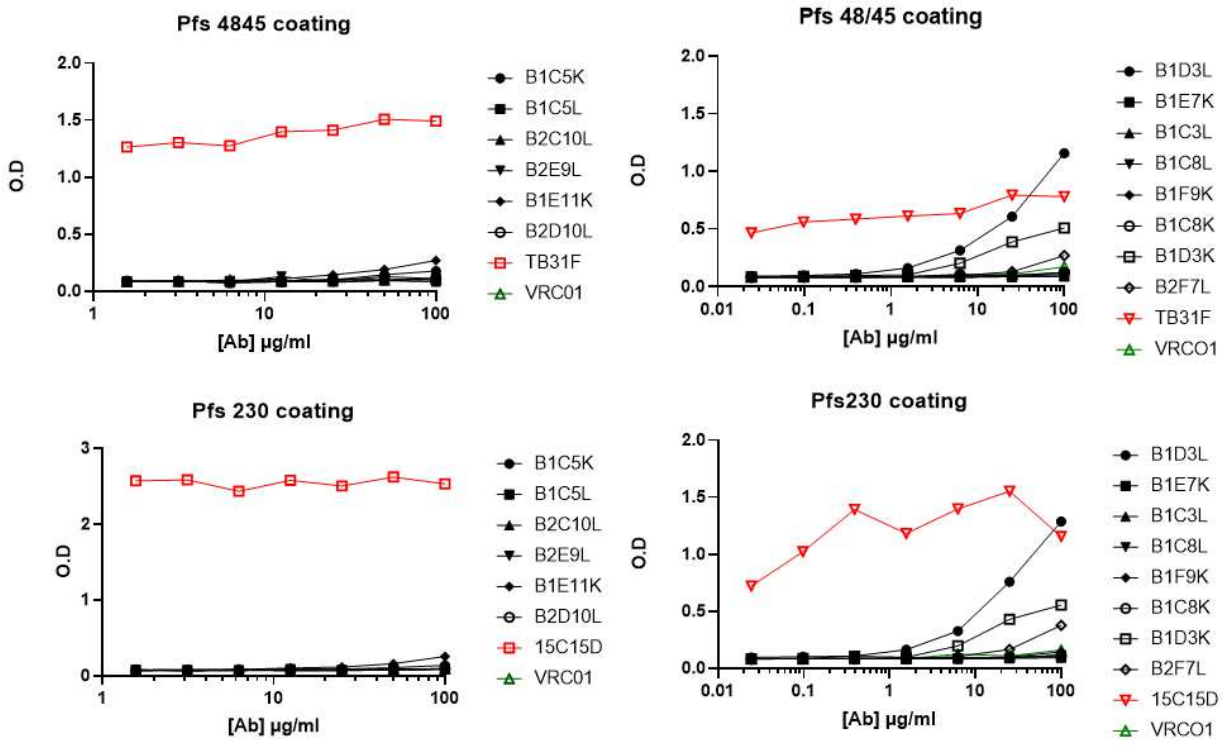

Figure 30: MAbs binding to recombinant Pfs48/45 and Pfs230 proteins.

Red curves: experiments positive controls (either 15C15D and TB31F). Green curves: negative control (VRCO1, an anti-HIV mAb).

As shown in figure 30, no mAb recognised the proteins, except for B1D3K and B1D3L. These mAbs gave a signal for both Pfs48/45 and Pfs230, but only at high concentration. These two proteins had no common sequence, suggesting non-specific binding at high concentration. In addition, both B1D3K and B1D3L were found to react on a panel of self-antigens (protocol detailed in Material and Method), in particular B1D3L (data not shown), reflecting their polyreactivity.

B1C5K and B1C5L, although reacting with a protein with a molecular weight similar to Pfs48/45 in the Western blot, did not bind to Pfs48/45 R06C, corresponding to epitope I of Pfs48/45. This suggests either a binding to the other epitopes of Pfs48/45 (II, III or IV) or that the conformation of the recognised epitope on the parasite was different from the one of the recombinant proteins. Of note, no human mAb has been described to date as able to bind to one of the three epitopes II, III or IV. Alternatively, B1C5K and B1C5L could be binding to a protein other than Pfs48/45 but still have the same molecular weight when observed in Western blot.

Similarly, the absence of Pfs230C1 (corresponding to domain 1) recognition by B2C10L and B2E9L may suggest binding to another Pfs230 domain than this one, to a conformational epitope not present in Pfs230C1, or to a different protein with a similar molecular weight as Pfs230. To date, the only anti-Pfs230 human mAb described in the literature binds domain 1 (163). More experiments are planned in the near future to test binding of B1C10L and B2E9L to the other recombinant domains of Pfs230.

1.2.6 Activity of the produced mAbs in SMFA

Two types of SMFAs were performed. HT-GFP-Luc *Pf* strain with a luminescence read-out SMFA was performed by our collaborators at TropIQ. SMFA using the WT strain and manual counting was performed by our collaborators at Radboud to confirm and complete the initial results obtained with the HT-GFP-Luc *Pf* strain. Unfortunately, results of these two types of SMFA were not always concordant, as discussed below and summarized table 10.

HT-GFP-Luc *Pf*-based SMFA :

SMFA using *Pf* NF54-HT-GFP-Luc strain and luminescence detection of oocysts is detailed in Material and Methods. In those first SMFA experiments, 5 Abs had TRA above 80% : B1C5K, B1C5L, B2C10L, B2E9L and B1E11K when tested at 500 µg/ml (see table 10, left half of the table). Interestingly, both B1C5 mAbs, with either kC an lC, were functional. When tested at lower concentrations, B1C5L and B1E11K retained a high-level of TRA (87.5% at 50 µg/ml and 89% at 100 µg/ml respectively). Five mAbs had an intermediate TRA between 50 to 80%: B1C3L, B1D3L, B1C8L, B1E7K and B1F9K when tested at 500 µg/ml. Finally, four mAbs were considered as having no TRA, with TRA scores below 50% at 500 µg/ml: B1D3K, B2D10L, B2F7L and B1C8K.

	% inh. Luciferase detection	% inh. Manual detection	
mAb	500 µg/ml	500 µg/ml	100 µg/ml
B1C5K	88.6	94	78
B1C5L	85.2	91	76
B2C10L	97.3	95	86
B2E9L	92.1	84	98
B1C8L	70.2	97	93
B1D3L	72.6	94	73
B1D3K	43.6		
B1F9K	67.7	92	76
B1E7K	74.7	-7	
B1C3L	68.8	**20**	
B2D10L	28.0		
B2F7L	16.2		
B1C8K	-15.2		
B1E11K	83.3	-35.0	

Table 10: SMFA levels of mAbs obtained following agnostic sorting, oocyst detection being performed by either luciferase detection or manual counting.

Green cells: inhibition percentages between 0 to 50%. Yellow cells: between 50 to 80%. Red cells: between 80 to 100%. MAbs are generally considered as TRAbs when TRA > 80%.

SMFA with manual counting:

Here SMFA were performed using WT *Pf* strain, manual dissection and microscopic counting.

- B1E11K titration:

The B1E11K mAb displayed an interesting binding profile when tested in gamete WT and KO SIFA and GE Western blot, suggesting binding to another antigen than Pfs230 and Pfs48/45, and was also considered as a TRAb following the HT-GFP-Luc SFMA. Thus, B1E11K was selected as a priority to undergo further SMFA at a lower concentration than in the previous assay, using a protocol with 20 mosquitoes fed per mAb, and WT parasites. Results presented in figure 31 were obtained with the same B1E11K batch as the one used for HT-GFP-Luc

SMFA experiments and the first GE Western blot analysis performed by our collaborators at Radboud.

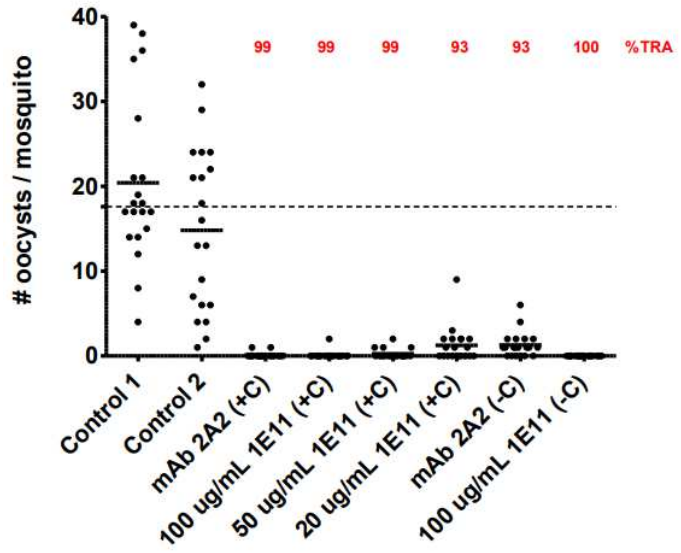

Figure 31: Testing of the first batch of B1E11K mAb in SMFA with the manual counting detection method.

Different mAb concentrations were assayed in the presence of complement (+C) or in its absence (-C). Controls 1 and 2 are experiments for which no mAbs was added to the mosquito bloodmeal. Red are TRA percentages (2A2 mAb : anti- Pfs230 mAb)

In this experiment, B1E11K again showed very high TRA levels with or without complement, even at concentrations as low as 20 µg/ml. These results therefore appeared to confirm the strong functionality of the mAb. **As SIFA results suggested recognition of proteins other than Pfs48/45 and Pfs230, the B1E11K mAb was certainly a good candidate as a TRAb binding to a novel target. Thus, the second part of my thesis work, was dedicated to the precise characterisation of B1E11K binding properties and the determination of its epitope.**

- <u>Confirmation of the activity of the mAb panel in SMFA:</u>

Monoclonal Abs having a TRA > 50% in HT-GFP-Luc were selected for confirmation of activity in further SMFA experiments (see table 10, right half of the table). The B1C3L and B1E7K mAbs in this assay showed lower TRA results than when tested in HT-GFP-Luc Pf SMFA. Conversely, B1D3L, B1C8L and B1F9K, which previously shown intermediate TRA, had TRA above 80%. **Surprisingly, the B1E11K mAb, which had previously shown high**

TRA levels, had no TRA in this experiment. As new B1E11K batches were used for this experiment, a confusion could have occurred, that could eventually explain these contradictory results. Investigations were conducted to try to understand where the error came from.

Overall, 7 mAbs were confirmed as having TRA at 500 µg/ml when tested at 500 µg/ml in manual counting: B1C5K, B1C5L, B2C10L, B2E9L, B1C8L, B1D3L, B1F9K.

<u>B1E11K quality controls:</u>

In an attempt to determine if a confusion occurred during B1E11K production and shipment, GE Western blot analysis was performed with all the B1E11K batches that were sent by our laboratory to our collaborators in Nijmegen.

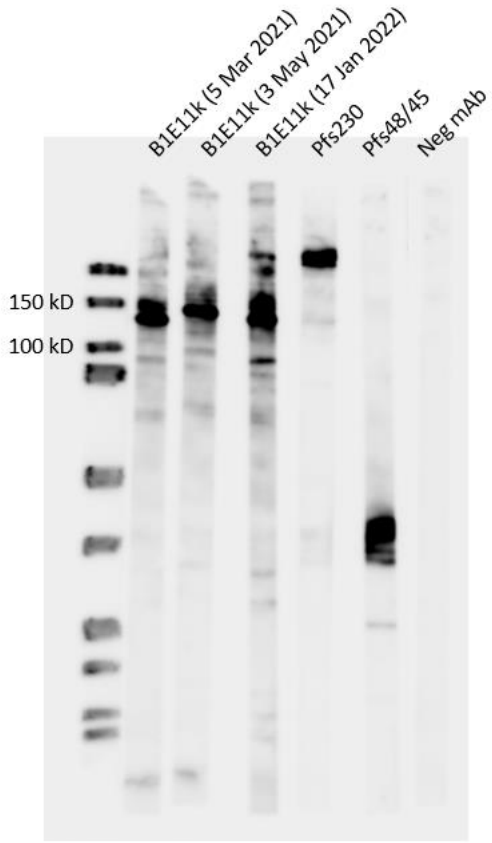

Figure 32: GE Western blot of the different B1E11K batches used for SMFA experiments.

Half a million of reduced gametocytes were deposited per lane. B1E11KmAbs were diluted at 5µg/ml. Anti-Pfs230 mAb: 15C15D. Anti Pfs48/45 mAb: TB31F. Negative control (anti-HIV) mAb: VRCO1.

As seen in figure 32, all batches had the same binding profile, suggesting that an early confusion most likely had occurred during the preparation and aliquoting of the B1E11K sample for the first SMFA experiment, this sample having then been used for the second B1E11K TRA titration using SMFA with manual counting that had also given a positive result.
As an alternative explanation, the presence of endotoxins in the first B1E11K batch that had given excellent levels in SMFA was also studied. The endotoxin contamination levels of eight different batches of B1E11K mAb were measured. Thirteen other mAbs produced in the laboratory over the last two years were also tested, among them some that did not show any TRA when tested in SMFA. Endotoxin contamination levels were around 10 UI/ml for all the tested mAbs, suggesting that endotoxin contamination was not the origin of the originally detected B1E11K TRA.

Interestingly, in this WB, particularly in the case of the Ab batch of January 17, 2022, the recognition pattern of B1E11K clearly showed a band with a molecular weight corresponding to the molecular weight of Pfs230, in a similar manner as a control mAb specific of Pfs230 (15C15D). This band was also present, although in a more faint way, in the first Western blot (figure 31), as well as with the other batches of Ab in the WB showed in Fig 34. .

Overall, the WB showed that B1E11K recognised multiple proteins of different molecular weight from the gametocyte extract. The precise investigation of the recognised proteins is detailed in part II of this thesis.

1.2.7 Sequences of the tested mAbs:

The obtained mAbs sequence characteristics are summarised in table 11. Finally, our mAb panel being too small, it was not possible to detect an enrichment of the same Ig gene among mAbs targeting the same antigen, or having high TRA levels.

	Heavy Chain					Light Chain			
mAb	V gene	D gene	J gene	CDR3 length	V region identity %	V gene	J gene	CDR3 length	V region identity %
B1C5K	IGHV1-8*01	IGHD3-10*01	IGHJ5*02	16	93.06%	IGKV1-5*03	IGKJ2*02	9	89.73%
B1C5L	IGHV1-8*01	IGHD3-10*01	IGHJ5*02	16	93.06%	IGLV1-44*01	IGLJ3*02	11	95.44%
B2C10L	IGHV1-2*02	IGHD4-11*01	IGHJ5*02	11	93.09%	IGLV2-11*01	IGLJ1*01	9	96.53%
B2E9L	IGHV3-33*01	IGHD3-10*01	IGHJ4*02	17	96.53%	IGLV1-51*02	IGLJ2*01	10	95.79%
B1C8L	IGHV4-61*02	IGHD3-16*01	IGHJ5*02	11	80.70%	IGLV1-51*02	IGLJ2*01	11	86.67%
B1D3L	IGHV1-18*01	IGHJ6*03	IGHD3-9*01	21	91.67%	IGLV1-47*01	IGLJ3*02	10	88.41%
B1D3K	IGHV1-18*01	IGHJ6*03	IGHD3-9*01	21	91.67%	IGKV2D-29*01	IGKJ1*01	9	97.62%
B1F9K	IGHV4-4*07	IGHD6-19*01	IGHJ2*01	14	58.22%	IGKV1-12*01	IGKJ3*01	9	100%
B1E7K	IGHV3-33*01	IGHD5-12*01	IGHJ4*02	17	95.14%	IGKV3-11*01	IGKJ2*04	10	97.47%
B1C3L	IGHV4-4*07	IGHD6-13*01	IGHJ5*02	17	100.00%	IGLV2-14*01	IGLJ2*01	10	90%
B2D10L	IGHV4-31*03	IGHD3-10*01	IGHJ4*02	22	85.61%	IGLV3-1*01	IGLJ2*01	10	96.06%
B2F7L	IGHV3-74*03	IGHD3-10*01	IGHJ6*02	19	85.42%	IGLV2-8*01	IGLJ1*01	10	100%
B1C8K	IGHV4-61*02	IGHD3-16*01	IGHJ5*02	11	80.70%	IGKV3-15*01	IGKJ1*01	10	96.42%
B1E11K	IGHV3-7*01	IGHD3-10*01	IGHJ4*01	9	90.74%	IGKV3-20*01	IGKJ2*04	9	90.20%

Table 11: Sequence characteristics of the produced mAbs following agnostic sort.

In the first column, mAbs are highlighted in yellow and blue for lambda or kappa Abs respectively. Gene usage, CDR3 length and V,D,J region identity are also indicated.

Among the panel of obtained mAbs, 6 were kappa (42%) and 8 were lambda (57%). These percentages are in accordance with physiological values, with roughly 1/3 of kappa Abs and 2/3 of lambda Abs found in a healthy individual (197). For three mAbs of the panel, both kappa and lambda sequences were retrieved for the same heavy chain, which represents 42% of our small panel of Abs, a very large proportion. Indeed, according to Tiller et al (183), this physiological phenomenon is usually observed for about 5% of the sequences. More Abs would have been needed to conclude the significance of this double light chain recovery phenomenon.
By comparison with physiological values, heavy chains CDR3 were 15.85 amino acid long on average (± 4.33), similar to the reference values of 15.5(± 3.2) (198).
For both heavy and light chains, the mutation rates of the V region were high: 88.25% on average for heavy chains (with the exception of B1F9K) and 94.31% on average for light chains.
In terms of IgG genes family used, they were either IGHV1, IGHV3 or the IGHV4. Of note, two mAbs, B2E9L and B1E7K were found to be of the IGHV3-33 family, a family predominant among Abs directed against the NANP repeats of the Pf CSP protein (199).

1.2.8 Summary of the characteristics of the mAbs isolated from donor A

In order to make the information presented above more intelligible, below in table 12 are summarized the different binding and functional properties of each mAb isolated. Results obtained to date are briefly recapitulated below:

B1C5K and B1C5L mAbs were obtained from the same MBC. They had similar binding profile in SIFA (high binding to WT gametes abolished with Pfs48/45 KO ones), but more surprisingly, they were both functional when tested at 500 µg/ml by either TropIQ or Radboud. Indeed, as mentioned before, it is generally rare that mAbs originating from the same cell are both functional (183). GE Western blot showed native Pf48/45 recognition, whereas ELISA performed on recombinant protein showed no binding, which may suggest binding to an epitope absent from recombinant Pfs48/45.

B2C10L and B2E9L mAbs both recognised WT but not Pfs48/45 KO gametes in SIFA. Their binding profile in Western blot suggested recognition of Pfs230, probably on an epitope not present on the recombinant protein as they were both negative in ELISA based on recombinant Pfs230. Both were functional at 100 µg/ml when tested in the presence of complement.

B1C8L was binding only at 100 µg/ml to WT gametes and not to KO gametes, but was found to be highly functional in manual counting SMFA. For now, its target remains unclear.

B1D3L and B1D3K mAbs were not reactive in SIFA despite high binding signals in gamete SIFA and gametocyte ELISA performed on in IgG supernatant. Among the two antibodies, only B1D3L was functional in manual counting SMFA. B1D3L Western blot binding profile suggested binding to Pfs230. Oddly enough, both mAbs were found reactive against recombinant Pfs48/45 and Pfs230 in ELISA. They were then positive when tested for polyreactivity.

B1F9K was found functional at 500 µg/ml in manual counting SMFA, even if it was neither binding in SIFA, nor in recombinant proteins-based ELISA.

B1E7K, B1C3L, B2D10L, B2F7L and B1C8K were not TRAbs and had either poor or no binding signal in SIFA. The study of antigens targeted by these antibodies will therefore not be performed.

Finally, B1E11K mAb profile in gamete SIFA was similar when using either WT or KO gametes. Its binding pattern in GE Western blot suggested binding to proteins of different size, and notably to a protein with the same molecular weight as Pfs230. Following contradictory results between SMFA experiments, B1E11K was finally not considered a TRAb.

Table 12: Summary of isolated mAbs characteristics

	IgG supernatant tests			SIFA						SMFA			GE WB	ELISA
				% pos GMT in WT SIFA			% pos GMT in KO SIFA			% inh. Luciferase detection	% inh. Manual detection			
mAb	SIFA	CGT ELISA	GMT ELISA	100 µg/ml	5 µg/ml	1 µg/ml	100 µg/ml	5 µg/ml	1 µg/ml	500 µg/ml	500 µg/ml	100 µg/ml		
B1C5K	NB	1190	2254	68.7	92.3	94.8	3.0	2.0	1.8	88.6	94	78	Pfs 48/45	NB
B1C5L	NB	1190	2254	77.5	82.7	92.5	7.2	1.6	1.0	85.2	91	76	Pfs 48/45	NB
B2C10L	NB	/	1691	66.5	58.6	68.9	3.1	4.0	4.6	97.3	95	86	Pfs230	NB
B2E9L	Hit	/	553	76.2	75.3	82.3	11.3	9.9	9.7	92.1	84	98	Pfs 230	NB
B1C8L	NB	150	435	60.7	2.5	2.0	2.1	1.0	1.0	70.2	97	93		NB
B1D3L	Hit	1395	173	3.0	2.0	2.0	6.4	1.1	0.7	72.6	94	73		Pf48/45R06C & Pfs230C1
B1D3K	Hit	1395	173	4.9	3.5	2.6	8.6	2.8	1.9	43.6				Pf48/45R06C & Pfs230C1
B1F9K	NB	/	440	1.5	1.9	2.0	1.0	0.8	0.9	67.7	92	76		NB
B1E7K	NB	/	409	60.9	2.8	1.1	5.6	1.5	1.0	74.7	-7			NB
B1C3L	NB	434	678	2.8	1.0	1.1	3.5	1.7	1.5	68.8	**20**			NB
B2D10L	NB	/	422	49.5	61.7	17.2	4.2	4.2	5.0	28.0			Multi. Bands & Pfs230	NB
B2F7L	Hit	/	403	18.5	9.5	3.8	5.5	4.7	5.3	16.2				NB
B1C8K	NB	150	435	10.5	1.0	0.8	3.8	0.6	1.3	-15.2				NB
B1E11K	NB	/	1290	27.8	30	19	18.8	18.8	19.9	83.3	-35.0		Multi. Bands & Pfs230	NB

NB: Not binding

1.3 Isolation of monoclonal TRAbs: conclusion and discussion

Our goal was to isolate naturally developed human TRAbs targeting new antigenic targets or new epitopes on known targets from a selected donor. Two different approaches were proposed, either sorting MBCs using stained live gametes as baits, or activating MBCs and doing a high throughput IgG screen using a gamet(ocyt)e extract ELISA.

From the two strategies that had been envisaged, following preliminary experiments, the second one was selected to be performed with cells from a donor who had been previously selected for the high level of TRAbs in his serum. Such donors are rare, and only a very limited number of vials of PBMCs were available from the donor selected by our collaborators at Radboud: Donor A. As time to complete our workplan was limited too, we had to decide early on which strategy was most likely to yield positive results. Preliminary results from the second approach appeared somehow more promising and it was selected. Therefore, we didn't have the opportunity to test our first approach on more samples, notably from Donor A. This direct sorting approach was thus only performed as a preliminary experiment, with PBMCs from a malaria donor whose serum did not demonstrate TRA and had relatively low titers against gamete proteins. One mAb targeting gametes was potentially isolated, no TRAb could be isolated. The limited results suggested that the approach could yield Abs of interest but we could not conclude on its effectiveness, and additional experiments would be necessary.

More exploitable results came from the activation and screening of MBCs from Donor A. While the amounts of MBCs sorted were quite low because of a high mortality rate when thawing the PBMC sample, 136 cell supernatants, corresponding to 12.4% of total sorted and activated cells, were reactive in GE ELISA. This high proportion of reactive MBCs may be explained by a high frequency of parasite-reactive cells due to a strong specific activation of the donor immune response, as he was sampled during an acute malaria crisis. In addition, screening was done using a gametocyte extract, thus containing a very large number of antigens to which the donor may have mounted an Ab response.

A total of 14 mAbs were produced, a number which may seem low. Many different steps are required to produce a mAb starting from an MBC lysate, most of them being very technical as they are performed on single cell, and this can jeopardise mAb final production yield. Furthermore, it is possible that within some wells selected for the binding characteristics of the

secreted IgG, the corresponding MBC died during the 11 days of activation, making amplification of genetic material impossible.

Among the 14 produced mAbs, half showed TRA at 500 µg/ml when tested in manual counting SMFA, and titration will have to be done to precisely determine mAbs IC_{80}. Among the 7 TRAbs, 4 were found to be directed against well-known proteins in GE Western blot: two against Pfs230 (B2C10L and B2E9L) and two against Pfs48/45 (B2C5L and B1C5K). As these mAbs did not show reactivity against Pfs230 (Pfs230 C1) or Pfs48/45 R06C in ELISA, Western blot and ELISA will have to be performed using others recombinant domains of the proteins for more precise epitope determination. For B2C10L and B2E9L, as all the anti-Pfs230 TRAbs described to date are complement dependent, SMFA will also be performed without complement to determine if this is also their case.

Finally, one TRAb was found to be polyreactive (B1D3L), and the two remaining mAbs (B1C8L and B1F9K) appeared to recognise a so far not characterised antigen. Further experiments such as immunoprecipitation on gametocyte extract followed by Mass Spectrometry will be useful help define the corresponding antigens.

Although it enabled the successful isolation of TRAbs, this project presents some limitations that will be discussed below, and improvements will be proposed.

As mentioned in the introduction, chronically *Pf*-infected individuals suffer modifications of their physiological immune response, including an increase of atypical memory B cells (AMB) compared to the healthy population (31). Numerous studies have investigated the role and impact of these AMBs, which is not clear to date, and some have shown that AMBs are responsible for functional immune responses (200)(201). These cells do not express CD27, this latter being a cluster of differentiation canonically expressed at the memory B cell surface. Our gating strategy being based on the selection of CD27+ cells, AMBs are missed, although being an important component of the B cell response to *Pf*.

Because the direct gamete sorting strategy relied on regular shipments of large quantities of gametes for set-up purposes; its implementation spread over several months (because of cell culture constrains, gametes could only be harvested every two weeks *a minima*). Once received, gametes were labelled with fluorochromes. As mentioned previously, the use of nucleic staining was not very suitable for two reasons: fluorescence intensity was dependent on cell viability, and the nucleic stain tended to leak on PBMCs, inducing false positive signals. Choosing the

anti-Pfs47 Ab therefore addressed these two issues. However, more stringent selection criteria could have been applied to ensure that MBCs that had non-specifically bound to a gamete were not sorted. This could have been done by only sorting cells giving high anti-Pfs47 Dylight signals, suggesting they were bound to more than one gamete, or by even using two types of fluorochromes for anti-Pfs47 antibodies, and sorting MBCs positive for the two, ensuring a fixation of at least two gametes. Finally, the use of anti-pfs47 was also not a perfect solution as Pfs47 is a protein expressed only by female gametes. Ideally, two Abs should have been used, one marking the female gametes, the other marking the male ones. However, the use of Abs directed against membrane antigens obviously prevents the binding of reactive BCRs against the targeted protein, but also against the surrounding proteins due to steric hindrance. One solution would be the use of *Plasmodium falciparum* strains containing a fluorescent reporter gene for male and female specific proteins. Sorting has already been performed with such strains by Lasonder et al (202), using PfDynGFP (for male selection) and Pf47GFP strains, and could therefore be considered for direct sorting experiments.

If the selection of gametes as performed for direct sorting presents some limitations, the same is true for the selection of MBC supernatants following agnostic sort. When using GE extract, the proportion of surface proteins is unknown and a low concentration of surface proteins in the extract may preclude selection. While gamete SIFA allows for better selection of antibodies only targeting surface proteins, the test as currently conducted is not perfect. Indeed, it requires gametes fixation with PFA, which can cause morphological changes, loss of epitopes or mislocalisation of target proteins (203). Ideally, SIFA on live gametes should be preferred (204).

To take advantage of both strategies, sorting gamete-binding MBC into cell culture wells and activating them for 11 days to screen their supernatant seemed an appealing method. Indeed, this would decrease the number of plated MBCs compared to agnostic sorting, making IgG supernatant screening in gametocyte extract ELISA less labor-intensive and costly. Such a protocol would also avoid the amplification of genetic material from MBCs that were non-specifically bound to gametes during sorting. As we feared that gametes may perturbate the IgG+ MBC proliferation, preliminary set-up experiments were made to verify healthy patient MBC activation rates when sorted with gametes. MBC -gamete complexes were artificially created by centrifugating the two cell populations together prior to sorting. After 11 days of culture, the activation percentage was 62.5%, with average IgG levels at 116 ng/ml and a

maximal concentration of 413.9 ng/ml in one well, these results suggesting that the presence of gametes had no impact on MBCs activation and that this strategy could be used in the future.

Once the MBCs of interest were selected and lysed, their genetic material was amplified by PCR. At this stage also, improvements could be considered. Indeed, it has been shown by Kreer et al (205) that the primer set developed by Tiller et al (183) allows a good amplification of families 1, 3 and 4, but a weak amplification of families 5, 6 and 7, and no amplification of family 2. This has to be put in perspective to the Ig gene amplification results obtained in this thesis, where only one IGHV5 Ab was amplified following the two sorts, all the other Abs being from families 1, 3 and 4! It would therefore be necessary in the future to update the currently used primer sets to avoid missing interesting Ig gene families.

When selected to be produced as mAbs, immunoglobulin genes are cloned into an IgG1 backbone, regardless of their initial subclass. The choice of IgG1s is justified by their optimal binding to C1Q and FcG receptors, allowing a stronger activation of the effector functions such as Ab dependent cell cytotoxicity or complement activation than with the other subtypes (and notably IgG2). This characteristic is of particular importance when working with anti-Pfs230 Abs, that have all been described to date as complement-dependent. However, Roeffen et al (164) demonstrated that when changing an IgG1 for an IgG 2a or 2b subtype, a previously “non-functional” mAb became a TRAb (63F2A2.2a or 63F2A2.2b) without the mechanism behind this acquisition of functionality being explained. Thus, using our pipeline, we can eventually miss Abs that were initially functional by changing their isotype.

Each reverse vaccinology project is centred around a reference test to determine the functionality of the mAbs once they are produced, and the reproducibility of this test is key to a successful pipeline. In the case of this project, the SMFA can only be performed if a sufficient number of parasites are available (a factor dependent on cell culture constraints), and it can currently only be used to test about 20 mAbs simultaneously. The high variability of this test has already been mentioned in the results section: to obtain reliable results, it must be performed on a large number of mosquitoes and repeated. For future sorts, a "barcoded SMFA" could be used. This test has been recently set-up by our TropIQ collaborators, following the protocol described by Sturm et al (206). Such a test allows high-throughput screening by performing SFMA on several mAbs in only one plate. Briefly, a blood meal is composed as for luciferase-based SMFA, but in each well are added different genetically modified *Asaia* bacteria, a *Pf*

prokaryotic symbiont. These bacteria carry individual short DNA barcode, that will be different from one well to another. Mosquitoes are released for feeding on blood meals, one mosquito feeding on only one meal in a single well in the vast majority of cases. Sequencing of the barcoded *Asaia* aspirated during the blood meal allows to determine in which well the mosquito has fed.

In stepping back, a future implementation of the pipeline may come from a new generation sequencing technique:10X genomics. Compared to the direct sorting strategy set-up in this thesis project, the use of 10X may enable the exploration of the full MBC repertoire able to recognise *Pf* gametes and the production of the corresponding Abs thanks to conservation of HC/LC pairing, without being restricted by the limitations of the current IgG gene amplification process used, while decreasing the work load and cost associated. Having such a large number of Ig sequences at our disposal could allow the study of possible enrichment among the IgG families involved in binding to the sexual stage antigens of *Plasmodium falciparum*.

Overall the approach has worked to isolate gamete-specific mAbs, including importantly mAbs to the well-defined targets Pfs230 and Pfs48/45, therefore it is likely that new targets will be discovered when repeating additional sorts. Donors having very high TRA serum being rare, optimisation of the pipeline is essential before new sorting experiments. The proposed implementations should improve the selection of MBCs of interest and mAbs produced, increase Ig gene recovery yield and the SMFA testing capacity of the produced mAbs.

2. THE B1E11K MAB: BINDING CHARACTERISTICS AND EPITOPE MAPPING

We sought to determine the antigen recognised by the B1E11K mAb, characterize its epitope and binding properties. To this end, a number of experiments were carried out, as described below, some of which are by our collaborators. Protein microarray experiments were done by the team of W. Stone (London School of Hygiene and Tropical Medicine), Western blots were done by our collaborators from Radboud University, mass-spectrometry by the EDYP platform headed by Y. Couté (CEA Grenoble), Growth Inhibition Assay (GIA) by the team of K. Miura (Maryland National Institute of Allergy and Infectious Diseases). We finally collaborated with the team of J-P Julien (University of Toronto) for structure determination, experiments were performed by R. Yoo, a PhD student.

2.1 Identification of the antigens recognized by the B1E11K mAb

As mentioned above, the B1E11K mAb did not recognise the Pfs230 and Pfs48/45 truncated constructs in ELISA. In Western blot, the mAb mostly bound 2 bands at around 130 and 150 kDa, corresponding to unidentified proteins. Bands of lower and higher molecular weight were also recognized suggesting cross-reactivity to diverse proteins or recognition of degradation products. Notably, as explained previously, a band was visible at 230 kDa, similar to the one given by the anti-Pfs230 control mAb, suggesting the potential recognition of Pfs230 by B1E11K. Various techniques were used to identify the B1E11K specificity.

2.1.1 Protein Microarray

Recognition by B1E11K of antigens from the gametocyte stage was tested using a protein microarray designed by Stone et al (65). Microarray chips were coated with recombinant proteins corresponding to putative antigens expressed at the gametocyte stage, but also proteins expressed at different steps of *Pf* lifecycle, some of them for which the expression at the sexual stage is not certain yet. Sequences of the recombinant proteins used in the microarray and recognised by B1E11K can be found in supplementary data 4.

Uniprot ID	Name	Gametocyte score
554_CFS_RM-TB22_0.03_2	Pf11.1 peptide used for immunisations	
977_PF3D7_0220000_e2s1_4	Liver Stage Antigen 3 (LSA3)	-13,58
1069_PF3D7_0309100_C_4	OMD protein	18,87
113_PF3D7_1149200_e2s1_1	ring infected erythrocyte surface antigen 3 (RESA3)	-25,32
637_PF3D7_0102200_e2s2_3	ring infected erythrocyte surface antigen (RESA)	-15,0263
224_PF3D7_1127500_C_1	Protein disulfide isomerase	12,9654
236_PF3D7_1036300-S2_1	Duffy binding like merozoite surface protein 2	-
120_PF3D7_0411700_1	conserved plasmodium protein	-
826_PF3D7_1038400_e2s1_3	Pf 11.1	24,6
402_PF3D7_1149200_e2s2_2	ring infected erythrocyte surface antigen 3	-25,3296
696_PF3D7_0804500_e3_3	uncharacterized protein	9,31
651_PF3D7_1038400_e7s1_3	Pf 11.1	24,6
643_PF3D7_1038400_e5s3_3	Pf 11.1	24,6
1070_PF3D7_0909000-S2_C_4	uncharacterized protein	-
86_PF3D7_1038400_e1s1_1	Pf 11.1	24,6
101_PF3D7_0522400_e3s1_1	uncharacterized protein	
sp|P68874|P230_PLAF7	Pfs 230	26,2

Table 13: B1E11K binding to recombinant Pf proteins displayed on a microarray.

B1E11K mAb binding to a set of recombinant proteins expressed at different steps of the parasite lifecycle are classified in a descending order. The first line of the table corresponds to microarray proteins for which B1E11K had the strongest binding, then hits are ranked according to their binding capacity in descending order. The right column indicated the "gametocyte score", as defined by Stone et al (54)*. When higher than –2.46, the protein presence is enriched in gametocytes. Pfs230 score (in grey) is shown for comparison, but Pfs230 was not present in this array. A value lower than –18.98, indicated that the protein was specific to the asexual stage.*

As seen in table 13, when tested on this microarray, B1E11K showed reactivity against several antigens, some expressed at the sexual stage (i.e Pf 11.1), others at the asexual stage (i.e LSA3, RESA, RESA3…).

In order to better understand the nature of the sequences potentially common to these proteins and recognized by B1E11K, we performed an analysis of their sequence. As these proteins contain numerous repeated amino acid patterns, we used the RADAR (Rapid Automatic Detection and Alignment of Repeats) software, from the EMBL Institute. As shown in table 14, most proteins analysed were rich in glutamic-acid repeats, of different size and composition.

554_CFS_RM-TB22_0.03_2 → Pf11.1 peptide used for immunisations	**VVPEVVEE x8 , adjacent.**
977_PF3D7_0220000_e2s1_4 → Liver Stage Antigen 3	EEIVAPTVEE X6 non adjacent EEIVAPSVEESVAPS x2 non adjacent EEIVAPSV x14 non adjacent VEENVEENVEEN Once, also present in RESA3.
1069_PF3D7_0309100_C_4 → OMD protein	No repeats
113_PF3D7_1149200_e2s1_1 → ring infected erythrocyte surface antigen 3	VDENVEEQx2 non adjacent QSVNEIVEE x2 adjacent DESGE x2 non adjacent
637_PF3D7_0102200_e2s2_3 → ring infected erythrocyte surface antigen	ENVEEYDEENVEE x3 VEENVEENVEEN X5
224_PF3D7_1127500_C_1 → Protein disulfide isomerase	No repeats
236_PF3D7_1036300-S2_1 → Duffy binding like merozoite surface protein 2	EDIEEETE x2 adjacent or EETEE x4 overlapping
120_PF3D7_0411700_1 → conserved plasmodium protein	No repeats
826_PF3D7_1038400_e2s1_3 → Pf 11.1	ELVEEVIPEE x4 (15 if only EEVIPEE) EELVEE x9 non adjacent EEVIPEE x14 non adjacent
402_PF3D7_1149200_e2s2_2 → ring infected erythrocyte surface antigen 3	ENVEENVEENVEEN x6 adjacent ENAEENAEENAEEN x1 EENIEE x6 non adjacent
696_PF3D7_0804500_e3_3 → uncharacterized protein	No repeats
651_PF3D7_1038400_e7s1_3 → Pf 11.1	PAPKKEK x 13 non adjacent PEELVEEVIP x3 non adjacent PEELIEEFVP x3 non adjacent EELVEE x13 non adjacent
643_PF3D7_1038400_e5s3_3 → Pf 11.1	EEVVPEEVVEEVIPEELIEELVP x2 non adjacent EEVIPEEVVEEVLPEELVEEVVPE x3 non adjacent EELVEE x23 non adjacent EEVIPEE x19 non adjacent
1070_PF3D7_0909000-S2_C_4 → uncharacterized protein	No repeats
86_PF3D7_1038400_e1s1_1 → Pf 11.1	EVIPEE x5 non adjacent EELVEE x23 non adjacent
101_PF3D7_0522400_e3s1_1 → uncharacterized protein	No repeats

Table 14: Analysis of repeated amino acid motifs among the different B1E11K protein "hits" from GE Western blot, immunoprecipitation and microarray.

Results were obtained using the Uniprot database and RADAR software.

Although Pfs230 was not part of the microarray, its sequence was retrieved from the database and also analysed using RADAR (data not shown).

Among all of the proteins, Pfs230, Pf11.1, RESA, RESA3 and LSA3 presented the most similar glutamic acid repeats, following an "EE-XX-EE" pattern. Precise repeat localisations among full-length proteins are indicated in supplementary data 5 to 10 and are highlighted in yellow. Pfs230 contains 7 adjacent EE-VG-EE repeats which are located in a domain of the protein which is cleaved upon gametocyte egress from erythrocytes. RESA and RESA3 contain respectively 20 and 9 EE-NV-EE overlapping repeats at the C-term of the protein, rendering this domain disordered. LSA3 contains 2 overlapping EE-NV-EE repeats. Finally, 221 non-adjacent EE-LV-EE repeats are spanning the whole Pf 11.1 megadalton protein.

As extensively described in the introduction, Pfs230 is expressed on gametocytes and gametes and is able to induce TRAbs, as well as Pf11.1. Pf11.1 is a megadalton protein expressed at the gametocyte stage and cleaved during gametocyte egress from RBCs.
RESA is an asexual-stage antigen and as described by Collins et al (207) "is localized in the micronemes of merozoites and also the membrane of red cells infected with ring-stage parasites". It has been described that anti-RESA Abs tend to correlate with the acquisition of natural immunity, and that both polyclonal or monoclonal anti-RESA Abs are able to inhibit erythrocyte invasion by merozoites in vitro (21). RESA3 belongs to the same Ring-infected Erythrocyte Surface Antigen family as RESA and shares high sequence homologies, notably at their C-terminal extremity, rich in EENVEE repeats (208). The functionality of anti-RESA3 Abs has so far been much less studied. Finally, LSA3 is expressed at the pre-erythrocytic stage and can induce protective Abs (209), but can also be found in infected red blood cells accordingly to Plasmodb. Of note, transcripts of LSA3 are also found in to okinetes according to the Malaria Cell Atlas.

Thus, B1E11K was found to cross react against several proteins of the asexual and sexual stage parasites rich in glutamic acid. As detailed below, investigations were undertaken to more precisely identify which were the antigens, then the epitopes, recognised.

2.1.2 Polyreactivity assay

To ensure that the ability of B1E11k to recognise different proteins in microarray and Western blot was not due to polyreactivity, the mAb was tested in ELISA against several human self-proteins, ssDNA and LPS and compared to 4.E10 (a known anti-HIV polyreactive Ab used as a positive control).

	B1E11K	4 E 10
ssDNA	0,0727	0,8608
GD1α	0,0451	0,8413
LPS	0,0466	0,6359
Transferrin	0,0625	0,4674
Apotransferrin	0,064	0,4795
Hemocyanin	0,0452	1,0091
Insulin	0,0496	1,2322
Cardiolipin	0,0403	1,0733
Albumin	0,0468	0,8253
Histone	0,0536	0,1788

Table 15: ELISA for polyreactivity of B1E11K.

O.D values for B1E11K and 4E10 Abs (at 50 µg/ml). Protocol described in material and methods.

The B1E11K mAb did not bind any of the antigens on the panel at a significant level, even at a high 50 ug/ml concentration, and therefore polyreactivity was ruled out.

2.1.3 Western blot

To further confirm the microarray results, our collaborators from Radboud University tested by Western blot B1E11K the binding to both sexual (gametocyte) and asexual stage parasite extracts. The binding of B1E11K to fragments of recombinant Pf11.1, RESA, RESA3 and LSA3 recombinant proteins were also tested.

Sequences of the recombinant protein fragments used can be found in supplementary data 5 to 10 and are written in light blue. Briefly, the recombinant "Pf11.1 protein" correspond to repeats of the VVPEVVEE motif, which spans Pf11.1. Recombinant RESA corresponds to amino acids 66 to 585 of the native protein and recombinant RESA3 to amino acids 570 to 1090. Finally, LSA3 corresponds to amino acid 67 to 822.

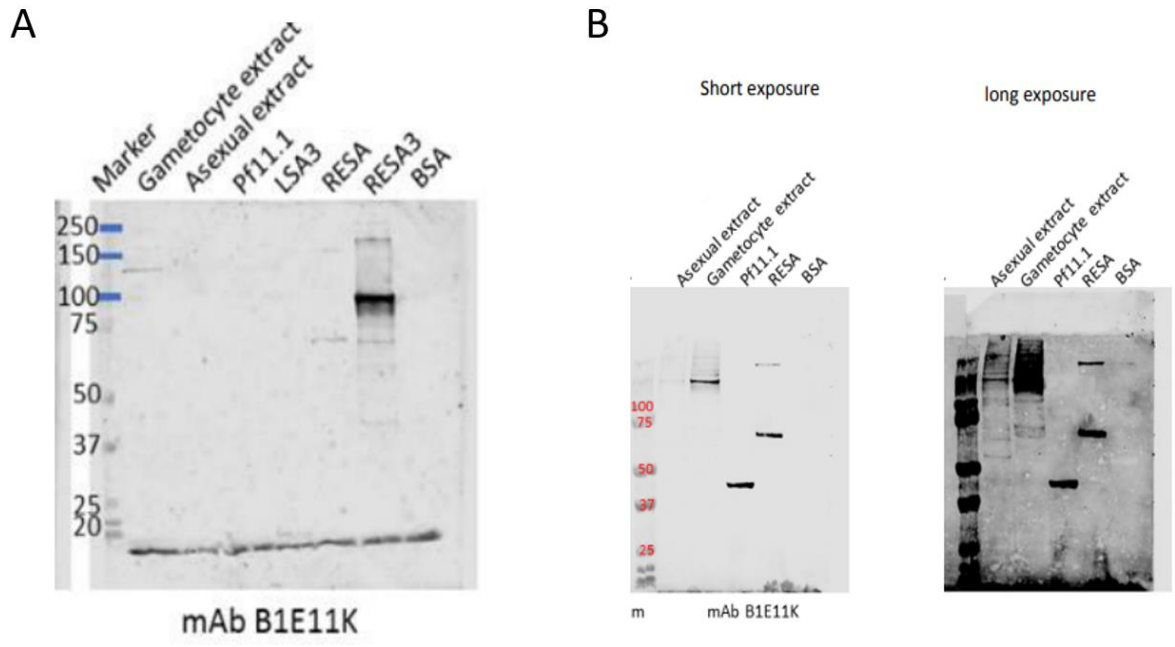

Figure 33: B1E11K binding to asexual and sexual parasite extracts and several recombinant proteins in Western blot analysis.

B1E11KmAb was diluted at 5µg/ml. A: B1E11K reactivity was tested against gametocyte / asexual extract (half a million of reduced gametocytes or asexual parasite was deposited per lane), and against the following truncated recombinant proteins: Pf11.1, LSA3, RESA, RESA3 (20 ng were deposited per lane). B: Western blot B was designed as a confirmation experiment, but showed contradictory results compared to Western blot A.

The results obtained were somehow different with the 2 Western blots (figure 33). However, the following information (which will have to be confirmed) could be retrieved:

B1E11K was shown to bind the two types of parasite extract, either gametocyte or asexual, with similar profiles for both types of extract: multiple bands with a main band at 130-140 kDa, as already obtained in the previous Western blots. Bands were of lower intensity for the asexual extract, suggesting the presence of lesser quantities of the recognised proteins.

Interestingly, recombinant RESA3 and Pf11.1 recombinant truncated proteins were recognised in Western blot A and B respectively. Their sequence includes the repeated EEXXEE motifs, which is in line with the hypothesis formulated previously, according to which B1E11K could recognize these types of motifs. Truncated recombinant LSA3 was not recognised in Western blot A, while it was the same construction recognised by B1E11K in microarray (which contains EENVEE motifs). Finally, truncated recombinant RESA was recognised in Western blot B and A (B1E11K recognition giving a band of very low intensity in the latter), although

the version of RESA used for the Western blot did not contain the EEXXEE motifs. It did, however, contain other many glutamic acid residues, spanning the whole sequence.

Thus, although not consistent, Western blot results suggested that B1E11K recognised proteins expressed at the asexual and sexual stage, and that they cross-react against the recombinant Pf11.1, RESA and RESA3 protein.

2.1.4 Gametocyte extract immunoprecipitation and mass spectrometry

Protein microarray and Western blot on recombinant proteins suggested that B1E11K could recognise Pf11.1, while Western blot against gametocyte extract suggested recognition of Pfs230. Thus, to confirm these results and verify that B1E11K did not recognise other proteins expressed at the sexual stage which were not selected for inclusion in the microarray, an immunoprecipitation (IPP) was performed with B1E11K on gametocyte extract, followed by mass spectrometry analysis to identify the immunoprecipitated antigens. Briefly, tosyl-activated beads were covalently decorated with B1E11K and incubated with gametocyte lysate to enable antigen capture. The immunoprecipitated antigens were eluted, and the elution fraction was run on a SDS Page gel and silver-stained. A negative control immunoprecipitation was performed using an anti-HIVgp120 Ab. Bands were selected and cut from the gel for mass spectrometry analysis on the basis of their presence in the sample immunoprecipitated by B1E11K and their absence in the negative control sample.

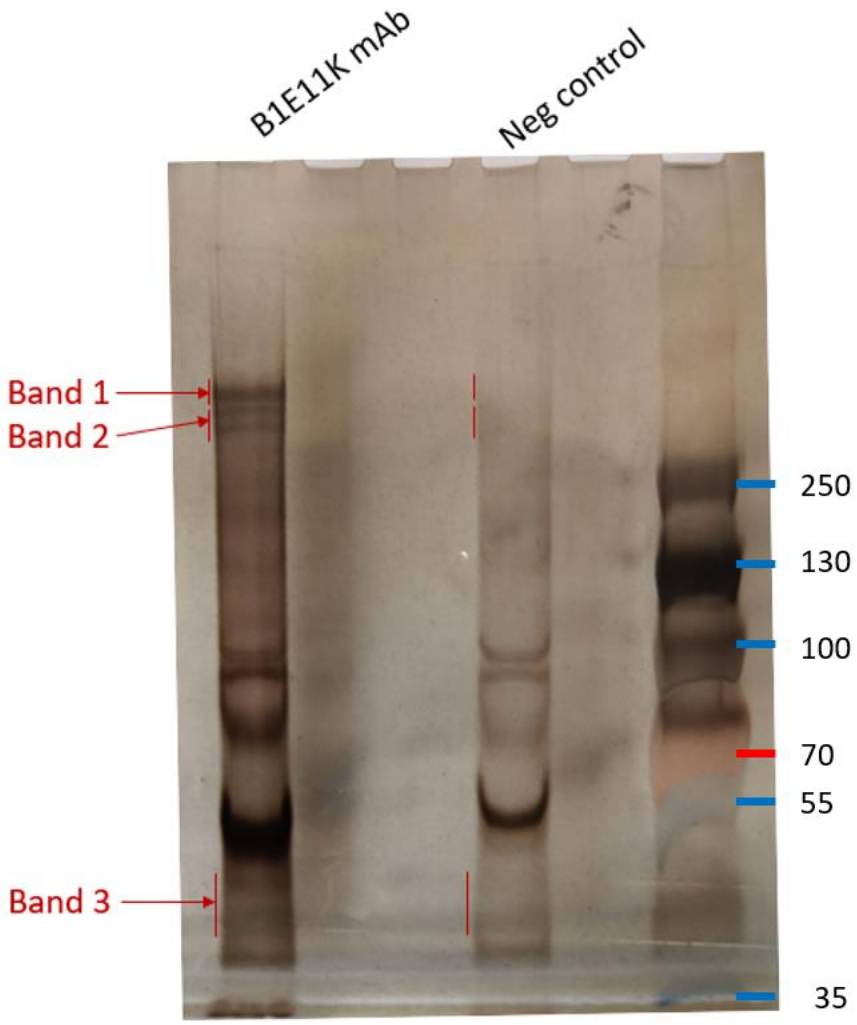

Figure 34: B1E11K immunoprecipitation results.

A Native Page 3-12% Bis Tris gel was used for protein separation (see Material and Methods) then silver stained. VRCO1, an anti-HIV mAb was used as a negative control.

Surprisingly, the recognition profile of the gametocyte extract by B1E11K was different from that of gametocyte extract Western blot, without multiple bands between 100 and 250 kDa. Of note, the intense band with a 66 kDa molecular weight, present in both lanes was due to the BSA used during the IPP.

As shown in figure 34, two bands with a molecular weight higher than 250 kDa, and a third one with a molecular weight lower than 55 kDa were seen in the B1E11K immunoprecipitate but were not present in the negative control. The 3 bands were cut and sent to Y. Couté at the Edyp platform (CEA Grenoble) for mass spectrometry analysis. Results were analysed by querying the entire proteome of *Plasmodium falciparum* (from the NF54 isolate) in the Uniprot database.

The results revealed Pfs230 as being the major component detected in bands 1 and 2. In bands 2 and 3, a small amount of EMP-1 trafficking protein was also detectable, but the level was too low to be considered as corresponding to specific binding.

Therefore, if the IPP showed Pfs230 as recognised, no other sexual stage proteins identified through the protein microarray, in particular Pf11.1, were identified. Several hypotheses may explain this result, such as the absence of binding of B1E11K to other proteins, the high abundancy of Pfs230 compared to the other proteins or potential technical issues with the experiments. Despite having chosen a gel suitable for high molecular weight proteins, the molecular weight of Pf11.1 being very high (estimated at 1 099 kDa), and the risk remains that Pf11.1 failed to enter the gel. However, it could also have been expected that degradation products of Pf11.1 successfully entered the gel. Such products were suspected to correspond to the 130-150 kDa bands observed in Western blot, which were not found in the IPP.
Moreover, since strips were cut from the gel for the downstream MS experiment according to an enrichment visible by eye in comparison to the control, it is possible we could have missed proteins of interest, not visible because present in small quantity. To overcome the limitations of gel migration or band selection against a negative control, it would have been possible to use an alternative technique and directly send the eluates to the MS platform, without having to run a gel, a technique used by the team of E. Sabido Aguade (Centre for Genomics Regulation, University Pompeu Fabra).

We decided to rule out that a confusion may have occurred during Ab production and that the Ab used for MS experiment was not B1E11K, but another Ab binding to Pfs230 and purified the same day. To explore this hypothesis, three different batches of B1E11K were sent to MALDI-TOF platform (Integrated Structural Biology Platform), together with B2E9L, an anti-Pfs230 Ab purified the same day as B1E11K.

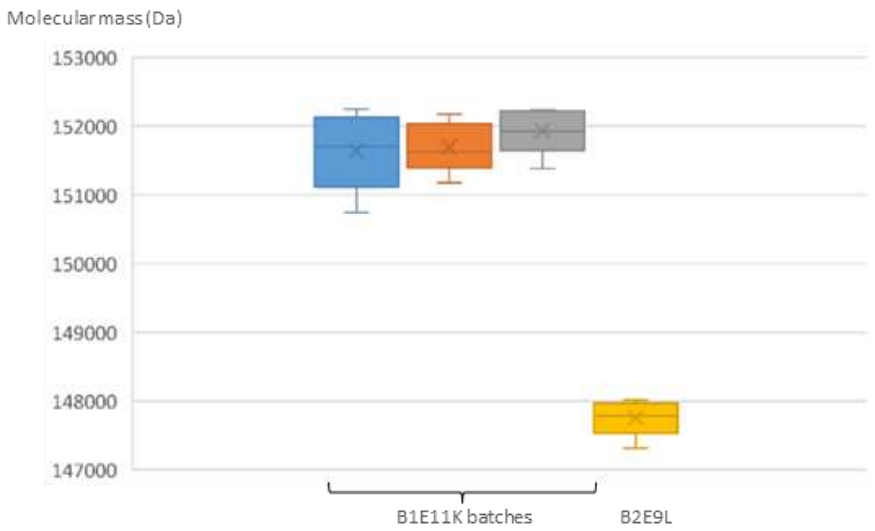

Figure 35: MALDI-TOF results of different B1E11K batches.

B1E11K batches are blue, orange and grey. Blue batch was used by TropIQ for their SMFA, grey batch was used for immunoprecipitation experiment. In yellow is B2E9L.

Figure 35 shows that the three B1E11K batches had the same molecular mass, therefore the Ab used for the immunoprecipitation was really B1E11K. Thus, the seemingly inconsistent results between immunoprecipitation, microarray and GE Western blot could not be explained by a difference in B1E11K batches. Of note, the theoretical molecular weight of B1E11K, calculated from its amino acid sequence is 144.04 kDa, while the average mass obtained in MALDI TOFF is 151.56 kDa. The difference between the two masses may be due to the presence of several glycosylation sites. Indeed, examination of the amino acid sequence of the heavy and light chains, revealed the presence of two consensus sequences for N-glycosylation in the heavy chain, one being in the Fab region.

2.1.5 Synthesis of peptides rich in glutamic-acid repeated motifs

Having identified amino-acid sequences that could potentially explain B1E11K cross-reactivity, nine peptides were synthesized (IBMM - SynBio3, P. Verdié team, Montpellier) to better characterise the binding of B1E11K to these EE-rich motifs. The peptides were synthesized with a biotin at the end terminus, followed by two aminohexanoyl residues (Ahx) used as spacers, and the sequences were terminated by two glycins. The addition of biotin allowed the use of streptavidin-coupled chips for BLI analysis, as described in the next section.

	Sequences synthesised	Molecular weight (g/mol)
Pfs230 *(P1)*	Biotin - Ahx- Ahx -EEVGEEVGEEVGEEVGEEVGEEVGEEVGEE-GG	2240
RESA *(P2)*	Biotin - Ahx – Ahx -EENVEENVEENVEENVEENVEENVEENVEENV-GG	2468
Pf11.1 *(P3)*	Biotin - Ahx – Ahx -EELVEEVIPEELVEEFIPEELVEEVIPEELVEEVIP-GG	2706
RESA *(8AA)*	Biotin - Ahx- Ahx -EENVEENV	1412.6
RESA *(10AA)*	Biotin - Ahx- Ahx - EENVEENVEE	1670.8
RESA *(12AA)*	Biotin - Ahx- Ahx - EENVEENVEENV	1884.1
RESA *(14AA)*	Biotin- Ahx- Ahx - EENVEENVEENVEE	2141.3
Pf11.1 *(VIP)*	Biotin - Ahx- Ahx - EELVEEVIPEELVEE	2236.3
Pf11.1 *(VVP)*	Biotin - Ahx- Ahx - EELVEEVVPEELVEE	2222.5

Table 16: List of the synthesised peptides with their amino-acid composition.
(In italic are the peptides abbreviated names used during analysis).

Two sets of peptides were sequentially synthesised: first the three upper peptides corresponding to Pfs230 (P1), RESA (P2) and Pf11.1 (P3) repeated motifs. Following experiments detailed below, suggesting that RESA was the preferentially recognised antigen, a second set of peptides was synthesised. These four peptides were designed to identify the minimal epitope allowing RESA binding. Of note, the Pf11.1 (P3) peptide sequence does not correspond to a sequence found naturally in the parasite, but to the fusion of two different EE-rich repeat motifs found on separate locations of the protein. Two alternative Pf11.1 peptides were thus synthesised, identical to the sequences naturally found in Pf11.1.

2.2 B1E11K binding to a panel of glutamic acid rich synthetic peptides

Interactions between the different peptides and B1E11K mAb were evaluated first by ELISA for rapid screening and peptide selection, then by BLI for precise characterisation of the interactions.

Of note, B2D10L having a similar binding profile than B1E11K when tested in gametocyte extract Western blot, its binding was also tested in ELISA and BLI with the same peptide panel than for B1E11K but showed no binding to any of the peptides.

2.2.1 Binding of the B1E11K whole IgG

2.2.1.1 IgG B1E11K binding to peptides in ELISA

B1E11K mAb binding to peptides was measured in ELISA, using streptavidin-coated plates to capture and orientate biotinylated peptides. EC50 values were determined as described in the Material and Methods section. As indicated figure 36A, B1E11K bound to the three P1, P2 and P3 peptides. However, binding to the RESA (P2) peptide was much stronger compared to the binding to of the Pfs 230 (P1) and Pf11.1 (P3) peptides. This motivated the synthesis of smaller RESA peptides for a more precise determination of the B1E11K minimal sequence recognized / minimal epitope. In contrast B2D10L recognition of the three peptides was very weak. Its binding was thus not investigated further in ELISA. When tested on the smaller RESA peptides panel, B1E11K mAb binding to P2 and RESA 14,12 or 10 AA was similar, with EC50s in the picomolar range, whereas no binding was observed for the 8 amino acid RESA peptide, suggesting the 10AA peptide contained the minimal epitope (see figures 36D and E). Finally, B1E11K mAb binding to Pf11.1 (VIP) and (VVP) was found to be similar to binding to Pf11.1 (P3), as indicated in 36F.

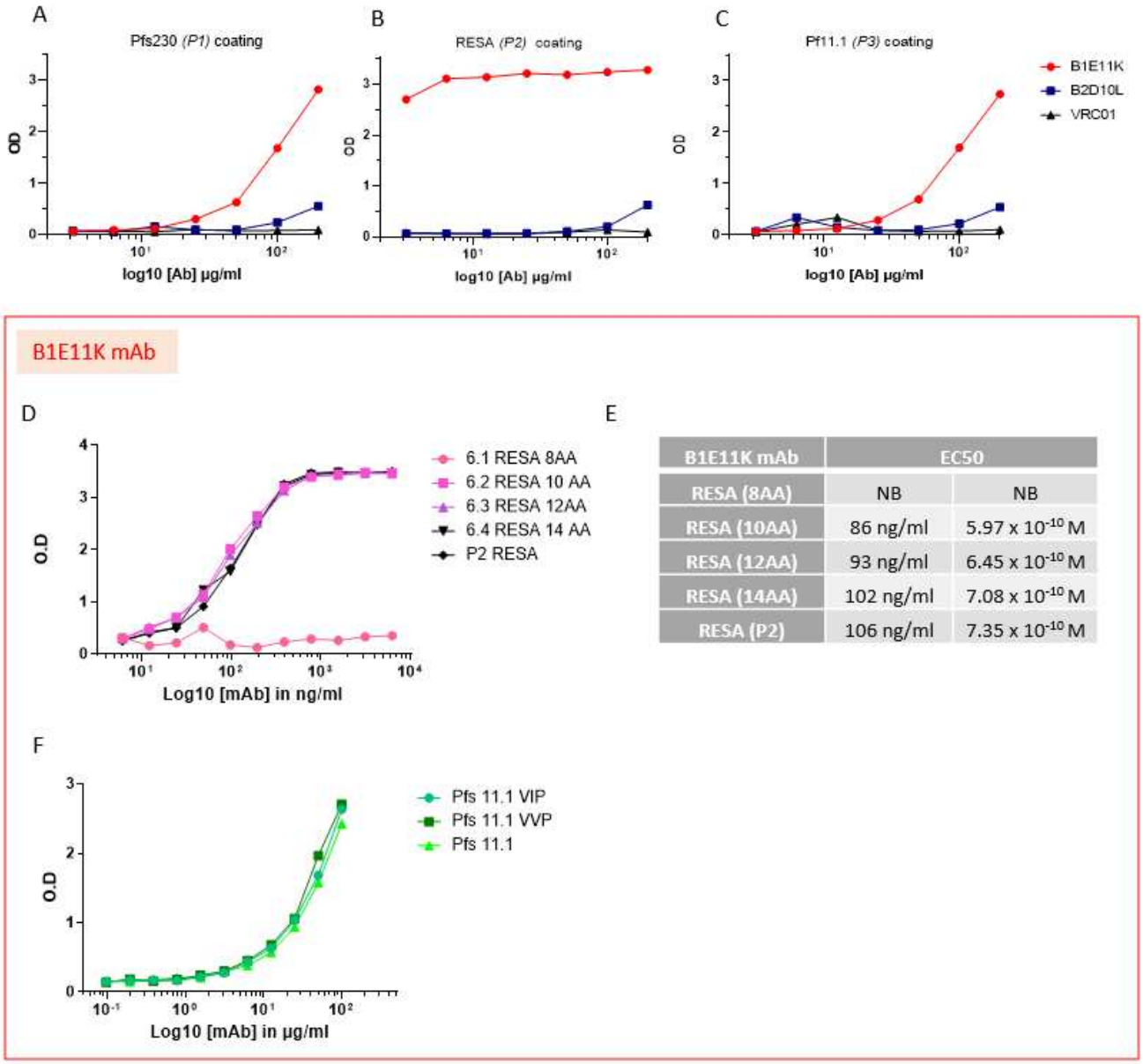

B1E11K mAb	EC50	
RESA (8AA)	NB	NB
RESA (10AA)	86 ng/ml	5.97 x 10^{-10} M
RESA (12AA)	93 ng/ml	6.45 x 10^{-10} M
RESA (14AA)	102 ng/ml	7.08 x 10^{-10} M
RESA (P2)	106 ng/ml	7.35 x 10^{-10} M

Figure 36: B1E11K binding to the different peptides in ELISA.

Potency of B1E11K and B2D10L mAbs binding to coated Pfs230 (P1) (A), RESA (P2) (B), Pf 11.1 (P3) (C). (VRCO1: anti-HIV mAb, negative control.) B1E11K mAb binding to RESA-derived peptides panel (D) and the corresponding calculated EC50 (E). (NB: not binding) BE11K mAb binding to Pf11.1-derived peptides panel (F). Of note, B1E11K mAb concentrations are not the same among the different experiments, but have been adapted to match B1E11K binding intensities on the different panels.

2.2.1.2 IgG B1E11K binding to peptides in BLI:

While ELISA helped to rapidly determine which peptides were recognised, BLI experiments were used to determine kinetic parameters: association and dissociation rate constants (k_{on} and k_{off}). Different set-up experiments were tested before performing the BLI experiments presented below. An initial configuration consisting in an anti-IgG Fc chip to capture B1E11K mAb and the soluble peptides as analytes was first attempted. However, their binding to B1E11K mAb could not be detected, as the peptides turned out to be too small of analytes. We finally immobilised the biotinylated peptides on streptavidin chips and used B1E11K as the analyte, as described in Material and Methods. The results obtained are presented in figure 39. It was not possible to determine B1E11K binding to Pfs230 *(P1)* and Pf11.1 *(P3)* using the same conditions as for the RESA peptide panel. Affinity of B1E11K for these peptides was so low for Pfs230 *(P1)* and Pf11.1 *(P3)* that constants determination would have required large quantities of peptides and Abs that were not available.

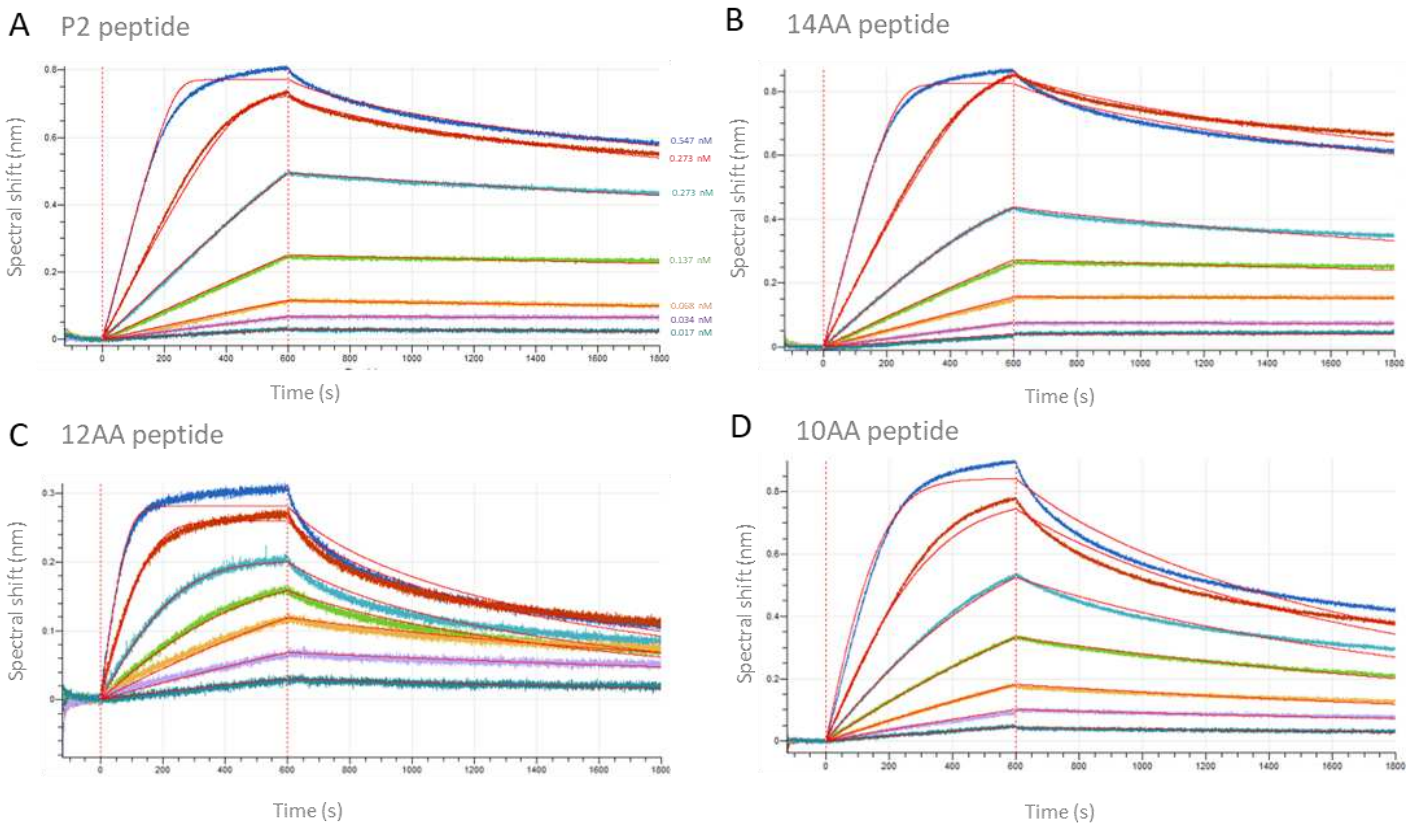

	K_D (M)	k_{on} ($M^{-1}s^{-1}$)	k_{off} (s^{-1})	Full R^2
RESA (P2)	6.12×10^{-12}	1.10×10^{8}	6.71×10^{-4}	0.9991
RESA (8AA)	NB			
RESA (10AA)	4.03×10^{-11}	2.76×10^{7}	1.11×10^{-3}	0.9949
RESA (12AA)	2.17×10^{-11}	8.70×10^{7}	1.89×10^{-3}	0.9881
RESA (14AA)	7.47×10^{-12}	7.69×10^{7}	5.74×10^{-4}	0.9991

Figure 37: BLI analysis of B1E11K mAb binding to the following RESA peptides: P2 (A), 14AA (B), 12AA (C), 10AA (D)

B1E11K concentrations used were the same for the four experiments, and ranging from 0.547 nM to 0.017 nM (two fold serial dilutions). Fitting model : 1:1 Langmuir and mass transfer.

Similarly to what is seen in ELISA, RESA 8AA was not recognised in BLI either, confirming RESA *(10AA)* contained the limiting epitope. B1E11K mAb recognised RESA P2, 14AA, 12AA, 10AA peptides. Because the two methods are different, comparison between the parameters measured with ELISA (EC_{50}) and BLI (K_D) is a bit hazardous. However, the affinity constants determined by BLI were in the same range as the EC50 values obtained using ELISA : in the picomolar range. The absence of progressive K_D increase with the shortening of the peptide may be explained by the avidity phenomenon. Briefly, the interactions between a mAb and its epitope are in fact a succession of attachment and detachment (k_{on} and k_{off}). A mAb having two Fabs, in case of detachment of one of the two arms, the other one can rapidly attach

itself in its place. This is particularly the case with the long repeats of RESA *(P2)*, where a succession of potential binding sites are placed next to each other, allowing the almost instantaneous rebinding of the mAb and giving low k_{off}, in the x 10^{-4} s^{-1} range.
One common solution to avoid the binding by each arm of the mAb of two closely ligands is to decrease the density of ligands coated on the sensorchips. Even if chips were coated with low concentrations of RESA (0.12 µg/ml) and the use of very short dipping times (15 sec), it was impossible to entirely get rid of the avidity phenomenon. As ITC experiments are performed in solution, they would have been more appropriate to get rid of the avidity phenomenon.

BLI results were analysed using the 1:1 Langmuir model coupled to the mass transfer model, as this was the best fit, however using the 1:1 interaction model is questionable when working with mAbs. The mass transfer model is used for interactions with a very low K_D, where the amount of available ligand becomes the limiting factor because of the rapidity of the reaction.

Finally, the experiments presented were only performed once, and it will be necessary in the future to perform at least duplicates of these measurements.

In order to study with precision the interactions between RESA *(P2)* and B1E11K binding site, the Fab of B1E11K was synthetised and its binding studied in ELISA and BLI (part 2.2.2).

2.2.2 Fab B1E11K

2.2.2.1 Fab production

In order to characterise the binding of B1E11K to the different peptides, while avoiding the bivalent binding and avidity phenomenon which occurs when working with mAbs, Fab production was performed as described in Material and Methods.

Several set-up experiments were performed, and different plasmid transfection ratios were tested, either a 1:1 (data not shown) or a 1:4 ratio (kappa: heavy), the latter being more appropriate to get rid of light chain dimers, as described by Spooner et al (210). Different affinity chromatography resins were also tested for Fab purification. The first one, the Pierce Protein L Agarose resin (Thermofisher, #20510) did not retain Fabs. This problem was solved using the Hi-Trap Kappaselect resin (Cytiva, #17545812), and SDS-PAGE analysis of the

purified Fab is shown in figure 38. In non-reducing conditions, two bands were visible at a molecular weight between 40 and 55 kDa. The higher molecular weight band may correspond to light chain dimers (MW: 47.23 kDa) or to glycosylated Fab (MW: 49.134 kDa) and the non-glycosylated Fab would correspond to the lower intensity band of lower molecular weight (MW: 47.134). Finally, the very low intensity band, with an approximative molecular weight of 25kDa most probably corresponds to light chain monomers, which are always produced in excess despite the 1:4 ratio.

Of note, we found out afterwards that the light chain dimers could have been removed by using an anti-CH1 column, but this column being very expansive, this solution has not been chosen for the moment.

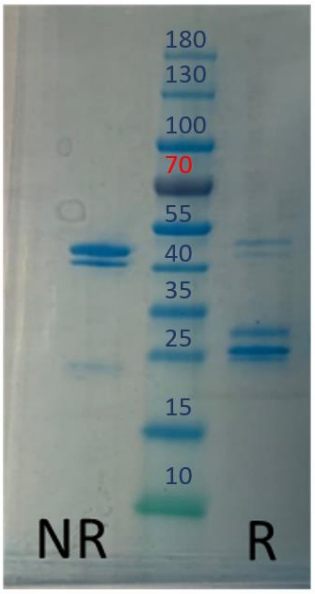

Figure 38: SDS PAGE analysis of purified B1E11K Fab transfected with a 1:4 ratio (light : heavy).

NR= non reduced, R= reduced, molecular weight page ruler plus, TF #26619

Treatment of the B1E11K and its Fab fragment with PNGase F, a glycosidase that removes N-linked oligosaccharides (kindly provided by N. Thielens, IBS) confirmed the presence of two Fab populations: one glycosylated and the other not. Indeed, as shown by SDS-PAGE analysis (figure 39), a shift in the migration of the Fab sample was observed following treatment with the glycosidase, confirming that roughly 75% of the fragment was produced glycosylated. A similar shift, although not as clear, was also observed with the full length the B1E11K mAb.

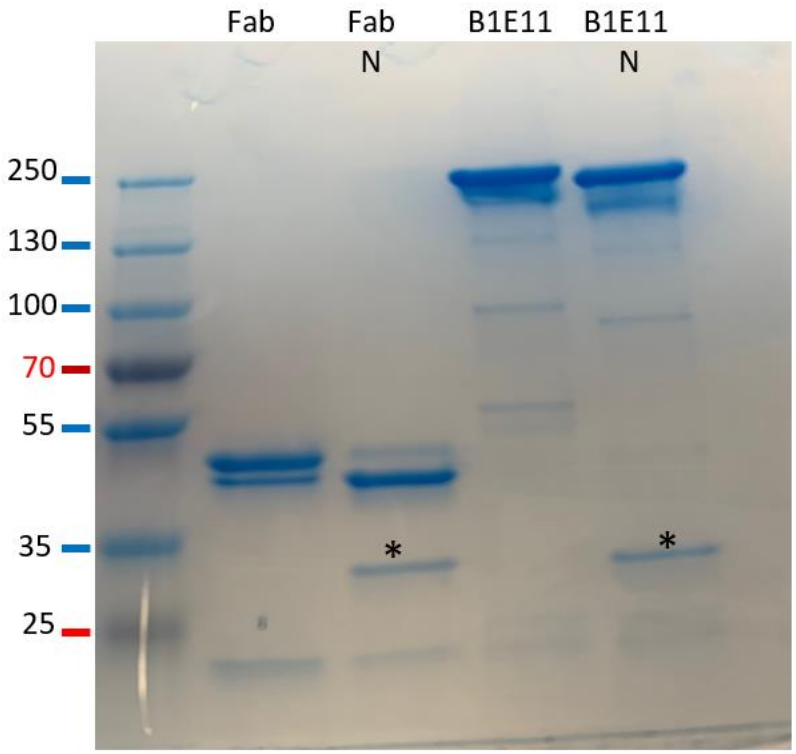

Figure 39: Non-reduced SDS gel of the B1E11K mAb and Fab with (N) or without N-glycanase treatment.

*Six micrograms of mAb or Fab were deposited in each well of a SDS-Page 4-20% gel. N : samples treated with PNGase F 10% (W/W), 2 x3h at 37 °C . *: bands due to the presence of glycanase.*

Thus, having successfully synthetised B1E11K Fab, it was then further used in ELISA and BLI experiments.

2.2.2.2 Fab B1E11K binding to peptides in ELISA

The produced Fab was then used to determine B1E11K binding to the peptide panels. As with the mAb, among P1, P2 and P3 peptides, RESA (P2) peptide was the one recognised with the highest potency, with an EC50 in the sub-nanomolar range (supplementary data 11). B1E11K Fab binding to RESA P2 and 14 AA was similar. A shift in IC50 was seen with RESA 10 and 12AA, conversely to what was observed with the mAb, reinforcing the hypothesis that the shift in affinity could have been hidden by the avidity effect.

A

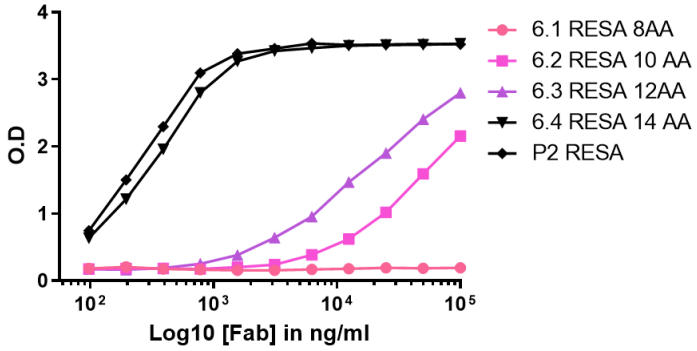

B

B1E11K Fab	EC50	
RESA (8AA)	NB	NB
RESA (10AA)	72.9 µg/ml	1.54 x 10^{-6} M
RESA (12AA)	23.5 µg/ml	4.98 x 10^{-7} M
RESA (14AA)	338.3 ng/ml	7.17 x 10^{-9} M
RESA (P2)	251.6 ng/ml	5 x 10^{-9} M

Figure 40: Summary of B1E11K Fab binding to the RESA peptides panel in ELISA (A) and the corresponding EC50.

(NB: not binding)

2.2.2.3 Fab B1E11K binding to peptides in BLI

RESA-P2 and B1E11K Fab binding analysis was performed using the same protocol as for B1E11K mAb, and the following results were obtained.

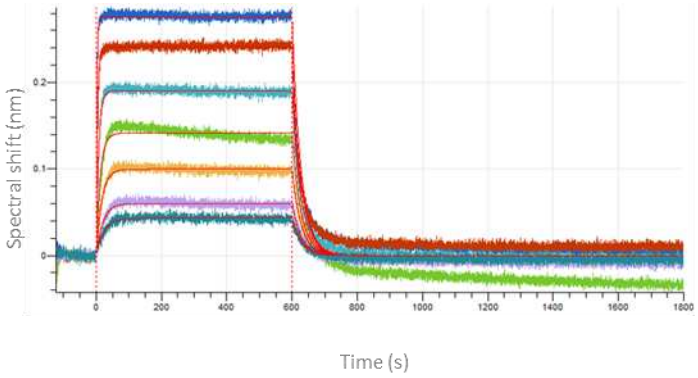

	KD (M)	k_{on} ($M^{-1}s^{-1}$)	K_{off} (s^{-1})	Full R^2
RESA (P2)	$5.05x10^{-8}$	$7.28x10^{5}$	$3.68x10^{-2}$	0.9858

Figure 41: Characteristics of B1E11K Fab binding to RESA (P2) peptide in BLI.

Interaction model used was 1:1 Langmuir. Fab concentration are spanning from 500 nM to 7,81nM (two-by-two sequential dilution).

Similarly to what was observed in ELISA, B1E11K Fab K_D (5.05 x 10^{-8} M) was lower compared to B1E11K mAb K_D (7.63 x 10^{-12} M), as shown figure 41. As for B1E11KmAb, to obtain more robust results, these experiments will be performed in duplicate or triplicate in the near future. Of note, kinetics could also have been determined at the steady-state, regarding the obtained curves.

To perform structural studies, the team of J-P Julien choose to synthetise the B1E11K Fab gene de-novo in a codon-optimized manner, getting rid of the N-glycosylation site present in the Fab HC variable part. This B1E11K Fab was also tested for its interaction with RESA-P2 peptides using BLI. K_D was 4.5 (± 0.7) x 10^{-8} M, k_{on} was 8 (± 2) x 10^5 M and k_{off} was 3.6 (± 0.4) x 10^{-2} M *(n=3)*, these results being in agreement with those obtained following the ELISA and BLI measures performed by our team. This suggests that the presence or absence of N-glycan has no impact on Fab binding to the RESA P2 peptide. The kinetics of the interaction between B1E11K Fab and P10 were also measured: K_D was 1.8 (± 0.3) x 10^{-7} M, k_{on} was 1.0 (± 0.4) x 10^4 M and k_{off} was 1.7 (± 0.6) x 10^{-1} M *(n=3*¸ with thus a change of 10 fold between the K_D obtained for the B1E11K Fab- RESA (P2) interaction versus the B1E11K Fab - RESA (10AA) interaction.

Results of B1E11K Fab binding to the other RESA peptides (14AA, 12AA and 10AA) are to come.

2.3 Research of the EENVEENVEE motif in the *Plasmodium falciparum* proteome

Knowing from ELISA and BLI experiments that the EENVEENVEE motif was B1E11K minimal epitope, this pattern was searched on the *Plasmodium falciparum* proteome using the Uniprot database (isolate NF54). The search aimed to complement the information provided by the microarray experiment, in case of proteins rich in this particular motif had not been selected in the composition of the chip. Of note, only RESA, RESA3 and LSA-3 protein were retrieved from the database and thus no protein particularly rich in EENVEENVEE was missed following microarray experiments.

2.4 Research of B1E11K cross-reactive motifs among the RESA protein

Collins et al (207) showed in the 90s that immunisation of Aotus monkeys with the EENVEE-rich region of RESA induced protective Ab responses against the development of parasitemia in some of the animals (2/5). These same animals also developed a cross-reactive serological response against the EENVEE and EENVEHDA motif, this latter spanning amino acids 900 to 909 of the protein. To explore B1E11K cross-reactivity to this EENVEHDA motif and to surrounding amino-acids, a third set of peptides was ordered (see table 17). Of note, precise EENVEHDA motif localisation is indicated in green in the RESA sequence (supplementary data 5).

	Sequences synthesised	Molecular weight (g/mol)
P10	Biotin - Ahx- Ahx -EENVEHDA	1392.6
P11	Biotin - Ahx- Ahx -EANVEHDAEENV	1805.8
P12	Biotin - Ahx- Ahx -EHDAEENVEHDA	1844
P13	Biotin - Ahx- Ahx -EENVEHDAEENV	1863

Table 17: EENVEHDA-derived synthetic peptides

B1E11K binding to this set of peptides was tested in a sandwich ELISA, using the same protocol as for previous peptides sets. B1E11K mAb (figure 42 A) and B1E11K Fab (figure 42 B) showed a very weak binding to P10, P11, P12, P13, similar to the binding observed with Pfs230 *(P1)* and Pf11.1 *(P3)*.

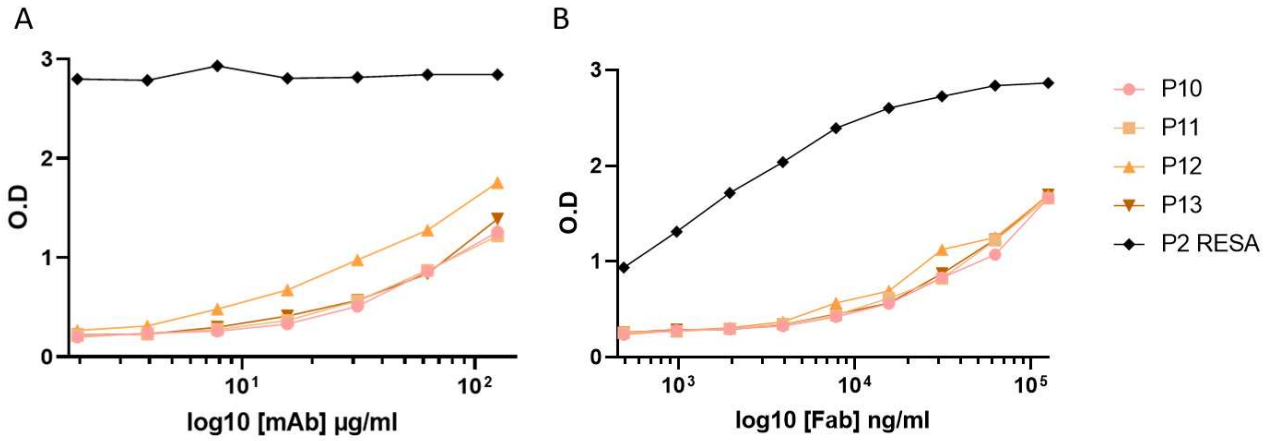

Figure 42 : B1E11K mAb and Fab binding to the EENVEHDA-derived set of peptides

2.5 B1E11K two-Fab binding to RESA (P2) peptide

The experiments presented in this last part of the thesis were entirely performed by J-P Julien's team, in particular by Randy Yoo, PhD student. The choice was made to present and discuss them, as they bring new and very interesting insights on B1E11K Fabs binding characteristics.

2.5.1 Fab B1E11K binding to peptides in ITC

Complementary to BLI experiments, J-P Julien team also tested B1E11K Fab binding to RESA-P2 and RESA 10 AA peptides using isothermal calorimetry (ITC).

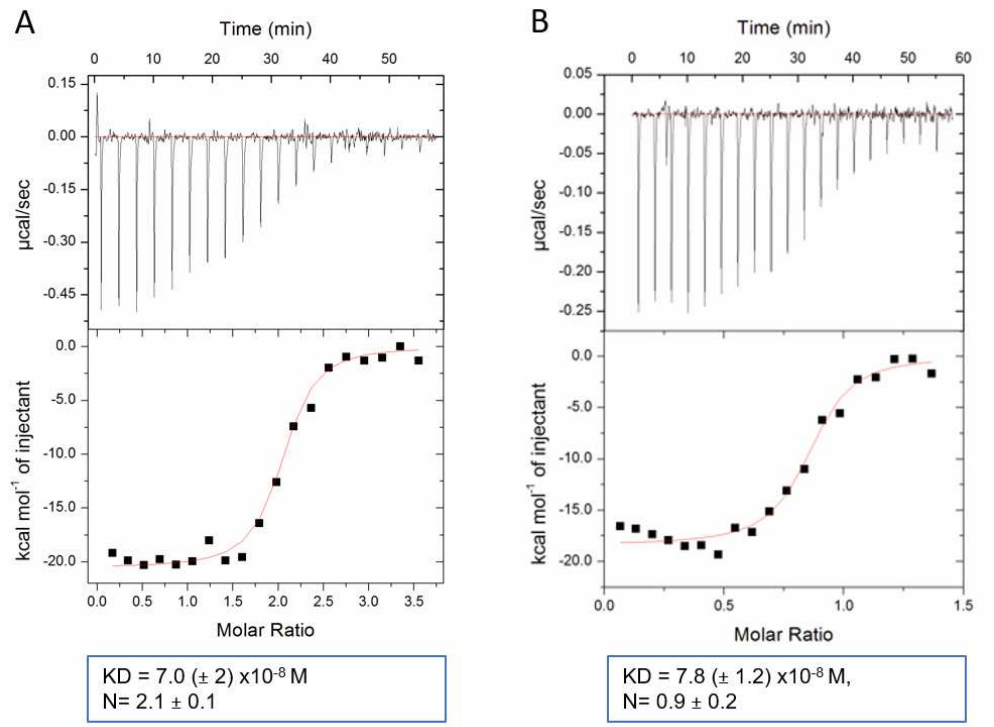

Figure 43: B1E11K Fab binding to RESA-P2 peptide (A) and RESA-10AA peptide (B) when measured in ITC.

Again, as seen in figure 43 A the values found for K_D when testing B1E11K Fab – RESA-P2 interaction were close to those obtained in BLI. In addition, when performing ITC experiments, the bivalent model was found to be the one best fitting the interaction, suggesting two Fabs could bind simultaneously on the RESA-P2 peptide. In addition, B1E11K Fab binding to RESA-10AA peptide (containing the limiting epitope) followed a monovalent interaction model (figure 43B).

In the light of these results, instead of the 1:1 Langmuir model used in BLI for fitting the Fab-RESA*(P2)* interaction, a 2:1 interaction model should have been used preferentially, to reflect the binding of two Fabs to a single RESA*(P2)* peptide.

This two Fabs binding hypothesis was confirmed when preparing Fab-RESA P2 complexes for crystallography experiments, as detailed below.

2.5.2 Homotypic B1E11K Fabs binding to RESA P2 peptide in electron microscopy:

As ITC data suggested binding of two Fabs to RESA *(P2)*, RESA *(P2)* complexes (6:1 ratio) were purified by SEC-MALS to perform electron microscopy experiments. A first peak was observed at 60 minutes, corresponding to 93 (+/- 2) kDa, i.e. the molecular weight of two Fabs and the peptide, and a second peak at 70 minutes corresponding to 49 (+/- 8) kDa, i.e. the molecular weight of a Fab bound to a peptide, confirming the hypothesis of double Fab binding (see supplementary data 9).

The electron microscopy results obtained using fractions of the first peak containing the 2:1 Fabs- RESA(P2) complexes are presented figure 44.

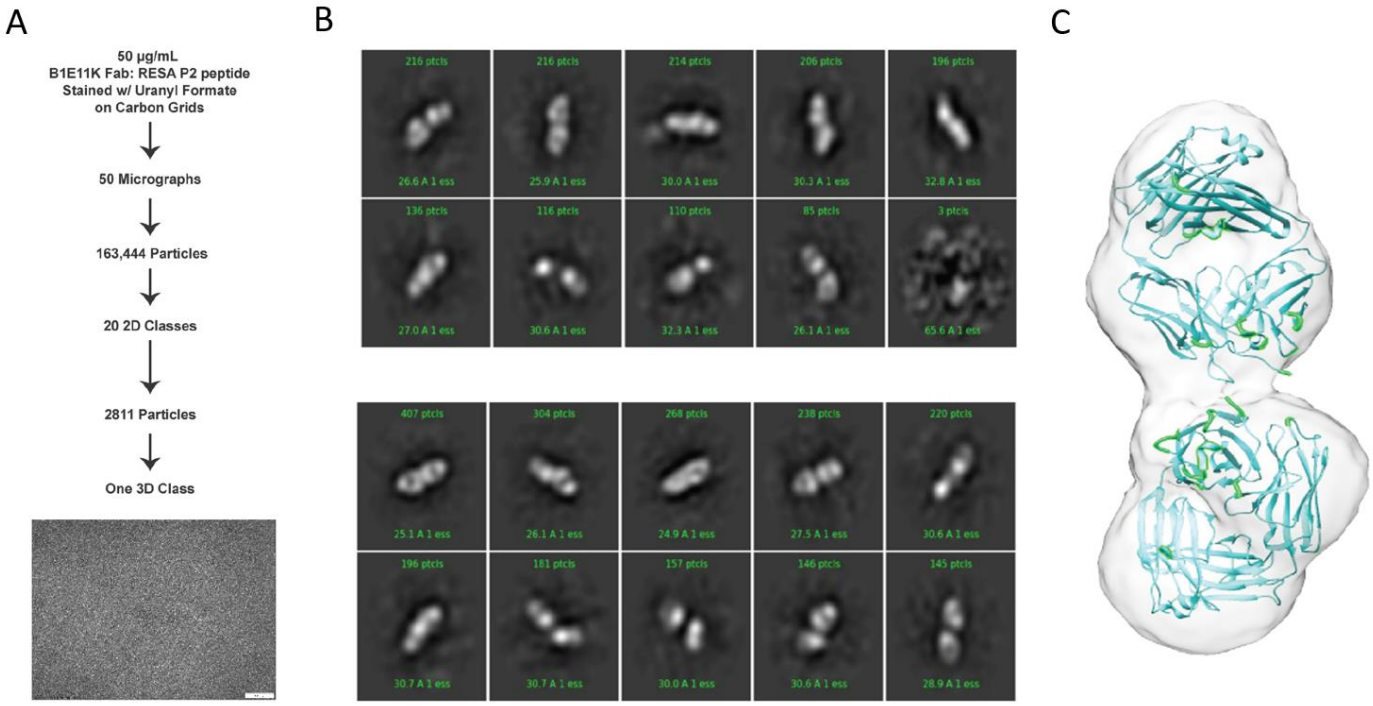

Figure 44: Electron microscopy imaging of two B1E11K Fabs in complex with one RESA *(P2)* peptide.

A :imaging process and obtained picture. B :images of the complexes using a magnifiction of 80,000X. Pixel size is 1.83 . C : complex 3D reconstruction.

The 2D classes revealed that the complex was flexible in nature, adopting many different conformations in which the Fabs engaged at various angles - the most predominant being a head-to-head approach, as showed in figure 44 B. Some particles consisted of a single Fab molecule, likely due to one of the two Fabs unbinding to the peptide due to the high off-rate. Overall, these findings highlighted the highly flexible and dynamic nature of the complex, which did not, however, block 3D reconstruction (figure 44 C). The resulting density permitted the fitting of two Fabs binding in a head-to-head conformation with substantial contacts between the two Fabs.

2.5.3 Homotypic B1E11K Fabs binding to RESA P2 peptide in crystallography experiments:

To fully understand both B1E11K peptide cross-reactivity and higher specificity to RESA, and to determine if complex formation involves homotypic interactions, X-ray crystallography experiments were performed. A crystal structure of the B1E11K:RESA P2 peptide complex at 3.0 A resolution was obtained (supplementary data 10). As expected from ITC, SEC-MALS, and nsEM data, the two Fabs engaged with the peptide with one Fab predominantly interacting with the N-terminal portion (designated hereafter “Fab A”) and the other interacting with mostly the C-terminal portion of the peptide (“Fab B”) as showed figure 45 A. Inspection of the electron density at the Fab:peptide interface revealed that the density at the interface was unambiguous and sufficient to generate a model with a high degree of confidence (figure 45B, 45C, and 45D).

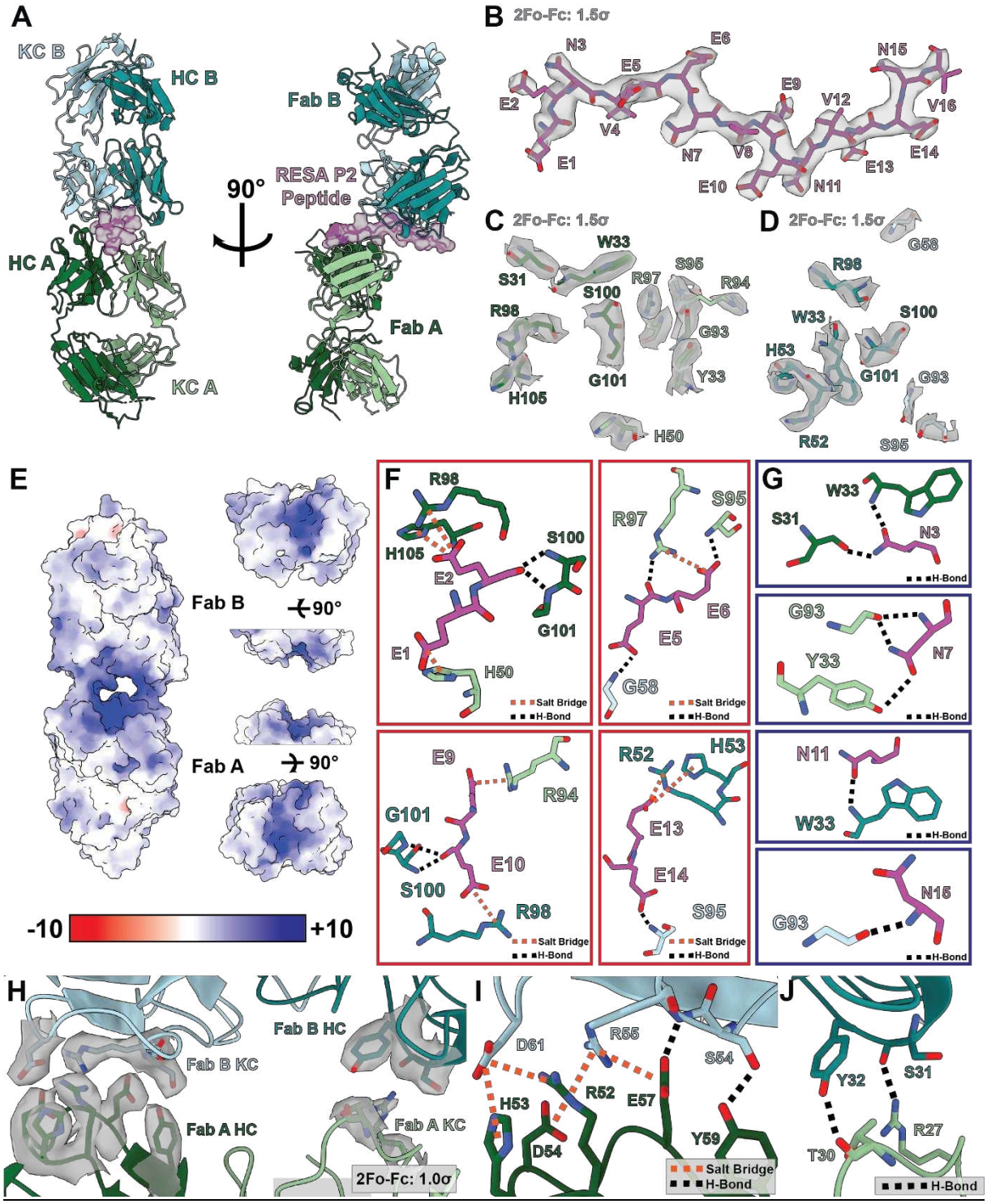

Figure 45: Cristallographic structure

A: General architecture of the B1E11K Fabs – RESA (P2) complex. RESA (P2) peptide is in pink. Fab A (dark green) and Fab B (light green) fixed the N-terminal and C-terminal part of the peptide respectively. B: electron density of RESA (P2) peptide. C: electron density of Fab A interacting amino acids. D: electron density of Fab B interacting amino acid. E: Couloumbic electrostatic surface coloring of the two B1E11K Fabs interacting together. F: B1E11K Fabs

amino acid engaged in interactions involving RESA P2 glutamic acids. G: B1E11K Fabs amino acid engaged in interactions involving RESA P2 asparagines. H: Fab-Fab interactions.

Each Fab formed a highly electropositive groove that closed off to form an off-shift tunnel when the two Fabs engaged with one another (figure 45E). The highly electropositive paratope of the Ab was complementary to the electronegative nature of the RESA, Pfs230, and Pf11.1 imparted to these proteins via their glutamic acid residue repeats. As expected, the interaction interface was highly dense in salt-bridges and hydrogen bonding interactions with minimal to no hydrophobic contacts (figure 45F).

RESA differed from Pfs230 and Pf11.1 as its repeats consisted of a polar amino acid residue: asparagine. The asparagine residues formed hydrogen bonding interactions with various side chains and backbone atoms in the paratope of B1E11K (figure 45G). The majority of interactions were mediated by the asparagine side chain. As Pfs230 and Pf11.1 lack polar residues and have either L or V amino-acid in these positions instead, binding capabilities of B1E11K were lower compared to RESA.

The crystal structure revealed that the two B1E11K Abs engaged in homotypic interactions (figures 45H, 45I and 45J). Among the two interfaces, the first was more extensively involving residues of the KCDR2 loop of Fab B and residues of HCDR2 of Fab A. Two salt-bridging networks were observed (figure 45I). First, Fab B's D61 sidechain participated in salt-bridging interactions with H53 and R52 of Fab A's HCDR2. The second network of salt bridges involved R55 of Fab B KCDR2 interacting with D54 and E57 of Fab A's HCDR2. In addition to these salt-bridging interactions, the backbone amide of R55 along with the sidechain hydroxyl of S54 participated in hydrogen bonding interactions with the side chains of E57 and Y59 of Fab A's HCDR2 loop. Finally, a less extensive hydrogen bonding interface involved the backbone carbonyl S31 and Y32 sidechain of Fab B's HCDR1 loop forming two hydrogen bonds with the R27 side chain and T30 backbone carbonyl KCDR1 of Fab A respectively (figure 45J).

Interestingly, some of the amino acids involved in homotypic interactions were mutated from germline (IGKV3-20 and IGHV3-7). This is the case for R27 and T30 in kC and H53 and R52 in HC. The latter two mutated amino acids also allowed binding to RESA, as do H50 and R94 in kC. This may suggest that B1E11K arose from an MBC select because of the double binding characteristics of it BCR, able to bind antigens with a strong affinity (amplified by the avidity

phenomenon), as well as able to engage in homotypic binding with neighbouring Fabs bound on adjacent repeats.

2.6 Growth inhibition assay

Finally, as micro-array and Western blot showed that B1E11K bound to RESA and RESA-3 recombinant proteins, because anti-RESA mAbs can have a growth inhibition activity, B1E11K was tested in Growth Inhibition Assay (GIA). Briefly, the test was performed as described by Malkin et al (211) : human erythrocytes parasitized with late trophozoite and schizont stages of *P.f* are cultured with the mAb to be tested, and results are compared to cultures performed with control mAbs. Thus, B1E11K was sent to the Miura lab to determine if it had GIA. Having a similar binding pattern to gametocyte extract in Western blot analysis, B2D10L was also selected.

mAb	Tested concentration (mg/ml)	Growth Inhibition Activity (%)
B1E11K	1	16.8
B2D10L	1	10.6
VRCO1	1	7.1
AMA1-C2 Std	0.456	49.4
AMA1-C2 Std	2.735	91.4

Table 18: B1E11K mAb growth inhibition activity.

The GIA was performed in the Miura lab. MAbs were used at 1 mg/ml unless otherwise specified. VRCO1 is an anti-HIV mAb used as a negative control. AMA1-C2 is a mAb with GIA, used as a positive control.

As indicated in table 18, B1E11K was not able to inhibit parasite erythrocytic growth, despite its ability to recognise the RESA and RESA-3 proteins. B2D10L also showed no functional activity.

2.7 The B1E11K mAb: conclusion and discussion

B1E11K was isolated through a screen based on its binding to gamete proteins in ELISA.

B1E11K recognition of gametes in SIFA is relatively low, around 20-30% of both WT and KO, which suggested that it did bind to a surface antigen, likely with a high affinity as the binding did not decrease significantly at lower Ab concentrations. Thus, the protein recognized at the surface may be expressed, at least at a level high enough to be detected, only on a fraction of the gametocytes. Although the B1E11K mAb did bind to a fraction of the gametes in SIFA, it finally did not show any functional activity in terms of reduction of transmission in the latest confirmation tests using manual counting SMFA, suggesting that the protein it targeted on the GMT surface was not involved in this process or that the Ab did not recognize a "transmission blocking" epitope.

We have shown that B1E11K highest affinity is for sequences from RESA and RESA3, proteins not expressed in gametes. Therefore, the selection of B1E11K in SIFA must have been through the binding to proteins with homologous sequences present in the gamete extract, such as Pfs230 and possibly Pfs11.1. Western blots of gametocyte extracts showed that B1E11K binds strongly to 2 proteins around 130 and 150 kDa, respectively. These may correspond to degradation products of Pfs11.1, as Pf11.1 is cleaved during gametocyte egress. In addition, Pfs230 appears to be also recognized in WB by the Ab. However, the identity of the antigen recognised in SIFA remains undefined. Indeed, only the cleaved form of Pfs230, i.e. devoid of the E rich domain, is supposed to be expressed at this stage.

Interestingly, ITC and electron microscopy experiments revealed the ability of two fabs to bind to a RESA *(P2)* peptide comprising eight overlapping EENVEE repeats, and crystallography experiments showed that the Fabs, when bound, engage in homotypic interactions, rendering peptide binding even more stable and stronger. As mentioned in introduction, this type of multiple Fab binding to repeats, which also allows homotypic binding, has been described for NANP repeats of the central part of the PfCSP. It has also been shown that such interactions stabilise the NANP-repeats region in a spiral-like conformation (212), not only for P. falciparum but also for CSP from other species, such as P. bergheii (213) and P. vivax (214). Currently, the EENVEE-rich C-terminal extremity of RESA is represented in Alphafold as a helix, but with a very low per-residue confidence score, and the same goes for RESA3 (see

supplementary data 11 and 12). The synthesis of a peptide that mimics the 20 overlapping EENVEE repeats found in RESA and the study of the B1E11K Fab binding to this long peptide in crystallography could provide insights on the conformational changes induced at the protein level.

Finally, B1E11K is one of the rare human mAbs against RESA described. Other anti-RESA human mAbs were obtained by Udomsangpetch (215) et al following EBV immortalisation in the 1980s. Though they proved to be able to inhibit parasite growth, their targeted epitopes were not determined. B1E11K is also one of the rare human mAbs described as having a cross-reactivity against glutamic-rich acids repeats. To our knowledge, MAb 33G2 is the only human Ab described that has similar properties (218) (219). It was described in the 1990s for its ability to block merozoite reinvasion of RBCs and was obtained following EBV immortalisation of MBC from a naturally immune Liberian donor. Its main antigen is Ag332 (220) and more precisely the epitope $Y(SVTEEIAEEDK)^2$ (1.9×10^8 M^{-1}). However, 33G2 was shown to cross-react with several glutamic acid-rich motifs of Pf11.1, the highest affinity constant being seen with EELVEEVIP (9.1×10^4 M^{-1}). Despite the ability of this mAb to bind Pf11.1, its TRA was not determined. Finally, 33G2 was also able to recognise RESA repeats, but with a much lower affinity than for B1E11K, in the order of 10^4 M^{-1}.

OVERALL CONCLUSION & DISCUSSION

My PhD project aimed to isolate human monoclonal Abs able to reduce the transmission of *P. falciparum* through the recognition of novel antigenic targets. Isolating mAbs for antigen discovery is more challenging than doing so against known antigens as commonly performed. Indeed, our approach required working with the whole *P. falciparum* pathogen and with complex functional assays. To our knowledge, in the malaria field, only one team used a similar approach to characterize antigens through an agnostic sorting followed by the screening of Ig containing supernatants: Tan et al (216) screened IgG and IgM producing cells from malaria naïve volunteers immunized with the PfSPZ vaccine and who were protected from controlled malaria infection. All human mAbs isolated to date following malaria infection or immunisation with the whole pathogen (irradiated sporozoite) target PfCSP. Concerning the sexual stage of the parasite, only one human mAb with TRA has been described to date: LMIV230-01. However, this mAb was obtained following immunisation with the domain 1 of Pfs230. Therefore, trying to obtain transmission reducing mAbs from naturally infected humans as we aimed for within this project was a first. The approach we took was overall successful, as we isolated seven different human mAbs with the sought-for activity. The isolation of mAbs recognizing the well-defined TRA target Pfs230 and Pfs48/45, clearly validated the strategy we used. Although no new target for TRAbs was described to date, the characterisation of the antigens recognized by some of the Abs isolated is still ongoing. Interestingly, preliminary results suggest that the anti-Pfs230 TRAbs we isolated may recognise a domain that has to date not been shown as involved in TRA. Furthermore, among the panel obtained, 2 mAbs with TRA appear to recognise a so far not characterised antigen, and further experiments will help define the corresponding proteins.

One of the Ab isolated, B1E11K, although not being able to reduce transmission, was shown to recognize proteins from various stages of the parasite, through the recognition of glutamate-rich motifs. The study of the binding of B1E11K to such repeated motifs in RESA brings new insights about immune responses towards repeated motifs found in *Pf* proteins. To date, most of the research on those concern the central NANP-repeats rich motifs of PfCSP. The evidence of homotypic binding between B1E11K Fabs bound to RESA *(P2)* peptide nicely supports the hypothesis formulated by Imkeller et al (217) that "antihomotypic affinity maturation may be a generalizable property of B cell responses if a repetitive antigen (malarial or other) brings two Abs into close proximity to optimize binding and promote clustering of surface Ig molecules through homotypic interactions ". Clustering of BCRs promotes MBCs activation and clonal expansion. To better understand how the B1E11K lineage evolved binding

to RESA repeats and homotypic interactions, germline reversion experiments will be carried out.

It has been demonstrated that some anti-RESA mAbs targeting EENVEE repeats region, and naturally developed during infection can have GIA (218). The molecular mechanisms behind this inhibition are yet not fully explained. Therefore isolating additional mAbs recognizing the EENVEENVEE motifs may allow the isolation of ones having the ability to inhibit growth, that could be either used for passive immunisations or to guide vaccine design. Indeed, the search for an erythrocytic stage vaccine, based on the RESA antigen, and more specifically EENVEE repeats, is at a standstill. As previously mentioned, encouraging results were obtained with monkey immunisations using EENVEE-rich repeats peptides, that induced GIA in two animals (207). Following these promising results, a vaccine was elaborated by Saul et al (219) in the early 2000s and administered in high transmission areas. However, it was not possible with this study to distinguish the protection conferred by vaccination to the one conferred by natural humoral responses (220). Different approaches can be envisioned for the obtention of further EENVEE-specific Abs. Additional Abs could be isolated through selection on peptides, from selected individuals whose serum showed GIA. Another option could be to resort to animal immunisation (possibly humanised mice) with the corresponding repeats, using for example decorated VLPs to increase immunogenicity. More broadly, mAbs cross-reacting against the EEVGEE (Pfs230) and/or the EELVEE (Pf11.1) repeats may be isolated using these approaches, ideally leading to the isolation of mAbs that could not only possess GIA but also TRA through the recognition of proteins from the different stage of P falciparum. Such cross-reacting mAbs able to have functional activities at different stages of the parasite cycle were defined by Nahrendorf et al (221) as “cross-stage protective malaria antigens” and could be particularly interesting for passive immunotherapies strategies.

BIBLIOGRAPHY

1. Chevillard C, Amen A, Besson S, Hannani D, Bally I, Dettling V, et al. Elicitation of potent SARS-CoV-2 neutralizing antibody responses through immunization with a versatile adenovirus-inspired multimerization platform. Molecular Therapy [Internet]. 2022;30(5):1913–25. Available from: https://doi.org/10.1016/j.ymthe.2022.02.011

2. Sulbaran G, Maisonnasse P, Amen A, Effantin G, Guilligay D, Dereuddre-Bosquet N, et al. Immunization with synthetic SARS-CoV-2 S glycoprotein virus-like particles protects macaques from infection. Cell Rep Med. 2022;3(2).

3. Phillips MA, Burrows JN, Manyando C, van Huijsduijnen RH, van Voorhis WC, Wells TNC. Malaria. Nat Rev Dis Primers. 2017;3.

4. Cowman AF, Healer J, Marapana D, Marsh K. Malaria: Biology and Disease. Cell [Internet]. 2016;167(3):610–24. Available from: http://dx.doi.org/10.1016/j.cell.2016.07.055

5. Kozlov M. Resistance to front-line malaria drugs confirmed in Africa. Nature. 2021;597(7878):604–604.

6. Maxmen A. Scientists hail historic malaria vaccine approval — but point to challenges ahead. Nature. 2021 Oct 8;

7. World Health Organization. World Malaria Report 2019. Geneva. [Internet]. 2019. 1–232 p. Available from: https://www.who.int/publications-detail/world-malaria-report-2019

8. WHO organisation. Global technical strategy for malaria. 2016.

9. Cox F. History of the discovery of the malaria parasitesand their vectors [Internet]. 2010. Available from: http://www.parasitesandvectors.com/content/3/1/5

10. Bousema T, Drakeley C. Epidemiology and infectivity of Plasmodium falciparum and Plasmodium vivax gametocytes in relation to malaria control and elimination. Clin Microbiol Rev. 2011;24(2):377–410.

11. Joice R, Nilsson SK, Montgomery J, Dankwa S, Egan E, Morahan B, et al. Plasmodium falciparum transmission stages accumulate in the human bone marrow. Sci Transl Med. 2014 Jul 6;6(244).

12. Venugopal K, Hentzschel F, Valkiūnas G, Marti M. Plasmodium asexual growth and sexual development in the haematopoietic niche of the host. [cited 2022 Jun 10]; Available from: www.nature.com/nrmicro

13. Meibalan E, Harvard MM. Biology of malaria transmission. Recent Advances in Malaria. 2016;87–124.

14. O. Billker, M.K Shaw, G. Margos, R.E Sinden. The roles of temperature pH and mosquito factors as triggers of male and female gametogenesis of Plasmodium berghei in vitro. Parasitology.

15. O. Billker, v. LIndo, M. Panico, A.E Etienne. Identification of xanthurenic acid as the putative inducer of malaria development in the mosquito. Letters to Nature . 1997;

16. OMS. Compendium of who malaria guidance. 2019. 1–31 p.

17. Hemingway J, Ranson H, Magill A, Kolaczinski J, Fornadel C, Gimnig J, et al. Averting a malaria disaster: Will insecticide resistance derail malaria control? The Lancet. 2016;387(10029):1785–8.

18. Conrad MD, Rosenthal PJ. Antimalarial drug resistance in Africa: the calm before the storm? Lancet Infect Dis. 2019;19(10):e338–51.

19. Eskenazi B, An S, Rauch SA, Coker ES, Maphula A, Obida M, et al. Prenatal Exposure to DDT and Pyrethroids for Malaria Control and Child Neurodevelopment: The VHEMBE Cohort, South Africa. Environ Health Perspect. 2018;126(11):119001.

20. Kurup SP, Butler NS, Harty JT. T cell-mediated immunity to malaria. Nat Rev Immunol [Internet]. 2019; Available from: http://dx.doi.org/10.1038/s41577-019-0158-z

21. Perlmann H, Perlmann P, Berzins K, Wåhlin B, Troye-Blomberg M, Hagstedt M, et al. Dissection of the human antibody response to the malaria antigen Pf155/RESA into epitope specific components. Immunol Rev. 1989;112(1):115–32.

22. Reiss T, Müller F, Pradel G. The impact of human complement on the clinical outcome of malaria infection. Mol Immunol [Internet]. 2022 Nov;151:19–28. Available from: https://linkinghub.elsevier.com/retrieve/pii/S0161589022004138

23. Inklaar MR, Barillas-Mury C, Jore MM. Deceiving and escaping complement – the evasive journey of the malaria parasite. Trends in Parasitology. Elsevier Ltd; 2022.

24. Ouédraogo AL, Roeffen W, Luty AJF, Vlas SJ de, Nebie I, Ilboudo-Sanogo E, et al. Naturally Acquired Immune Responses to Plasmodium falciparum Sexual Stage Antigens Pfs48/45 and Pfs230 in an Area of Seasonal Transmission. Infect Immun [Internet]. 2011 Dec 1 [cited 2019 Feb 18];79(12):4957–64. Available from: http://www.ncbi.nlm.nih.gov/pubmed/21969000

25. Cohen S, McGregor IA, Carrington S. Gamma-globulin and acquired immunity to human malaria. Nature. 1961;192(4804):733–7.

26. Tran TM, Li S, Doumbo S, Doumtabe D, Huang CY, Dia S, et al. An intensive longitudinal cohort study of malian children and adults reveals no evidence of acquired immunity to plasmodium falciparum infection. Clinical Infectious Diseases. 2013;57(1):40–7.

27. Snow RW, Omumbo JA, Lowe B, Molyneux CS, Obiero JO, Palmer A, et al. Relation between severe malaria morbidity in children and level of Plasmodium falciparum transmission in Africa. Lancet. 1997;349(9066):1650–4.

28. Langhorne J, Ndungu FM, Sponaas AM, Marsh K. Immunity to malaria: More questions than answers. Nat Immunol. 2008;9(7):725–32.

29. Whittaker C, Slater H, Nash R, Bousema T, Drakeley C, Ghani AC, et al. Global patterns of submicroscopic Plasmodium falciparum malaria infection: insights from a systematic review and meta-analysis of population surveys. Lancet Microbe. 2021;2(8):e366–74.

30. Ouédraogo AL, Gonçalves BP, Gnémé A, Wenger EA, Guelbeogo MW, Ouédraogo A, et al. Dynamics of the human infectious reservoir for malaria determined by mosquito feeding assays and ultrasensitive malaria diagnosis in Burkina Faso. Journal of Infectious Diseases. 2016;213(1):90–9.

31. Portugal S, Obeng-Adjei N, Moir S, Crompton PD, Pierce SK. Atypical memory B cells in human chronic infectious diseases: An interim report. Cell Immunol [Internet]. 2017 Nov [cited 2019 Apr 16];321:18–25. Available from: http://www.ncbi.nlm.nih.gov/pubmed/28735813

32. Portugal S, Tipton CM, Sohn H, Kone Y, Wang J, Li S, et al. Malaria-associated atypical memory B cells exhibit markedly reduced B cell receptor signaling and effector function. Elife. 2015;4(MAY):1–21.

33. Greta E Weiss*, Peter D. Crompton*, Shanping Li*, Laura A. Walsh* S. Atypical memory B cells are greatly expanded in individuals living in a malaria-endemic area. Bone. 2014;23(1):1–7.

34. Coppi A, Natarajan R, Pradel G, Bennett BL, James ER, Roggero MA, et al. The malaria circumsporozoite protein has two functional domains, each with distinct roles as sporozoites journey from mosquito to mammalian host. Journal of Experimental Medicine. 2011 Feb 14;208(2):341–56.

35. Herrington DA, Clyde DF, Losonsky G, Cortesia M, Murphy JR, Davis J, et al. Safety and immunogenicity in man of a synthetic peptide malaria vaccine against Plasmodium falciparum sporozoites. 1987.

36. Ripley W, Sherwood1 JA, Neva3 FA, Hoffman1 SL, Hollingdale4 MR, Hockmeyer1 WT, et al. Safety and efficacy of a recombinant DNA Plasmodium falciparum sporozoite vaccine. 1987.

37. Foquet L, Hermsen CC, van Gemert GJ, van Braeckel E, Weening KE, Sauerwein R, et al. Vaccine-induced monoclonal antibodies targeting circumsporozoite protein prevent Plasmodium falciparum infection. Journal of Clinical Investigation. 2014 Jan 2;124(1):140–4.

38. Fidel Zavala, James Tam, Allan Cochrane, Isabella Quakyi, Ruth Nussenzweig, Victor Nuessenzweig. Rationale for development of a synthetic vaccine against Plasmodium falciparum malaria. Sciences. 1985;

39. Drakeley CJ, Eling W, Teelen K, Bousema JT, Sauerwein R, Greenwood BM, et al. Parasite infectivity and immunity to Plasmodium falciparum gametocytes in Gambian children. Vol. 26, Parasite Immunology. 2004.

40. Saeed M, Roeffen W, Alexander N, Drakeley CJ, Targett GAT, Sutherland CJ. Plasmodium falciparum antigens on the surface of the gametocyte-infected erythrocyte. PLoS One. 2008 May 28;3(5).

41. Miura K, Takashima E, Deng B, Tullo G, Diouf A, Moretz SE, et al. Functional comparison of plasmodium falciparum transmission-blocking vaccine candidates by the standard membrane-feeding assay. Infect Immun. 2013 Dec;81(12):4377–82.

42. Carter R, Gwadz RW, McAuliffe FM. Plasmodium gallinaceum: Transmission-blocking immunity in chickens. I. Comparative immunogenicity of gametocyte- and gamete-containing preparations. Exp Parasitol. 1979;47(2):185–93.

43. Healer J, Mcguinness D, Hopcroft P, Haley S, Carter R, Riley E. Complement-Mediated Lysis of Plasmodium falciparum Gametes by Malaria-Immune Human Sera Is Associated with Antibodies to the Gamete Surface Antigen Pfs230 [Internet]. Vol. 65, INFECTION AND IMMUNITY. 1997. Available from: https://journals.asm.org/journal/iai

44. Miura K, Swihart BJ, Deng B, Zhou L, Pham TP, Diouf A, et al. Transmission-blocking activity is determined by transmission-reducing activity and number of control oocysts in Plasmodium falciparum standard membrane-feeding assay. Vaccine. 2016 Jul 29;34(35):4145–51.

45. Stone WJR, Churcher TS, Graumans W, van Gemert GJ, Vos MW, Lanke KHW, et al. A scalable assessment of Plasmodium falciparum transmission in the standard membrane-feeding assay, using transgenic parasites expressing green fluorescent protein-luciferase. Journal of Infectious Diseases. 2014 Nov 1;210(9):1456–63.

46. Miura K, Stone WJR, Koolen KM, Deng B, Zhou L, van Gemert GJ, et al. An inter-laboratory comparison of standard membrane-feeding assays for evaluation of malaria transmission-blocking vaccines. Malar J. 2016 Sep 9;15(1).

47. Drakeley CJ, Bousema JT, Akim NIJ, Teelen K, Roeffen W, Lensen AH, et al. Transmission-reducing immunity is inversely related to age in Plasmodium falciparum gametocyte carriers. Parasite Immunol. 2006 May;28(5):185–90.

48. Stone WJR, Dantzler KW, Nilsson SK, Drakeley CJ, Marti M, Bousema T, et al. Naturally acquired immunity to sexual stage P. Falciparum parasites. Parasitology. 2016;143(2):187–98.

49. Bousema T, Roeffen W, Meijerink H, Mwerinde H, Mwakalinga S, van Gemert GJ, et al. The dynamics of naturally acquired immune responses to Plasmodium falciparum sexual stage antigens Pfs230 & Pfs48/45 in a low endemic area in Tanzania. PLoS One. 2010;5(11).

50. le Roch KG, Johnson JR, Florens L, Zhou Y, Santrosyan A, Grainger M, et al. Global analysis of transcript and protein levels across the Plasmodium falciparum life cycle. Genome Res. 2004 Nov;14(11):2308–18.

51. Kaslow DC, Quakyi IA, Keister DB. Minimal variation in a vaccine candidate from the sexual stage of Plasmodium falciparum. Vol. 32, Molecular and Biochemical Parasitology. 1989.

52. Duffy PE, Kaslow DC. A Novel Malaria Protein, Pfs28, and Pfs25 Are Genetically Linked and Synergistic as Falciparum Malaria Transmission-Blocking Vaccines. Vol. 65, INFECTION AND IMMUNITY. 1997.

53. G. Pradel. Proteins of the malaria parasite sexual stages expression function and potential for transmission blocking strategies. Parasitology. 2007;

54. Stone WJR, Campo JJ, Ouédraogo AL, Meerstein-Kessel L, Morlais I, Da D, et al. Unravelling the immune signature of Plasmodium falciparum transmission-reducing immunity. Nat Commun [Internet]. 2018;9(1):1–14. Available from: http://dx.doi.org/10.1038/s41467-017-02646-2

55. Eksi S, Czesny B, van Gemert GJ, Sauerwein RW, Eling W, Williamson KC. Malaria transmission-blocking antigen, Pfs230, mediates human red blood cell binding to exflagellating male parasites and oocyst production. Mol Microbiol. 2006 Aug;61(4):991–8.

56. Gomes PS, Bhardwaj J, Rivera-Correa J, Freire-De-Lima CG, Morrot A. Immune escape strategies of malaria parasites. Vol. 7, Frontiers in Microbiology. Frontiers Media S.A.; 2016.

57. Burton DR. What are the most powerful immunogen design vaccine strategies?: A structural biologist's perspective. Cold Spring Harb Perspect Biol. 2017;9(11).

58. R. Rosenberg, R.A. Wirtz, I. Schneider, R. Burge. An estimation of the number of malaria sporozoites ejected by a feeding mosquito.

59. Triller G, Scally SW, Costa G, Pissarev M, Kreschel C, Bosch A, et al. Natural parasite exposure induces protective human anti- malarial antibodies. 2018;47(6):1197–209.

60. Gilson PR, Crabb BS. Morphology and kinetics of the three distinct phases of red blood cell invasion by Plasmodium falciparum merozoites. Int J Parasitol. 2009 Jan;39(1):91–6.

61. Tonwong N, Sattabongkot J, Tsuboi T, Iriko H, Takeo S, Sirichaisinthop J, et al. Natural Infection of Plasmodium falciparum Induces Inhibitory Antibodies against Gametocyte Development in Human Hosts. Vol. 65, Jpn. J. Infect. Dis. 2012.

62. Gardner MJ, Hall N, Fung E, White O, Berriman M, Hyman RW, et al. Genome sequence of the human malaria parasite Plasmodium falciparum. Nature. 2002;419(6906):498–511.

63. Swearingen KE, Lindner SE. Plasmodium Parasites Viewed through Proteomics. Trends Parasitol. 2018;34(11):945–60.

64. McCall MBB, Kremsner PG, Mordmüller B. Correlating efficacy and immunogenicity in malaria vaccine trials. Semin Immunol. 2018;39(August):52–64.

65. Barry AE, Arnott A. Strategies for Designing and Monitoring Malaria Vaccines Targeting Diverse Antigens. Front Immunol. 2014 Jul 28;5.

66. Scherf A, Lopez-Rubio JJ, Riviere L. Antigenic Variation in Plasmodium falciparum . Annu Rev Microbiol. 2008;62(1):445–70.

67. Wright GJ, Rayner JC. Plasmodium falciparum Erythrocyte Invasion: Combining Function with Immune Evasion. PLoS Pathog. 2014;10(3).

68. Scally SW, Julien JP. Peek-Peak-Pique: Repeating Motifs of Subtle Variance Are Targets for Potent Malaria Antibodies. Immunity. 2018;48(5):851–4.

69. D J Kemp, R L Coppel and, Anders RF. Repetitive Proteins and Genes of Malaria. http://dx.doi.org/101146/annurev.mi41100187001145 [Internet]. 2003 Nov 28 [cited 2022 Jul 22];41(1):181–181. Available from: https://www.annualreviews.org/doi/abs/10.1146/annurev.mi.41.100187.001145

70. Pholcharee T, Oyen D, Flores-Garcia Y, Gonzalez-Paez G, Han Z, Williams KL, et al. Structural and biophysical correlation of anti-NANP antibodies with in vivo protection against P. falciparum. Nat Commun. 2021;12(1).

71. Langowski MD, Khan FA, Savransky S, Brown DR, Balasubramaniyam A, Harrison WB, et al. Restricted valency (NPNA)n repeats and junctional epitope-based circumsporozoite protein vaccines against Plasmodium falciparum. NPJ Vaccines. 2022;7(1):16–23.

72. Bigman LS, Iwahara J, Levy Y. Negatively Charged Disordered Regions are Prevalent and Functionally Important Across Proteomes. J Mol Biol. 2022 Jul 30;434(14).

73. Hou N, Jiang N, Ma Y, Zou Y, Piao X, Liu S, et al. Low-Complexity Repetitive Epitopes of Plasmodium falciparum Are Decoys for Humoural Immune Responses. Front Immunol. 2020;11(April):1–13.

74. Rappuoli R, Aderem A. A 2020 vision for vaccines against HIV, tuberculosis and malaria. Nature. 2011;473(7348):463–9.

75. WHO. Word Malaria Report 2021. Word Malaria report Geneva: World Health Organization. (2021). Licence: CC. 2021. 2013–2015 p.

76. Laurens MB. RTS,S/AS01 vaccine (Mosquirix™): an overview. Hum Vaccin Immunother. 2019;

77. Olotu A, Fegan G, Wambua J, Nyangweso G, Leach A, Lievens M, et al. Seven-Year Efficacy of RTS,S/AS01 Malaria Vaccine among Young African Children. New England Journal of Medicine. 2016 Jun 30;374(26):2519–29.

78. Prudêncio M, Costa JC. Research funding after COVID-19. Nat Microbiol. 2020;5(August):2020.

79. Vaccine M, Roadmap T, Global WHO. 2013 Update to the Malaria Vaccine Technology Roadmap. 2013;

80. Duffy PE, Patrick Gorres J. Malaria vaccines since 2000: progress, priorities, products. Vol. 5, npj Vaccines. Nature Research; 2020.

81. Reuling IJ, van de Schans LA, Coffeng LE, Lanke K, Meerstein-Kessel L, Graumans W, et al. A randomized feasibility trial comparing four antimalarial drug regimens to induce Plasmodium falciparum gametocytemia in the controlled human malaria infection model. Elife. 2018;7:1–19.

82. Stanisic DI, McCarthy JS, Good MF. Controlled human malaria infection: Applications, advances, and challenges. Infect Immun. 2018 Jan 1;86(1).

83. R. s. NUSSENZWEIG J. VANDERBERG H. MosT C. ORTON. Protective immunity produced by the injection of X irradiated sporozoites of Plasmodium berghei.

84. Rieckmann KH, Beaudoin IRL, Cassells JS, Sell KW. Use of attenuated sporozoites in the immunization of human volunteers against falciparum malaria *. 57:261–5.

85. Sissoko MS, Healy SA, Katile A, Zaidi I, Hu Z, Kamate B, et al. Safety and efficacy of a three-dose regimen of Plasmodium falciparum sporozoite vaccine in adults during an intense malaria transmission season in Mali: a randomised, controlled phase 1 trial. Lancet Infect Dis. 2022 Mar 1;22(3):377–89.

86. Oneko M, Steinhardt LC, Yego R, Wiegand RE, Swanson PA, Kc N, et al. Safety, immunogenicity and efficacy of PfSPZ Vaccine against malaria in infants in western Kenya: a double-blind, randomized, placebo-controlled phase 2 trial. Nat Med. 2021 Sep 1;27(9):1636–45.

87. Kublin JG, Mikolajczak SA, Sack BK, Fishbaugher ME, Seilie A, Shelton L, et al. Complete attenuation of genetically engineered Plasmodium falciparum sporozoites in human subjects. Sci Transl Med. 2017;9(371):1–12.

88. Mwakingwe-Omari A, Healy SA, Lane J, Cook DM, Kalhori S, Wyatt C, et al. Two chemoattenuated PfSPZ malaria vaccines induce sterile hepatic immunity. Nature. 2021;595:15.

89. Casares S, Brumeanu TD, Richie TL. The RTS,S malaria vaccine. Vol. 28, Vaccine. 2010. p. 4880–94.

90. Agnandji ST, Lell B, Fernandes JF, Abossolo BP, Kabwende AL, Adegnika AA, et al. Efficacy and Safety of the RTS,S/AS01 Malaria Vaccine during 18 Months after Vaccination: A Phase 3 Randomized, Controlled Trial in Children and Young Infants at 11 African Sites. PLoS Med. 2014;11(7).

91. Tan J, Sack BK, Oyen D, Zenklusen I, Piccoli L, Barbieri S, et al. A public antibody lineage that potently inhibits malaria infection through dual binding to the circumsporozoite protein. Nat Med. 2018;24(4):401–7.

92. Pringle JC, Carpi G, Almagro-Garcia J, Zhu SJ, Kobayashi T, Mulenga M, et al. RTS,S/AS01 malaria vaccine mismatch observed among Plasmodium falciparum isolates from southern and central Africa and globally. Sci Rep. 2018;8(1).

93. Datoo MS, Natama MH, Somé A, Traoré O, Rouamba T, Bellamy D, et al. Efficacy of a low-dose candidate malaria vaccine, R21 in adjuvant Matrix-M, with seasonal administration to children in Burkina Faso: a randomised controlled trial. The Lancet. 2021;397(10287):1809–18.

94. Kariu T, Ishino T, Yano K, Chinzei Y, Yuda M. CelTOS, a novel malarial protein that mediates transmission to mosquito and vertebrate hosts. Mol Microbiol. 2006 Mar;59(5):1369–79.

95. Bergmann-Leitner ES, Mease RM, de la Vega P, Savranskaya T, Polhemus M, Ockenhouse C, et al. Immunization with pre-erythrocytic antigen CelTOS from plasmodium falciparum elicits cross-species protection against heterologous challenge with Plasmodium berghei. PLoS One. 2010;5(8).

96. Khan F, Porter M, Schwenk R, DeBot M, Saudan P, Dutta S. Head-to-head comparison of soluble vs. Qβ VLP circumsporozoite protein vaccines reveals selective enhancement of NANP repeat responses. PLoS One. 2015;10(11):1–18.

97. McCoy ME, Golden HE, Doll TA, Yang Y, Kaba SA, Zou X, et al. Mechanisms of protective immune responses induced by the Plasmodium falciparum circumsporozoite protein-based, self-assembling protein nanoparticle vaccine. Malar J. 2013;12(1).

98. Janitzek CM, Matondo S, Thrane S, Nielsen MA, Kavishe R, Mwakalinga SB, et al. Bacterial superglue generates a full-length circumsporozoite protein virus-like particle vaccine capable of inducing high and durable antibody responses. Malar J. 2016;15(1):1–9.

99. Mallory KL, Taylor JA, Zou X, Waghela IN, Schneider CG, Sibilo MQ, et al. Messenger RNA expressing PfCSP induces functional, protective immune responses against malaria in mice. NPJ Vaccines. 2021;6(1):1–12.

100. Bliss CM, Bowyer G, Anagnostou NA, Havelock T, Snudden CM, Davies H, et al. Assessment of novel vaccination regimens using viral vectored liver stage malaria vaccines encoding ME-TRAP. Sci Rep [Internet]. 2018;8(1):1–17. Available from: http://dx.doi.org/10.1038/s41598-018-21630-4

101. Tiono AB, Nébié I, Anagnostou N, Coulibaly AS, Bowyer G, Lam E, et al. First field efficacy trial of the ChAd63 MVA ME-TRAP vectored malaria vaccine candidate in 5-17 months old infants and children. PLoS One. 2018;13(12):1–19.

102. Rampling T, Ewer KJ, Bowyer G, Edwards NJ, Wright D, Sridhar S, et al. Safety and efficacy of novel malaria vaccine regimens of RTS,S/AS01B alone, or with concomitant ChAd63-MVA-vectored vaccines expressing ME-TRAP. NPJ Vaccines. 2018 Dec 1;3(1).

103. Bargieri DY, Andenmatten N, Lagal V, Thiberge S, Whitelaw JA, Tardieux I, et al. Apical membrane antigen 1 mediates apicomplexan parasite attachment but is dispensable for host cell invasion. Nat Commun. 2013;

104. Beeson JG, Drew DR, Boyle MJ, Feng G, Fowkes FJI, Richards JS. Merozoite surface proteins in red blood cell invasion, immunity and vaccines against malaria. FEMS Microbiol Rev. 2016;40(3):343–72.

105. Illingworth JJ, Alanine DG, Brown R, Marshall JM, Bartlett HE, Silk SE, et al. Functional comparison of blood-stage plasmodium falciparummalaria vaccine candidate antigens. Front Immunol. 2019;10(JUN):1–17.

106. Payne RO, Silk SE, Elias SC, Miura K, Diouf A, Galaway F, et al. Human vaccination against RH5 induces neutralizing antimalarial antibodies that inhibit RH5 invasion complex interactions. JCI Insight. 2017;2(21):1–19.

107. Minassian AM, Silk SE, Barrett JR, Nielsen CM, Miura K, Diouf A, et al. Reduced blood-stage malaria growth and immune correlates in humans following RH5 vaccination. Med [Internet]. 2021;2(6):701-719.e19. Available from: https://doi.org/10.1016/j.medj.2021.03.014

108. Dutta S, Dlugosz LS, Drew DR, Ge X, Ababacar D, Rovira YI, et al. Overcoming Antigenic Diversity by Enhancing the Immunogenicity of Conserved Epitopes on the Malaria Vaccine Candidate Apical Membrane Antigen-1. PLoS Pathog. 2013;9(12):1–17.

109. Sirima SB, Richert L, Chêne A, Konate AT, Campion C, Dechavanne S, et al. PRIMVAC vaccine adjuvanted with Alhydrogel or GLA-SE to prevent placental malaria: a first-in-human, randomised, double-blind, placebo-controlled study. Lancet Infect Dis. 2020 May 1;20(5):585–97.

110. Mordmüller B, Sulyok M, Egger-Adam D, Resende M, de Jongh WA, Jensen MH, et al. First-in-human, Randomized, Double-blind Clinical Trial of Differentially Adjuvanted PAMVAC, A Vaccine Candidate to Prevent Pregnancy-associated Malaria. Clinical Infectious Diseases. 2019 Oct 15;69(9):1509–16.

111. Stanisic DI, Fink J, Mayer J, Coghill S, Gore L, Liu XQ, et al. Vaccination with chemically attenuated Plasmodium falciparum asexual blood-stage parasites induces parasite-specific cellular immune responses in malaria-naïve volunteers: A pilot study. BMC Med. 2018 Oct 8;16(1).

112. Coelho CH, Rappuoli R, Hotez PJ, Duffy PE. Transmission-Blocking Vaccines for Malaria: Time to Talk about Vaccine Introduction. Trends Parasitol [Internet]. 2019;35(7):483–6. Available from: https://doi.org/10.1016/j.pt.2019.04.008

113. Challenger JD, Olivera Mesa D, Da DF, Yerbanga RS, Lefèvre T, Cohuet A, et al. Predicting the public health impact of a malaria transmission-blocking vaccine. Nat Commun [Internet]. 2021;12(1):1–12. Available from: http://dx.doi.org/10.1038/s41467-021-21775-3

114. Carter R. Transmission blocking malaria vaccines. Vaccine. 2001 Mar 21;19(17–19):2309–14.

115. Takashima E, Tachibana M, Morita M, Nagaoka H, Kanoi BN, Tsuboi T. Identification of Novel Malaria Transmission-Blocking Vaccine Candidates. Front Cell Infect Microbiol. 2021;11(November):1–8.

116. McLeod B, Miura K, Scally SW, Bosch A, Nguyen N, Shin H, et al. Potent antibody lineage against malaria transmission elicited by human vaccination with Pfs25. Nat Commun. 2019;10(1).

117. de Jong RM, Tebeje SK, Meerstein-Kessel L, Tadesse FG, Jore MM, Stone W, et al. Immunity against sexual stage Plasmodium falciparum and Plasmodium vivax parasites. Immunol Rev. 2020;293(1):190–215.

118. Skinner J, Huang CY, Waisberg M, Felgner PL, Doumbo OK, Ongoib A, et al. Plasmodium falciparum gametocyte-specific antibody profiling reveals boosting through natural infection and identifies potential markers of gametocyte exposure. Infect Immun. 2015;83(11):4229–36.

119. Barr PJ, Green KM, Gibson HL, Bathurst IC, Quakyi IA, Kaslow DC. Recombinant Pfs25 Protein of Plasmodium falciparum elicits Malaria Transmission-blocking immunity in experimental Animals [Internet]. Available from: http://rupress.org/jem/article-pdf/174/5/1203/1101983/1203.pdf

120. Chaturvedi N, Bharti PK, Tiwari A, Singh N. Strategies & recent development of transmission-blocking vaccines against Plasmodium falciparum. Vol. 143, Indian Journal of Medical Research. Indian Council of Medical Research; 2016. p. 696–711.

121. Outchkourov NS, Roeffen W, Kaan A, Jansen J, Luty A, Schuiffel D, et al. Correctly folded Pfs48/45 protein of Plasmodium falciparum elicits malaria transmission-blocking immunity in mice. Proceedings of the National Academy of Sciences [Internet]. 2008;105(11):4301–5. Available from: http://www.pnas.org/cgi/doi/10.1073/pnas.0800459105

122. Singh SK, Plieskatt J, Chourasia BK, Fabra-García A, Garcia-Senosiain A, Singh V, et al. A Reproducible and Scalable Process for Manufacturing a Pfs48/45 Based Plasmodium falciparum Transmission-Blocking Vaccine. Front Immunol. 2021 Jan 11;11.

123. Lennartz F, Brod F, Dabbs R, Miura K, Mekhaiel D, Marini A, et al. Structural basis for recognition of the malaria vaccine candidate Pfs48/45 by a transmission blocking antibody. [cited 2018 Oct 22]; Available from: www.nature.com/naturecommunications

124. Pfs R, Keisterb DB, Muratovab O, Kaslowb DC. Recombinant Pfs230, a plasmodium falciparum gametocyte protein indueces antisera that recudes the infectivity of Plasmodium falciparum. 1995;75:33–42.

125. Bustamante PJ, Woodruff DC, Oh J, Keister DB, Muratova O, Williamson KC. Differential ability of specific regions of Plasmodium falciparum sexual-stage antigen, Pfs230, to induce malaria transmission-blocking immunity. Parasite Immunol. 2000;22(8):373–80.

126. Tachibana M, Wu Y, Iriko H, Muratova O, MacDonald NJ, Sattabongkot J, et al. N-terminal prodomain of Pfs230 synthesized using a cell-free system is sufficient to induce complement-dependent malaria transmission-blocking activity. Clinical and Vaccine Immunology. 2011;18(8):1343–50.

127. Farrance CE, Rhee A, Jones RM, Musiychuk K, Shamloul M, Sharma S, et al. A plant-produced Pfs230 vaccine candidate blocks transmission of Plasmodium falciparum. Clinical and Vaccine Immunology. 2011;18(8):1351–7.

128. Lee SM, Plieskatt J, Krishnan S, Raina M, Harishchandra R, King CR. Expression and purification optimization of an N-terminal Pfs230 transmission-blocking vaccine candidate. Protein Expr Purif. 2019 Aug 1;160:56–65.

129. Scherf A, Behr C, Sarthou J -L, Pla M, Rogier C, Trape J -F, et al. Immune response in mouse and malaria-exposed humans to peptides derived from Pfl1-1, a highly repetitive megadalton protein of Plasmodium falciparum. Eur J Immunol. 1993;23(7):1574–81.

130. Draper SJ, Sack BK, King CR, Nielsen CM, Rayner JC, Higgins MK, et al. Malaria Vaccines: Recent Advances and New Horizons. Cell Host Microbe [Internet]. 2018;24(1):43–56. Available from: https://doi.org/10.1016/j.chom.2018.06.008

131. Kurtovic L, Reiling L, Opi DH, Beeson JG. Recent clinical trials inform the future for malaria vaccines. Communications Medicine [Internet]. 2021;1(1):1–5. Available from: http://dx.doi.org/10.1038/s43856-021-00030-2

132. Healy SA, Anderson C, Swihart BJ, Mwakingwe A, Gabriel EE, Decederfelt H, et al. Pfs230 yields higher malaria transmission-blocking vaccine activity than Pfs25 in humans but not mice. Journal of Clinical Investigation. 2021 Apr 1;131(7).

133. de Graaf H, Payne RO, Taylor I, Miura K, Long CA, Elias SC, et al. Safety and Immunogenicity of ChAd63/MVA Pfs25-IMX313 in a Phase I First-in-Human Trial. Front Immunol. 2021;12(July):1–13.

134. Healy SA, Anderson C, Swihart BJ, Mwakingwe A, Gabriel EE, Decederfelt H, et al. Pfs230 yields higher malaria transmission-blocking vaccine activity than Pfs25 in humans but not mice. Journal of Clinical Investigation. 2021;131(7):1–10.

135. Phase T, Mccall M. First-in-Human Clinical Trial Initiated for Novel Malaria Transmission Blocking Vaccine. 2021;(July).

136. Chichester JA, Green BJ, Jones RM, Shoji Y, Miura K, Long CA, et al. Safety and immunogenicity of a plant-produced Pfs25 virus-like particle as a transmission blocking vaccine against malaria: A Phase 1 dose-escalation study in healthy adults. Vaccine. 2018 Sep 18;36(39):5865–71.

137. Kapulu MC, Da DF, Miura K, Li Y, Blagborough AM, Churcher TS, et al. Comparative assessment of transmission-blocking vaccine candidates against plasmodium falciparum. Sci Rep. 2015;5(January):1–15.

138. Bruno L, Cortese M, Rappuoli R, Merola M. Lessons from Reverse Vaccinology for viral vaccine design. Curr Opin Virol. 2015;11:89–97.

139. Rappuoli R. Reverse vaccinology Rino Rappuoli. Curr Opin Microbiol. 2000;445–50.

140. Serruto D, Bottomley MJ, Ram S, Giuliani MM, Rappuoli R. The new multicomponent vaccine against meningococcal serogroup B, 4CMenB: Immunological, functional and structural characterization of the antigens. Vaccine [Internet]. 2012;30(SUPPL. 2):B87–97. Available from: http://dx.doi.org/10.1016/j.vaccine.2012.01.033

141. Rappuoli R, Bottomley MJ, D'Oro U, Finco O, de Gregorio E. Reverse vaccinology 2.0: Human immunology instructs vaccine antigen design. J Exp Med [Internet]. 2016;213(4):469–81. Available from: http://www.jem.org/lookup/doi/10.1084/jem.20151960

142. Dennis R. Burton. Antibodies viruses and vaccines. Nature reivew immunology.

143. Finco O, Rappuoli R. Designing vaccines for the twenty-first century society. Vol. 5, Frontiers in Immunology. Frontiers Research Foundation; 2014.

144. Ahmad K, Malik HS, Bloom K, Milks KJ, Straight a F, Carroll CW, et al. Structure of RSV Fusion Glycoprotein. Science (1979). 2013;340(May):1113–7.

145. Hsieh C lin, Goldsmith JA, Schaub JM, Divenere AM, Kuo H che, Javanmardi K, et al. Structure-based design of prefusion-stabilized SARS-CoV-2 spikes. 2020;0826(July):1–9.

146. McLeod B, Mabrouk MT, Miura K, Ravichandran R, Kephart S, Hailemariam S, et al. Vaccination with a structure-based stabilized version of malarial antigen Pfs48/45 elicits ultra-potent transmission-blocking antibody responses. Immunity. 2022 Sep 13;55(9):1680-1692.e8.

147. Rappuoli R, Gregorio E De, Del G, Phogat S, Pecetta S. Vaccinology in the post − COVID-19 era. 2021;118(3):1–7.

148. Julien JP. Antibodies against Plasmodium falciparum malaria at the molecular level. Nat Rev Immunol [Internet]. Available from: http://dx.doi.org/10.1038/s41577-019-0209-5

149. Traggiai E, Becker S, Subbarao K, Kolesnikova L, Uematsu Y, Gismondo MR, et al. An efficient method to make human monoclonal antibodies from memory B cells: Potent neutralization of SARS coronavirus. Nat Med. 2004;10(8):871–5.

150. Lanzavecchia A, Corti D, Sallusto F. Human monoclonal antibodies by immortalization of memory B cells. Curr Opin Biotechnol. 2007;18(6):523–8.

151. Corti D, Lanzavecchia A. E ffi cient Methods To Isolate Human Monoclonal Antibodies from Memory B Cells and Plasma Cells. 2014;1–9.

152. Lu RM, Hwang YC, Liu IJ, Lee CC, Tsai HZ, Li HJ, et al. Development of therapeutic antibodies for the treatment of diseases. Vol. 27, Journal of Biomedical Science. BioMed Central Ltd.; 2020.

153. Guillaume Desoubeaxu, Mireia Pelegrin. Anticorps monoclonaux en infectiologie.

154. Daily JP. Monoclonal Antibodies — A Different Approach to Combat Malaria. New England Journal of Medicine [Internet]. 2022 Aug 4;387(5):460–1. Available from: http://www.nejm.org/doi/10.1056/NEJMe2207865

155. Kisalu NK, Idris AH, Weidle C, Flores-Garcia Y, Flynn BJ, Sack BK, et al. A human monoclonal antibody prevents malaria infection by targeting a new site of vulnerability on the parasite. Nat Med. 2018 May 1;24(4):408–16.

156. Gaudinski MR, Berkowitz NM, Idris AH, Coates EE, Holman LA, Mendoza F, et al. A Monoclonal Antibody for Malaria Prevention. New England Journal of Medicine. 2021;385(9):803–14.

157. Wang LT, Pereira LS, Flores-Garcia Y, O'Connor J, Flynn BJ, Schön A, et al. A Potent Anti-Malarial Human Monoclonal Antibody Targets Circumsporozoite Protein Minor Repeats and Neutralizes Sporozoites in the Liver. Immunity. 2020 Oct 13;53(4):733-744.e8.

158. Wu RL, Idris AH, Berkowitz NM, Happe M, Gaudinski MR, Buettner C, et al. Low-Dose Subcutaneous or Intravenous Monoclonal Antibody to Prevent Malaria. N Engl J Med [Internet]. 2022 Aug 4;387(5):397–407. Available from: http://www.ncbi.nlm.nih.gov/pubmed/35921449

159. Sherrard-Smith E, Sala KA, Betancourt M, Upton LM, Angrisano F, Morin MJ, et al. Synergy in anti-malarial pre-erythrocytic and transmission-blocking antibodies is achieved by reducing parasite density. Elife. 2018;

160. van der Boor SC, Smit MJ, van Beek SW, Ramjith J, Teelen K, van de Vegte-Bolmer M, et al. Safety, tolerability, and Plasmodium falciparum transmission-reducing activity of monoclonal antibody TB31F: a single-centre, open-label, first-in-human, dose-escalation, phase 1 trial in healthy malaria-naive adults. Lancet Infect Dis [Internet]. 2022 Aug; Available from: https://linkinghub.elsevier.com/retrieve/pii/S1473309922004285

161. de Jong RM, Meerstein-Kessel L, Da DF, Nsango S, Challenger JD, van de Vegte-Bolmer M, et al. Monoclonal antibodies block transmission of genetically diverse Plasmodium falciparum strains to mosquitoes. Vol. 6, npj Vaccines. Nature Research; 2021.

162. Kundu P, Semesi A, Jore MM, Morin MJ, Price VL, Liang A, et al. Structural delineation of potent transmission-blocking epitope I on malaria antigen Pfs48/45. Nat Commun [Internet].

2018 Dec 26 [cited 2019 Jan 14];9(1):4458. Available from: http://www.nature.com/articles/s41467-018-06742-9

163. Coelho CH, Tang WK, Burkhardt M, Galson JD, Muratova O, Salinas ND, et al. A human monoclonal antibody blocks malaria transmission and defines a highly conserved neutralizing epitope on gametes. Nat Commun [Internet]. 2021;1–12. Available from: http://dx.doi.org/10.1038/s41467-021-21955-1

164. Roeffen W, Geeraedts F, Eling W, Beckers P, Kumar N, Lensen T, et al. Transmission Blockade of Plasmodium falciparum Malaria by Anti-Pfs230-Specific Antibodies Is Isotype Dependent. Vol. 63, INFECTION AND IMMUNITY. 1995.

165. Plasmodium Falciparum a comparison of the activity of Pfs230 specific antibiodies in an assay of transmission blocking immunity and specific competition ELISAs.

166. Quakyi IA, Carter R, Rener J, Kumar N, Good MF, Miller LH. The 230-kDa gamete surface protein of Plasmodium falciparum is also a target for transmission-blocking antibodies. The Journal of Immunology. 1987;139(12).

167. Coelho CH, Tang WK, Burkhardt M, Galson JD, Muratova O, Salinas ND, et al. A human monoclonal antibody blocks malaria transmission and defines a highly conserved neutralizing epitope on gametes. Nat Commun. 2021 Dec 1;12(1).

168. Roeffen W, Teelen K, van As J, vd Vegte-Bolmer M, Eling W, Sauerwein R. Plasmodium falciparum: Production and characterization of rat monoclonal antibodies specific for the sexual-stage Pfs48/45 antigen. Exp Parasitol. 2001;97(1):45–9.

169. Vermeulen AN, Ponnudurai T, Beckers PJA, Verhave JP, Smits MA, Meuwissen JHET. Sequential expression of antigens on sexual stages of Plasmodium falciparum accessible to transmission blocking antibodies in the mosquito [Internet]. Available from: http://rupress.org/jem/article-pdf/162/5/1460/1095706/1460.pdf

170. Stura EA, Satterthwait AC, Calvo JC, Stefanko RS, Langeveld JP, Kaslow DC. Crystallization of an intact monoclonal antibody (4B7) against Plasmodium falciparum malaria with peptides from the Pfs25 protein antigen. Acta Crystallogr D Biol Crystallogr [Internet]. 1994 Jul 1 [cited 2022 Jun 9];50(4):556–62. Available from: https://onlinelibrary.wiley.com/doi/full/10.1107/S0907444994001782

171. Mulder Bert, Roeffen Will, Sauerwein Robert, Tchuinkam Timoléon, Boudin Crhistian, Verhave Jan Peter. Anti Pfs25 monoclonal antibody 32F81 blocks transmission from Plasmodium falciparum gametocyte carriers in Cameroon.

172. Scally SW, McLeod B, Bosch A, Miura K, Liang Q, Carroll S, et al. Molecular definition of multiple sites of antibody inhibition of malaria transmission-blocking vaccine antigen Pfs25. Nat Commun [Internet]. 2017;8(1). Available from: http://dx.doi.org/10.1038/s41467-017-01924-3

173. Feng BZ, Hoffmann KN, Nussenzweig RS, Tsuji M, Fujioka H, Aikawa M, et al. Pfs2400 can mediate antibody dependent malaria transmission inhibition and may e the plasmodium falciparum 11.1 gene product. 1993;177(February).

174. Canepa GE, Molina-Cruz A, Yenkoidiok-Douti L, Calvo E, Williams AE, Burkhardt M, et al. Antibody targeting of a specific region of Pfs47 blocks Plasmodium falciparum malaria

transmission. NPJ Vaccines [Internet]. 2018 Dec 10 [cited 2018 Dec 24];3(1):26. Available from: http://www.nature.com/articles/s41541-018-0065-5

175. Farrance CE, Chichester JA, Musiychuk K, Shamloul M, Rhee A, Manceva SD, et al. Human Vaccines Antibodies to plant-produced Plasmodium falciparum sexual stage protein Pfs25 exhibit transmission blocking activity. 2011; Available from: https://doi.org/10.4161/hv.7.0.14588

176. Jones RM, Chichester JA, Mett V, Jaje J, Tottey S, Manceva S, et al. A plant-produced Pfs25 VLP malaria vaccine candidate induces persistent transmission blocking antibodies against plasmodium falciparum in immunized mice. PLoS One. 2013;8(11).

177. MacLeod DT, Choi NM, Briney B, Garces F, Ver LS, Landais E, et al. Early Antibody Lineage Diversification and Independent Limb Maturation Lead to Broad HIV-1 Neutralization Targeting the Env High-Mannose Patch. Immunity [Internet]. 2016 [cited 2018 Dec 28];44(5):1215–26. Available from: http://www.ncbi.nlm.nih.gov/pubmed/27192579

178. Walker LM, Huber M, Doores KJ, Falkowska E, Pejchal R, Julien JP, et al. Broad neutralization coverage of HIV by multiple highly potent antibodies. Nature. 2011 Sep 22;477(7365):466–70.

179. Dejnirattisai W, Zhou D, Ginn HM, Duyvesteyn HME, Supasa P, Case JB, et al. The antigenic anatomy of SARS-CoV-2 receptor binding domain. Cell. 2021 Apr 15;184(8):2183-2200.e22.

180. Lindner JM, Cornacchione V, Sathe A, Be C, Srinivas H, Riquet E, et al. Human Memory B Cells Harbor Diverse Cross-Neutralizing Antibodies against BK and JC Polyomaviruses. Immunity [Internet]. 2019;50(3):668-676.e5. Available from: https://doi.org/10.1016/j.immuni.2019.02.003

181. Christian Gaebler, Henning Gruell, Klara Velinzon, Johannes F. Scheid, Michel C. Nussenzweig, Florian Klein. Isolation of HIV 1 reactive antibodies using cell surface expressed gp160.

182. Garrone P, Neidhardt EM, Garcia E, Galibert L, van Kooten C, Banchereau J. Fas Ligation Induces Apoptosis of CD40-activated Human B Lymphocytes.

183. Tiller T, Meffre E, Yurasov S, Tsuiji M, Nussenzweig MC, Wardemann H. Efficient generation of monoclonal antibodies from single human B cells by single cell RT-PCR and expression vector cloning. J Immunol Methods [Internet]. 2008 Jan 1 [cited 2018 Jun 12];329(1–2):112–24. Available from: http://www.ncbi.nlm.nih.gov/pubmed/17996249

184. Vos MW, Stone WJR, Koolen KM, van Gemert GJ, van Schaijk B, Leroy D, et al. A semi-automated luminescence based standard membrane feeding assay identifies novel small molecules that inhibit transmission of malaria parasites by mosquitoes. Sci Rep. 2015 Dec 21;5.

185. Ponnudurai T, Lensen AHW, van Gemert GJA, Bensink MPE, Bolmer M, Meuwissen JHET. Infectivity of cultured Plasmodium falciparum gametocytes to mosquitoes. Parasitology. 1989;98(2):165–73.

186. Lasonder E, Rijpma SR, van Schaijk BCL, Hoeijmakers WAM, Kensche PR, Gresnigt MS, et al. Integrated transcriptomic and proteomic analyses of P. Falciparum gametocytes: Molecular insight into sex-specific processes and translational repression. Nucleic Acids Res. 2016 Jul 27;44(13):6087–101.

187. Silvestrini F, Lasonder E, Olivieri A, Camarda G, van Schaijk B, Sanchez M, et al. Protein export marks the early phase of gametocytogenesis of the human malaria parasite Plasmodium falciparum. Molecular and Cellular Proteomics. 2010;9(7):1437–48.

188. Punjani, Rubinstein, Fleet, Brubaker. cyroSPARC algorithms for rapid unsupervised cryo EM structure determination.

189. Winter G, Waterman DG, Parkhurst JM, Brewster AS, Gildea RJ, Gerstel M, et al. DIALS: Implementation and evaluation of a new integration package. Acta Crystallogr D Struct Biol. 2018;74:85–97.

190. McCoy AJ, Grosse-Kunstleve RW, Adams PD, Winn MD, Storoni LC, Read RJ. Phaser crystallographic software. J Appl Crystallogr. 2007 Jul 13;40(4):658–74.

191. Adams PD, Afonine P v., Bunkóczi G, Chen VB, Davis IW, Echols N, et al. PHENIX: A comprehensive Python-based system for macromolecular structure solution. Acta Crystallogr D Biol Crystallogr. 2010;66(2):213–21.

192. Emsley P, Cowtan K. Coot: Model-building tools for molecular graphics. Acta Crystallogr D Biol Crystallogr. 2004 Dec;60(12 I):2126–32.

193. Adasme MF, Linnemann KL, Bolz SN, Kaiser F, Salentin S, Haupt VJ, et al. PLIP 2021: Expanding the scope of the protein-ligand interaction profiler to DNA and RNA. Nucleic Acids Res. 2021 Jul 2;49(W1):W530–4.

194. Morbach H, Eichhorn EM, Liese JG, Girschick HJ. Reference values for B cell subpopulations from infancy to adulthood. Clin Exp Immunol [Internet]. 2010 Nov [cited 2018 Jun 19];162(2):271–9. Available from: http://doi.wiley.com/10.1111/j.1365-2249.2010.04206.x

195. Huang J, Doria-Rose NA, Longo NS, Laub L, Lin CL, Turk E, et al. Isolation of human monoclonal antibodies from peripheral blood B cells. [cited 2018 Jun 8]; Available from: https://www.ncbi.nlm.nih.gov/pmc/articles/PMC4844175/pdf/nihms659449.pdf

196. Muir L, McKay PF, Petrova VN, Klymenko O v, Kratochvil S, Pinder CL, et al. Optimisation of ex vivo memory B cell expansion/differentiation for interrogation of rare peripheral memory B cell subset responses. Wellcome Open Res [Internet]. 2017 [cited 2018 Jun 8];2:97. Available from: https://www.ncbi.nlm.nih.gov/pmc/articles/PMC5843844/pdf/wellcomeopenres-2-14259.pdf

197. Abe M, Goto T, Kosaka M, Wolfenbarger D, Weiss DT, Solomon A. Differences in kappa to lambda (k:l) ratios of serum and urinary free light chains [Internet]. Available from: https://academic.oup.com/cei/article/111/2/457/6483314

198. Shi B, Ma L, He X, Wang X, Wang P, Zhou L, et al. Comparative analysis of human and mouse immunoglobulin variable heavy regions from IMGT/LIGM-DB with IMGT/HighV-QUEST. Theor Biol Med Model. 2014 Jul 3;11(1).

199. Kisalu NK, Idris AH, Weidle C, Flores-Garcia Y, Flynn BJ, Sack BK, et al. A human monoclonal antibody prevents malaria infection by targeting a new site of vulnerability on the parasite. Nat Med [Internet]. 2018;24(4):408–16. Available from: http://dx.doi.org/10.1038/nm.4512

200. Pérez-Mazliah D, Ndungu FM, Aye R, Langhorne J. B-cell memory in malaria: Myths and realities. Vol. 293, Immunological Reviews. Blackwell Publishing Ltd; 2020. p. 57–69.

201. Muellenbeck MF, Ueberheide B, Amulic B, Epp A, Fenyo D, Busse CE, et al. Atypical and classical memory B cells produce plasmodium falciparum neutralizing antibodies. Journal of Experimental Medicine. 2013 Feb;210(2):389–99.

202. Lasonder E, Rijpma SR, van Schaijk BCL, Hoeijmakers WAM, Kensche PR, Gresnigt MS, et al. Integrated transcriptomic and proteomic analyses of P. Falciparum gametocytes: Molecular insight into sex-specific processes and translational repression. Nucleic Acids Res. 2016;44(13):6087–101.

203. Richter KN, Revelo NH, Seitz KJ, Helm MS, Sarkar D, Saleeb RS, et al. Glyoxal as an alternative fixative to formaldehyde in immunostaining and super-resolution microscopy. EMBO J. 2018 Jan 4;37(1):139–59.

204. Singh K, Burkhardt M, Nakuchima S, Herrera R, Muratova O, Gittis AG, et al. Structure and function of a malaria transmission blocking vaccine targeting Pfs230 and Pfs230-Pfs48/45 proteins. Commun Biol. 2020 Dec 1;3(1).

205. Kreer C, Döring M, Lehnen N, Ercanoglu MS, Gieselmann L, Luca D, et al. openPrimeR for multiplex amplification of highly diverse templates. J Immunol Methods [Internet]. 2020;480(September 2019):112752. Available from: https://doi.org/10.1016/j.jim.2020.112752

206. Sturm A, Vos MW, Henderson R, Eldering M, Koolen KMJ, Sheshachalam A, et al. Barcoded Asaia bacteria enable mosquito in vivo screens and identify novel systemic insecticides and inhibitors of malaria transmission. PLoS Biol. 2021 Dec 1;19(12).

207. Collins WE, Anders RF, Pappaioanou M, Campbell GH, Brown G v., Kemp DJ, et al. Immunization of Aotus monkeys with recombinant proteins of an erythrocyte surface antigen of Plasmodium falciparum. Nature. 1986;323(6085):259–62.

208. Badaut C, Guyonnet L, Milet J, Renard E, Durand R, Viwami F, et al. Immunoglobulin response to Plasmodium falciparum RESA proteins in uncomplicated and severe malaria. Malar J. 2015;14(1):1–13.

209. Brahimi K, Badell E, Sauzet JP, BenMohamed L, Daubersies P, Guérin-Marchand C, et al. Human antibodies against Plasmodium falciparum liver-stage antigen 3 cross-react with Plasmodium yoelii preerythrocytic-stage epitopes and inhibit sporozoite invasion in vitro and in vivo. Infect Immun. 2001;69(6):3845–52.

210. Spooner J, Keen J, Nayyar K, Birkett N, Bond N, Bannister D, et al. Evaluation of Strategies to Control Fab Light Chain Dimer During Mammalian Expression and Purification: A Universal One-Step Process for Purification of Correctly Assembled Fab. Biotechnol Bioeng [Internet]. 2015;112:1472–7. Available from: http://onlinelibrary.wiley.com/doi/10.1002/bit.25550/abstract

211. Malkin EM, Diemert DJ, McArthur JH, Perreault JR, Miles AP, Giersing BK, et al. Phase 1 clinical trial of apical membrane antigen 1: An asexual blood-stage vaccine for Plasmodium falciparum malaria. Infect Immun. 2005 Jun;73(6):3677–85.

212. Oyen D, Torres JL, Cottrell CA, Richter King C, Wilson IA, Ward AB. Cryo-EM structure of P. falciparum circumsporozoite protein with a vaccine-elicited antibody is stabilized by somatically mutated inter-Fab contacts [Internet]. Vol. 4, Sci. Adv. 2018. Available from: https://www.science.org

213. Kucharska I, Thai E, Srivastava A, Rubinstein JL, Pomès R, Julien JP. Structural ordering of the plasmodium berghei circumsporozoite protein repeats by inhibitory antibody 3d11. Elife. 2020 Oct 1;9:1–25.

214. Kucharska I, Hossain L, Ivanochko D, Yang Q, Rubinstein JL, Pomès R, et al. Structural basis of Plasmodium vivax inhibition by antibodies binding to the circumsporozoite protein repeats. Elife. 2022 Jan 1;11.

215. Udomsangpetch R, Lundgren K, Berzins K, Wåhlin B, Perlmann H, Troye-Blomberg M, et al. Human monoclonal antibodies to Pf 155, a major antigen of malaria parasite Plasmodium falciparum. Science (1979). 1986;231(4733):57–9.

216. Tan J, Sack BK, Oyen D, Zenklusen I, Piccoli L, Barbieri S, et al. A public antibody lineage that potently inhibits malaria infection through dual binding to the circumsporozoite protein. Nat Med. 2018 May 1;24(4):401–7.

217. Imkeller K, Scally SW, Bosch A, Marti GP, Costa G, Triller G, et al. Antihomotypic affinity maturation improves human B cell responses against a repetitive epitope. Science (1979). 2018;360(6395):1358–62.

218. Astagneau P, Chougnet C, Lepers JP, Andriamangatiana-Rason MD, Deloron P. Antibodies to the 4-mer repeat of the ring-Infected erythrocyte surface antigen (Pf155/RESA) protect against plasmodium falciparum malaria. Int J Epidemiol. 1994;23(1):169–75.

219. Saul. Human phase I vaccine trials of 3 recombinant asexual stage malaria antigens with Montanide ISA720 adjuvant.

220. Genton B, Al-Yaman F, Betuela I, Anders RF, Saul A, Baea K, et al. Safety and immunogenicity of a three-component blood-stage malaria vaccine (MSP1, MSP2, RESA) against Plasmodium falciparum in Papua New Guinean children. Vaccine. 2003;22(1):30–41.

221. Nahrendorf W, Scholzen A, Sauerwein RW, Langhorne J. Cross-stage immunity for malaria vaccine development. Vaccine [Internet]. 2015;33(52):7513–7. Available from: http://dx.doi.org/10.1016/j.vaccine.2015.09.098

ANNEXES

Specificity	Fluorochrome	Working dilution	Brand	Ex max	Em max
Viability	live /dead Aqua	1/200	Thermofisher (#L34957)	405	525
Anti-CD3	Vioblue	1/50	Miltenyi (#130-114-519)	400	425
Anti-IgG	PerCP – Vio 700	1/10	Miltenyi (#130-107-056)	482	676
Anti-IgA	Anti IgA PerCP – Vio 700	1/50	Miltenyi (#130-116-885)		
Anti-CD20	Anti CD20 PE Vio 770	1/50	Miltenyi (#130-111-345)	565	776
Anti-CD19	Anti CD19 PE Vio 770	1/10	Miltenyi (#130-113-649)		
Anti-IgD	PE	1/50	Miltenyi (#130-110-643)	565	575
Anti-IgA	PE	1/50	Miltenyi (#130-113-476)		
Anti-IgM	PE	1/50	Miltenyi (#130-093-075)		
Anti-CD27	APC	1/10	Miltenyi (#130-108-336)	652	660
Nucleic acid	SYTO 61	1/5000	Thermofisher (#S11343)	628	645
Females gametes (anti Pfs 47)	Anti Pfs47/45 dylight	5 µL/ ml 100 000 cells/ 100 µl	Fluorochrome coupled to mAb by Radboud	652	672

Annex 1: Fluorochromes table

Ex: excitation. Em: emission.

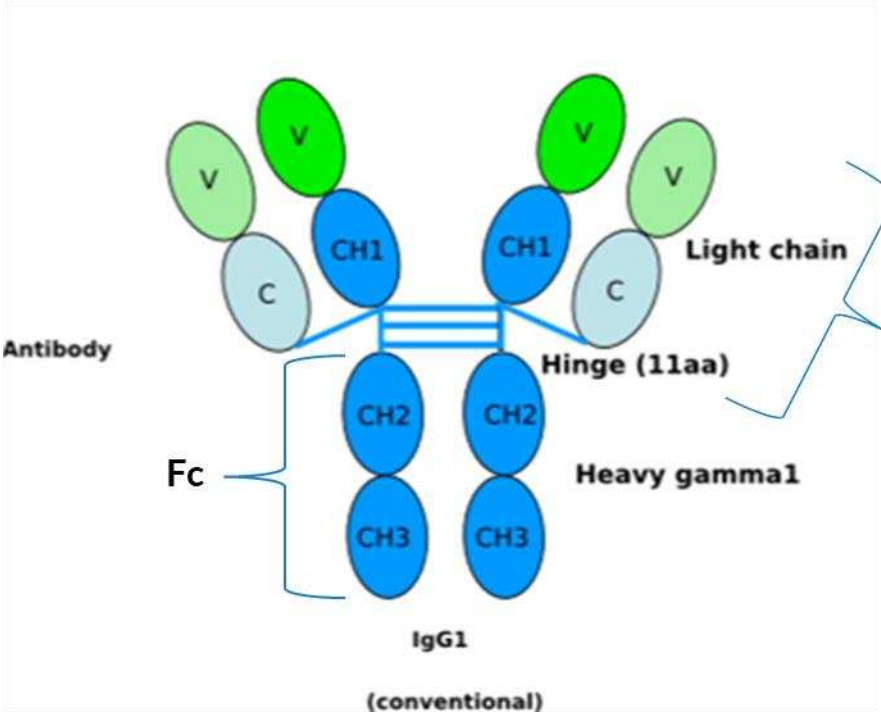

Annex 2: Structure of an Immunoglobulin

IgG are homodimeric flexible Y shaped proteins of 150 kDa. Each monomer is composed of two polypeptidic chains: one chain of 50 kDa, called "heavy" chain (HC) and one of 25 kDA, called "light" chain (LC), light-coloured in the scheme. It exists two types of Lc: either Lamda chain or Kappa chain, depending on the gene which encoded the chain, and only one kind is present on one antibody.

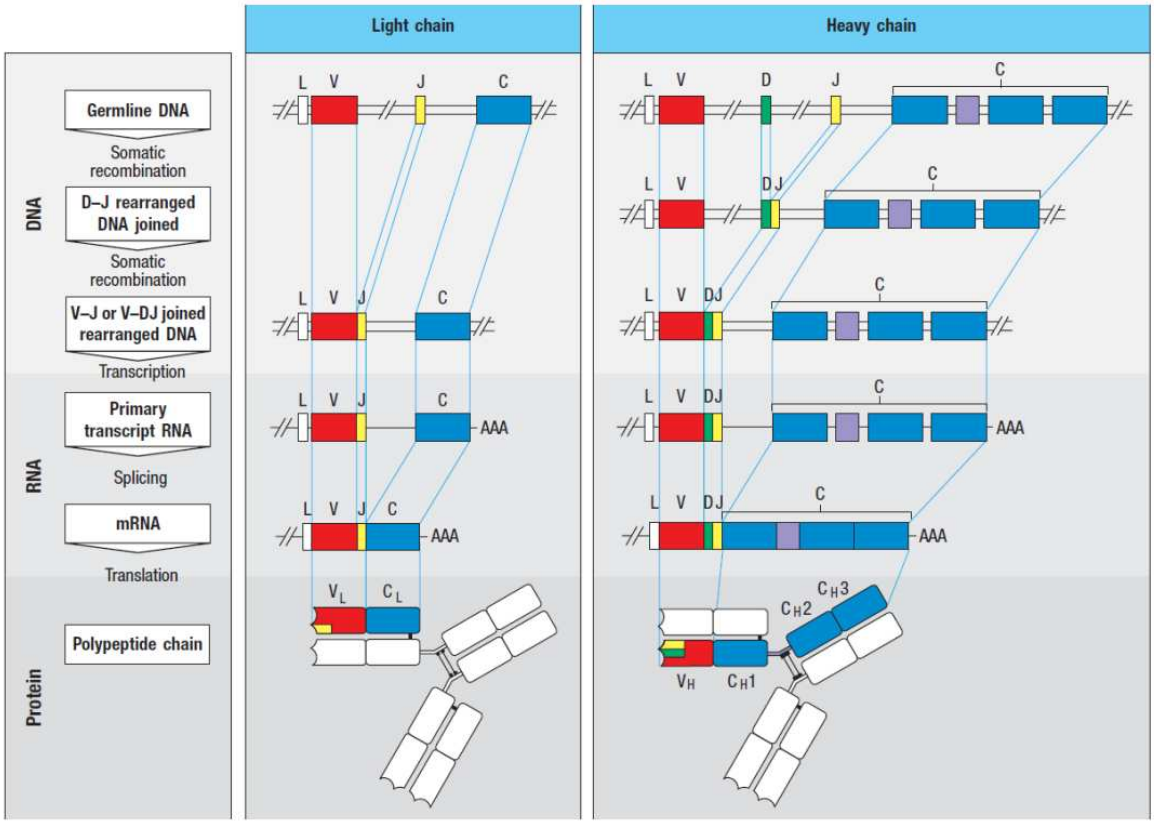

Annex 3: V, D and J genes recombination ensures an immense diversity of antibody variable regions

Heavy chains are composed of VH segment (for variable heavy), DH segment (for determining heavy) and JH segment (for joining heavy segments). Light chains are composed of VL and JL segments only. On a chromosome, there are several versions of V, D and J genes, and only one of each type is selected to encode for the variable part.

	Primers sets	IgG gene family amplified	Primer sequence
HC plate	H1 forward	5' L-VH 1	ACAGGTGCCCACTCCCAGGTGCAG
		5' L-VH 3	AAGGTGTCCAGTGTGARGTGCAG
		5' L-VH 4/6	CCCAGATGGGTCCTGTCCCAGGTGCAG
		5' L-VH 5	CAAGGAGTCTGTTCCGAGGTGCAG
	H1 reverse	3' CH1	GGAAGGTGTGCACGCCGCTGGTC
LC plate	L1 forward	5' LVL 1	GGTCCTGGGCCCAGTCTGTGCTG
		5' LVL 2	GGTCCTGGGCCCAGTCTGCCCTG
		5' LVL 3	GCTCTGTGACCTCCTATGAGCTG
		5' LVL 4/5	GGTCTCTCTCSCAGCYTGTGCTG
		5' LVL 6	GTTCTTGGGCCAATTTTATGCTG
		5' LVL 7	GGTCCAATTCYCAGGCTGTGGTG
		5' LVL 8	GAGTGGATTCTCAGACTGTGGTG
	L1 reverse	3' CL	CACCAGTGTGGCCTTGTTGGCTTG
KC plate	K1 forward	5' LVK 1/2	ATGAGGSTCCCYGCTCAGCTGCTGG
		5' LVK 3	CTCTTCCTCCTGCTACTCTGGCTCCCAG
		5' LVK 4	ATTTCTCTGTTGCTCTGGATCTCTG
	K1 reverse	3' CK 543	GTTTCTCGTAGTCTGCTTTGCTCA

Annex 4: Primers set for IgG genes amplification: first round or hemi-nested PCR (PCR1)

	Primers sets	IgG gene familiy amplified	Primer sequence
HC plate	H2 forward	5'Agel VH1/5	CTGCAACCGGTGTACATTCCGAGGTGCAGCTGGTGCAG
		5'Agel VH3	CTGCAACCGGTGTACATTCTGAGGTGCAGCTGGTGGAG
		5'Agel VH4	CTGCAACCGGTGTACATTCCCAGGTGCAGCTGCAGGAG
		5'Agel VH3-23	CTGCAACCGGTGTACATTCTGAGGTGCAGCTGTTGGAG
		5'Agel VH4-34	CTGCAACCGGTGTACATTCCCAGGTGCAGCTACAGCAGTG
	H2 reverse	3' IgG (internal)	GTTCGGGGAAGTAGTCCTTGAC
LC plate	L2 forward	5' AgeI VL 1	CTGCTACCGGTTCCTGGGCCCAGTCTGTGCTGACKCAG
		5' AgeI VL 2	CTGCTACCGGTTCCTGGGCCCAGTCTGCCCTGACTCAG
		5' AgeI VL 3	CTGCTACCGGTTCTGTGACCTCCTATGAGCTGACWCAG
		5' AgeI VL 4/5	CTGCTACCGGTTCTCTCTCSCAGCYTGTGCTGACTCA
		5' AgeI VL 6	CTGCTACCGGTTCTTGGGCCAATTTTATGCTGACTCAG
		5' AgeI VL 7/8	CTGCTACCGGTTCCAATTCYCAGRCTGTGGTGACYCAG
	L2 reverse	3' XhoI CL	CTCCTCACTCGAGGGYGGGAACAGAGTG
KC plate	K2 forward	5' Pan VK	ATGACCCAGWCTCCABYCWCCCTG
	K2 reverse	3' CK 494	GTGCTGTCCTTGCTGTCCTGCT

Annex 5: Primers set for IgG genes amplification: second round or hemi-nested PCR (PCR2)

Oligo Name	Oligo Sequence (5'-3')
SL 5′ VH1	GGGTTTTCCTTGTTGCTATTCTCGAGGGTGTCCAGTGTCAGGTGCAGCTGGTGCAG
SL 5′ VH1/5	GGGTTTTCCTTGTTGCTATTCTCGAGGGTGTCCAGTGTCAGGTGCAGCTGCAGGAGTCGGGCCCA
SL 5′ VH3	GGGTTTTCCTTGTTGCTATTCTCGAGGGTGTCCAGTGTGAGGTGCAGCTGGTGGAG
SL 5′ VH3–23	GGGTTTTCCTTGTTGCTATTCTCGAGGGTGTCCAGTGTGAGGTGCAGCTGTTGGAG
SL 5′ VH4	GGGTTTTCCTTGTTGCTATTCTCGAGGGTGTCCAGTGTCAGGTGCAGCTGCAGGAG
SL 5′ VH 4–34	GGGTTTTCCTTGTTGCTATTCTCGAGGGTGTCCAGTGTCAGGTGCAGCTACAGCAGTG
SL 5′ VH 1–18	GGGTTTTCCTTGTTGCTATTCTCGAGGGTGTCCAGTGTCAGGTTCAGCTGGTGCAG
SL 5′ VH 1–24	GGGTTTTCCTTGTTGCTATTCTCGAGGGTGTCCAGTGTCAGGTCCAGCTGGTACAG
SL 5′ VH3–33	GGGTTTTCCTTGTTGCTATTCTCGAGGGTGTCCAGTGTCAGGTGCAGCTGGTGGAG
SL 5′ VH 3–9	GGGTTTTCCTTGTTGCTATTCTCGAGGGTGTCCAGTGTGAAGTGCAGCTGGTGGAG
SL 5′ VH4–39	GGGTTTTCCTTGTTGCTATTCTCGAGGGTGTCCAGTGTCAGCTGCAGCTGCAGGAG
SL 5′ VH 6–1	GGGTTTTCCTTGTTGCTATTCTCGAGGGTGTCCAGTGTCAGGTACAGCTGCAGCAG
SL 5' VH7-4-1	GGGTTTTCCTTGTTGCTATTCTCGAGGGTGTCCAGTGTCAGGTGCAGCTGGTGCAATC
SL 5' VH 5-51*03	GGGTTTTCCTTGTTGCTATTCTCGAGGGTGTCCAGTGTGAGGTGCAGCTGGTGCAGTCTG
SL 5′ VH1-3	GGGTTTTCCTTGTTGCTATTCTCGAGGGTGTCCAGTGTCAGGTCCAGCTTGTGCAG
SL5-VH3-23-04	GGGTTTTCCTTGTTGCTATTCTCGAGGGTGTCCAGTGTGAGGTGCAGCTGGTGGAG
SL5-VH4-30-2-04	GGGTTTTCCTTGTTGCTATTCTCGAGGGTGTCCAGTGTCAGCTGCAGCTGCAGGAG
SL 3′ JH 1/2/4/5	GATGGGCCCTTGGTGCTAGCTGAGGAGACGGTGACCAG
SL 3′ JH 3	GATGGGCCCTTGGTGCTAGCTGAAGAGACGGTGACCATTG
SL 3′ JH 6	GATGGGCCCTTGGTGCTAGCTGAGGAGACGGTGACCGTG
SL 5′ VL 1	TTTTTCTAGTAGCAACTGCAACCGGTGTACACCAGTCTGTGCTGACTCAG
SL 5′ VL 2	TTTTTCTAGTAGCAACTGCAACCGGTGTACACCAGTCTGCCCTGACTCAG
SL 5′ VL 3	TTTTTCTAGTAGCAACTGCAACCGGTGTACACTCCTATGAGCTGACTCAG
SL 5′ VL 4/5	TTTTTCTAGTAGCAACTGCAACCGGTGTACACCAGCCTGTGCTGACTCA
SL 5′ VL 6	TTTTTCTAGTAGCAACTGCAACCGGTGTACACAATTTTATGCTGACTCAG
SL 5′ VL 7/8	TTTTTCTAGTAGCAACTGCAACCGGTGTACACCAGACTGTGGTGACTCAG
SL 5′ VL 1-51	TTTTTCTAGTAGCAACTGCAACCGGTGTACACCAGTCTGTGTTGACGCAG
SL 5′ VL 1-40	TTTTTCTAGTAGCAACTGCAACCGGTGTACACCAGTCTGTGCTGACGCA
SL 5' VL 3-27	TTTTTCTAGTAGCAACTGCAACCGGTGTACACTCCTATGAGCTGACACAGCCATCCTC
SL 5' VL 3-21	TTTTTCTAGTAGCAACTGCAACCGGTGTACACTCCTATGTGCTGACTCAG
SL 5' VL 1-47	TTTTTCTAGTAGCAACTGCAACCGGTGTACACCAGTCTGTGCTGACTCA
SL 5′ VL 3-10	TTTTTCTAGTAGCAACTGCAACCGGTGTACACTCCTATGAGCTGACACAG
SL 5' VL 2-8/2-14	TTTTTCTAGTAGCAACTGCAACCGGTGTACACCAGTCTGCCCTGACT
SL 5′ VL 4-69	TTTTTCTAGTAGCAACTGCAACCGGTGTACACCAGCTTGTGCTGACTCA
SL 5' VL 9-49	TTTTTCTAGTAGCAACTGCAACCGGTGTACACCTGTGCTGACTCAGCCACCTT
SL 5' V8-61	TTTTTCTAGTAGCAACTGCAACCGGTGTACACGACCCAGGAGCCATCGTTCT
SL 3′ CL	TGTTGGCTTGAAGCTCCTCACTCGAGGGCGGGAACAGAGTG
SL 5′ VK 1–5	TTTTTCTAGTAGCAACTGCAACCGGTGTACACGACATCCAGATGACCCAGTC
SL 5′ VK 1–9	TTTTTCTAGTAGCAACTGCAACCGGTGTACACGACATCCAGTTGACCCAGTCT
SL 5′ VK 1D–43	TTTTTCTAGTAGCAACTGCAACCGGTGTACACGCCATCCGGATGACCCAGTC
SL 5′ VK 2–24	TTTTTCTAGTAGCAACTGCAACCGGTGTACACGATATTGTGATGACCCAGAC
SL 5′ VK 2–28	TTTTTCTAGTAGCAACTGCAACCGGTGTACACGATATTGTGATGACTCAGTC
SL 5′ VK 2–30	TTTTTCTAGTAGCAACTGCAACCGGTGTACACGATGTTGTGATGACTCAGTC
SL 5′ VK 3–11	TTTTTCTAGTAGCAACTGCAACCGGTGTACACGAAATTGTGTTGACACAGTC
SL 5′ VK 3–15	TTTTTCTAGTAGCAACTGCAACCGGTGTACACGAAATAGTGATGACGCAGTC
SL 5′ VK 3–20	TTTTTCTAGTAGCAACTGCAACCGGTGTACACGAAATTGTGTTGACGCAGTCT
SL 5′ VK 4–1	TTTTTCTAGTAGCAACTGCAACCGGTGTACACGACATCGTGATGACCCAGTC
SL 5' VK 3–20*02	TTTTTCTAGTAGCAACTGCAACCGGTGTACACGAAATTGTGTTGACACAGTCTCCAGCCAC
SL 5' VK 2D-29*02	TTTTTCTAGTAGCAACTGCAACCGGTGTACACGATATTGTGATGACCCAGACT
SL5-VK-3-7	TTTTTCTAGTAGCAACTGCAACCGGTGTACACGAAATTGTAATGACACAGTCT
SL 5' VK 1-12	TTTTTCTAGTAGCAACTGCAACCGGTGTACACGACATCCAGATGACCCAGTCT
SL 5' VK 1-39*01	TTTTTCTAGTAGCAACTGCAACCGGTGTACACGACATCCAGATGACCCAGTCT
SL 3′ JK 1	AAGACAGATGGTGCAGCCACCGTACGTTTAATCTCCAGTCGTGTC
SL 3′ JK 1/4	AAGACAGATGGTGCAGCCACCGTACGTTTGATCTCCACCTTGGTC
SL 3′ JK 2	AAGACAGATGGTGCAGCCACCGTACGTTTGATCTCCAGCTTGGTC
SL 3′ JK 3	AAGACAGATGGTGCAGCCACCGTACGTTTGATATCCACTTTGGTC
SL 3′ JK 5	AAGACAGATGGTGCAGCCACCGTACGTTTAATCTCCAGTCGTGTC
SL 3′ JK 1	AAGACAGATGGTGCAGCCACCGTACGTTTGATTTCCACCTTGGTC

Annex 6: Primers for IgG genes cloning

SUPPLEMENTARY DATA

Fractions	R0.10C IgG	Total IgG w/o R0.10C IgG	230CMB IgG	230CMB (conc)	Total IgG w/o RO.10C 230CMB IgG	Total IgG w/o RO.10C 230CMB IgG (C-)
TRA (%)	91,5 *(86,4-94,7)*	99,5 *(99-99,7)*	-2,5 *(- 38,6 – 24,2)*	99,3 *(98,6- 99,6)*	99,5 *(99-99,8)*	99,8 *(99,5- 99,9)*

Supplementary data 1: Donor A serum characteristics, from Stone et al (54), when depleted of anti-Pfs48/45 and anti-Pfs230 Abs.

Experiment performed by Stone and al(54) *. Total purified IgGs of this donor had a 99,4% TRA. (conc) = IgG at 9 times the physiological concentration. (C-) = SMFA experiment performed without complement.*

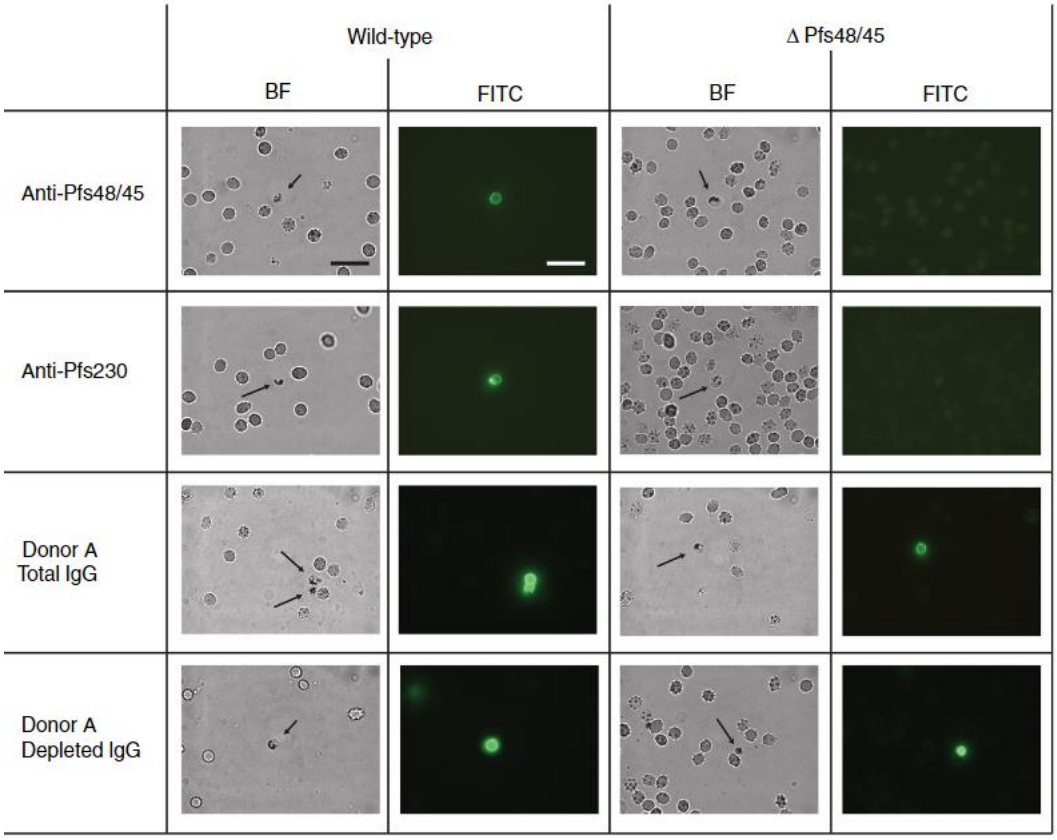

Supplementary data 2: Gamete SIFA results obtained by Stone et al (54) with donor A serum, either depleted in anti-Pfs48/45 and Pfs230 Abs or not.

Experiment performed by Stone and al (54) *.Gametes were either wild-type or Pfs48/45 KO. MAbs 45.1 (anti-Pfs48/45) and 2A2 (anti-Pfs230) were used as controls.*

	Plate	Well	GCT ELISA	GMT ELISA
1	P1.1	C15	567	101
2	P1.1	G21	434	678
3	P1.1	G23	5207	1028
4	P1.1	H14	1190	2254
5	P1.1	H16	446	1464
6	P1.1	K20	297	362
7	P1.1	N14	150	435
8	P1.1	N20	242	469
9	P1.1	O6	237	343
10	P1.1	O14	182	340
11	P1.1	O23	478	322
12	P1.2	B6	1395	173
13	P1.2	D20	1950	1116
14	P1.2	G19	370	603
15	P1.2	G22	476	257
16	P1.2	G23	445	320
17	P1.2	H18	134	1467
18	P1.2	H23	379	108
19	P1.2	I20	438	150
20	P1.2	I22	411	369
21	P1.2	I23	389	194

	Plate	well	GMT ELISA
22	P1.2	B3	491
23	P1.2	B7	550
24	P1.2	B8	422
25	P1.2	B15	370
26	P1.2	B19	521
27	P1.2	B20	403
28	P1.2	C11	488
29	P1.2	C19	438
30	P1.2	C23	352
31	P1.2	D7	376
32	P1.2	D15	352
33	P1.2	D19	396
34	P1.2	F2	389
35	P1.2	F13	351
36	P1.2	H2	365
37	P1.2	H4	367
38	P1.2	L2	393
39	P1.2	L21	1691
40	P2.2	H11	1821
131	P2.2	N6	688
132	P2.2	H21	729
133	P2.2	K22	676

	Plate	well	GMT ELISA
85	P4.2	B3	706
86	P4.2	B4	690
87	P4.2	B7	503
88	P4.2	B8	441
89	P4.2	B9	487
90	P4.2	B11	475
91	P4.2	C2	598
92	P4.2	C3	463
93	P4.2	C7	485
94	P4.2	C12	495
95	P4.2	C18	463
96	P4.2	C19	493
97	P4.2	D2	564
98	P4.2	D3	481
99	P4.2	D4	468
100	P4.2	D5	539
101	P4.2	D21	460
102	P4.2	E2	461
103	P4.2	E6	598
104	P4.2	E7	454
105	P4.2	F2	550
106	P4.2	*F8*	*440*
107	P4.2	F14	434
108	P4.2	F20	470
109	P4.2	G3	440
110	P4.2	H3	508
111	P4.2	H5	468
112	P4.2	H11	490
113	P4.2	I2	438
114	P4.2	J5	440
115	P4.2	M4	442
116	P4.2	N2	441
117	P4.2	N6	559

64	P3.2	B2	429
65	P3.2	B3	408
66	P3.2	B4	626
67	P3.2	B11	409
68	P3.2	B19	567
69	P3.2	C15	547
70	P3.2	D2	455
71	P3.2	D9	1290
72	P3.2	E7	455
73	P3.2	E15	570
74	P3.2	F7	425
75	P3.2	F9	426
76	P3.2	F11	732
77	P3.2	G4	409
78	P3.2	G13	568
79	P3.2	H4	440
80	P3.2	H15	427
81	P3.2	H16	564
41	P7.2	B2	463
42	P7.2	B3	519
43	P7.2	B4	473
44	P7.2	B7	5190
45	P7.2	B8	519
46	P7.2	B13	422
47	P7.2	B19	610
48	P7.2	C2	432
49	P7.2	C7	571
50	P7.2	C8	433
51	P7.2	D4	412
52	P7.2	D6	489
53	P7.2	E3	553
54	P7.2	E8	424
55	P7.2	F4	402
56	P7.2	F7	436
57	P7.2	F8	529
58	P7.2	H2	420
59	P7.2	H4	415
60	P7.2	H18	403
61	P7.2	J10	405
62	P7.2	N2	426
63	P7.2	O16	448

118	P 5.2	B4	634
119	P 5.2	B7	413
120	P 5.2	B11	501
121	P 5.2	B15	470
122	P 5.2	B19	489
123	P 5.2	D2	447
124	P 5.2	D7	657
125	P 5.2	E7	442
126	P 5.2	F11	425
127	P 5.2	F19	406
128	P 5.2	H5	409
129	P 5.2	J2	520
130	P 5.2	K4	429
82	P 6.2	C2	406
83	P 6.2	E3	468
84	P 6.2	F20	1452
134	P 6.2	C12	349
135	P 6.2	C17	344
136	P 6.2	E19	341

Supplementary data 3: IgG supernatant tested in gamet (oocyte) ELISA and gamete SIFA

In yellow are clear positive hits in SIFA, detected by both the software and by eye. In orange are doubtful hits in SIFA, not considered positive by eye but for which the software detected more than 10% of positive gametes.

554_CFS_RM-TB22_0.03_2 → Pf11.1 peptide used for immunisations

MVVPEVVEEVVPEVVEEVVPEVVEEVVPEVVEEVVPEVVEEVVPEVVEEVVPEVVEEVVPEVVEEVV
PEELHHHHHH

977_PF3D7_0220000_e2s1_4 → Liver Stage Antigen 3

SDINKSWKKNTYVDKKLNKLFNRSLGESQVNGELASEEVKEKILDLLEEGNTLTESVDDNKNLEEAEDIKENILL
SNIEEPKENIIDNLLNNIGQNSEKQESVSENVQVSDELFNELLNSVDVNGEVKENILEESQVNDDIFNSLVKSVQ
QEQQHNVEEKVEESVEENDEESVEENVEENVEENDDESVASSVEESIASSVDESIDSSIEENVAPTVEEIVAPTV
EEIVAPSVVESVAPSVEESVEENVEESVAENVEESVAENVEESVAENVEESVAENVEESVAENVEESVAENVEEI
VAPTVEESVAPTVEEIVAPSVEESVAPSVEEIVVPTVEESVAENVEEIVAPSVEEIVAPSVEEIVAPTVEESVAP
TVEEIVAPSVEESVAPSVEEIVVPTVEESVAENVEESVAENVEEIVAPSVEEIVAPSVEEIVAPSVEEIVAPSVE
EIVAPSVEEIVAPSVEEIVAPSVEEIVAPSVEEIVAPTVEEIVAPTVEEIVAPSVEEIVAPTVEESVAENVATNL
SDNLLSNLLGGIETEEIKDSILNEIEEVKENVVTTILENVEETTAESVTTFSNILEEIQENTITNDTIEEKLEEL
HENVLSAALENTQSEEEKKEVIDVIEEVKEEVATTLIETVEQAEEESASTITEIFENLEENAVESNENVAENLEK
LNETVFNTVLDKVEETVEISGESLENNEMDKAFFSEIFDNVKGIQENLLTGMFRSIETSIVIQSEEKVDLNENVV
SSILDN

1069_PF3D7_0309100_C_4 → OMD protein

MLEMNMIMKIYYIFLLFVFILIERCVDNDVINKTQENYLDHRDFEKDMDELDLSGLEYDIENVEEIAQKDSYNYV
TQIYVYIRIDEEYKKYINHLELMRLGQRFMTILQNAMINVQLKKTGTGIFTCFYENKSITDDLATYFLIQKEVDF
IEVGFDKRYPEGRHAPITDSDMRVFIKNEELYPYDVP

113_PF3D7_1149200_e2s1_1 → ring infected erythrocyte surface antigen 3

GNFGYNGSSNSGAQFTDRCSRNLYCETLPINPYADSENPIVVSQVFGLPSEKPTFTLEGTPDIDHTNILGFNEKL
MTDVNRYRYSNNYEAIPHTREFNPLIVDKVLFDYNEKVDNLGRSGGDIIKKMQTLWDEIMDINKRKYDFLKTKLQ
KTYSQYKVQYDMPKEVYESKWGQCLKLINQGGDNLEERLNTQFKNWYRQKYLNLEEYRRLTVLNQIAWKALSNQI
QYTCRKIMNSNISSFKHISELKSLEQRAAKDAQEEMRKRAEKQKKKKSKRRGWLCCGGGDNETVEPQQEEPVQDV
GEHQINEYGDILPSLKVSINNSAINYYDAVKDGKYLDDDSSDALYTDEDLLFDLEKQKYMDMLDGSEDESVEDNE
EEHSGEANEEELSVDENVEEQNVDESGEQQSDDESGEHQSVNEIVEEQSVNEIVEEQTVDEIVEQETVDENVEEQ
AVDENEEQQTVDENVEQQTIDESQVQEEISTIQENIEEVVSEVQQDSEVDRTLHVPDTRFYDILGVGVNADMK

637_PF3D7_0102200_e2s2_3 → ring infected erythrocyte surface antigen

NEAYQVLGDIDKKRWYNKYGYDGIKQVNFMNPSIFYLLSSLEKFKDFTGTPQIVTLLRFFFEKRLSMNDLENKSE
HLLKFMEQYQKEREAHVSEYLLNILQPCIAGDSKWNVPIITKLEGLKGSRFDIPILESLRWIFKHVAKTHLKKSS
KSAKKLQQRTQANKQELANINNNLMSTLKEYVGSSEQMNSITYNFENINSNVDNGNQSKNISDLSYTDQKEILEK
IVSYIVDISLYDIENTALNAAEQLLSDNSVDEKTLKKRAQSLKKLSSIMERYAGGKRNDKKAKKYDTQDVVGYIM
HGISTINKEMKNQNENVPEHVQHNAEANVEHDAEENVEHDAEENVEENVEENVEENVEENVEENVEENVEENVEE
NVEENVEENVEENVEENVEENVEENVEEYDEENVEEVEENVEEYDEENVEEVEENVEENVEENVEENVEEYDEEN
VEEVEENVEENVEENVEENVEENVEEVEENVEENVEENVEENVEENVEENVEEYDEENVEEHNEEYDE

224_PF3D7_1127500_C_1 → Protein disulfide isomerase

MLEMIIKFLIFNLLLYLFRCNTKVNFTYPQNDFLRIDSENIEEAFENNDYWLINFYAPQCVYCKFIWDKLRYIQR
SIQNENRTKIYFGEVNCDNQKGYTVCEIYGAMRVPQLKLFKGSELISTYSNDITNYNNIKSWIYYITTPLFVGVQ
DENELKSYETENNIFLTCSENLPADLFDVAKLYKEECYFINITNPDMCTRMNIKTNELHVMSAYNHSTYDLDTLD
RELLKLFVNKNRFPLVMKIDHRNFFNIRSSGNNLMLLLLDMKKNPNAYILEYKQYAEKYKNHNDILFGYIDGKYY
EENLELYGTDSDYYPQIIVFSKNPREYYFEGYFNIDNVDNIIYDVKNKRIYHKFEEFTKFRIILIKFKKHIKYIL
KKAFKTDFLSFIGFICSVIMMLLTAILVIHTIYKYYMSYTHNTYIEKEEKSEYPYDVP

236_PF3D7_1036300-S2_1 → Duffy binding like merozoite surface protein 2

INYTDIKTLSPSEYLIEKCPECKCTKKNLQDVFELTFDGKALLEKLKKEESPVSNSVNALPEPGQITLPDPSLKQ
TTQQENQPVVETPVTTAVINEHQGQTEPNKGDNNNERENHESNVGSIQEVNQGSVSEESHSKTIDPSKIDDRLEL
SSGSSSLEQHSKEDVKKGCALELVPLSLSDIEQIANESEDVLEEIEEEINTDGEIEYITEEEIKEDIEEETEEDI
EEETEEETEEETEEEADEETVKEIEDKPEQEIKNKSLEEKQIDKNTDTSEKKGFNNSEKDEKARNLISKNYKNYN
ELDKNVHTLVNSIISLLEEGNGSDSTLNSLSKDITNLFKN

+

MKGLKVFMRSFVYFVLVCNLINNVIICHKINYENIEENPQINDQNIMEILNSSVLNNNMKKEKEKNILYDISYYI
EYLKIINSLDNKYNDKFHKAILNIDTTKKKKEKKNIDLIYYSGKKYNNNIKDIKKQLHKSFYV

826_PF3D7_1038400_e2s1_3 → Pf 11.1

VIPEEVVEEIITEEIAEEIIPKELVEEVIPEEVVVEIIPEKLVEEFVSEELVEELVPEEIVEKVVPEELVEEIVP
EELVEEVVPEELVEEVIPEELVEEFIPEEVVEEVLPEQLVEEVISEVVEEVVPEELVEEVIPEEVVEELVAEEVI
EEVIPKELIEEAITEEVEEVIPEEIVEEVIPEEVVKEVIPEVEIEEILPEELIEELVAKEVIEEVITEEVAEEVI
PEEIVQEVIPEEVVEEIITEVEIEEVLPEELIDEVVPEEVTEEVITEEVMPEEVVKEVIPEEIAEEVIPKELVEE
VIPEEVVEEIIPEVEIEEVLPEEVIEEVVPEVEIEELIPDEVVEEVLPEELVEEVIPEEVAVEVVPEEVIEEAVP
EEIVEEFIPEEQIEEVIQEEIIEQVVPEELIEEVVPEEIIEEVIPEEIVEEVIYEEVIPEELVEEVIAEKLVKEI
VPEQVREEVTLEEIVEEMIPEEFVEEVAPEVEIEEIIPEELIEEVIPEVLVEEAVPEELIEKVIPEVLVEEIIYK
EGIPEVLIEEVIPEELVQEVIPEEIVEEVVPEEFIEEMIPQEVVKEVITEKFIEEMIPEEVVEEVIPEEFIEEMI
PEVVVEEVVPEELVEEMLPEELIEVVVPEELIEEVIPEELVEEVVAEELVEEVIPEEL

402_PF3D7_1149200_e2s2_2 → ring infected erythrocyte surface antigen 3

PDTRFYDILGVGVNADMKEISESYFKLAKQYYPPKYSVNEGMLKFKQISEAYQILGDIDKRKMYNKFGYDGIKGV
NFIHPTIYYMLASLEKFAFYTGSPQIVTLMKFLFEKKLTVNDLDTKSEHLSKIMGVYQKERETYISENLISRLQP
YIDSIRNWDVQIKDQIYELMGSPFDIAIIDSIGWTLQYVSMSHMKNPKKAIKKLETRSKKNKETVAYENNKLMNI
LREYFGNNEQINSITYNMEYNTLNENNENGYRKILNLNHKKQKKLFEEIISYIVNISLSDIENTVKNSAESILTV
EGLDEKKLSKRIESLRMLANAIRKYILRGKKGKKYKNKDAKSLSGNIANEINLINKELQNLKEHTQANIPEHIEE
NVQENMEENVEENVEENVEENVEENVEENVEENVEENVEENVEENVEENVEENIEENVEENVEENIEENIEENAEENVE
ENIEENIEENIEENIEENIEENVEENVEENIEENVEENVEENAEENAEENAEENAEENDETPQEHNEEYDE

696_PF3D7_0804500_e3_3 → uncharacterized protein

LKIYEILPGLQVVFIKEIEIKHDVSPKKCICEEKIHELKERRKKEEHENEGISIFNLSYFLSSNYHKKQSNTRSD
EKMNSSYNYSYNRMPSDNNKSNNLLNGSAQNVNTNDSKKTVQLYSFQKNDKKKEKNTNSSFNSISHLKSPSENSE
EMDIHSDKEGYQSVIIGGINFGYLGFNFSKFMNNKKKITIIDAYLLSTTHLVTISNNGTIALIKI

651_PF3D7_1038400_e7s1_3 → Pf 11.1

KVVPEELVEEVIPEEIVEEVIPEELIEEFVPEELVEEEVPEELVEEVIPEVLVEEVIPEEFVEEVIPEELVEEVI
PEELFEEVVPEELVEEVIPEEIVEEVIPEELIEEVVPEVLVEEVIPEELVEEVIPEELFEEVVPEELVAEVIPEE
IVEEVIPEELIEEFVPEELVEEEVPEELVEEVIPEVLVEEEVPEELVEEVIPEELVEEMLPEELIEVVVPEELVE
EVVPEIVEEVVPEELVEEVIPEEVVEEVLPEKLVEEVVPEIVEEVAPEVVEEVIPEELVEEIIPEILVEEVVPIE
VVEEAVPEVVVEEVVPEKIVEEVVPEKVLEEVIPELLVEEIVPIEVVGEIVPEEVVEKIVPMEVVEELLPEVVEE
VPHEIVEEEVVKEVIPEDEKKVEIVEIIIEEKVEKIPKKKVIEKKKEKEKIRKPKKKVEKEIKPKEVKGVKGKLK
KDVKAKHLKGSKVKITEDIQKKMEDDIKEKIMEKELKEEIKDKEYLRKVIPKEEKKEPIPKKGKSVEPKKEKQAG
VKKEKVPETKKEKAPAPKKEKVQAPKKEKVPAPKKEKPAVPKKEKVPEPKKEKVPEPKKEKAPAPKKEKVQAPKK
EKAPAPKKEKAPAPKKEKAPAPKKEKAPAPKKEKPAVPKKEKPAVPKKEKVPETKKEKVPETKKEKVPETKKEKV
PVPKKEKVPAPKKEKVPAPKKEKVPAPKKEKPAVPKKEKVPETKKEKAPEPKKEKAPEPKKEKAPEPKKEKAPEP
KKEKAPAPKKEKVPVPKKEKVPAPKKEKVPAPKKEKPAVPKKEKVPETKKEKEKDSQPKKEKAKETSRPPKKEKE
KGK

643_PF3D7_1038400_e5s3_3 → Pf 11.1

EELIEVVVPEELVEEVVPEELVEEVVPEEVVEEVIPEELIEELVPEVEIEEILPEELIEELVPEEIIEEVIPKEL
IEEVIPEVVVEEVVPEVLVEEVVPEELVEEVIPEVLVEEEVPEELVEDVIPEELVEEVVPEELVEEVIPEEVVEE
VLPEELVEEVVPEEIVEEVIPEELVEEEVPEELVEEVIPEEVVEEVIPEEVPEKVIPEKLVEELIPEEVVEELIP
EEVVEEMVPIEVVEEVVPTEVLEEVIPEIVVEEVVPEELVEEVIPEELVEEVIPEIVVEEVVPEELVEEVIPEEL
VEEVVPEELVEEVVPEEIVEELLPKEIVEEVIYEEQVEEVIHEELVAEVIPEEVVEEVVPEVVEEVVPEIVAEVI
PEEVVEEVVPEVVEEVVPEVVEEVIPEEVVEEVIPEEFIEEMIPEEIVEEVVPEVVEEVIPEELVAEVIPEELVE
EVIPEVLFEEEIPEVVVEEVVPEVVEEEIPEVVVEEVVPEVVEEVIPEEVVEELIPEEVVEEMVPIEIVEEVVPT
EVLEEVIPEIVVEEVVPEELVEEVIPEELVEEVVPEELVEEVVPEVVEEVVPEVVEEVVPEELVEEVIPEVVVEE
VVPEELVEEVIPEELVEEIIPEEIVEEVIPEELIEEVVPEVLVEEVIPEELVEEVIPEELFEEVVPEELVAEVIP

EEIVEEVIPEELIEEFVPEELVEEEVPEELVEEVIPEVLVEEVIPEEFVEEVIPEEIVEEVIPEEIVEEVIPEEV
VEEVVPEIVAEVIPEEVVEEVVPEIVAE

1070_PF3D7_0909000-S2_C_4 → uncharacterized protein

MLEYNDICVCINNLNNMKVKKAFFMVQDLFIKKYNCNKKKRKLFLRNIFISEILYRYKIIKKTEIIFNMNNEPPC
DNYMKYSIISKRLYRNYTFDYIIDLIDVNGKVCFMKYISCLNKINHYFKNIKLKSIEIINSSSLENNYSSFETLN
SISSEEFSDLEKKNKNIYSKNNIKGRSKNQKEKKKKKKKSESMCDKCISNVYIDFSHFNLAYEDEDNEVFYYVTK
KEYALLRRSSSFSYYIEKEGKKEENKTIKKKTVERVEDINMTHLDVEHDHIKEDDRKNSEPEQYKKINKNKKNHL
YINKKSHSIEQNSQNISLEKCDEKSDFNTVIYFYVNLLIPSNFIYIIASLIEATLFKSWIPFYTFPFKFGITDCK
LLKERGLIDKMVYTKIAMPWIIRDRYLLMDVWICEDFEYSRGIFLYATNFPRNTEINNNVNFDTDNCIEIDMSIH
AFICPKSFDKTNVKCYVEISPNMNFNEFFISFITKVFIKSCITHFIKVCKEFEINEDYNKELQKNIFFYDKLRKA
AKEYKIYYPYDVP

86_PF3D7_1038400_e1s1_1 → Pf 11.1

MKTKYKTLMVNIDDNDLGKRGNKIKPKHKKVEINLNDNNLSNNESKRKSRRKKVKVNLKDNLAKREGKMKRRNKK
EKRRKEKDNKKMNELKLKREYKESYLLDNKSDMDVIRNDKFSYFTLYKNNLFPNSNNYFLHMLKTYDEENKGIDE
NTDINENVEENEYVDKNTEGDKDGDEDKGGGESEGGDGHGSAGDSAGGDRGGDENKDKDNEENKDKKGNKDDDDE
EEEEEEEDDEEKEEKDEKDEKDEKDEKDEKDEKDEKDEKDEKDEKDEKDEKDEKGEKDESKGEEKFLKEEKMPKK
EENMQDKIERDKEFEGFKDEYFTQMEGGAYGITVEHEGQKLRETLTEGVEGYEKVIEEMEQTKLDEFLLPTNEGK
SDDFVSEMEEERLFNFVSYMEEEVKDKMFIEREQGTEEEVIHEDLSDEKIGIEKKELETFVQDVSDEVLQDEQLI
EEEKLTEEEKLTEEEKLTEEEKLTEDEQLIEEEKLTEEEKLTEEEKLTEEEKLTEEEKLTEEEKLTEEEKLTEEE
KLTEEEKLTEEEIFIEEDKISPKEVEEPLEDVLMEKMEKEYKEILHEGKSVVTQDMDEKLLSENLEDDLIPEEII
EELVDEELVEEVTAEEIVEEFVAEVEIEEKIPKELVEEVMPEEDVDEVVPEELVEEVVPEELIEGVIPEELVEDV
IPEKVLEKVIPEEIIEELVLEEVVEEIKHEELVEEEIPEEVTEEVIPDEVVEEVIPEELIEKVVKEELVEKVVAE
EIVEEVVPEELVEKVVAEEIVEEVIPEELIEEVITEKPAEEVIPEELVEEVIPKEIVEEVLPEEVVKEVIPEEVV
EEVIPEELVEEVIPEEIVEEVVPEELVEEMKPEEVVEEVISEELVEEMKPEEVVEEMKPEEVVEEVTPEKVVEEV
VPEELVEEMKPEEVVEEVISEE

101_PF3D7_0522400_e3s1_1 → uncharacterized protein

YEMFLTAIEKLFSESTNSLKEPLKIHLKNSQSKILHKTRNGKYCSFSDYEMNERIKVGSLRKKKRKKEIDIMKKK
EKIKNIYKKGYSDGSSFKKEERYYFDIPKNNTGFRITPKEGIELHVIFKKHDIKALNELKEDIKYFKNVEMCILR
HNKEYSSEHHLNNTPRDEMYVKKSCNCYNISKQVSMDENNKYNINIEHNDNNIENFENNNSNSNSNSNNYYMNNN
FPVYNDPKQHNVNNINNEIISIDYDLIIENGFKNDVPPTFNNISNYENLEINFTSECFNAFFNFIKYIEFYYLYK
GGCTKIFNIVPSIEECIKYSEYRKTFNQKNSKMNDEYAEEFMNKFEASCPIHLLTKLRLLSDERIYSKEYFNNIQ
KGEWKKLFYNFIKNKKGKNYMIDENLEKLDRWFTHDMLFNLVLPQINFTYIPLNLNHYNNNKIYYNKCFLSYNIS
CSFLFKQEKLSSMKKRYAIYMHNFNIHSLFVLFKRNKKFLINKKFCPIYLIEKLGIKNHCVYNEISHKCMNPYDI
HPHNFNEEYLLEQNFITQNIQNGHNYNKDINDKNYKDNFNQNYDYEKSKKNYKGSILNSLGKNTNNIDIHHEVNN
NLPSDIMRSNSTCSNYKIHYEHNYNNIEHYDNTVNYKENKKCSHIITTKEKEAYMRSAGQRGRNHLFYNEYYNNT
TKGRYKNMYMNNLNYNKYNDNNCDNNCDNNCDHYCDNNCDNNNYYYEKDYMCHIFFNNDNKVNDNMQYKYIDGNI
DTNNVDKKKIPIENLQSFKNEYISQKHNMNKNKMIHENDINYNKNNVDSKTDDKKGFWKFILGKKYKGEDDSIKN
NKSNYNTILGTNFDLLIYNKINKLPNCTMIFINDYSNNIREMDIYICKYIININNLIPIMNFIPKNNICLEIFLK
YDNIIDKDVIEALTLYLSMGSARKKIVQVCIEQL

Supplementary data 4: Sequences of the recombinant proteins used in the protein microarray.

>tr|Q8I0U6|Q8I0U6_PLAF7 Ring-infected erythrocyte surface antigen OS=Plasmodium falciparum (isolate 3D7) OX=36329 GN=PF3D7_0102200 PE=4 SV=1

MRPFHAYSWIFSQQYMDTKNVKEKNPTIYSFDDEEKRNENKSFLKVLCSKRGVLPIIGIL
YIILNGNLGYNGSSSSGVQFTDRCSRNLYGETLPVNPYADSENPIVVSQVFGLPFEKPTF
TLESPPDIDHTNILGFNEKFMTDVNRYRYSNNYEAIPHISEFNPLIVDKVLFDYNEKVDN
LGRSGGDIIKKMQTLWDEIMDINKRKYDSLKEKLQKTYSQYKVQYDMPKEAYESKWTQCI
KLIDQGGENLEERLNSQFKNWYRQKYLNLEEYRRLTVLNQIAWKALSNQIQYSCRKIMNS
DISSFKHINELKSLEHRAAKAAEAEMKKRAQKPKKKKSRRGWLCCGGGDIETVEPQQEEP
VQTVQEQQVNEYGDILPSLRASITNSAINYYDTVKDGVYLDHETSDALYTDEDLLFDLEK
QKYMDMLDTSEEESVKENEEEHTVDDEHVEEHTADDEHVEEPTVADDEHVEEPTVADEHV
EEPTVAEEHVEEPTVAEEHVEEPASDVQQTSEAAPTIEIPDTLYYDILGVGVNADMNEIT
ERYFKLAENYYPYQRSGSTVFHNFRKVNEAYQVLGDIDKKRWYNKYGYDGIKQVNFMNPS
IFYLLSSLEKFKDFTGTPQIVTLLRFFFEKRLSMNDLENKSEHLLKFMEQYQKEREAHVS
EYLLNILQPCIAGDSKWNVPIITKLEGLKGSRFDIPILESLRWIFKHVAKTHLKKSSKSA
KKLQQRTQANKQELANINNNLMSTLKEYVGSSEQMNSITYNFENINSNVDNGNQSKNISD
LSYTDQKEILEKIVSYIVDISLYDIENTALNAAEQLLSDNSVDEKTLKKRAQSLKKLSSI
MERYAGGKRNDKKAKKYDTQDVVGYIMHGISTINKEMKNQNENVPEHVQHNAEANVEHDA
EENVEHDAEENVEENVEENVEENVEENVEENVEENVEENVEENVEENVEENVEENVEENV
EENVEENVEEYDEENVEEVEENVEEYDEENVEEVEENVEENVEENVEENVEEYDEENVEE
VEENVEENVEENVEENVEENVEEVEENVEENVEENVEENVEENVEENVEEYDEENVEEHN
EEYDE

Supplementary data 5: RESA protein sequence from Uniprot database

Written in light blue are the amino acid comprised in the truncated recombinant RESA protein that what used to test B1E11K binding in Western blot. In yellow are highlighted the EENVEE repeats. In green is highlighted EENVEHDA motif.

>tr|Q8IHN1|Q8IHN1_PLAF7 Ring-infected erythrocyte surface antigen OS=Plasmodium falciparum (isolate 3D7) OX=36329 GN=PF3D7_1149200 PE=4 SV=1

MKPYSSYSSAFSKQYMGTKSVKAKNPTIYSFEEEKQNENMSLLKSLCSKRLVLPILGILY
IILNGNFGYNGSSNSGAQFTDRCSRNLYCETLPINPYADSENPIVVSQVFGLPSEKPTFT
LEGTPDIDHTNILGFNEKLMTDVNRYRYSNNYEAIPHTREFNPLIVDKVLFDYNEKVDNL
GRSGGDIIKKMQTLWDEIMDINKRKYDFLKTKLQKTYSQYKVQYDMPKEVYESKWGQCLK
LINQGGDNLEERLNTQFKNWYRQKYLNLEEYRRLTVLNQIAWKALSNQIQYTCRKIMNSN
ISSFKHISELKSLEQRAAKDAQEEMRKRAEKQKKKKSKRRGWLCCGGGDNETVEPQQEEP
VQDVGEHQINEYGDILPSLKVSINNSAINYYDAVKDGKYLDDDSSDALYTDEDLLFDLEK
QKYMDMLDGSEDESVEDNEEEHSGEANEEELSVDENVEEQNVDESGEQQSDDESGEHQSV
NEIVEEQSVNEIVEEQTVDEIVEQETVDENVEEQAVDENEEQQTVDENVEQQTIDESQVQ
EEISTIQENIEEVVSEVQQDSEVDRTLHVPDTRFYDILGVGVNADMKEISESYFKLAKQY
YPPKYSVNEGMLKFKQISEAYQILGDIDKRKMYNKFGYDGIKGVNFIHPTIYYMLASLEK
FAFYTGSPQIVTLMKFLFEKKLTVNDLDTKSEHLSKIMGVYQKERETYISENLISRLQPY
IDSIRNWDVQIKDQIYELMGSPFDIAIIDSIGWTLQYVSMSHMKNPKKAIKKLETRSKKN
KETVAYENNKLMNILREYFGNNEQINSITYNMEYNTLNENNENGYRKILNLNHKKQKKLF
EEIISYIVNISLSDIENTVKNSAESILTVEGLDEKKLSKRIESLRMLANAIRKYILRGKK
GKKYKNKDAKSLSGNIANEINLINKELQNLKEHTQANIPEHIEENVQENMEENVEENVEE
NVEENVEENVEENVEENVEENVEENVEENVEENIEENVEENVEENIEENIEENAEENVEE
NIEENIEENIEENIEENIEENVEENVEENIEENVEENVEENAEENAEENAEENAEENDET
PQEHNEEYDE

Supplementary data 6: RESA3 protein sequence from Uniprot database

Written in light blue are the amino acid comprised in the truncated recombinant RESA3 protein that what used to test B1E11K binding in Western blot. In yellow are the EENVEE repeats.

GSTtagVVPEVVEEVVPEVVEEVVPEVVEEVVPEVVEEVVPEVVEEVVPEVVEEVVPEVVEEVVPEVVEEVVPEV
VEEVVPEEL

Supplementary data 7: Sequence of the Pfs11.1 fragment used in Western blot experiment

>tr|Q8I6U6|Q8I6U6_PLAF7 Gametocyte-specific protein
OS=Plasmodium falciparum (isolate 3D7) OX=36329
GN=PF3D7_1038400 PE=4 SV=2
MKKESYRFLNISINNGSDKKKKSNFFVKIKNGTDLKDTKKDRIRFHFYFYFFIVKIILLS
LLIWTVIYSNNCSNGKYKSTLYIVGNHLRFRGFRILAENEYEMKTKYKTLMVNIDDNDLG
KRGNKIKPKHKKVEINLNDNNLSNNESKRKSRRKKVKVNLKDNLAKREGKMKRRNKKEKR
RKEKDNKKMNELKLKREYKESYLLDNKSDMDVIRNDKFSYFTLYKNNLFPNSNNYFLHML
KTYDEENKGIDENTDINENVEENEYVDKNTEGDKDGDEDKGGGESEGGDGHGSAGDSAGG
DRGGDENKDKDNEENKDKKGNKDDDDEEEEEEEEDDEEKEEKDEKDEKDEKDEKDEKDEK
DEKDEKDEKDEKDEKDEKDEKGEKDESKGEEKFLKEEKMPKKEENMQDKIERDKEFEGFK
DEYFTQMEGGAYGITVEHEGQKLRETLTEGVEGYEKVIEEMEQTKLDEFLLPTNEGKSDD
FVSEMEEERLFNFVSYMEEEVKDKMFIEREQGTEEEVIHEDLSDEKIGIEKKELETFVQD
VSDEVLQDEQLIEEEKLTEEEKLTEEEKLTEEEKLTEDEQLIEEEKLTEEEKLTEEEKLT
EEEKLTEEEKLTEEEKLTEEEKLTEEEKLTEEEKLTEEEIFIEEDKISPKEVEEPLEDVL
MEKMEKEYKEILHEGKSVVTQDMDEKLLSENLEDDLIPEEIIEELVDEELVEEVTAEEIV
EEFVAEVEIEEKIPKELVEEVMPEEDVDEVVPEELVEEVVPEELIEGVIPEELVEDVIPE
KVLEKVIPEEIIEELVLEEVVEEIKHEELVEEEIPEEVTEEVIPDEVVEEVIPEELIEKV
VKEELVEKVVAEEIVEEVVPEELVEKVVAEEIVEEVIPEELIEEVITEKPAEEVIPEELV
EEVIPKEIVEEVLPEEVVKEVIPEEVVEEVIPEELVEEVIPEEIVEEVVPEELVEEMKPE
EVVEEVISEELVEEMKPEEVVEEMKPEEVVEEVTPEKVVEEVVPEELVEEMKPEEVVEEV
ISEELVEEMKPEEVVEEVTPEKVVEEVVPEELVEEMKPEEVVEEVISEELVEEMKPEEVV
EEVISEELVEEMKPEEVVEEVTPEKVVEEVVPEELVEEMKPEEVVEEVISEELVEEMKPE
EVVEEVTPEKVVEEVVPEELVEEMKPEEVVEEVISEELVEEMKPEEVVEEVVPEELVEEV
IPEEVVEEIIPEEVVHEAKHEELFEKTVPEVEVQEIIPKELVEVIPEEVLPEELIEEVIP
EEIIEEVIPEEVVEEVIPEEIVQEVIPEDLMEEVVPEEIIEEKILEEIVEEEIHEEIVEE
IISEEVVEEVVPAEVVEEMIPEKLVEEVIPEELVEEVISEELVEEVVPVEVLEEVVPVEV
LEEVIPEEVVEEVIPEEFIEEMIPEEIVEEVVPEVVEEVIPEELVEEVVPVELLEEVIPE
ELLEEVIPEELVEEVVPEELVEDVIPEELIAEVVSEELVEEEIPEEVLEEVIPEELVEEV
IPEELVEEVIPEVLVEEVIPEELVEEVIPEVLVEEEVPEELVEEVIPELLVAEVIPEELV
AEVIPEEFVEEVIPEEVVEELVPEELVEEVIPEEIVEEVVEEVVEEIIPEEVIEEVIPEE
IVKEVVPEVLVEEVVPEEIVEEVVPEEIVEEVVPEELVEEVVPEELIEEVIPEELVEEVI
PEVLVEEVIPEVLVEEMVLEELVEEVIPEVLVEEMVPEEVVEKMVLEEVVEEVIPEEVVE
EVIPEEDVEQVIPEELIEEVVPEEVIEEVITEEVVEEVLPEELVEKVVEEEILEEVIPEE
LVEEVVREELIEEVVTEELVEKVVEEEIVEEVVLAEVVEEVIPQEIVEEVIPEEVVEEVI
PKEIVEEVIPEELVEEVVPEELVAEVIPEELVAEVIPEELIEEVVTEELVEEVIPEEVVE
EVIPEEVVEEVVPEELVEEVVPEELVEEVVPEEIVEELLPKEVVEEVIYEEQVEEVIPEE
LVAEVIPEKLVEEVIPEELVEEVIPEELVEEVVPEVVEEVVPEELVEEVIPEELVEEVIP
EVLVEEEVPEELVEEVIPEELVEEMLPEELIEVVVPEELVEEVVPEELVEEVVPEEVVEE
VIPEELIEELVPEVEIEEILPEELIEELVPEEIIEEVIPKELIEEVIPEVVVEEVVPEVV
EEVVPEIVEEVVPEVVEEVVPEEIIEEKISEEVVEEVLPKEIVEEVIPEELVEEVVPEEL
VAEVIPEELVEEVIPEVLFEEEIPEVVVEEVVPEVVEEEIPEVVVEEVVPEVVEEVIPEE
LVEEVIPEELIEEVIPEEVAEEVLPEELIEEVIPEELVEEVVPEELVAEVIPEEIVEEVV
REELVEEVVPEEVVEEVIPKEIVEEVVSEEVVEEVIPKEIVEEEVPEELVEVVPEELVEE
VVPEELVEEVVPEELVEEVVPEELVEEVVPEELVEEVVPEVVEEVQEQLVEEFIPEEVVE
ELVPEELVEEVIPEELVEEVIPEEIVEEVLPEEVVKEVIPEEVVEEVIPEELVEEVIPEE
IVEEVLPEEVVKEVIPEEVVEEVIPEELVEEVIPEELVEEVIPEELVEEVVSEELVEEVI
PEEIVEEVIPEELLEEVVEEVVPEIVEEVVPEVVEEVITEEVIPEELIKEVIPEELVEEV
IPEEIVEEVIPEEIVEEVISEEVVEEVVPEVVVEEVIPEEIVEEVLPKEIVEEVISEKVV
EEMIPEELVEEVIPEEVVEEVIPEVEIEEILPEELIEELVAEEVIEEVIPKELIEEVIPE
KLIEDVVPEEIVEEVLPEEVVKEVIPEEVVEEVLPEELVEEVIPEVVEEVVPEELVEEVL
PKEVVEEVIPEVEIEEILPEEIIEELVAKEVIEEVIPKELIEEAITEEVVEEMIPEEIIE
EVVPEEVIEEVITEEVVEEVVPEEVIEEVITEEVVEEAIPEEVVEEVIPEVEIEEVLPEE
LIEELVPEEVTEEVITEEVVEEAISEVVEEVIPEEIVKEVIPEEVVEEIITEEIAEEIIP
KELVEEVIPEEVVVEIIPEKLVEEFVSEELVEELVPEEIVEKVVPEELVEEIVPEELVEE
VVPEELVEEVIPEELVEEFIPEEVVEEVLPEQLVEEVISEVVEEVVPEELVEEVIPEEVV

EELVAEEVIEEVIPKELIEEAITEEVEEVIPEEIVEEVIPEEVVKEVIPEVEIEEILPEE
LIEELVAKEVIEEVITEEVAEEVIPEEIVQEVIPEEVVEEIITEVEIEEVLPEELIDEVV
PEEVTEEVITEEVMPEEVVKEVIPEEIAEEVIPKELVEEVIPEEVVEEIIPEVEIEEVLP
EEVIEEVVPEVEIEELIPDEVVEEVLPEELVEEVIPEEVAVEVVPEEVIEEAVPEEIVEE
FIPEEQIEEVIQEEIIEQVVPEELIEEVVPEEIIEEVIPEEIVEEVIYEEVIPEELVEEV
IAEKLVKEIVPEQVREEVTLEEIVEEMIPEEFVEEVAPEVEIEEIIPEELIEEVIPEVLV
EEAVPEELIEKVIPEVLVEEIIYKEGIPEVLIEEVIPEELVQEVIPEEIVEEVVPEEFIE
EMIPQEVVKEVITEKFIEEMIPEEVVEEVIPEEFIEEMIPEVVVEEVVPEELVEEMLPEE
LIEVVVPEELIEEVIPEELVEEVVAEELVEEVIPEELVEKVVPEVVEEFIHEVVEEVVPE
VVEEVVPEVVEEVVPEVVEEVVPEVVEEVVPEVVEEVVPEVVEEVVPEVVEEVVPEVVEE
VVPEVVEEVVPEELVEEVIPEVLFEEEIPEELVEVVPVELLEEAIPEELVEEVIPEELVE
EVIPEELVEEVIPEELVEEVILEELVEEVIPEELVEEVIPEELVEEVIPEVLVEEEIPEK
LVEEDIPEKLVEEVVPEELVEVVIPEELVEEVIPEELVKEVIPEELVKEVVPEELVEEEI
PKVVEEVLPEELVEEVMLEEVVEEVVPEIVEEVVPEELVEEVVPEVVEEVVPEEIVEEVI
PEELVEEVVKEELVEEVVKEELVEEVVKEELVEEVIPEVLVEEVVPEELLEEVIPKVLVE
EVIPELLVEEVVPEVIEEVVPEVVEEVVPEELLEEVIPEVLVEEEIPEKLVEEVVPEELV
EEVIPEVLVEEVVPEELVEEVISEELVEEVIPEELVEEVIPEEVVEEVVPEVVEEVVPEV
VEEVVPEVVEEVVPEVVEEVVPEVVEEVVPEVVEEVVPEVVEEVVPEVVEEVVPEVVEEV
VPEELIEEVIPEEIVEEVIPEELVAEVIPEKLVEEVIPEELVEEVIPEELVEEVIPEELV
EEVLPEEVVEEAVPEVVEEIVPEELIEEVIPEELIKEVVPEEVIEEVITEEVVEEVLPEE
IVEEVLPEEVIEEVVPEEVLPEEVVEEVVPEELVEEVVPEELVEEVIPEELVEEVL
PEEVVEEVVPKELVEELIPEELVEEVIPEELVEEVVPEELVAEVIPEELVEEVIPEELVE
EVIPEELVEEEIPEELVEEVILEELVEEVVPEELIEEVVPEELIEEVVPEELIEEVVEKV
IPEEIIEEVVPEEVIEEVITEEVVEEVVPEKVIEEVITEEVVEEVVPEEVIDEVITEEVV
EEVVPEEVIEEVIIEEVVEEVVPEEVIEEVITEEVVEEAIPEELVEEVIPEVLVEEEIPE
ELVEEVILEELVEEVVAEELIEEVVEEVIPEKLVEEVIPEEIVEEVIPEELVEVVVPEEL
VEEVIPEELVEEVIHEELVEEVIPEELVEEVIHEEIVEEVIPEEVVEEVIPEEIVEEVVP
EELLEEVIPELLVEEVVPEVVEEVVPVELLEEVVEEVITEEVIPEELIKEVISEELVEEL
IPEEVVQEVITEEVLEEVIPEEIVEELIPEKLIGEVVPEKVVEEVVLEEVVEEVIPEEIV
EEVITEEVLAEEIVEEFVPEELVEEMLPEEVVEERVREVEIEEEMVPEVLVEEVLPEVVEE
VITEEVVEEMVPEEVVEEMVPKEIVEEVLPEEVVEEVIPEEVVEEMVPEVLVEEVVPEEI
VEKVVPEEVVEEVVAEEIIEEVITEEVVEEIVPGEVVEEMVPEEIIEEVVPEEVIEEVIT
EEVVEEVIPEELVEEVIPEISVEVEIPEVLVEEVIPEKLVKVVPEELVEEVIPEELVEEV
ITEALVEEVVDVVVPEEIFEEVLPEEVVEEVIPEEVVEEMVPEEVVEEVVPEELVEEVIP
EEVVEKVVPEQLVEKVVPEELVEKVLPEELVEEVVPEELIEEVVTEEVIEEIIPEEIIEE
IIPEEVVEERVSIEVVEELVPEELIEEVVAEEIFEEVVPEKLIEEVVAEELIEEMVPEVV
EEVVEEIIPEEVIEEVIPEEIREEIIPEEVVEEVIEEVIPEELIEEEISREIVEEVIPEE
VVEEMMPEEVIEEVIPEEIREEMIPEEVVEEMIPEIEIEQVLPEELIEELVPEVEIEEIL
PEELIEELVPEGVIEEVIPKELIEEVIPEELIKEVVPEEVVEEVIPKEIVEEVVPEELIE
EVIPEELIEEVVPEEMIEEVIPEELIEEVVPEEMIEEVIPEELIEEVVPEEVKEEVIPVE
LIEEVVPEEMIEEVISEEVVEEVIPEELVEEVLPEVFVEEIVPKELVEEVIPEEIVEEVI
PEELVEEVIPEELVEEVISEELLEEVIPELLVEEVVPEVIEEVVPEVVEEVIPEVVEEVV
TEELVEEVIPEEVVEEMIPGVEIEEVLPEELVEEVIPEEIVEEVISEEDFEEVIPEALVE
EVIPELLVEEVVLEELIEEVIPEVVEEVIPEEVVEEVIPEEVVEKVVPEELVEEVIPEEL
VEEVIPEEVPEEVVPEELVEEVISEELVEEVIPEEIVEEVIPEEIVEEVMPEEVAEEVVP
EELVEEEVPEELVEEVIPEVLVEEVIPEEIVEEVVPEEVVEVVIPEEFIEEIIPEEVVVE
VTPEELIEEMKPEELFEEVIPKELIEEIIPEELIKEVIPEEIIEEVISKEIVEEVVEEEI
IEEVIPEEIVEEVVPEELVEKKVPEEIVEEVIYEEFLEEIMPEELIEEMKPEELIEEIIP
REIVEEIITEEVVEEMKPEELVEEMVPEEVVEEMVPEEVVEEMVPEEVVEEVITEKLIEE
VVPEEIIEELIPEELVEEVIPEKLIEEMIPEEVVEEMLLEEVVEEVVPEVEIEEMIPEQL
VEEVVPEELVEKEIPEVVEEIITEEVVEEMVPEEVVEEMVPEEVVEEVILEKLIEEVVPV
EVIEEVVPEEVIEEVIPEKLIEEIIPEVLVEEVVPEELIEEVIPEVLFEEVVPEVVEEVV
PEELVEKVVPEEIVEEVIPEFVEEVISEEIVEEVVTEELIEEMIPEEVVEEVIPEELVEE
VVPVELIEEVVPVELLEEVIPEELVEEVVPVELIEEVVPVELLEEVIPEEVVEEVIPEVV
KEVVPEVVEEVVPEVVEEVVPEVVEEVVPEVVEEVVPEELIEEVIPEELIKEVLPEEVIE
ELKPEELIEEIIPEEVVEEVIPEELIEEMIPELLVEEEVPEELVEEVIPEVLVEEMVPEE
IVEEVIPEELIAEFAPEELFEKVIPEEVVEELVSEELVEEVLPEVVEEVLPEVFEEVIPE
EVIEEIVPEEVMEEVVPKELIEEVIPEELIEEVIPEEVAEEVVPEKLIEEVIPEELIKEV
VPEELIEEVITEEVVEEAISEELVEEVVPEEVVEEVIPEELIEEVVPEELIEEIIPEELV
EEVIPEELVEEVVPEELVEEVIPEELVEEVVPEELVEKLIPEELVEEVIPELLVEEVVPE
EVVEELIPEELVEEVIPEELVEEVIPEEVPEEVIRELVEEVIPEELVEEVIPEEVPEEV
VPEELVQEVIPEELVEEVVHEEVPEEVVPEKLVEEVIPEELFEEVVPEEVPEEVVPEELV
EEVISEELVEEVIPEELVEEFIPEELVEEVIPEELVEEVIPEELVEEFIPEELVEEVIPE

ELVEEVIPEVLVEEEIPEKLVEEVVPEELVEEVIPEVLVEEVVTEEVPEEVVPEELVAEV
VPEELVKEVIPEELVEEVIPEEIVEEVIPEEVVEEVVPEELVEEVIPEEVVEEVIPEELV
EEVVPVELVEEVVPEELVEEVIPEELVEEVIPEEIVEEVIPEEVVEEVIPEEIVEEVISE
ELIEEVVPVELLEEVVPVEVLEDVIPEEVVEEVIPEEFIEEMIPEEIIEEAIPEEIVEEV
IPEVVEEVVPEELVEEVIPEEVVEKVVPEELVEEVIPEELVEEVIPEEVPEEVVPEELVE
EVISEELVEEIIPEELVEEVIPEEVVEEVVPEELVEEVIPEELVEEVIPEELVEEVIPEV
VEEVIPEKLVEEVVPEELIEEMIPEEIVEEVVPEVVEEVIPEELIEEVIPEELVEEVIPE
KLIEEMIPEELVEEVILEEVVEEVIPEEVVEEVLPEELVEEVVPEELVEEVAPVELLEEV
IPEELLEEVIPEELVEEVIPEELVEDVIPEELVEEVIPEELVEEIIPEELVEEVIPEVLV
EEEVPEELVEEVIPEELVEEVIPEELVEELIPEVLEEVIPEKLVEEVVPVELLEEVIPEE
LIEEVVPEVLVEVIPEKVVEEVIHEEIVKEVVPEELVEEVVPEEIVEEVVPEEVLEEVIP
KVLLEEEIPEKLVEEVIPEELIEEVVPEELVEEVMPEEVVEEVVPEELVEEVIPEEVVEE
VIPEELVEEVVPVELLEEIVPVELLEEVIPEELVEEVIPEELVEEVVPEELVAEVIPEKL
VEEVIPEKLVEEVIPEELVEEVVPEELVAEVIPEKLVEEVIPEELVEEIIPEELVEEVVP
EELVEEVVPEELVEEVIPEELVEEVIPEVLVEEEVPEELVEEVIPEELVEEMLPEELIEV
VVPEELVEEVVPEELVEEVVPEEVVEEVIPEELIEELVPEVEIEEILPEELIEELVPEEI
IEEVIPKELIEEVIPEVVVEEVVPEVLVEEVVPEELVEEVIPEVLVEEEVPEELVEDVIP
EELVEEVVPEELVEEVIPEEVVEEVLPEELVEEVVPEEIVEEVIPEELVEEEVPEELVEE
VIPEEVVEEVIPEEVPEKVIPEKLVEELIPEEVVEELIPEEVVEEMVPIEVVEEVVPTEV
LEEVIPEIVVEEVVPEELVEEVIPEELVEEVIPEIVVEEVVPEELVEEVIPEELVEEVVP
EELVEEVVPEEIVEELLPKEIVEEVIYEEQVEEVIHEELVAEVIPEEVVEEVVPEVVEEV
VPEIVAEVIPEEVVEEVVPEVVEEVVPEVVEEVIPEEVVEEVIPEEFIEEMIPEEIVEEV
VPEVVEEVIPEELVAEVIPEELVEEVIPEVLFEEEIPEVVVEEVVPEVVEEEIPEVVVEE
VVPEVVEEVIPEEVVEELIPEEVVEEMVPIEIVEEVVPTEVLEEVIPEIVVEEVVPEELV
EEVIPEELVEEVVPEELVEEVVPEVVEEVVPEVVEEVVPEELVEEVIPEVVVEEVVPEEL
VEEVIPEELVEEIIPEEIVEEVIPEELIEEVVPEVLVEEVIPEELVEEVIPEELFEEVVP
EELVAEVIPEEIVEEVIPEELIEEFVPEELVEEEVPEELVEEVIPEVLVEEVIPEEFVEE
VIPEEIVEEVIPEEIVEEVIPEEVVEEVVPEIVAEVIPEEVVEEVVPEVVEEVVPEVIEE
VVPEVIEEVVPEVVEEVVPEVVEEVVPEVVEEVVPVEVLEEVIPEEVVEEVIPEEFIEEM
IPEEIVEEVVPEVVEDVIPEELIAEVVSEELFEEEIPEELVEVVPVELLEEVIPEELVEE
VIPEELVEEVVPEELVEEVVPEELVEEVIPEELFEEVVPEELVEEVIPEEIVEEVIPEEL
IEEFVPEELVEEEVPEELVEEVIPEVLVEEVIPEEFVEEVIPEELVEEVIPEELFEEVVP
EELVEEVIPEEIVEEVIPEELIEEVVPEVLVEEVIPEELVEEVIPEELFEEVVPEELVAE
VIPEEIVEEVIPEELIEEFVPEELVEEEVPEELVEEVIPEVLVEEEVPEELVEEVIPEEL
VEEMLPEELIEVVVPEELVEEVVPEIVEEVVPEELVEEVIPEEVVEEVLPEKLVEEVVPE
IVEEVAPEVVEEVIPEELVEEIIPEILVEEVVPIEVVEEAVPEVVVEEVVPEKIVEEVVP
EKVLEEVIPELLVEEIVPIEVVGEIVPEEVVEKIVPMEVVEELLPEVVEEVPHEIVEEEV
VKEVIPEDEKKVEIVEIIIEEKVEKIPKKKVIEKKKEKEKIRKPKKKVEKEIKPKEVKGV
KGKLKKDVKAKHLKGSKVKITEDIQKKMEDDIKEKIMEKELKEEIKDKEYLRKVIPKEEK
KEPIPKKGKSVEPKKEKQAGVKKEKVPETKKEKAPAPKKEKVQAPKKEKVPAPKKEKPAV
PKKEKVPEPKKEKVPEPKKEKAPAPKKEKVQAPKKEKAPAPKKEKAPAPKKEKAPAPKKE
KAPAPKKEKPAVPKKEKPAVPKKEKVPETKKEKVPETKKEKVPETKKEKVPVPKKEKVPA
PKKEKVPAPKKEKVPAPKKEKPAVPKKEKVPETKKEKAPEPKKEKAPEPKKEKAPEPKKE
KAPEPKKEKAPAPKKEKVPVPKKEKVPAPKKEKVPAPKKEKPAVPKKEKVPETKKEKEKD
SQPKKEKAKETSRPPKKEKEKGK

Supplementary data 8: Pf11.1 protein sequence from Uniprot database

The VVPEVVEE amino acid repeats are highlighted in blue, as they compose the recombinant "Pf11.1 protein" that what used to test B1E11K binding in Western blot. In yellow are the EENVEE repeats.

>tr|O96275|O96275_PLAF7 Liver stage antigen 3 OS=Plasmodium falciparum (isolate 3D7) OX=36329 GN=PF3D7_0220000 PE=4 SV=1

MTNSNYKSNNKTYNENNNEQITTIFNRTNMNPIKKCHMREKINKYFFLIKILTCTILIWA
VQYANNSDINKSWKKNTYVDKKLNKLFNRSLGESQVNGELASEEVKEKILDLLEEGNTLT
ESVDDNKNLEEAEDIKENILLSNIEEPKENIIDNLLNNIGQNSEKQESVSENVQVSDELF
NELLNSVDVNGEVKENILEESQVNDDIFNSLVKSVQQEQQHNVEEKVEESVEENDEESVE
ENVEENVEENDDESVASSVEESIASSVDESIDSSIEENVAPTVEEIVAPTVEEIVAPSVV
ESVAPSVEESVEENVEESVAENVEESVAENVEESVAENVEESVAENVEESVAENVEESVA
ENVEEIVAPTVEESVAPTVEEIVAPSVEESVAPSVEEIVVPTVEESVAENVEEIVAPSVE
EIVAPSVEEIVAPTVEESVAPTVEEIVAPSVEESVAPSVEEIVVPTVEESVAENVEESVA
ENVEEIVAPSVEEIVAPSVEEIVAPSVEEIVAPSVEEIVAPSVEEIVAPSVEEIVAPSVE
EIVAPSVEEIVAPTVEEIVAPTVEEIVAPSVEEIVAPTVEESVAENVATNLSDNLLSNLL
GGIETEEIKDSILNEIEEVKENVVTTILENVEETTAESVTTFSNILEEIQENTITNDTIE
EKLEELHENVLSAALENTQSEEEKKEVIDVIEEVKEEVATTLIETVEQAEEESASTITEI
FENLEENAVESNENVAENLEKLNETVFNTVLDKVEETVEISGESLENNEMDKAFFSEIFD
NVKGIQENLLTGMFRSIETSIVIQSEEKVDLNENVVSSILDNIENMKEGLLNKLENISST
EGVQETVTEHVEQNVYVDVDVPAMKDQFLGILNEAGGLKEMFFNLEDVFKSESDVITVEE
IKDEPVQKEVEKETVSIIEEMEENIVDVLEEEKEDLTDKMIDAVEESIEISSDSKEETES
IKDKEKDVSLVVEEVQDNDMDESVEKVLELKNMEEELMKDAVEINDITSKLIEETQELNE
VEADLIKDMEKLKELEKALSEDSKEIIDAKDDTLEKVIEEEHDITTTLDEVVELKDVEED
KIEKVSDLKDLEEDILKEVKEIKELESEILEDYKELKTIETDILEEKKEIEKDHFEKFEE
EAEEIKDLEADILKEVSSLEVEEEKKLEEVHELKEEVEHIISGDAHIKGLEEDDLEEVDD
LKGSILDMLKGDMELGDMDKESLEDVTAKLGERVESLKDVLSSALGMDEEQMKTRKKAQR
PKLEEVLLKEEVKEEPKKKITKKKVRFDIKDKEPKDEIVEVEMKDEDIDEDIEEDVEEDI
EEDKVEDIDEDIDEDIDEDIGEDKDEVIDLIVQKEKRIEKVKEKKKKLEKKVEEGVSGLK
KHVDEVMKYVQKIDKEVDKEVSKALESKNDVTNVLKQNQDFFSKVKNFVKKYKVFAAPFI
SAVAAFASYVVGFFTFSLFSSCVTIASSTYLLSKVDKTINKNKERPFYSFVFDIFKNLKH
YLQQMKEKFSKEKNNNVIEVTNKAEKKGNVQVTNKTEKTTKVDKNNKVPKKSRTQKSK

Supplementary data 9: LSA3 protein sequence from Uniprot database

Written in light blue are the amino acid comprised in the truncated recombinant LSA3 protein that what used to test B1E11K binding in Western blot. In yellow are the EENVEE repeats.

>sp|P68875|P230_PLAFO Gametocyte surface protein P230 OS=Plasmodium falciparum (isolate NF54) OX=5843 GN=PF230 PE=1 SV=1

MKKIITLKNLFLIILVYIFSEKKDLRCNVIKGNNIKDDEDKRFHLFYYSHNLFKTPETKEKKNKKECFYKNGGIY
NLSKEIRMRKDTSVKIKQRTCPFHKEGSSFEMGSKNITCFYPIVGKKERKTLDTIIIKKNVTNDHVVSSDMHSNV
QEKNMILIRNIDKENKNDIQNVEEKIQRDTYENKDYESDDTLIEWFDDNTNEENFLLTFLKRCLMKIFSSPKRKK
TVVQKKHKSNFFINSSLKYIYMYLTPSDSFNLVRRNRNLDEEDMSPRDNFVIDDEEEEEEEEEEEEEEEEEEEE
EEEEYDDYVYEESGDETEEQLQEEHQEEVGAESSEESFNDEDEDSVEARDGDMIRVDEYYEDQDGDTYDSTIKNE
DVDEEVGEEVGEEVGEEVGEEVGEEVGEEVGEEVGEEVGEEVGEEGEEVGEGVGEEVGEEEGEEVGEEEGEYVDEKER
QGEIYPFGDEEEKDEGGESFTYEKSEVDKTDLFKFIEGGEGDDVYKVDGSKVLLDDDTISRVSKKHTARDGEYGE
YGEAVEDGENVIKIIRSVLQSGALPSVGVDELDKIDLSYETTESGDTAVSEDSYDKYASNNTNKEYVCDFTDQLK
PTESGPKVKKCEVKVNEPLIKVKIICPLKGSVEKLYDNIEYVPKKSPYVVLTKEETKLKEKLLSKLIYGLLISPT
VNEKENNFKEGVIEFTLPPVVHKATVFYFICDNSKTEDDNKKGNRGIVEVYVEPYGNKINGCAFLDEDEEEEKYG
NQIEEDEHNEKIKMKTFFTQNIYKKNNIYPCYMKLYSGDIGGILFPKNIKSTTCFEEMIPYNKEIKWNKENKSLG
NLVNNSVVYNKEMNAKYFNVQYVHIPTSYKDTLNLFCSIILKEEESNLISTSYLVYVSINEELNFSLFDFYESFV
PIKKTIQVAQKNVNNKEHDYTCDFTDKLDKTVPSTANGKKLFICRKHLKEFDTFTLKCNVNKTQYPNIEIFPKTL
KDKKEVLKLDLDIQYQMFSKFFKFNTQNAKYLNLYPYYLIFPFNHIGKKELKNNPTYKNHKDVKYFEQSSVLSPL
SSADSLGKLLNFLDTQETVCLTEKIRYLNLSINELGSDNNTFSVTFQVPPYIDIKEPFYFMFGCNNNKGEGNIGI
VELLISKQEEKIKGCNFHESKLDYFNENISSDTHECTLHAYENDIIGFNCLETTHPNEVEVEVEDAEIYLQPENC
FNNVYKGLNSVDITTILKNAQTYNINNKKTPTFLKIPPYNLLEDVEISCQCTIKQVVKKIKVIITKNDTVLLKRE
VQSESTLDDKIYKCEHENFINPRVNKTFDENVEYTCNIKIENFFNYIQIFCPAKDLGIYKNIQMYYDIVKPTRVP
QFKKFNNEELHKLIPNSEMLHKTKEMLILYNEEKVDLLHFYVFLPIYIKDIYEFNIVCDNSKTMWKNQLGGKVIY
HITVSKREQKVKGCSFDNEHAHMFSYNKTNVKNCIIDAKPKDLIGFVCPSGTLKLTNCFKDAIVHTNLTNINGIL
YLKNNLANFTYKHQFNYMEIPALMDNDISFKCICVDLKKKKYNVKSPLGPKVLRALYKKLNIKFDNYVTGTDQNK
YLMTYMDLHLSHKRNYLKELFHDLGKKKPADTDANPESIIESLSINESNESGPFPTGDVDAEHLILEGYDTWESL
YDEQLEEVIYNDIESLELKDIEQYVLQVNLKAPKLMMSAQIHNNRHVCDFSKNNLIVPESLKKKEELGGNPVNIH
CYALLKPLDTLYVKCPTSKDNYEAAKVNISENDNEYELQVISLIEKRFHNFETLESKKPGNGDVVVHNGVVDTGP
VLDNSTFEKYFKNIKIKPDKFFEKVINEYDDTEEEKDLESILPGAIVSPMKVLKKKDPFTSYAAFVVPPIVPKDL
HFKVECNNTEYKDENQYISGYNGIIHIDISNSNRKINGCDFSTNNSSILTSSVKLVNGETKNCEININNNEVFGI
ICDNETNLDPEKCFHEIYSKDNKTVKKFREVIPNIDIFSLHNSNKKKVAYAKVPLDYINKLLFSCSCKTSHTNTI
GTMKVTLNKDEKEEEDFKTAQGIKHNNVHLCNFFDNPELTFDNNKIVLCKIDAELFSEVIIQLPIFGTKNVEEGV
QNEEYKKFSLKPSLVFDDNNNDIKVIGKEKNEVSISLALKGVYGNRIFTFDKNGKKGEGISFFIPPIKQDTDLKF
IINETIDNSNIKQRGLIYIFVRKNVSENSFKLCDFTTGSTSLMELNSQVKEKKCTVKIKKGDIFGLKCPKGFAIF
PQACFSNVLLEYYKSDYEDSEHINYYIHKDKKYNLKPKDVIELMDENFRELQNIQQYTGISNITDVLHFKNFNLG
NLPLNFKNHYSTAYAKVPDTFNSIINFSCNCYNPEKHVYGTMQVESDNRNFDNIKKNENVIKNFLLPNIEKYALL
LDDEERQKKIKQQQEEEQQEQILKDQDDRLSRHDDYNKNHTYILYDSNEHICDYEKNESLISTLPNDTKKIQKSI
CKINAKALDVVTIKCPHTKNFTPKDYFPNSSLITNDKKIVITFDKKNFVTYIDPTKKTFSLKDIYIQSFYGVSLD
HLNQIKKIHEEWDDVHLFYPPHNVLHNVVLNNHIVNLSSALEGVLFMKSKVTGDETATKKNTTLPTDGVSSILIP
PYVKEDITFHLFCGKSTTKKPNKKNTSLALIHIHISSNRNIIHGCDFLYLENQTNDAISNNNNNSYSIFTHNKNT
ENNLICDISLIPKTVIGIKCPNKKLNPQTCFDEVYYVKQEDVPSKTITADKYNTFSKDKIGNILKNAISINNPDE
KDNTYTYLILPEKFEEELIDTKKVLACTCDNKYIIHMKIEKSTMDKIKIDEKKTIGKDICKYDVTTKVATCEIID
TIDSSVLKEHHTVHYSITLSRWDKLIIKYPTNEKTHFENFFVNPFNLKDKVLYNYNKPINIEHILPGAITTDIYD
TRTKIKQYILRIPPYVHKDIHFSLEFNNSLSLTKQNQNIIYGNVAKIFIHINQGYKEIHGCDFTGKYSHLFTYSK
KPLPNDDDICNVTIGNNTFSGFACLSHFELKPNNCFSSVYDYNEANKVKKLFDLSTKVELDHIKQNTSGYTLSYI
IFNKESTKLKFSCTCSSNYSNYTIRITFDPNYIIPEPQSRAIIKYVDLQDKNFAKYLRKL

Supplementary data 10: EEVGEE repeats localisation among Pf 230 protein, from Uniprot database

Pfs230 also contains a glutamic-acid rich repeated region. Both regions are cleaved from gametocyte during its erythrocyte egress, and usually mAbs generated against those regions do not fix gametes (127)

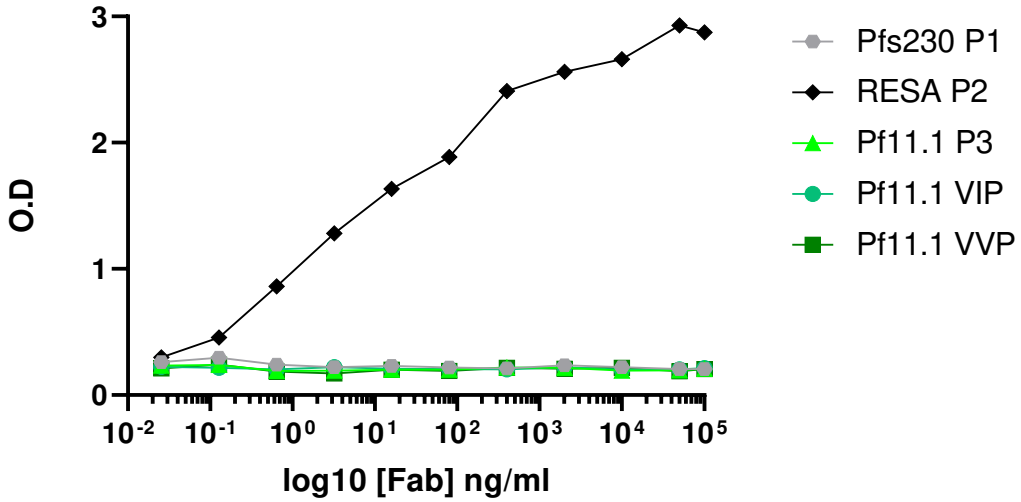

Supplementary data 11: B1E11K Fab binding to Pfs230 (P1), RESA (P2), Pf11.1 (P3), Pf11.1 VIP, Pf11.1 VVP peptides.

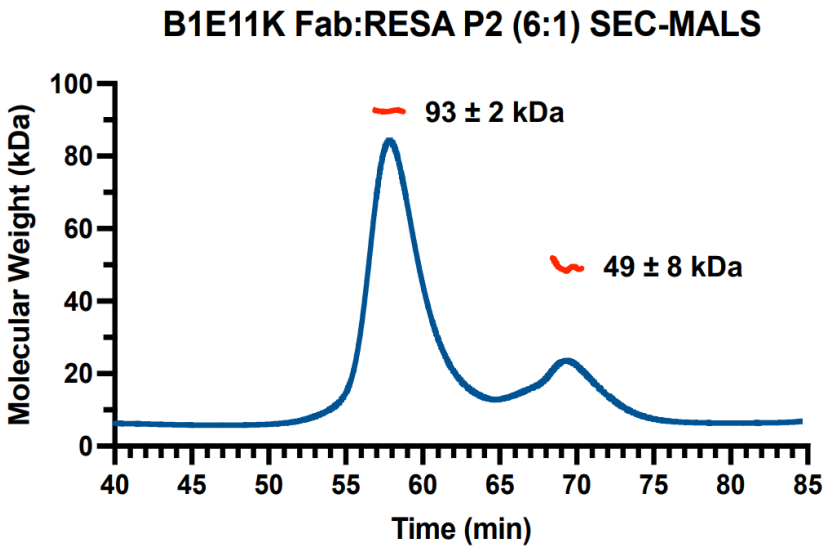

Supplementary data 9: SEC-MALS profiles of B1E11K Fab in complex with RESA *(P2)*

	B1E11K-RESA P2
Space group	$C222_1$
Cell dimensions	
a,b,c (Å)	78.6, 186.1, 131.5
α, β, γ (°)	90, 90, 90
Resolution (Å)	49.0–2.97 (3.08–2.97)
<I/σI>	10.2 (1.5)
Refinement Statistics	
R_{factor}/R_{free}	21.9/26.6
Rms deviations from ideality	
Bond lengths (Å)	0.002
Bond angle (°)	0.49
Ramachandran plot (%)	
Favoured regions	95.8
Allowed regions	4.2

Statistics for the highest-resolution shell are shown in parentheses.

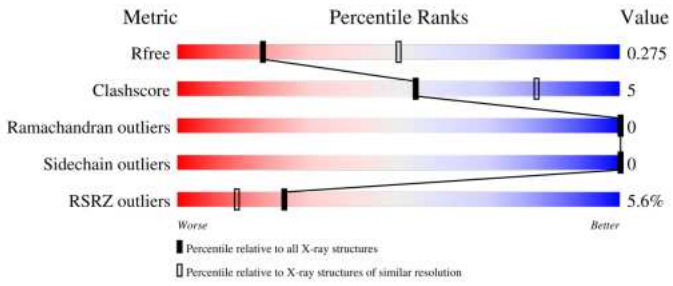

Supplementary data 10: Key statistics of B1E11K Fab – PRESA *(P2)* interactions in crystallography experiments

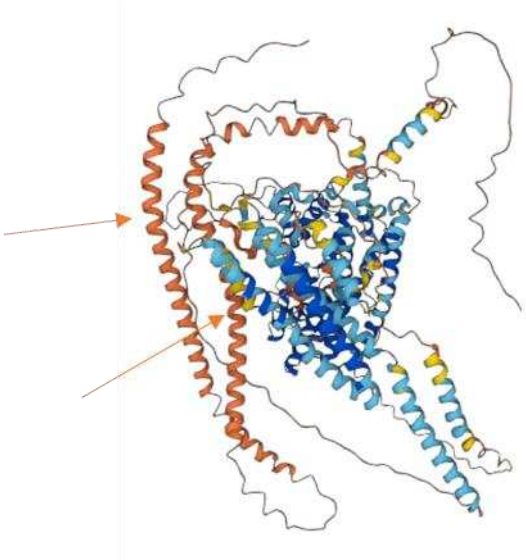

Supplementary data 11: Alphafold prediction of RESA folding.

The two arrows indicate the localisation of the EENVEE repeats, which are modelized as helices with a very low per-residue confidence score (pLDDT <50).

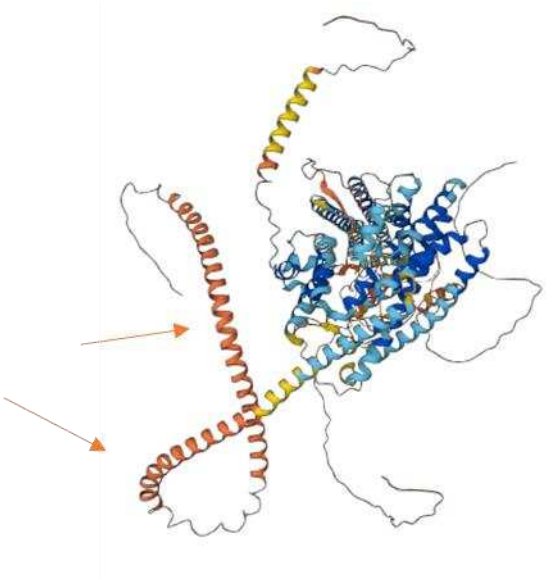

Supplementary data 12: Alphafold prediction of RESA3 folding.

The two arrows indicate the localisation of the EENVEE repeats, which are modelized as helices with a very low per-residue confidence score (pLDDT <50).

APPENDIX : PUBLISHED ARTICLES

As mentioned in the introduction, the following two papers present two anti-SARS-CoV-2 vaccine candidates.

The first one, called “ADDomer” and developed by P.Fender team, is a non-infectious particle, formed by the spontaneous assembly of protein subunits derived from type 3 human adenovirus. Using the Spy Tag-Spy Catcher system, it was possible to graft SARS-CoV-2 RBDs onto the surface of the virus-like particles (VLP). Of note, this system is derived from *Streptococcus pyogenes*, and allows a covalent and spontaneous attachment between the aspartate residue of the ST peptide and the lysine of the SC peptide. Once the correct conformation of the ADDomer-RBD construct had been verified, the next step was to assess the immunogenicity of this vaccine candidate in an animal model, and the mouse model was chosen. The results of ELISA and neutralisation tests demonstrated the ability of this vaccine platform to induce specific and functional anti-RBD antibodies. Moreover, while some vaccines based on the use of human adenovirus (type 3, type 5) as vectors have seen their performance diminish because of anti-adenoviral pre-immunity present in the general population, this was not the case with this candidate, which even showed higher Ab titers in the case of pre-immunisation with ADDomer.

The second vaccine candidate, developed by the team of W. Weissenhorn, consists of liposomes decorated with SARS-CoV-2 trimeric spikes. To increase antigen stability, a two-proline substitution (“2P spike”) and a reticulation with formaldehyde were used. As for the first vaccine candidate, spicule conformation and subsequent liposomes decoration was verified before injection into animals, in this case non-human primates. The results of ELISA and neutralisation tests not only demonstrated that the vaccine candidate was able to induce high levels of antibodies, but also high neutralisation titers. Of note, in the vaccinated group, none of the macaques developed symptoms, suggesting induction of a sterilizing immunity.

Molecular Therapy
Original Article

Elicitation of potent SARS-CoV-2 neutralizing antibody responses through immunization with a versatile adenovirus-inspired multimerization platform

Christopher Chevillard,[1,5] Axelle Amen,[1,3,5] Solène Besson,[1,5] Dalil Hannani,[2] Isabelle Bally,[1] Valentin Dettling,[1] Evelyne Gout,[1] Christophe J. Moreau,[1] Marlyse Buisson,[1] Salomé Gallet,[1] Daphna Fenel,[1] Emilie Vassal-Stermann,[1] Guy Schoehn,[1] Pascal Poignard,[1,3,4] Marie-Claire Dagher,[1] and Pascal Fender[1]

[1]CNRS, Univ. Grenoble Alpes, CEA, UMR5075, Institut de Biologie Structurale, 38042 Grenoble, France; [2]University Grenoble Alpes, CNRS, UMR 5525, VetAgro Sup, Grenoble INP, TIMC, 38000 Grenoble, France; [3]CHU Grenoble Alpes, 38000 Grenoble, France; [4]Department of Immunology and Microbiology, The Scripps Research Institute, La Jolla, CA 92037, USA

Virus-like particles (VLPs) are highly suited platforms for protein-based vaccines. In the present work, we adapted a previously designed non-infectious adenovirus-inspired 60-mer dodecahedric VLP (ADDomer) to display a multimeric array of large antigens through a SpyTag/SpyCatcher system. To validate the platform as a potential COVID-19 vaccine approach, we decorated the newly designed VLP with the glycosylated receptor binding domain (RBD) of SARS-CoV-2. Cryoelectron microscopy structure revealed that up to 60 copies of this antigenic domain could be bound on a single ADDomer particle, with the symmetrical arrangements of a dodecahedron. Mouse immunization with the RBD decorated VLPs already showed a significant specific humoral response following prime vaccination, greatly reinforced by a single boost. Neutralization assays with SARS-CoV-2 spike pseudo-typed virus demonstrated the elicitation of strong neutralization titers, superior to those of COVID-19 convalescent patients. Notably, the presence of pre-existing immunity against the adenoviral-derived particles did not hamper the immune response against the antigen displayed on its surface. This plug and play vaccine platform represents a promising new highly versatile tool to combat emergent pathogens.

INTRODUCTION

Although genomic vaccines have recently demonstrated their capacity to elicit protective immune responses,[1] protein-based vaccines remain highly attractive due to their lower cost, and ease of transport and storage, crucial to reach developing countries and remote locations, as well as better social acceptance, as recently highlighted by hesitancy regarding COVID-19 RNA vaccines. Protein immunogenicity is highly increased through presentation to the immune system in a multimeric manner, and a number of vaccine platforms have been developed to this aim, with various advantages and limitations.[2] We have previously reported that a non-infectious virus-like particle (VLP) derived from human adenovirus of type 3 and consisting of 60 identical penton base monomers could be exploited to display epitopes of interest on its surface.[3–5] In this vaccine platform, named ADDomer, exposed loops of the penton base protein were engineered to allow insertion of foreign peptides such as a linear neutralizing epitope from Chikungunya virus. However, this design did not permit the insertion of structurally complex antigens. To overcome this limitation while keeping the immunogenicity advantage of ADDomer, we describe here a redesigned platform offering a highly versatile capacity to display large and structurally complex antigens with potential post-translational modifications. In order to decorate the adenovirus-based VLPs with large antigens, the SpyTag/SpyCatcher system[6–9] was combined with the ADDomer technology. In this system, derived from *Streptococcus pyogenes,* an aspartate residue from the 13 amino acid SpyTag peptide (ST) can spontaneously create a covalent bond with a lysine residue encompassed in the complementary SpyCatcher module (SC). We thus genetically inserted the sequence coding for the ST peptide into the "variable loop" of the ADDomer that was previously used for small antigen insertion, yielding a VLP with 60 potential attachment sites for complex antigens engineered with an SC anchor.

In order to assess the newly developed platform, we decided to first test it as a potential candidate vaccine to elicit neutralizing antibodies (NAbs) against the severe acute respiratory syndrome coronavirus 2 (SARS-CoV-2). SARS-CoV-2 is an enveloped positive strand RNA virus belonging to the beta-coronavirus genus from the Coronaviridae family. It is the etiological agent of coronavirus disease 2019

Received 28 October 2021; accepted 7 February 2022;
https://doi.org/10.1016/j.ymthe.2022.02.011.

[5]These authors contributed equally

Correspondence: Pascal Fender, CNRS, Univ. Grenoble Alpes, CEA, UMR5075, Institut de Biologie Structurale, 38042 Grenoble, France
E-mail: pascal.fender@ibs.fr
Correspondence: Pascal Poignard, CNRS, Univ. Grenoble Alpes, CEA, UMR5075, Institut de Biologie Structurale, 38042 Grenoble, France
E-mail: pascal.poignard@ibs.fr

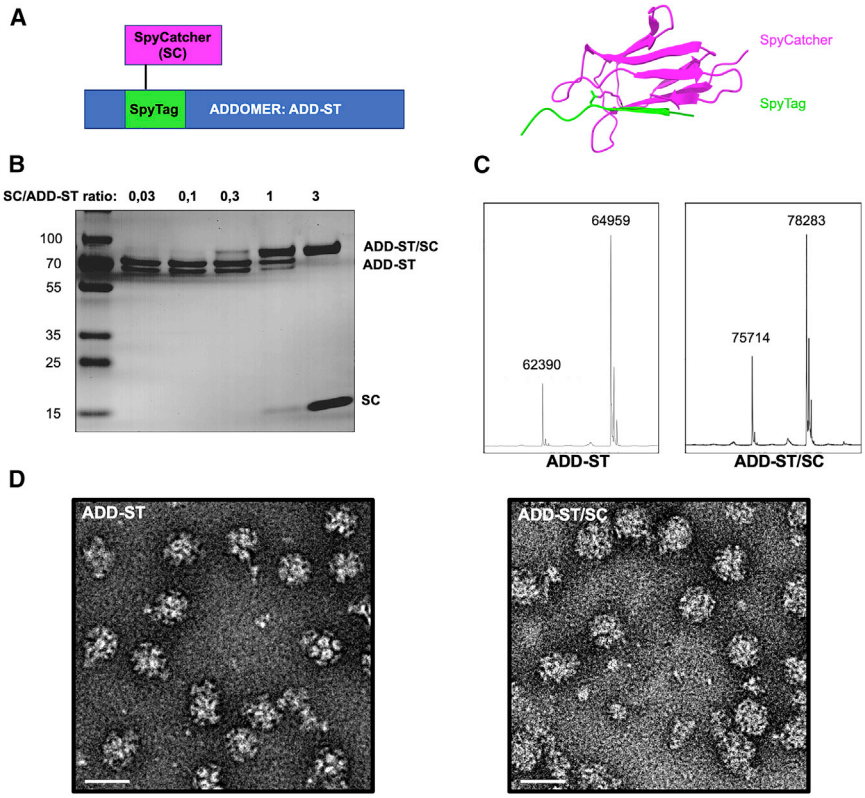

Figure 1. Application of the SpyTag/SpyCatcher cross-linking method to the ADDomer technology

(A) Diagram showing the internal insertion of SpyTag in the internal loop of an ADDomer monomer. Spytag (in green) can make an isopeptidic bond with SpyCatcher (in purple). Structure of a SpyTag covalently linked to a SpyCatcher is shown on the right (PDB code: 4MLI). (B) SDS-PAGE profile of reduced and boiled samples of ADD-ST after interaction with incremental ratio of SC showing the apparition of a higher MW covalent adduct (ADD-ST/SC). (C) Electrospray ionization graphs of ADD-ST and ADD-ST/SC showing the shift of the peaks by 13.3 kDa. The doublet is due to an alternative start of translation in ADD-ST and display the same mass shift of 13.3 kDa. (D) Negative staining electron micrographs of ADD-ST and ADD-ST/SC (bar, 30 nm).

(COVID-19), and at the origin of the pandemic that started in December 2019, leading to 5,542,359 deaths as of January 19, 2022 (https://covid19.who.int/), and vast socio-economic consequences.[10] Protection against SARS-CoV-2 infection and COVID-19 can be mediated by neutralizing Abs targeting the envelope trimeric glycoprotein spike (S) exposed at the surface of the virus.[11,12] Accordingly, spike-based vaccine approaches eliciting SARS-CoV-2 NAb responses have been successful at preventing COVID-19.[13–15] The ectodomain of the S protein is divided into the S1 and S2 domains. The Spike protein binds to the host angiotensin-converting enzyme 2 (ACE2), which serves as an entry receptor, as previously reported with SARS-CoV, responsible for the 2002–2004 SARS outbreak.[16–19] A subdomain of S1, named receptor binding domain (RBD), is the contact interface between the virus and the ACE2 receptor. Numerous studies have shown that the RBD comprises multiple distinct antigenic sites and is a prime target for NAbs in COVID-19 convalescent patients.[20–23] These NAbs[24] strongly inhibit cell infection by SARS-CoV-2 by competing with the RBD-ACE2 interaction. Moreover, anti-RBD NAbs have been shown to confer protection against SARS-CoV-2 challenge in animal models of COVID-19, as well as to prevent COVID-19 in humans, thus confirming the interest of using RBD as a vaccine immunogen.[25–27]

This prompted us to use the RBD as the antigen to be displayed on our newly designed VLP platform in order to engineer a novel COVID-19 vaccine approach. Here, we report that the newly designed platform can successfully be decorated with SARS-CoV-2 RBD and is highly immunogenic in mice, eliciting high neutralizing Ab titers.

RESULTS

Internal insertion of ST in ADDomer results in efficient SC cross-linking

ADDomer is a non-infectious 30-nm nanoparticle, formed from 12 bricks of the homo-pentameric penton base from the human adenovirus type 3. The ST sequence was inserted in the ADDomer gene in a region coding for the exposed flexible loop called the variable loop (Figure 1A). Due to the spontaneous homo-oligomerization of the 12-pentameric penton base, 60 copies of ST are exposed on the surface of the ADDomer-ST (ADD-ST) particle. To assess whether the newly inserted ST sequence was accessible and functional on ADD-ST, incubation with a different ratio of SC was performed. After boiling of samples, SDS-PAGE profile clearly showed that the incremental SC/ADD-ST ratio is correlated with the apparition of a band of higher molecular weight and the decrease of the intensity of bands related to unlinked moieties. Importantly, there was no remaining signal for undecorated ADD-ST after SC addition at the highest ratio, thus reflecting the full decoration of the nanoparticle (Figure 1B). This result suggests an efficient and concentration-dependent formation of the ADD-ST/SC complex. Mass spectroscopy analysis confirmed that the ADD-ST doublet shifted by 13.3 kDa (Figure 1C), which corresponds to the molecular weight (MW) of SC. The two peaks observed in mass spectroscopy is due to a second initiation codon in ADD-ST (starting at Methionine 25) without affecting the particle stability,[28] and SC can bind to each form indifferently, as shown by a similar shift of their MW corresponding to the addition of SC. Negative staining electron microscopy imaging performed on ADD-ST alone and ADD-ST fully decorated by SC showed that the integrity of the particle was not affected by the presence of SC and the grainy appearance of ADD-ST/SC likely reflects the presence of SC at the particle surface (Figure 1D). Altogether, these data show that SC cross-linking to ADD-ST is operational and can result in saturated decoration of the nanoparticle.

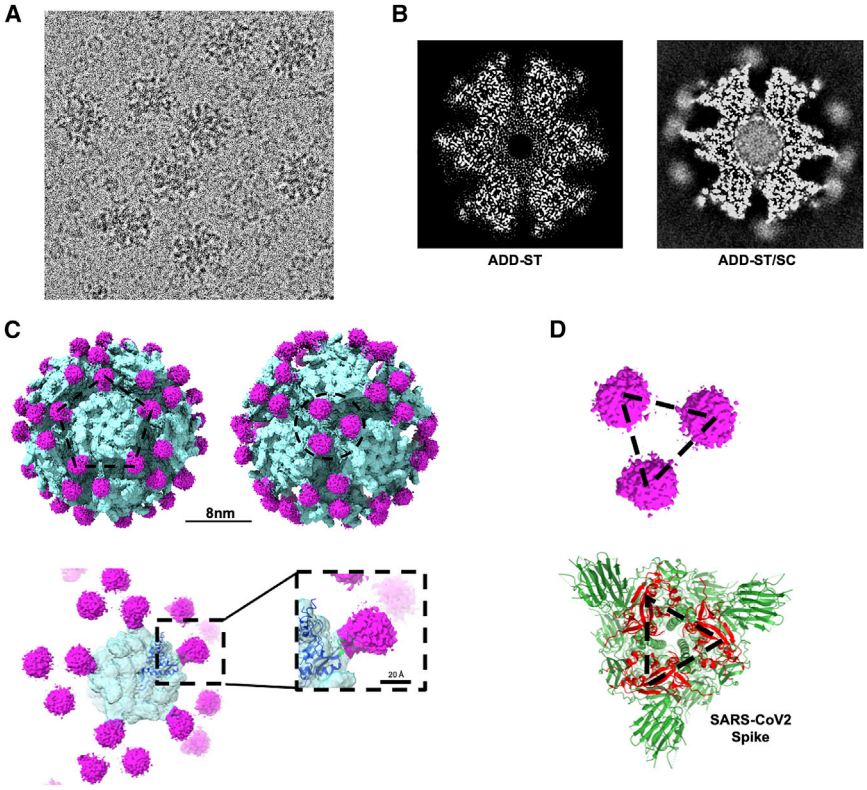

Figure 2. Cryo-EM reconstruction of ADD-ST decorated with SC

(A) Representative 2D picture of the particles frozen on ice (bar, 30 nm). (B) Section through the density of the 3D reconstruction without (ADD-ST) or with SC (ADD-ST/SC). (C) Isosurface representation of the ADDomer-ST/SC 3D structure showing the extra density of SC in purple onto the non-decorated ADD-ST scaffold in light blue. The particle is represented along either the 5- or 3-fold-axis (left and right, upper panel; bars, 80 and 20Å, respectively). Focus on a pentameric complex of ADD-ST/SC with a close-up view onto a single SC/ST interaction (dashed line boxes in the lower panel). The atomic resolution structure (dark blue) of the HAd3 penton base (PDB 4AQQ) has been fitted into the ADDomer EM density (light blue). (D) Organization of SC along the 3-fold axis of the particle (upper panel) and comparison with SARS-CoV-2 RBD architecture (in red) within the Spike protein structure (in green, PDB 6VXX) at the same scale.

Cryoelectron microscopy analysis enables visualization of SC decoration on ADD-ST

In order to visualize the SC arrangement around the ADDomer particle, a structural study by cryoelectron microscopy (cryo-EM) was used. Fully decorated ADD-ST/SC particles were imaged on a Glacios electron microscope (Figure 2A). Image analysis was performed and the obtained 3D structure was compared with the structure of an undecorated ADDomer particle (EMD-0198). An extra-density corresponding to SC bound to the ADDomer "variable loop" was clearly visible in ADD-ST/SC both in the density slice of the 3D map (Figure 2B) and in the isosurface representation of the structure (Figure 2C, purple density and supplementary movie). The resolution of the ADDomer particle is around 2.8 Å, allowing to clearly see the aminopeptidic chain. However, the ST/SC part is not rigidly attached to the ADDomer, which explains why the corresponding density is fuzzy, and the structure not better defined (Figure S1). The ADDomers have 2, 3, and 5 axes of symmetry (the latter two are shown in Figure 2C), which is a characteristic of a dodecahedron, meaning that SCs are distributed accordingly. Interestingly, along the 3-fold axis, SCs are ∼4.7 nm apart, which is close to the RBD in the trimeric spike protein of SARS-CoV-2 (∼4.1 nm), suggesting that the decorated particles would closely mimic the natural trimeric arrangement of RBDs (Figure 2D). Both the multivalency of SC displayed by the particle and the arrangements they have around the different symmetry axis could be an asset for vaccination purpose if an antigen is fused to this module.

Secreted RBD fused to SC is glycosylated and can be displayed at different ratios on the ADD-ST particle

To take advantage of the spontaneous and covalent linking of SC to ADD-ST, we reasoned that SC could be used as a versatile carrier to easily and efficiently fuse antigens, like in this SARS-CoV-2 vaccine development (Figure 3A), and in broader perspectives to diverse soluble proteins of interest. In the present study, the SARS-CoV-2 RBD was fused to the N-terminus of the SC (RBD-SC) and a melittin signal peptide was added to allow protein post-translational modifications (PTMs) such as glycosylations and secretion from insect cells. To assess whether the secreted and purified RBD-SC was glycosylated, it was treated with N-glycosydase (PNGaseF), and the result showed a shift in the migration of the related band in SDS-PAGE gel, indicating that RBD-SC was indeed glycosylated (Figure 3B). As previously performed with unfused SC (Figure 1B), incremental amounts of RBD-SC were added to ADD-ST in order to decorate the particle with different ratio of cargos (from 0.03 to 3 copies of SC *per* particle monomers). The SDS-PAGE gel profile (Figure 3C) showed the correlated apparition of a band at higher MW with increased concentrations of RBD-SC. This result reflects the covalent linking of RBD-SC to the ADD-ST monomers, whereas the band corresponding to non-decorated ADD-ST monomer progressively faded away, disappearing when the particle is fully decorated. This result showed that the ADDomer platform can be decorated with different numbers of antigen copies exposed on its surface. Altogether, these experiments demonstrated that SC fusion to large antigens (∼40 kDa for RBD-SC) with post-translational modifications enable their covalent linking to the ADDomer platform and that the ratio of decoration can be adjusted according to desired applications.

ADDomers decorated of glycosylated RBD bind to ACE2

RBD is the subdomain of the SARS-CoV-2 spike protein that binds to the human ACE2 receptor. To assess the function of RBDs

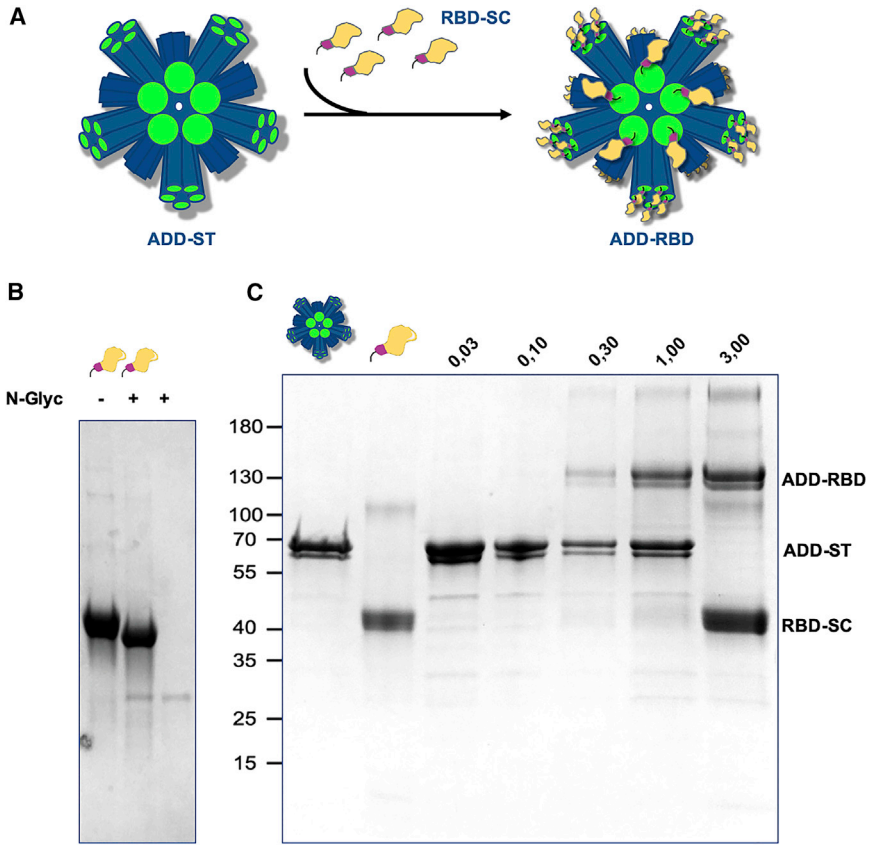

Figure 3. Fusion of SARS-CoV-2 RBD to SC enables its surface presentation on ADDomer particles

(A) Schematic representation of the spontaneous RBD-SC binding to ADD-ST to give ADD-RBD. (B) SDS-PAGE gel with RBD-SC before (–) and after (+) treatment with N-glycosidase and in absence of SC-RBD. The decrease of the molecular weight of SC-RBD after treatment indicates that it is glycosylated. (C) SDS-PAGE gel of reduced and boiled samples showing from left to right, the marker, bands of ADD-ST alone, SC-RBD alone and a fix amount of ADD-ST incubated with different ratio of RBD-SC (*per* particle monmer). The additional upper bands reflect the covalent adduct between ADD-ST and RBD-SC and thus the apparition of ADD-RBD. As expected, the increasing intensities of the ADD-RBD bands correlate with a decrease of non-decorated ADD-ST monomer.

linked to the ADDomer particles, three different approaches were used. First, binding experiments at the molecular scale were performed using surface plasmon resonance (SPR) on immobilized dimeric human ACE2 fused to the Fc domain of human immunoglobulin (Ig)G.[29] Sensorgrams of ADD-RBD binding to immobilized human ACE2 showed a clear concentration-dependent binding of the RBD-decorated particles on ACE2 and a stable interaction with no visible dissociation at the end of injections (Figure 4A). The extremely slow dissociation rate ($4.57\ 10^{-4}\ s^{-1}$) agreed with a sub-nanomolar "apparent" K_D (3.09×10^{-10} M). This apparent K_D is the result of an avidity with the decorated particle effect since the K_D of RBD-SC alone is slightly higher ($1.53\ 10^{-8}$ M; Figure S2). In any case, this result showed that the RBD is functional and that our platform somehow mimics viruses that evolved to take advantage of multivalent interactions with cellular receptors. In a second experiment at the cell scale, the direct binding of ADD-RBD onto HeLa cells stably expressing ACE2 was visualized by immunofluorescence using anti-ADDomer antibodies. The green signal seen at the periphery of HeLa-ACE2 cells in the presence of ADD-RBD contrasted with the absence of signal observed with the same cells but in presence of undecorated ADD-ST particles. This result demonstrated that RBD at the surface of the particles induced the interaction with ACE2 present at the surface of the HeLa-Ace2 cells (Figure 4B). Finally, a competition experiment between a pseudo-typed virus harboring the SARS-CoV-2 spike and either RBD-SC or ADD-RBD was performed. Negative control was made with undecorated ADD-ST alone. As expected, both RBD-SC alone and ADD-RBD were able to compete with the pseudo-typed virus with a slightly higher efficiency for the RBD-decorated particle (Figure 4C). Altogether, these experiments showed that RBD-SC is properly folded and can bind the ACE2 receptor at the molecular and cellular scales when applied alone (RBD-SC) or linked to the ADDomer particles (ADD-RBD).

RBD-decorated ADDomer elicits rapid anti-CoV2 Ab responses in mice, not negatively impacted by adenovirus pre-immunity

Multivalent exposition of RBD antigens at the surface of the particle is likely to result in a better activation of the humoral system than RBD alone. However, one cannot exclude that ADDomer itself could also play an indirect role in the anti-SARS-CoV-2 response, especially in a population with pre-existing adenovirus immunity. To address these two points, four groups of 10 mice were designed (Figure 5A). The two first control groups were injected with RBD-SC alone in group 1 or with the same amount of unlinked RBD-SC plus naked-ADDomer (i.e., not displaying the antigen) in group 2. The two other groups (groups 3 and 4) were vaccinated with ADD-RBD (i.e., RBD displayed at the particle surface) but group 4 was pre-immunized with naked-ADDomer 2 weeks before the injection of ADD-RBD, in order to investigate whether anti-HAdV-3 penton base antibodies, as may possibly be found in individuals previously infected with adenovirus type 3, may impact the immunogenicity of ADD-RBD (Figure 5B). The presence of anti-ADDomer (i.e., HAdV-3 penton base adenovirus) antibodies in group 4 was checked by ELISA 1 day before the first immunization with ADD-RBD. The results (Figure S3) show that all group 4 mice did mount an antibody response against naked-ADDomer. Then, the immune response against RBD

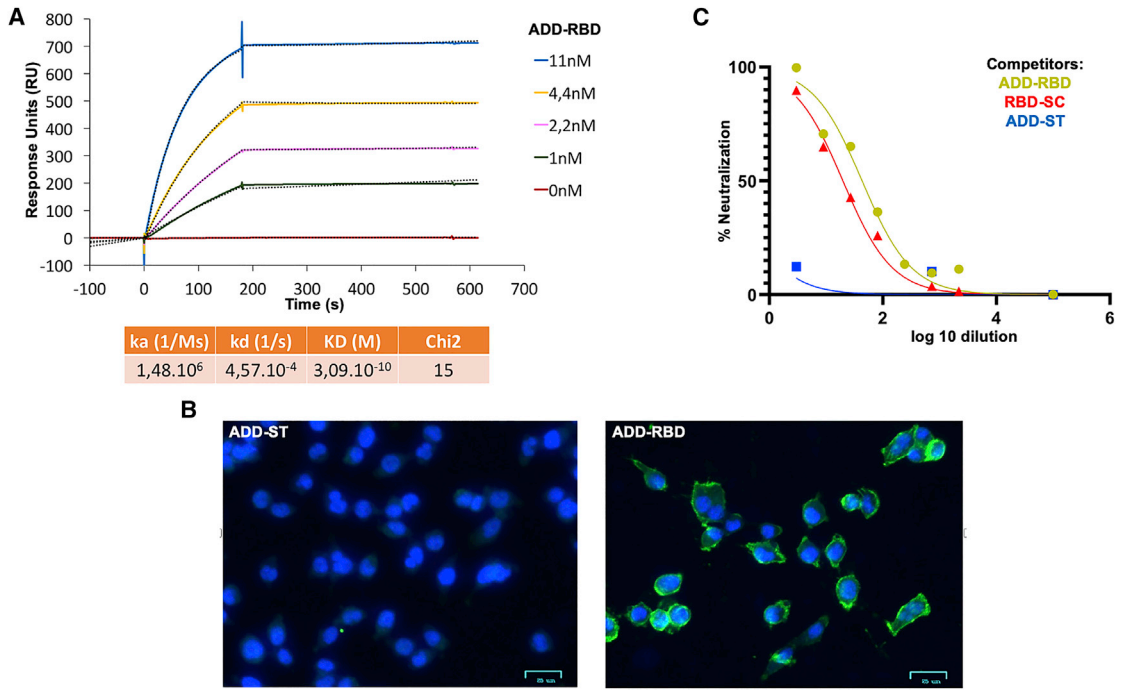

Figure 4. Functional characterization of the ADDomer particles decorated with SARS-CoV-2 RBD

(A) Surface plasmon resonance sensorgrams obtained by injection of different amounts of ADD-RBD to the immobilized ectodomain of the human ACE2 receptor fused to IgG Fc constant domain[29] and kinetic analysis. (B) Immunofluorescence microscopy images of HeLa-ACE2 cell at 4°C with double staining with Hoechst (blue) and anti-ADDomer Ab and an Alexa 488-conjugated secondary Ab (green) in presence of non-decorated ADD-ST (left) or ADD-RBD (right) particles. (C) Competition of pseudotyped SARS-CoV-2 virus encoding luciferase with either ADD-ST (blue), RBD-SC (red) and ADD-RBD (gold) at different dilutions.

was monitored by ELISA at days 13 (post first immunization), 27, and 41 (post second immunization). The RBD-decorated particles induced a significant anti-SARS-CoV-2 response after the first immunization (day 13, Figure 5C), whereas no response was detectable in controls of group 1 (RBD-SC alone) or group 2 (ADDomer with not displayed SC-RBD). Interestingly, anti HAdV-3 penton base pre-immunity did not negatively impact the anti-RBD response. A trend toward a stronger anti-RBD response was even observed at this stage.

Immunization boost increases both the amplitude and the duration of the response induced by ADD-RBD particles, independently of the anti-vector immunity

Two weeks after the second immunization (day 27), the anti-RBD response was clearly boosted for groups 3 and 4 that were injected with ADD-RBD, whereas the control groups 1 and 2 showed more heterogeneous responses (Figure 6A). This observation confirms that our vaccine platform displaying multivalent RBD antigens yields a rapid and efficient humoral response. The ADDomer technology applied to RBD antigen also demonstrated a long-lasting immunogenic effect with anti-SARS-CoV-2 RBD antibodies remaining at the highest level at day 41 (Figure 6B). The difference between mice pre-immunized by ADDomer (group 4) or not (group 3) was less pronounced than after the first immunization, both groups reaching high and comparable levels. Altogether, these results showed that the second immunization enabled a high and long-lasting Ab response against the SARS-CoV-2 RBD using the ADDomer platform and that anti-vector pre-immunity is possibly beneficial in particular to the initial responses (Figure 6C).

RBD-decorated ADDomer immunization elicits strong neutralizing Ab responses

Since the RBD is critical for binding to the SARS-CoV-2 receptor ACE2, antibodies elicited through immunization with the RBD (RBD-SC or ADDomer-RBD) can hinder the interaction between the Spike proteins and ACE2, blocking viral entry. The ability to neutralize the virus depends on the affinity of the antibodies for the RBD domain, as well as on the epitope recognized. To assess the potency and efficacy of the antibodies induced in the four immunized groups of mice, the neutralization potency of sera (day 41) from vaccinated mice was assessed using SARS-CoV-2 spike (Wuhan strain) pseudo-typed lentivirus and ACE2-expressing HeLa cells. Only a partial and heterogeneous neutralization was obtained from group 1 and 2 sera in which RBD-SC was not displayed on ADDomer, even after two immunizations (Figure 7A, upper panels). Of note, sera from mice immunized with RBD-decorated ADDomer (groups 3 and 4) showed a better neutralization titer after a single immunization than groups 1 and 2 after 2 immunizations (Figure S4). After the second immunization, strong virus neutralization was observed in all mice from groups 3 and 4

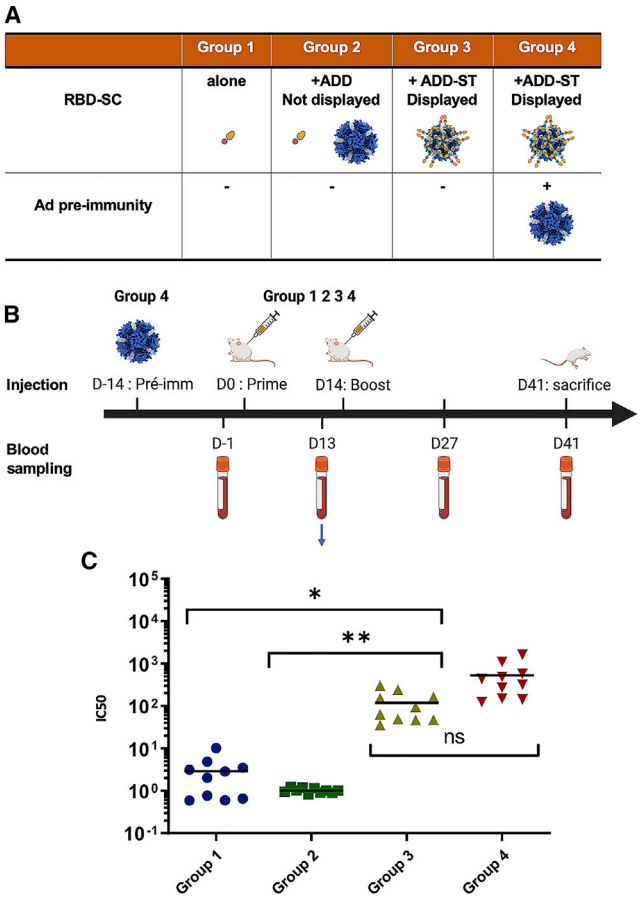

Figure 5. Immunization studies on mice inoculated with the same amount of RBD under different conditions

(A) Different groups were constituted to address the respective role of RBD-SC alone (group 1), RBD-SC in presence of naked-ADDomer (group 2), and RBD-SC displayed by ADDomer (ADD-RBD) either in adenovirus naive or adenovirus pre-immunized mice (group 3 and 4 respectively). (B) Immunization schedule and blood sampling for all groups. (C) IC50 of anti RBD response 13 days after the first immunization (n = 10). Lines are mean values and Kruskal-Wallis tests, were performed followed by a Dunn's multiple comparison tests.

(Figure 7A, lower panels). Neutralization titers (ND_{50}) clearly showed that mice vaccinated with RBD-decorated ADDomer had significantly higher neutralizing activity than mice immunized with the same amount of antigen when not displayed on the platform (Figure 7B). Moreover, in accordance with the ELISA results (Figure 5C), the anti-vector response (group 4) slightly increased the neutralization titer compared with the naïve group (group 3), which emphasizes that a pre-existing HAdV-3 penton base immunity could be beneficial for our novel vaccine platform (Figure 7B). The neutralizing Ab titers reached in groups 3 and 4 were overall superior to those from a cohort of convalescent COVID-19 patients composed of 50% mild (oxygen below 2 L/min) and 50% severe (intensive care unit) cases, and measured at 6 months after hospitalization (Figure 7B).[30]

DISCUSSION

In this study, we designed a novel and highly versatile vaccine platform amenable to large antigens by adapting the ST/SC technology to ADDomer, an adenovirus-inspired VLP.[5,6] This technology has already been described for designing VLP-derived vaccine; however, in these approaches, SC was the moiety grafted to the VLPs while the antigens were fused to the ST.[7,31] In our novel vaccine technology, we used the opposite configuration with ST insertion in an internal loop of ADDomer, which minimized the risk of steric hindrance and functional impact on the spontaneous oligomerization of ADDomers. Insertion of ST in a surface-exposed loop of ADDomer did not impair the spontaneous assembly of 12 pentameric bricks (Figure 1D), thus creating a universal generic platform for multivalent antigen display. Experiments of saturating cross-linking with SC alone suggested that a full decoration (i.e., 60 copies) of the particle can be achieved (Figure 1B). Despite the flexibility of the loop in which ST was inserted, cryo-EM reconstruction of the ADD-ST/SC complex clearly showed an extra density corresponding to the SC interacting with ST fused to the ADDomer. The data thus strongly suggested that the ADDomer could be used to display a multimerized array of antigens, a property that is crucial for the elicitation of strong Ab responses.[32–34] Interestingly, the characteristic 2-, 3-, and 5-fold symmetry axis of a dodecahedron are easily visible in the 3D structure (Figure 2C), this spatial configuration showing that the SCs are distributed at different distances from each other according to the symmetry axis. Such distribution of the antigen could potentially further favor the immunogenicity of the VLP by offering different patterns of presentation of the antigen at the particle surface.

The COVID pandemic led us to first evaluate our newly designed platform as an anti-SARS-CoV-2 vaccine to be displayed through fusion to the SC N-terminus. It is worth noting that in the 3-fold axis of ADDomer, the SC adopts a pseudo-trimeric arrangement, which on the RBD decorated VLP closely mimics the tridimensional configuration of this domain in the SARS-CoV-2 spike glycoprotein (Figure 2D). The distance between SC in such configuration is 4.7 nm, which is in the same range as that between RBDs in the trimeric Spike protein (4.1 nm). Expressing soluble RBD fused to SC in insect cells resulted in N-glycosylation as expected,[35] and did not affect the structure of SC, which retained its ability to cross-link to the ADD-ST vaccine platform in a dose-dependent manner (Figure 3C). The proper folding of the glycosylated RBD exposed at the surface of the particles and its ability to bind ACE2 were assessed in a functional viral entry assay via competition with SARS-CoV-2 Spike pseudo-typed virions (Figure 4C). An SPR experiment confirmed the high-affinity interaction of ADD-RBD to ACE2, the highly stable interaction observed suggesting an avidity effect of the multivalent particle exposing multiple copies of RBD (Figure 4A). Moreover, this experiment also shows that expressing RBD in insect cells leads to a functional SARS-CoV-2 glycoprotein domain. Several vaccines using the baculovirus expression system in insect cells have been approved, such as vaccines against papillomavirus or hepatitis B. The Novavax COVID-19 vaccine candidate, based on an insect cell-produced trimeric S protein, is also advancing toward approval trials.[36]

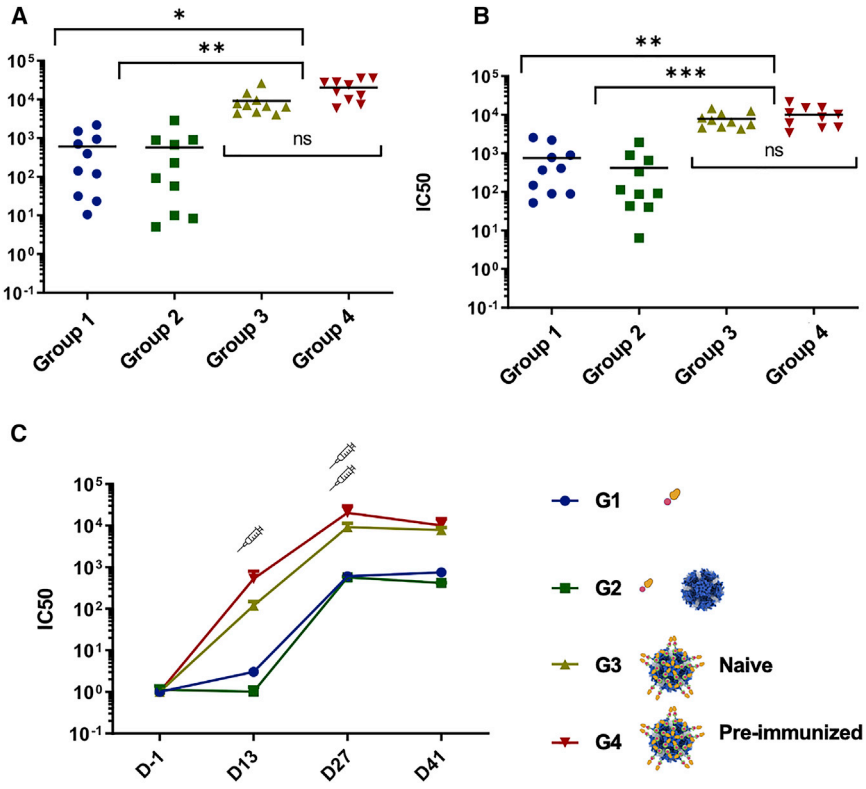

Figure 6. Anti-RBD Ab in all groups of mice 2 and 4 weeks after the booster immunization

(A) IC50 of anti-RBD for each individual mice from all groups, 2 weeks after the booster injection. (B) Same data, 4 weeks after the booster injection. Lines are mean values. Kruskall-Wallis tests, were performed followed by a Dunn's multiple comparison tests. (C) Means of the anti-RBD response from all mice according to their groups and the time after the first immunization performed at day 0.

The ability of the RBD-decorated ADDomer to elicit an anti-SARS-CoV-2 humoral response was then studied in mice. As expected, we confirmed that displaying the RBD in a multimerized manner led to a strong improvement in immunogenicity (groups 3 and 4 versus groups 1 and 2). Indeed, this was clearly apparent from the first injection, where the groups with decorated particles showed a significant anti-RBD response at day 13 as measured in ELISA (Figure 5C), whereas no response was observed for the other groups. This observation is in agreement with experiments reported with other vaccine platforms that showed that injection of RBD or S-trimer alone did not produce significant responses.[31,37] In our experiment, we chose to inject 5μg of RBD, but a dose-response study would be necessary to determine the optimal amount. As a comparison, similar experiments carried out with a similar 60-mer platform showed that 0.9 μg instead of 5 μg of RBD resulted in a similar immune response paving the way to dose-sparing.[38] After the second immunization, although a response was observed in the non-decorated groups, the titers attained in the decorated groups were about 10-fold greater (Figure 6A). Notably, the anti-RBD response in the latter groups endured over time with similar titers at 2 and 4 weeks following the second immunization (Figure 6B). The anti-SARS-CoV-2 RBD sera were further assessed for their capacity to neutralize S-protein pseudotyped lentivirus particles (Figure 7). As seen for binding responses, a neutralizing activity was observed in the RBD-decorated groups after the first immunization. Overall, a good correlation between ELISA and neutralizing titers was observed. Strong neutralizing titers were attained in all mice immunized with ADD-RBD after the boost immunization, superior to those of convalescent COVID-19 patients (Figure 7B), showing the ability of our vaccine platform to elicit functional Ab responses with a potential protective activity. The low titers obtained in mice immunized with RBD and naked ADDomer (no decoration) again demonstrated that the high immunogenicity achieved with decorated VLPs originated from the multimeric display of the antigen. A limitation of our study is that cellular responses were not measured. It is known that CD8 T cell responses likely play an important role in protecting against severe forms of COVID-19. In contrast to mRNA and viral vector vaccines, VLPs are not optimal platforms to elicit CD8 T cell responses, due to the lack of endogenous antigen production. This hurdle may indeed represent a limitation for such vaccines, including our approach. However, CD8 responses may be elicited by VLPs under certain circumstances through cross-presentation following uptake by dendritic cells, and additional work will be necessary to evaluate whether ADDomer may potentially elicit specific CD8 T cells.

Overall, the data are in adequacy with results obtained with similar vaccine platforms using multimeric display of the SARS-CoV-2 RBD on scaffolds such as the 24-mer ferritin, the 60-mer dodecahedral thermophilic aldolase.[31,39,40,41] In contrast to these latter vaccine platforms, our particles originate from a human virus, Adenovirus serotype 3 (HAd3), which is known to have a relatively high seroprevalence.[42,43]

However, if HAdV-3 is globally among the most common types implicated in HAdV infections, a great variation is observed by geographic regions. Indeed, HAdV-3 accounts for 15% to 87% of adenoviral respiratory infections with a greater prevalence in Asia than in western countries.[44] Neutralizing antibodies against HAdV-3 are mainly directed against the hexon protein, which is not present in ADDomer made only of penton bases.

A potentially detrimental impact of pre-existing immunity on the immunogenicity of adenovirus-based viral vectors has been described,[45,46] which thus led us to explore whether such effect may also be encountered with our adenovirus-derived VLP platform.

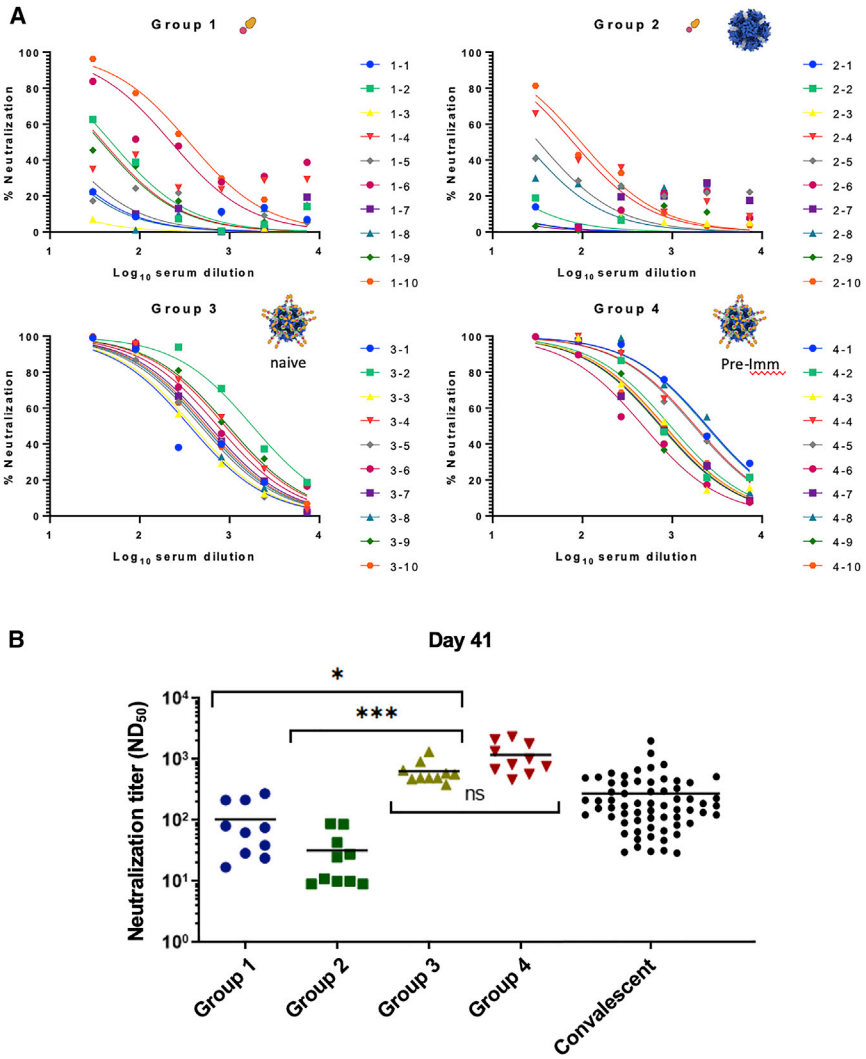

Figure 7. Neutralization study of mice sera on SARS-CoV-2 pseudo-typed virus and comparison with COVID-19 convalescent patients

(A) Curves showing the percentage of neutralization of individual sera of mice from all groups on viral infection by SARS-CoV-2 pseudo-typed virus. This pseudo-typed virus encodes luciferase as a reporter of cell infection and was preincubated with three-time serial dilutions of sera. Luciferase expression was compared to the one of non-neutralized virus. (B) Comparison of the neutralization titer at 50% of the maximal effect (ND50) from all individual mice with the mean represented by a line. Statistical analysis using Kruskall-Wallis tests followed by a Dunn's multiple comparison tests demonstrates the superiority of neutralization of sera from mice immunized with RBD-decorated ADDomer particles versus both non-decorated particles and COVID-19 convalescent patients.

Interestingly, in contrast to adenovirus-viral vectors, pre-immunity against the VLP had no detrimental effect on the immunogenicity of our adenovirus-inspired VLP platform. Indeed, mice with immunity to ADDomer at the time of the first immunization appeared to respond with somehow greater Ab titers against RBD than naive mice, although the difference was not found significant (group 4 versus group 3, Figure 5C). This potential beneficial effect may be in particular explained by the formation of immune complexes leading to a better uptake by antigen-presenting cells, via Fc receptors, resulting in an increase in immunogenicity.[47] Of note, the prevalence, in individuals who have been infected with HAdV-3, of antibodies directed against the penton base, which is the only component of ADDomer, is not precisely known. Our present work anticipates that our platform could be used whatever the HAdV-3 immunological status of the patients, and the potential presence of anti-penton antibodies.

In conclusion, we designed a new adenovirus-inspired VLP platform that achieves high immunogenicity against the displayed antigen. In contrast to current platforms using the ST/SC system, we opted to engineer the ST on the VLP side, within the exposed VL. Thanks to this design, it can be envisaged to add another ST in a second exposed loop, such as the RGD (RGDL), to further increase stoichiometry (up to 120 attachment sites). Moreover, for mosaic vaccine approaches, the RGDL can be used to insert another orthogonal attachment site such as a snoop tag to display a second antigen. As an added value, the use of two different attachment tags/loops allows for differential antigenic stoichiometries and display patterns. Indeed, the RGDLs are more central on the pentameric building block of the ADDomer than the VLs, which are exposed on the periphery, resulting in a greater distance between the VLs than the RGDLs at the pentamer level. Displaying antigens through attachment to these two loops will therefore lead to various patterns of antigen display at the VLP scale, as shown in Figure S5. This will offer a large range of combinations to vary the stoichiometry of decoration as well as the distance between the antigens to potentially optimize immunogenicity.[48] The versatility of the vaccine platform can thus be exploited to generate mosaic particles displaying RBDs from different betacoronaviruses or SARS-CoV-2 variants to broaden NAb responses and protect against current and future variants of concern. A recent work described that 60-mer mosaic nanoparticles with four to eight distinct RBDs from betacoronaviruses can be generated. Remarkably, the codisplay of the SARS-CoV-2 RBD along with other RBDs showed that the combination of antigens on the same particle did not affect the elicitation of neutralizing antibodies against a particular RBD.[37] Moreover, neutralization of both "matched" and "mismatched" strains was observed after mosaic priming, suggesting that such particles might protect against several betacoronaviruses at once after a single injection.

More generally, our new versatile platform constitutes a putative tool in the preparedness to fight emerging pathogens that will remain to be investigated in viral challenge trials.

MATERIALS AND METHODS

Baculovirus production

The baculovirus expression system was used for both the production of ADDomer-SpyTag (ADD-ST) and for the RBD fused to SpyCatcher (RBD-SC). Synthetic DNA (Genscript) was cloned in the pACEBac1 using the restriction sites BamHI and HindIII. For RBD-SC, the SARS-CoV-2 spike sequence (320–554) was cloned upstream of the SC, and a hexa His-Tag was added in the C-terminus of SC. This fusion protein was secreted using the melittin signal peptide present in the vector. Recombinant baculoviruses were made by transposition with an in-house bacmid expressing yellow fluorescent protein, as previously described.[5] Baculovirus was amplified on Sf21 cells at low multiplicity of infection (MOI) and after two amplification cycles was used to infect insect cells for 64 to 72 h at high MOI. For ADD-ST production, the infected cells were pelleted and recovered, whereas for RBD-SC, cells were discarded and the supernatant was saved.

Protein purification

ADDomer and ADD-ST purification

The ADDomer and ADD-ST were purified according to classical protocol.[49] Briefly, after lysis of the insect cell pellet by three cycles of freeze-thaw in the presence of Complete protease inhibitor cocktail (Roche), and removal of debris, the lysate was loaded onto a 20% to 40% sucrose density gradient. The gradient was centrifuged for 18 h at 4°C on an SW41 Rotor in a Beckman XPN-80 ultracentrifuge. The dense collected fractions at the bottom of the tubes were dialyzed against Hepes 10 mM pH 7.4, NaCl 150 mM, and then loaded onto a Macroprep Q cartridge (Bio-Rad). After elution by a 150- to 600-mM linear NaCl gradient in Hepes 10 mM pH 7.4, ADDomer-containing fractions were checked by SDS-PAGE and concentrated on Amicon (MWCO: 100 kDa) with buffer exchange to Hepes 10 mM pH 7.4, NaCl 150 mM.

SC purification

After lysis of the insect cell pellet as described above in the presence of Complete EDTA-free protease inhibitor cocktail, the clarified lysate was diluted five times in wash buffer (Hepes 10 mM pH 7.4, NaCl 150 mM, imidazole 10 mM) and loaded onto a His Gravitrap column (Cytiva) by gravity, with two passages of the lysate onto the column. The column was washed with the same buffer, then eluted by 200 mM Imidazole. The fractions were analyzed by SDS-PAGE, pooled, and Imidazole was withdrawn by buffer exchange using Amicon ultrafiltration devices (MWCO: 4 kDa).

RBD-SC purification

The insect cell supernatant was centrifuged after thawing for 15 min at 7,500 g and loaded onto a Hepes 10 mM pH 7.4 pre-equilibrated Heparin column (Cytiva) of 5 mL for 500 mL of supernatant. The column was washed with Hepes 10 mM pH 7.4 for 25 mL then eluted for 10 mL with 0 to 500 mM linear NaCl gradient in Hepes 10 mM pH 7.4. The eluate was supplemented with 30 mM Imidazole-HCl and incubated with Ni-NTA beads (Qiagen), 2 mL of beads for 500 mL culture, for at least 1 h at 4°C under gentle agitation. The beads were then poured into an empty column and the protein was eluted by two column volumes of 250 mM Imidazole in Hepes 10 mM pH 7.4, NaCl 150 mM. It was then submitted to buffer exchange using an Amicon device (MWCO 30 kDa).

RBD purification

The following reagent was produced under HHSN272201400008C and obtained through BEI Resources, NIAID, NIH: Vector pCAGGS containing the SARS-CoV2, Wuhan-Hu-1 Spike Glycoprotein RBD, NR-52309. Vector NR-52309 from BEI Resources was used for mammalian expression of the RBD alone used for ELISA. EXPI293 cells grown in EXPI293 expression medium were transiently transfected with the vector according to the manufacturer's protocol (Thermo Fisher Scientific). Five days after transfection, the medium was recovered and filtered through a 0.45-mm filter. Two-step protein purification on Aktä Xpress, with a HisTrap HP column (GE Healthcare) and a Superdex 75 column (GE Healthcare) was performed using 20 mM Tris pH 7.5 and 150 mM NaCl buffer. For the HisTrap, a wash step in 75 mM imidazole was performed and RBD was eluted in buffer supplemented with 500 mM imidazole before loading onto the gel filtration column run in equilibration buffer.

N-glycosidase treatment

RBD-SC was incubated for 1 h at 37°C with the N-glycosidase PGNase F (kindly provided by Dr Nicole Thielens) at 1:100 ratio, then run on gel next to the same amount of untreated RBD-SC.

Complex formation

ADD-SpyTag + SpyCatcher (ADD-ST/SC) for Cryo-EM

The purified ADD-ST was mixed with an excess of purified SC (ratio 1:4). The protein mix was incubated overnight at 25°C under shaking in a Thermomixer (300 rpm). A purification step on a sucrose gradient was performed to remove the SC in excess and to recover only the fully decorated ADD-ST/SC at the bottom of the gradient. Buffer exchange was done in 10 mM Hepes, 150 mM NaCl, and the sample was concentrated to 1.5 mg/mL.

ADD-SpyTag + SpyCatcher-RBD (ADD-RBD) for characterization and mice immunization experiments

Covalent complex formation was obtained by incubation of purified ADD-ST with purified RBD protein fused to SC (RBD-SC). Incubation was performed at 25°C under agitation on a Thermomixer at 300 rpm. RBD-SC ratio per ADD-ST was varied according to the experiment, as indicated in the text. For immunization experiments, a ratio of 40 copies of RBD-SC per ADD-ST was chosen to leave minimal free RBD-SC. This ratio was calculated on SDS-PAGE using ImageLab software (Bio-Rad). Integrity of the ADD-RBD was checked by negative staining electron microscopy.

In vivo *experiments and vaccination*

Vaccination experiments were performed according to ethical guidelines, under a protocol approved by the Grenoble Ethical Committee for Animal Experimentation and the French Ministry of Higher Education and Research (reference number: APAFIS#27765–2020102114206782 v2). Five-week-old female Balb/c mice were purchased from Janvier (Le Genestet St. Isle, France). For all mice groups, vaccines were in PBS and adjuvanted with one volume of ADDavax (InvivoGen). All the mice received two vaccine doses at 2 weeks of interval (day 0 and day 14) starting at 8 weeks of age. Each mice group received subcutaneously the corresponding vaccine as indicated within the paper in 100 μL final volume, in the right flank. The pre-immunized group received 2 weeks before the first dose of vaccine (day −15) the ADDomer vector alone (5 μg in 100 μL final volume, in the right flank). The day before each vaccination, and 2 and 4 weeks after the last vaccination, 100 μL of blood was withdrawn for serologic tests. For retro-orbital blood sampling, mice were anesthetized with 4% Isoflurane.

ELISA

The antigens (either RBD or ADDomer) were diluted at 1 μg/mL in PBS, and 50 μL was coated overnight at 4°C, in a 96-well plate (Maxisorp NUNC Immunoplate, #442404). Plates were washed using a ThermoScientific Microplate washer (#5165040). After three washes with 100 μL of PBS-Tween 0.05%, plates were blocked with PBS-BSA 3% for 1 h. Mouse serum was serially diluted in PBS and incubated for 1 h (50 μL/well) at room temperature. After five washes with PBS-Tween 0.05%; a goat anti-mouse IgG (H + L) secondary Ab linked to horseradish peroxidase (JIR 115-035-062) diluted at 1:2,500 in PBS-Tween 0.05% was added for 1 h. After five washes, 50 μL of transmembrane domain substrate was distributed per well. The enzymatic reaction was stopped after 70 s by addition of 50 μL of H_2S0_4 (1 M), and plates were read at 450 nm with a TECAN Spark 10M plate reader.

Electron microscopy

Negative staining

Samples of 3.5 μL were adsorbed on the clean side of a carbon film previously evaporated on mica and then stained using 2% (w/v) Sodium Silico Tungstate pH 7.4 for 30 s. The sample/carbon ensemble was then transferred to a grid and air-dried. Images were acquired under low-dose conditions (<30 e−/Å2) on an F20 electron microscope operated at 120 kV using a CETA camera.

Cryo-EM

Quantifoil grids (300 mesh, R 1.2/1.3) were negatively glow-discharged at 30 mA for 45 s; 3.5 μL of the sample were applied onto the grid, and excess solution was blotted away with a Vitrobot Mark IV (FEI) (blot time: 6 s, blot force: 0, 100% humidity, 20°C), before plunge-freezing in liquid ethane. The grid was transferred onto a 200-kV Thermo Fisher Glacios microscope equipped with a K2 summit direct electron detector for data collection. Automated data collection was performed with SerialEM, acquiring one image per hole, in counting mode. Micrographs were recorded at a nominal ×36,000 magnification, giving a pixel size of 1.145 Å (calibrated using a β-galactosidase sample) with a defocus ranging from −0.6 to −2.35 μm. In total, 1,038 movies with 40 frames per movie were collected with a total exposure of 40 e−/$Å^2$.

Image processing and cryo-EM structure refinement

Movie drift correction was performed with Motioncor2[50] using frames from 2 to 40. CTF determination was performed with Relion 3.1.2 (Scheres 2012). A total of 939 movies of 1,038 were kept at this stage. Particle selection was done using the Laplacian filter with a diameter between 30 and 40 nm. A total of 77,323 particles were automatically selected, boxed into 480 × 480-$pixel^2$ boxes and submitted to 2D classification. After extensive selection and generation of an initial model imposing I1 symmetry, 3D refinement followed by CTF Refine and post-processing generated a final reconstruction including 10,163 particles with a resolution of 2.76 Å (Fourier Shell = 0.143) (applied B-factor −82)

Immunofluorescence microscopy

HeLa-ACE2 cells (kindly provided by Dr David Nemazee) were seeded on polylysine-coated glass coverslips the day before the experiment. Coverslips were incubated for 1 h at 4°C with 0.75 μg of either ADD-ST or ADD-RBD in 50μL of pre-chilled DMEM. Coverslips were washed three times in cold PBS then fixed for 10 min with −20°C methanol. Fixed cells were blocked for 1 h in PBS supplemented by 3% normal goat serum, then incubated for 1 h with 1:1,000 rabbit HAd3 anti penton base serum. After three PBS washes, cells were incubated with 1/250 antiRabbit Alexa 488 Ab (ThermoFisher A32721), washed three times in PBS, then nuclei were counterstained with Hoechst 33258 for 3 min before mounting. Observations were done on a Zoe microscope (Bio-Rad).

Surface plasmon resonance

Surface plasmon resonance experiment was performed on a T200 instrument. Anti-human Fc polyclonal antibody (Jackson Immunoresearch, 109-005-008) diluted at 25 μg/mL in 10 mM sodium acetate pH 5 was immobilized on CM5 sensor chips using the amine coupling chemistry according to the manufacturer's instructions (Cytiva) to get an immobilization level of 14,000 RU. ACE-2 –Fc (GenScript Z033484) was diluted at 1.2 μg/mL in HBS P+ (Cytiva) to get an capture level of 100 RU. For interaction measurements, ADD-RBD (ranging from 1 nM to 11nM in HBSP+) was injected over captured ACE-2 Fc in HBS P+ buffer at 30 μL/min. Anti-human Fc polyclonal antibody flow cell was used for correction of the binding response. Regeneration of the surfaces was achieved by 10 mM Glycine pH2. Binding curves were analyzed using BIAEvaluation software (GE Healthcare) and data was fit to a 1:1 Langmuir with drifting baseline interaction model.

Neutralization assays and pseudo-typed SARS-CoV-2 virion production

Pseudovirus production and titration

Neutralization assays were performed using lentiviral pseudotypes harboring the SARS-CoV-2 spike and encoding luciferase. Briefly,

gag/pol and luciferase plasmids were co-transfected with a SARS-CoV-2 spike plasmid with a C-term deletion of 18aa at 1:0.4:1 ratio on adherent HEK293T cells. Supernatants containing the produced pseudoviruses were harvested 72 h after transfection, centrifuged, filtered through 0.45 μm and concentrated 50 times on Amicon Ultra (MWCO 100KDa), aliquoted and stored at −80°C. Before use, supernatants were tittered using HeLa ACE-2 cells to determine the appropriate dilution of pseudovirus necessary to obtain about 150,000 relative light units (RLU) per well in a 48-well plate.

Neutralization assay

Serial 3-fold dilutions starting from 1/10 dilution (serum), or 6 μg/mL (known bNAbs) were let in contact with the pseudoviruses for 1 h at 37°C in 96-w white plates (Greiner #675083), before addition of HeLa ACE2 cells. Plates were incubated 24 h at 37°C, protected from evaporation, then cells were fed with 60 μL of DMEM (Gibco 11,966-025) supplemented with 10% FBS (VWR 97068-086), and incubated for another 24 h. Medium in each well was aspirated and replaced by 45 μL of 1X cell lysis buffer (OZ Bioscience # LUC1000) for a 60-min incubation under agitation; 30 μL of luciferin substrate was then added and RLU was measured instantly by a luminometer. For competition with ADD-ST, ADD-RBD, and RBD-SC, the same protocol was used with initial concentration of 150μg/mL for ADD-ST, 200μg/mL and ADD-RBD and 50μg/mL for RBD-SC alone. Serums from a cohort of Grenoble region hospitalized convalescent patients were obtained with their consent, 6 to 8 months following COVID-19 diagnosis. The study was approved by the "Comité de Protection des Personnes SUD-EST I" on 20 August 2020 (ref 2020-84).

Statistical analyses

As the half maximal inhibitory concentration (IC50) and median effective dose (ED50) datasets followed a non-normal, heteroscedastic distribution, a non-parametric test was used for comparison of the different groups. Kruskall-Wallis tests were performed followed by a Dunn's multiple comparison tests for each figure. Differences were considered significant when p value was below 0.05. Statistics were performed using GraphPad software, version 9.

SUPPLEMENTAL INFORMATION

Supplemental information can be found online at https://doi.org/10.1016/j.ymthe.2022.02.011.

ACKNOWLEDGMENTS

We are grateful to the "CNRS Prematuration program," to the "ANR-Flash COVID" and to "Région Auvergne-Rhône-Alpes, AuRA" for the financial support to this work. This project has received funding from the European Research Council (ERC) under the European Union's Horizon 2020 research and innovation program (grant agreement No 682286). D.H. is supported by GEFLUC Dauphiné-Savoie, Ligue contre le Cancer Comité Isère, Université Grenoble Alpes IDEX Initiatives de Recherche Stratégiques and Fondation du Souffle-Fonds de recherche en santé respiratoire (FdS-FRSR). We thank Aymeric Peuch for help with the usage of the EM computing cluster and Emmanuelle Neumann for the training of C.C. in negative staining and Leandro Estrozi for help with image analysis. We thank Philippe Mas, Dr Matthieu Roustit, and Dr Sebastian Dergan-Dylon for help with statistical analysis. We thank David Nemazee for HeLa-ACE2 cells and SARS-CoV-2 spike expression plasmid, and Pierre Charneau for plasmids encoding for lentiviral proteins and luciferase. We thank Olivier Epaulard and Julien Lupo for the COVID-19 patients cohort study. This work used the platforms of the Grenoble Instruct-ERIC center (ISBG; UAR 3518 CNRS-CEA-UGA-EMBL) within the Grenoble Partnership for Structural Biology (PSB), supported by FRISBI (ANR-10-INBS-05-02) and GRAL, financed within the University Grenoble Alpes graduate school (Écoles Universitaires de Recherche) CBH-EUR-GS (ANR-17-EURE-0003). The electron microscope facility is supported by the Auvergne-Rhône-Alpes Region, the Fondation Recherche Medicale (FRM), the fonds FEDER and the GIS-Infrastructures en Biologie Sante et Agronomie (IBISA). I.B.S. acknowledges integration into the Interdisciplinary Research Institute of Grenoble (IRIG, CEA). V.D. has an internship of Master de Biologie, École Normale Supérieure de Lyon, Université Claude Bernard Lyon I, Université de Lyon, 69342 Lyon Cedex 07, France.

AUTHOR CONTRIBUTIONS

P.F., M.C.D., and P.P. conceived the experiments. Vector production and purification were performed by C.C., V.D., and S.G. Structural analysis was performed by G.S., D.F., and C.C. Animal experiments were performed by D.H. and S.B. Molecular interaction studies was performed by E.G., C.M., and E.V.S. Immunological characterization and virus neutralization was performed by A.A., I.B., and M.B. With input from all authors, P.F. and P.P. wrote the manuscript.

DECLARATION OF INTERESTS

We declare no competing interests.

REFERENCES

1. Bok, K., Sitar, S., Graham, B.S., and Mascola, J.R. (2021). Accelerated COVID-19 vaccine development: milestones, lessons, and prospects. Immunity *54*, 1636–1651.
2. Nguyen, B., and Tolia, N.H. (2021). Protein-based antigen presentation platforms for nanoparticle vaccines. NPJ Vaccin. *6*, 70.
3. Fender, P., Ruigrok, R.W., Gout, E., Buffet, S., and Chroboczek, J. (1997). Adenovirus dodecahedron, a new vector for human gene transfer. Nat. Biotechnol. *15*, 52–56.
4. Besson, S., Vragniau, C., Vassal-Stermann, E., Dagher, M.C., and Fender, P. (2020). The adenovirus dodecahedron: beyond the platonic story. Viruses *12*, 718.
5. Vragniau, C., Bufton, J.C., Garzoni, F., Stermann, E., Rabi, F., Terrat, C., Guidetti, M., Josserand, V., Williams, M., Woods, C.J., et al. (2019). Synthetic self-assembling ADDomer platform for highly efficient vaccination by genetically encoded multiepitope display. Sci. Adv. *5*, eaaw2853.
6. Zakeri, B., Fierer, J.O., Celik, E., Chittock, E.C., Schwarz-Linek, U., Moy, V.T., and Howarth, M. (2012). Peptide tag forming a rapid covalent bond to a protein, through engineering a bacterial adhesin. Proc. Natl. Acad. Sci. *109*, E690–E697.
7. Brune, K.D., Leneghan, D.B., Brian, I.J., Ishizuka, A.S., Bachmann, M.F., Draper, S.J., Biswas, S., and Howarth, M. (2016). Plug-and-Display: decoration of Virus-Like Particles via isopeptide bonds for modular immunization. Sci. Rep. *6*, 19234.
8. Li, L., Fierer, J.O., Rapoport, T.A., and Howarth, M. (2014). Structural analysis and optimization of the covalent association between SpyCatcher and a peptide tag. J. Mol. Biol. *426*, 309–317.

9. Keeble, A.H., and Howarth, M. (2020). Power to the protein: enhancing and combining activities using the Spy toolbox. Chem. Sci. *11*, 7281–7291.

10. Zhou, P., Yang, X.-L., Wang, X.-G., Hu, B., Zhang, L., Zhang, W., Si, H.-R., Zhu, Y., Li, B., Huang, C.-L., et al. (2020). A pneumonia outbreak associated with a new coronavirus of probable bat origin. Nature *579*, 270–273.

11. Khoury, D.S., Cromer, D., Reynaldi, A., Schlub, T.E., Wheatley, A.K., Juno, J.A., Subbarao, K., Kent, S.J., Triccas, J.A., and Davenport, M.P. (2021). Neutralizing antibody levels are highly predictive of immune protection from symptomatic SARS-CoV-2 infection. Nat. Med. *27*, 1205–1211.

12. McMahan, K., Yu, J., Mercado, N.B., Loos, C., Tostanoski, L.H., Chandrashekar, A., Liu, J., Peter, L., Atyeo, C., Zhu, A., et al. (2021). Correlates of protection against SARS-CoV-2 in rhesus macaques. Nature *590*, 630–634.

13. Polack, F.P., Thomas, S.J., Kitchin, N., Absalon, J., Gurtman, A., Lockhart, S., Perez, J.L., Pérez Marc, G., Moreira, E.D., Zerbini, C., et al. (2020). Safety and efficacy of the BNT162b2 mRNA covid-19 vaccine. N. Engl. J. Med. *383*, 2603–2615.

14. Jackson, L.A., Anderson, E.J., Rouphael, N.G., Roberts, P.C., Makhene, M., Coler, R.N., McCullough, M.P., Chappell, J.D., Denison, M.R., Stevens, L.J., et al. (2020). An mRNA vaccine against SARS-CoV-2 — preliminary report. N. Engl. J. Med. *383*, 1920–1931.

15. Heath, P.T., Galiza, E.P., Baxter, D.N., Boffito, M., Browne, D., Burns, F., Chadwick, D.R., Clark, R., Cosgrove, C., Galloway, J., et al. (2021). Safety and efficacy of NVX-CoV2373 covid-19 vaccine. N. Engl. J. Med. *385*, 1172–1183.

16. Shang, J., Ye, G., Shi, K., Wan, Y., Luo, C., Aihara, H., Geng, Q., Auerbach, A., and Li, F. (2020). Structural basis of receptor recognition by SARS-CoV-2. Nature *581*, 221–224.

17. Yan, R., Zhang, Y., Li, Y., Xia, L., Guo, Y., and Zhou, Q. (2020). Structural basis for the recognition of SARS-CoV-2 by full-length human ACE2. Science *367*, 1444–1448.

18. Lan, J., Ge, J., Yu, J., Shan, S., Zhou, H., Fan, S., Zhang, Q., Shi, X., Wang, Q., Zhang, L., et al. (2020). Structure of the SARS-CoV-2 spike receptor-binding domain bound to the ACE2 receptor. Nature *581*, 215–220.

19. Starr, T.N., Greaney, A.J., Hilton, S.K., Ellis, D., Crawford, K.H.D., Dingens, A.S., Navarro, M.J., Bowen, J.E., Tortorici, M.A., Walls, A.C., et al. (2020). Deep mutational scanning of SARS-CoV-2 receptor binding domain reveals constraints on folding and ACE2 binding. Cell *182*, 1295–1310.e20.

20. Piccoli, L., Park, Y.-J., Tortorici, M.A., Czudnochowski, N., Walls, A.C., Beltramello, M., Silacci-Fregni, C., Pinto, D., Rosen, L.E., Bowen, J.E., et al. (2020). Mapping neutralizing and immunodominant sites on the SARS-CoV-2 spike receptor-binding domain by structure-guided high-resolution serology. Cell *183*, 1024–1042.e21.

21. Barnes, C.O., West, A.P., Huey-Tubman, K.E., Hoffmann, M.A.G., Sharaf, N.G., Hoffman, P.R., Koranda, N., Gristick, H.B., Gaebler, C., Muecksch, F., et al. (2020). Structures of human antibodies bound to SARS-CoV-2 spike reveal common epitopes and recurrent features of antibodies. Cell *182*, 828–842.e16.

22. Robbiani, D.F., Gaebler, C., Muecksch, F., Lorenzi, J.C.C., Wang, Z., Cho, A., Agudelo, M., Barnes, C.O., Gazumyan, A., Finkin, S., et al. (2020). Convergent antibody responses to SARS-CoV-2 in convalescent individuals. Nature *584*, 437–442.

23. Brouwer, P.J.M., Caniels, T.G., van der Straten, K., Snitselaar, J.L., Aldon, Y., Bangaru, S., Torres, J.L., Okba, N.M.A., Claireaux, M., Kerster, G., et al. (2020). Potent neutralizing antibodies from COVID-19 patients define multiple targets of vulnerability. Science *369*, 643–650.

24. Barnes, C.O., Jette, C.A., Abernathy, M.E., Dam, K.-M.A., Esswein, S.R., Gristick, H.B., Malyutin, A.G., Sharaf, N.G., Huey-Tubman, K.E., Lee, Y.E., et al. (2020). SARS-CoV-2 neutralizing antibody structures inform therapeutic strategies. Nature *588*, 682–687.

25. Alsoussi, W.B., Turner, J.S., Case, J.B., Zhao, H., Schmitz, A.J., Zhou, J.Q., Chen, R.E., Lei, T., Rizk, A.A., McIntire, K.M., et al. (2020). A potently neutralizing antibody protects mice against SARS-CoV-2 infection. J. Immunol. *205*, 915–922.

26. Zost, S.J., Gilchuk, P., Case, J.B., Binshtein, E., Chen, R.E., Nkolola, J.P., Schäfer, A., Reidy, J.X., Trivette, A., Nargi, R.S., et al. (2020). Potently neutralizing and protective human antibodies against SARS-CoV-2. Nature *584*, 443–449.

27. O'Brien, M.P., Forleo-Neto, E., Musser, B.J., Isa, F., Chan, K.-C., Sarkar, N., Bar, K.J., Barnabas, R.V., Barouch, D.H., Cohen, M.S., et al. (2021). Subcutaneous REGEN-COV antibody combination to prevent covid-19. N. Engl. J. Med. *385*, e70.

28. Fuschiotti, P., Schoehn, G., Fender, P., Fabry, C.M.S., Hewat, E.A., Chroboczek, J., Ruigrok, R.W.H., and Conway, J.F. (2006). Structure of the dodecahedral penton particle from human adenovirus type 3. J. Mol. Biol. *356*, 510–520.

29. Lei, C., Qian, K., Li, T., Zhang, S., Fu, W., Ding, M., and Hu, S. (2020). Neutralization of SARS-CoV-2 spike pseudotyped virus by recombinant ACE2-Ig. Nat. Commun. *11*, 2070.

30. Epaulard, O., Buisson, M., Nemoz, B., Maréchal, M.L., Terzi, N., Payen, J.-F., Froidure, M., Blanc, M., Mounayar, A.-L., Quénard, F., et al. (2021). Persistence at one year of neutralizing antibodies after SARS-CoV-2 infection: influence of initial severity and steroid use. J. Infect. https://doi.org/10.1016/j.jinf.2021.10.009.

31. Tan, T.K., Rijal, P., Rahikainen, R., Keeble, A.H., Schimanski, L., Hussain, S., Harvey, R., Hayes, J.W.P., Edwards, J.C., McLean, R.K., et al. (2021). A COVID-19 vaccine candidate using SpyCatcher multimerization of the SARS-CoV-2 spike protein receptor-binding domain induces potent neutralising antibody responses. Nat. Commun. *12*, 542.

32. Kanekiyo, M., Wei, C.-J., Yassine, H.M., McTamney, P.M., Boyington, J.C., Whittle, J.R.R., Rao, S.S., Kong, W.-P., Wang, L., and Nabel, G.J. (2013). Self-assembling influenza nanoparticle vaccines elicit broadly neutralizing H1N1 antibodies. Nature *499*, 102–106.

33. Kanekiyo, M., Bu, W., Joyce, M.G., Meng, G., Whittle, J.R.R., Baxa, U., Yamamoto, T., Narpala, S., Todd, J.-P., Rao, S.S., et al. (2015). Rational design of an epstein-barr virus vaccine targeting the receptor-binding site. Cell *162*, 1090–1100.

34. Bachmann, M.F., and Zinkernagel, R.M. (1997). Neutralizing antiviral B cell responses. Annu. Rev. Immunol. *15*, 235–270.

35. Watanabe, Y., Allen, J.D., Wrapp, D., McLellan, J.S., and Crispin, M. (2020). Site-specific glycan analysis of the SARS-CoV-2 spike. Science *369*, 330–333.

36. Shinde, V., Bhikha, S., Hoosain, Z., Archary, M., Bhorat, Q., Fairlie, L., Lalloo, U., Masilela, M.S.L., Moodley, D., Hanley, S., et al. (2021). Efficacy of NVX-CoV2373 covid-19 vaccine against the B.1.351 variant. N. Engl. J. Med. *385*, 1172–1183.

37. Cohen, A.A., Gnanapragasam, P.N.P., Lee, Y.E., Hoffman, P.R., Ou, S., Kakutani, L.M., Keeffe, J.R., Wu, H.-J., Howarth, M., West, A.P., et al. (2021). Mosaic nanoparticles elicit cross-reactive immune responses to zoonotic coronaviruses in mice. Science *371*, 735–741.

38. Walls, A.C., Fiala, B., Schäfer, A., Wrenn, S., Pham, M.N., Murphy, M., Tse, L.V., Shehata, L., O'Connor, M.A., Chen, C., et al. (2020). Elicitation of potent neutralizing antibody responses by designed protein nanoparticle vaccines for SARS-CoV-2. Cell *183*, 1367–1382.e17.

39. He, L., Lin, X., Wang, Y., Abraham, C., Sou, C., Ngo, T., Zhang, Y., Wilson, I.A., and Zhu, J. (2021). Single-component, self-assembling, protein nanoparticles presenting the receptor binding domain and stabilized spike as SARS-CoV-2 vaccine candidates. Sci. Adv. *7*, eabf1591.

40. Salzer, R., Clark, J.J., Vaysburd, M., Chang, V.T., Albecka, A., Kiss, L., Sharma, P., Gonzalez Llamazares, A., Kipar, A., Hiscox, J.A., et al. (2021). Single-dose immunisation with a multimerised SARS-CoV-2 receptor binding domain (RBD) induces an enhanced and protective response in mice. FEBS Lett. *595*, 2323–2340.

41. Saunders, K.O., Lee, E., Parks, R., Martinez, D.R., Li, D., Chen, H., Edwards, R.J., Gobeil, S., Barr, M., Mansouri, K., et al. (2021). Neutralizing antibody vaccine for pandemic and pre-emergent coronaviruses. Nature *594*, 553–559.

42. Vogels, R., Zuijdgeest, D., van Rijnsoever, R., Hartkoorn, E., Damen, I., de Béthune, M.-P., Kostense, S., Penders, G., Helmus, N., Koudstaal, W., et al. (2003). Replication-deficient human adenovirus type 35 vectors for gene transfer and vaccination: efficient human cell infection and bypass of preexisting adenovirus immunity. JVI *77*, 8263–8271.

43. Arnberg, N. (2012). Adenovirus receptors: implications for targeting of viral vectors. Trends Pharmacol. Sci. *33*, 442–448.

44. Haque, E., Banik, U., Monwar, T., Anthony, L., and Adhikary, A.K. (2018). Worldwide increased prevalence of human adenovirus type 3 (HAdV-3) respiratory infections is well correlated with heterogeneous hypervariable regions (HVRs) of hexon. PLoS ONE *13*, e0194516.

45. Lanzi, A., Ben Youssef, G., Perricaudet, M., and Benihoud, K. (2011). Anti-adenovirus humoral responses influence on the efficacy of vaccines based on epitope display on adenovirus capsid. Vaccine *29*, 1463–1471.

46. Anchim, A., Raddi, N., Zig, L., Perrieau, P., Le Goffic, R., Ryffel, B., and Benihoud, K. (2018). Humoral responses elicited by adenovirus displaying epitopes are induced independently of the infection process and shaped by the toll-like receptor/MyD88 pathway. Front Immunol. *9*, 124.

47. Heyman, B. (2003). Feedback regulation by IgG antibodies. Immunol. Lett. *88*, 157–161.

48. Veneziano, R., Moyer, T.J., Stone, M.B., Wamhoff, E.-C., Read, B.J., Mukherjee, S., Shepherd, T.R., Das, J., Schief, W.R., Irvine, D.J., et al. (2020). Role of nanoscale antigen organization on B-cell activation probed using DNA origami. Nat. Nanotechnol. *15*, 716–723.

49. Fender, P. (2014). Use of dodecahedron "VLPs" as an alternative to the whole adenovirus. Methods Mol. Biol. *1089*, 61–70.

50. Zheng, S.Q., Palovcak, E., Armache, J.-P., Verba, K.A., Cheng, Y., and Agard, D.A. (2017). MotionCor2: anisotropic correction of beam-induced motion for improved cryo-electron microscopy. Nat. Methods *14*, 331–332.

Cell Reports
Medicine

Article

Immunization with synthetic SARS-CoV-2 S glycoprotein virus-like particles protects macaques from infection

Graphical abstract

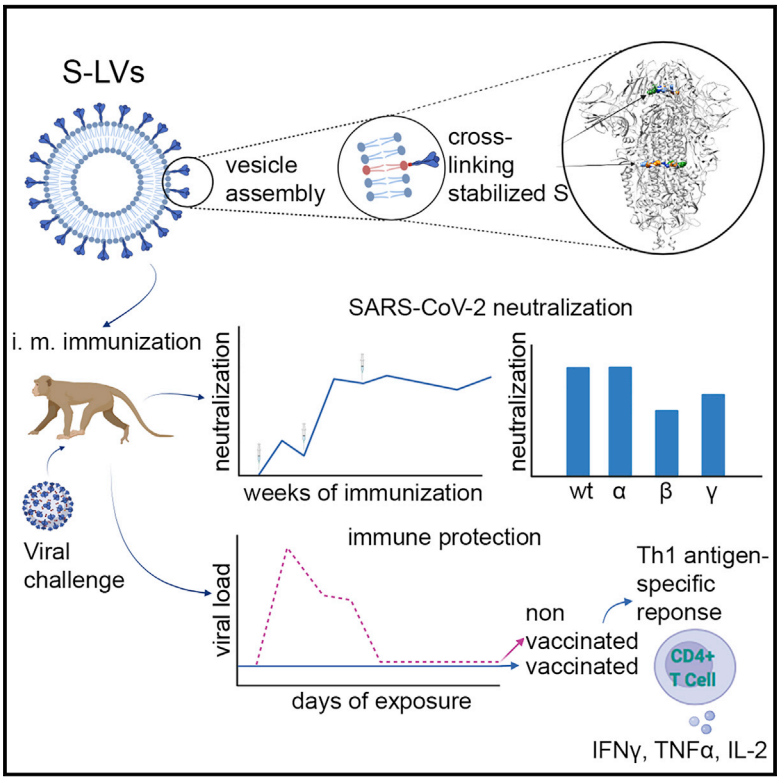

Highlights

- S glycoprotein formaldehyde cross-linking stabilizes S in the prefusion conformation
- Vaccination of cynomolgus macaques with S lipid particles induces neutralization
- Vaccination protects macaques against a SARS-CoV-2 challenge
- Sterilizing protection correlates with nasopharyngeal anti-S IgG and IgA titers

Authors

Guidenn Sulbaran, Pauline Maisonnasse, Axelle Amen, ..., Pascal Poignard, Roger Le Grand, Winfried Weissenhorn

Correspondence

winfried.weissenhorn@ibs.fr (W.W.), roger.le-grand@cea.fr (R.L.G.)

In brief

Sulbaran et al. find that formaldehyde cross-linked S lipid nanoparticles induce potent neutralizing antibody titers upon cynomolgus macaque vaccination. Notably, vaccinated animals develop sterilizing immunity as highlighted upon virus challenge. Thus, the study provides a path to induce sterilizing immunity correlating with mucosal immune responses, which are desired to prevent virus spreading.

Sulbaran et al., 2022, Cell Reports Medicine 3, 100528
February 15, 2022
https://doi.org/10.1016/j.xcrm.2022.100528

CellPress

Cell Reports Medicine

CellPress
OPEN ACCESS

Article

Immunization with synthetic SARS-CoV-2 S glycoprotein virus-like particles protects macaques from infection

Guidenn Sulbaran,[1,7] Pauline Maisonnasse,[2,7] Axelle Amen,[1] Gregory Effantin,[1] Delphine Guilligay,[1] Nathalie Dereuddre-Bosquet,[2] Judith A. Burger,[3] Meliawati Poniman,[3] Marloes Grobben,[3] Marlyse Buisson,[1] Sebastian Dergan Dylon,[1] Thibaut Naninck,[2] Julien Lemaitre,[2] Wesley Gros,[2] Anne-Sophie Gallouët,[2] Romain Marlin,[2] Camille Bouillier,[2] Vanessa Contreras,[2] Francis Relouzat,[2] Daphna Fenel,[1] Michel Thepaut,[1] Isabelle Bally,[1] Nicole Thielens,[1] Franck Fieschi,[1] Guy Schoehn,[1] Sylvie van der Werf,[4,5] Marit J. van Gils,[3] Rogier W. Sanders,[3,6] Pascal Poignard,[1] Roger Le Grand,[2,*] and Winfried Weissenhorn[1,8,*]

[1]Univ. Grenoble Alpes, CEA, CNRS, Institut de Biologie Structurale (IBS), Grenoble, France
[2]Center for Immunology of Viral, Auto-immune, Hematological and Bacterial Diseases (IMVA-HB/IDMIT), Université Paris-Saclay, Inserm, CEA, Fontenay-aux-Roses, France
[3]Department of Medical Microbiology and Infection Prevention, Amsterdam University Medical Centers, University of Amsterdam, Location AMC, Amsterdam, the Netherlands
[4]Molecular Genetics of RNA Viruses, Department of Virology, Institut Pasteur, CNRS UMR 3569, Université de Paris, Paris, France
[5]National Reference Center for Respiratory Viruses, Institut Pasteur, Paris, France
[6]Department of Microbiology and Immunology, Weill Medical College of Cornell University, New York, NY, USA
[7]These authors contributed equally
[8]Lead contact
*Correspondence: winfried.weissenhorn@ibs.fr (W.W.), roger.le-grand@cea.fr (R.L.G.)
https://doi.org/10.1016/j.xcrm.2022.100528

SUMMARY

The severe acute respiratory syndrome coronavirus 2 (SARS-CoV-2) pandemic has caused an ongoing global health crisis. Here, we present as a vaccine candidate synthetic SARS-CoV-2 spike (S) glycoprotein-coated lipid vesicles that resemble virus-like particles. Soluble S glycoprotein trimer stabilization by formaldehyde cross-linking introduces two major inter-protomer cross-links that keep all receptor-binding domains in the "down" conformation. Immunization of cynomolgus macaques with S coated onto lipid vesicles (S-LVs) induces high antibody titers with potent neutralizing activity against the vaccine strain, Alpha, Beta, and Gamma variants as well as T helper (Th)1 $CD4^+$-biased T cell responses. Although anti-receptor-binding domain (RBD)-specific antibody responses are initially predominant, the third immunization boosts significant non-RBD antibody titers. Challenging vaccinated animals with SARS-CoV-2 shows a complete protection through sterilizing immunity, which correlates with the presence of nasopharyngeal anti-S immunoglobulin G (IgG) and IgA titers. Thus, the S-LV approach is an efficient and safe vaccine candidate based on a proven classical approach for further development and clinical testing.

INTRODUCTION

Severe acute respiratory syndrome coronavirus 2 (SARS-CoV-2), a betacoronavirus closely related to SARS-CoV-1, is the etiological agent of coronavirus disease (COVID-19), which quickly developed into a worldwide pandemic[1,2] causing more than five million deaths as of November 2021 (https://covid19.who.int/) and highlighting the urgent need for effective infection control and prevention.

An important correlate of protection of antiviral vaccines is the generation of neutralizing antibodies.[3–5] The main SARS-CoV-2 target for inducing neutralizing antibodies is the spike (S) glycoprotein composed of the S1 subunit that harbors the receptor-binding domain (RBD) and the S2 membrane fusion subunit that anchors the S trimer in the virus membrane.[6] RBD binding to the cellular receptor ACE 2 (ACE2) leads to virus attachment, and subsequent S2-mediated fusion with endosomal membranes establishes infection.[7–9] S is synthesized as a trimeric precursor polyprotein that is proteolytically cleaved by furin and furin-like proteases in the Golgi generating the non-covalently linked S1-S2 heterotrimer.[10] The structure of S reveals a compact heterotrimer composed of the S1 N-terminal domain (NTD), the receptor-binding domain (RBD) , two subdomains, S2, the transmembrane region, and a cytoplasmic domain. The conformation of RBD is in a dynamic equilibrium between either all RBDs in a closed, receptor-inaccessible conformation or one or two RBDs in the "up" conformation.[8,11–14] Only the S RBD in the up position allows receptor binding,[15,16] which triggers the

S2 post-fusion conformation in proteolytically cleaved S.[14] S is also highly glycosylated, which affects infection[17] and access to neutralizing antibodies.[18]

Antibodies targeting the S glycoprotein were identified upon SARS-CoV-2 seroconversion,[19] which mostly target RBD that is immunodominant.[20,21] This led to the isolation of many neutralizing antibodies, which confirmed antibody-based vaccination strategies.[22–36] Many of these antibodies have been shown to provide *in vivo* protection against SARS-CoV-2 challenge in small animals and non-human primates[28,36–39] or are in clinical development and use.[40]

The magnitude of antibody responses to S during natural infection varies greatly and correlates with disease severity and duration.[41,42] Basal responses are generally maintained for months[43–45] or decline within weeks after infection,[41] most notably in asymptomatic individuals.[46] Thus, any vaccine-based approach aims to induce long-lasting immunity.

A number of animal models have been developed to study SARS-CoV-2 infection including the macaque model, which demonstrated an induction of innate, cellular, and humoral responses upon infection,[47–51] conferring partial protection against reinfection.[52,53] Consequently, many early vaccine candidates provided protection in the macaque model including the currently licensed vaccines based on S-specific mRNA delivery[54,55] (BNT162b2, Pfizer/BioNTech; mRNA-1273, Moderna), adenovirus vectors[56,57] (ChAdOx1 nCoV-19, Oxford/AstraZeneca; Ad*26*.COV2.S, Johnson & Johnson), and inactivated SARS-CoV-2[58,59] (PiCoVacc/CoronaVac, Sinovac). Numerous other approaches have been evaluated as well.[60]

Employing the classical subunit approach, S subunit vaccine candidates have generated different levels of neutralizing antibody responses in pre-clinical testing.[61–65] Using self-assembly strategies of S or RBDs further increased immune responses[66,67] and protected against infection.[68–70]

Antigens can be also presented via liposomes, which provide a highly controllable degree of multivalency and stability and a prolonged circulating half-life *in vivo.*[71,72] Notably, liposomes coated with viral glycoproteins such as the HIV-1 envelope (Env) induced more efficient immune responses than did immunization with single glycoprotein trimers.[73–76] This is in line with more efficient B cell activation and with the generation of germinal centers (GCs) by multivalent presentation of Env trimers versus soluble trimers.[73]

Here, we developed synthetic virus-like particles employing liposomes that are decorated with S glycoprotein trimers that have been treated by formaldehyde cross linking, which in turn stabilized S in the native conformation over a long time period. Serum antibody recognition of cross-linked versus non-cross-linked S did not show significant binding differences. A small group of cynomolgus macaques was immunized with S-LVs, which produced high S-specific antibody titers and Th1 $CD4^+$ T cell responses. Potent neutralization of wild-type (WT) SARS-CoV-2 and of Alpha pseudovirus variants was observed after two immunizations, while Beta and Gamma pseudovirus variants were neutralized at reduced potency. Challenge of the animals with SARS-CoV-2 demonstrated that S-LV immunization protected the animals from infection revealing no detection of genomic RNA (gRNA) upon infection in nasal and tracheal swabs nor in bronchoalveolar lavages (BALs), thus suggesting sterilizing immunity. This indicates that S-LVs are potential candidates for further clinical development of a safe protein-based SARS-CoV-2 vaccine.

RESULTS

S-LV formation and characterization

The S glycoprotein construct 2P[8] was expressed in mammalian cells and purified by Ni^{2+}-affinity and size-exclusion chromatography (SEC) (Figure S1A), with yields up to 10 mg/L using Expi293F cells. This produced native trimers as determined by negative staining electron microscopy and 2D class averaging of the single particles (Figure S1B). Since S revealed low thermostability (melting temperature [Tm] = 42°C) as reported previously,[8] it was chemically cross-linked with 4% formaldehyde (FA) producing a higher molecular weight species as determined by SDS-PAGE (Figure S1C). FA cross-linking preserved the native structure (Figure S1D) over longer time periods (Figures S1E) by increasing the thermostability to a Tm of 65°C. The cryo-electron microscopy structure of FA-cross-linked S (FA-S) at 3.4°C resolution (Figure S2; Table S1) revealed two major sites of cross linking (Figure 1A). RBD residues R408 and K378 cross-linked neighboring RBDs producing S trimers in the closed "RBD-down" conformation (Figures 1A and 1B). The second site introduced inter-S2 subunit bonds by cross-linking R1019 of the central S2 helix and/or S2 K776 with S2 HR1 K947 (Figure 1C). FA-S was incubated with liposomes (phosphatidylcholine 60%, cholesterol 36%, DGS-NTA 4%), and efficiently captured via its C-terminal His-tag. Free, unbound Fa-S was removed from the S proteoliposomes by sucrose gradient centrifugation (Figure S1F), and decoration of the liposomes with FA-S (S-LV) was confirmed by negative staining electron microscopy (Figure 1D).

S-LV immunization induced potent neutralizing antibody responses in cynomolgus macaques

S-LVs were produced for a small vaccination study of cynomolgus macaques to evaluate the immunogenicity and elicitation of neutralizing antibodies. Four cynomolgus macaques were immunized with 50 μg S-LVs adjuvanted with monophospholipid A (MPLA) liposomes by the intra-muscular route at weeks 0, 4, 8, and 19 (Figure 2A). Sera of the immunized macaques were analyzed for binding to S, FA-S, and the RBD in 2 week intervals. The results revealed similar S-specific antibody (Ab) titers for all animals. S effective dose (ED_{50}) titers increased from ∼75 on week 4 to ∼10,000 on week 6 and to ∼20,000 on week 12, after the first, second, and third immunizations, respectively (Figure 2B). Slight reductions in titers were detected against FA-S (Figure 2C). Titers against RBD alone reached effective doses (ID50s) of ∼100 on week 4 and ∼4,500 on week 6, as well as slight increases on week 12 for some animals (Figure 2D). This suggests that the first and second immunizations induced significant RBD titers, while the third immunization boosted non-RBD antibodies since the week 12 S-specific titers were >4 times higher than the RBD-specific titers in contrast to previous time points at which this ratio was lower (Figure 2C). A fourth immunization did not further boost antibody generation, and titers at week 22 were lower or comparable to week 12 titers (Figures

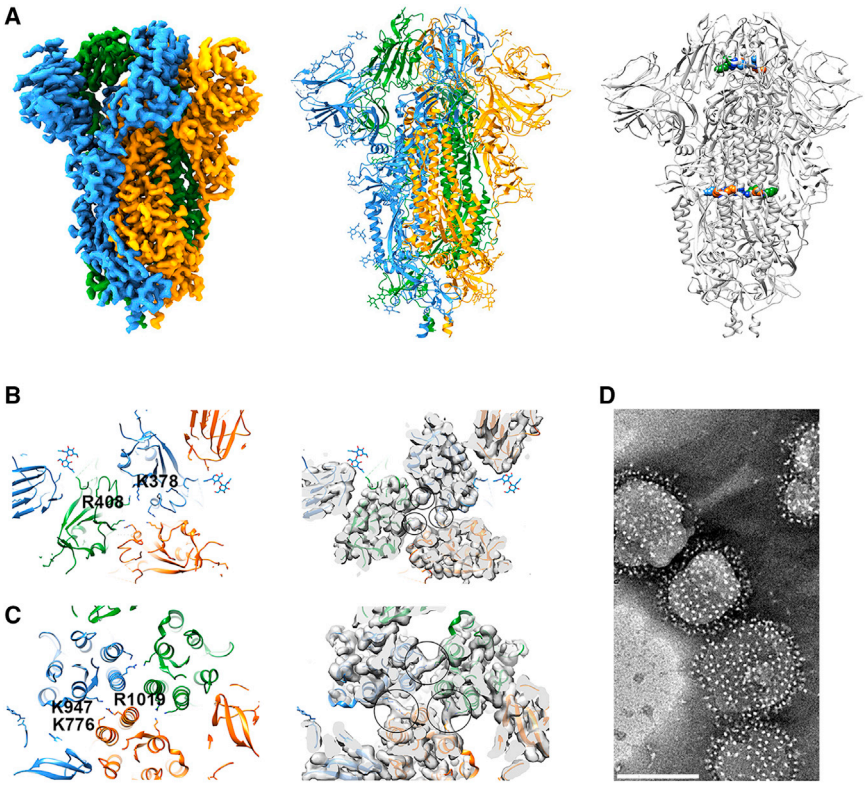

Figure 1. Structural characterization of cross-linked SARS-CoV-2 S (FA-S)- and FA-S-coated lipid vesicles (LVs)

(A) Right panel, cryo-EM density of FA-S with all three RBDs down; each protomer is colored differently. The structure was calculated from 126,719 particles imposing C3 symmetry. . Middle panel, molecular model of FA-S refined to a resolution of 3.4 Å shown as ribbon. Modeled *N*-linked glycans are shown as all atom models. Right panel, two major cross-linking sites were identified that covalently link RBDs and the S2 subunits from different protomers.

(B) Close-up of the cross-linking sites between RBDs. FA-cross-linked amino groups of K378 and R408 of neighboring protomers as indicated by the continuous density connecting side chains (right panel).

(C) Close-up of the cross-linking sites between S2 (left panel). Continuous density between the central helix R1019 as well as S2 K776 to S2 HR1K947 suggested two alternative cross-links between protomers with equal occupancy (right panel).

(D) FA-cross-linked S glycoprotein was incubated with liposomes containing 4% DGS-NTA lipids, purified by sucrose gradient density centrifugation, and analyzed by negative staining electron microscopy, revealing regular decoration of the liposomes with the S glycoprotein. Counting S on 50 S-LVs (negative staining EM 2D vision) indicated 231 ± 92 trimers. We thus estimate that approximately or at least 460 ± 184 S trimers are attached to the LVs. Scale bar, 200 nm.

2B, 2C, and 2D). We conclude that S-LV immunization induced primarily RBD-specific antibodies after the first and second immunizations, while the third immunization increased the generation of non-RBD antibodies significantly.

Serum neutralization titers using a WT pseudovirus were elicited in all four animals. At week 2 after the first immunization, ID50 titers between 100 and 1,000 were observed, which dropped close to baseline at week 4 but was significantly increased at week 6, 2 weeks after the second immunization demonstrating ID50s between 5,000 and ~20,000. The ID50s then decreased at week 8 and increased from 20,000 to ~40,000 at week 10, 3 weeks after the third immunization. At week 19, neutralization potency decreased but was still high, indicating that three immunizations induced robust neutralization titers. The fourth immunization boosted neutralization titers to the same level as the third immunization (Figure 3A).

Since antibody titers indicated the induction of high levels of RBD-specific antibodies, in order to understand the part of anti-RBD antibodies in serum neutralization, we depleted the serum at week 10 by anti-RBD affinity chromatography, resulting in no detectable RBD antibodies by ELISA. RBD-specific Ab-depleted serum showed 10% to 30% neutralization compared with the complete serum, indicating some level of non-RBD-specific neutralization. While RBD-specific Ab neutralization largely dominated in two animals, the fraction of non-RBD-specific Ab neutralization activity (Figure 3B) appeared greater in the other two, suggesting a participation of these Abs in the high neutralization titers (Figure 3A).

S-LV immunization protected cynomolgus macaques from SARS-CoV-2 infection

In order to determine the extent of S-LV-vaccination-induced protection, vaccinated and non-vaccinated animals (n = 4) were infected with the primary SARS-CoV-2 isolate (BetaCoV/France/IDF/0372/2020) with a total dose of 1×10^5 plaque-forming units (PFU). Infection was induced by combining intra-nasal (0.25 mL into each nostril) and intra-tracheal (4.5 mL) routes at week 24, 5 weeks after the last immunization. Viral loads in the control animal group peaked in the trachea at 3 days post-exposure (dpe) with a median value of 6.0 $\log_{10}$ copies/mL and in the nasopharynx between 4 and 6 dpe with a median copy number of 6.6 $\log_{10}$ copies/mL (Figure 4A). Viral loads decreased subsequently, and no virus was detected on 10 dpe in the trachea, while some animals showed viral detection up to 14 dpe in the nasopharyngeal swabs (Figure 4A). In the BAL, three control (Ctrl) animals out of four showed detectable viral loads at 3 dpe, and two of them remained detectable at 7 dpe with mean value of 5.4 and 3.6 $\log_{10}$ copies/mL, respectively. Rectal fluids tested positive in one animal, which also had the highest tracheal and nasopharyngeal viral loads (Figures S3A and S3B). Viral subgenomic RNA (sgRNA), which is believed to estimate the number of infected and productively infected cells collected with the swabs or during the lavage, showed peak copy numbers between 3/4 and 6 dpe in the tracheal and nasopharyngeal fluids, respectively (Figure 4B). In the BALs, the two animals presenting high genomic viral loads also showed detectable sgRNA at 3 and 7 dpe, with medians of 5.1 and 3.1 $\log_{10}$ copies/mL, respectively (Figure 4B).

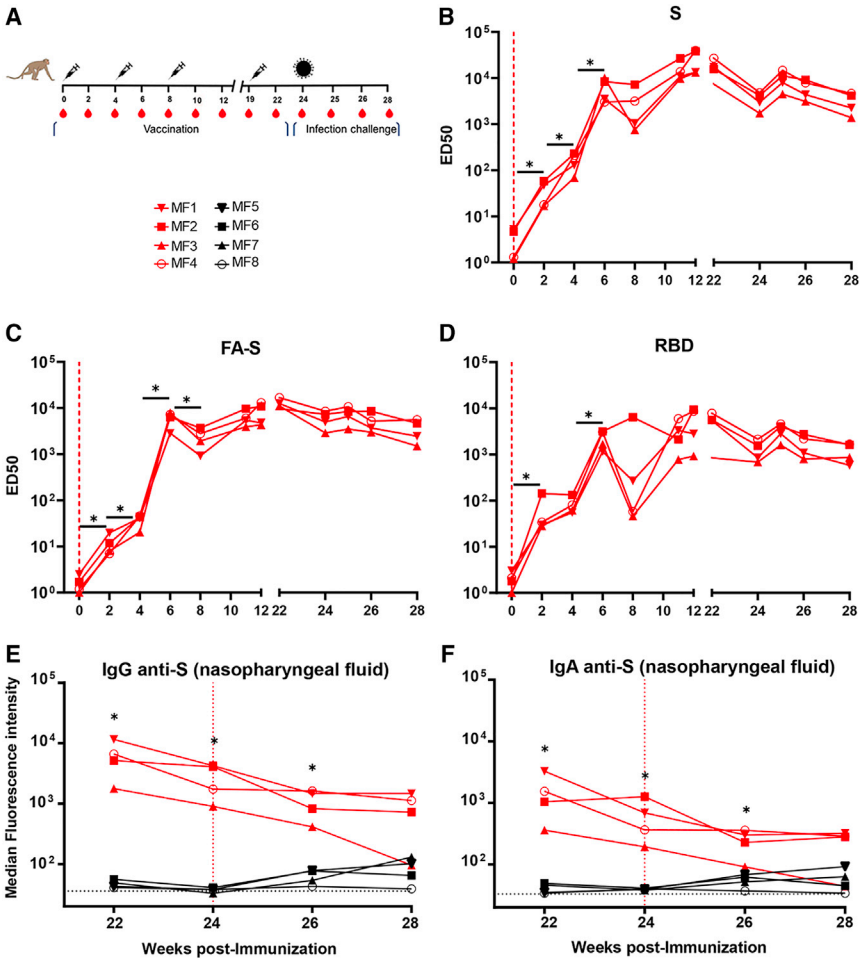

Figure 2. Antibody responses induced by S-LV vaccination of cynomolgus macaques

(A) Scheme of vaccination, challenge, and sampling. Syringes indicate the time points of vaccination, red drops indicate the time of serum collection, and the virus particle indicates the time point of challenge. Symbols of identifying individual macaques are used in all figures.

(B) ELISA of SARS-CoV-2 S-protein-specific IgG determined during the study at weeks 0, 2, 4, 6, 8, 10, 12, 22, 24, 26, and 28. Ab titers of individual animals are shown.

(C) ELISA of SARS-CoV-2 FA-S-protein-specific IgG determined during the study at the indicated weeks.

(D) ELISA of SARS-CoV-2 S RBD-specific IgG determined during the study at the indicated weeks.

(B–D) Differences between matched groups were compared using the Wilcoxon signed-rank test ($p < 0.1$).

(E and F) Detection of S-specific IgG (E) and IgA (F) in nasopharyngeal fluids. Relative mean fluorescence intensity (MFI) of IgG and IgA binding to SARS-CoV-2 S measured with a Luminex-based serology assay in nasopharyngeal swabs. The background level is indicated by dotted lines. The vertical red line indicates the day of challenge. Groups were compared using the Mann-Whitney U test (*$p < 0.05$).

Data presented are from technical duplicates.

In contrast to control animals, neither gRNA nor sgRNA was detected at any point in the vaccinated group (Figures 4A and 4B). The mean gRNA peaks in the trachea and nasopharynx (6.0 and 6.6 $\log_{10}$ copies/mL, respectively) of the control group were higher ($p = 0.0286$) than those of the vaccinated group. The area under the curve was also higher in the trachea of the control group (6.2 $\log_{10}$, $p = 0.286$). In the BAL, the difference was not statistically significant due to the low number of animals. The complete absence of viral RNA in the vaccinated group, both in the upper and lower respiratory tract, strongly suggested that sterilizing immunity was induced by vaccination. ID50 antibody titers against S, FA-S, and the RBD decreased slightly from the day of infection (week 24) to 4 weeks pe (Figures 5A, 5B, and5C), although a small increase in Ab titers is observed at 1 week pe (week 25). Ab titers also correlated with a slight decrease in neutralization from week 24 to 4 weeks pe, although one animal showed a small increase in neutralization on week 25, 1 week pe (Figure 5D). This demonstrated that challenge of vaccinated animals did not significantly boost their immune system. In contrast, the control group started to show clear detection of S-, FA-S-, and RBD-specific IgG on week 2 pe (week 26) (Figures 5A, 5B, and 5C), which correlated with the detection of neutralization at week 2 pe in most animals (Figure 5D). Protection of vaccinated animals further correlated with the presence of significant S- and RBD-specific IgG and IgA in nasopharyngeal fluids (Figures 2E and S4). This indicated that S-LV vaccination induced mucosal immunity that very likely contributed to the sterilizing effect of vaccination.

Similar to previous observations,[50,70] during the first 14 dpe, all control animals showed mild pulmonary lesions characterized by non-extended ground-glass opacities (GGOs) detected by chest CT (Figure S5A). Vaccinated animals showed no significant impact of challenge on CT scores. The only animal showing a lesion score >10 was in the control group. Whereas all control animals experienced monocytoses between 2 and 8 dpe, probably corresponding to a response to infection, monocyte counts remained stable after challenge for the vaccinated monkeys (Figure S5B), in agreement with the absence of detectable anamnestic response in the latter animals.

The levels of CD4- and CD8-specific T cells were measured in both groups of animals. Before exposure, Th1-type $CD4^+$ T cell responses were observed in all vaccinated macaques following *ex vivo* stimulation of peripheral blood mononuclear cells (PBMCs) with S-peptide pools (Figures 6, S6, and S7). None had detectable anti-S $CD8^+$ T cells (Figure S8). No significant difference was observed at 14 dpe, also in agreement with the absence of an anamnestic response in vaccinated animals. In contrast, the anti-S Th1 $CD4^+$ response increased post-exposure for most of the control animals (Figures 6 and S6).

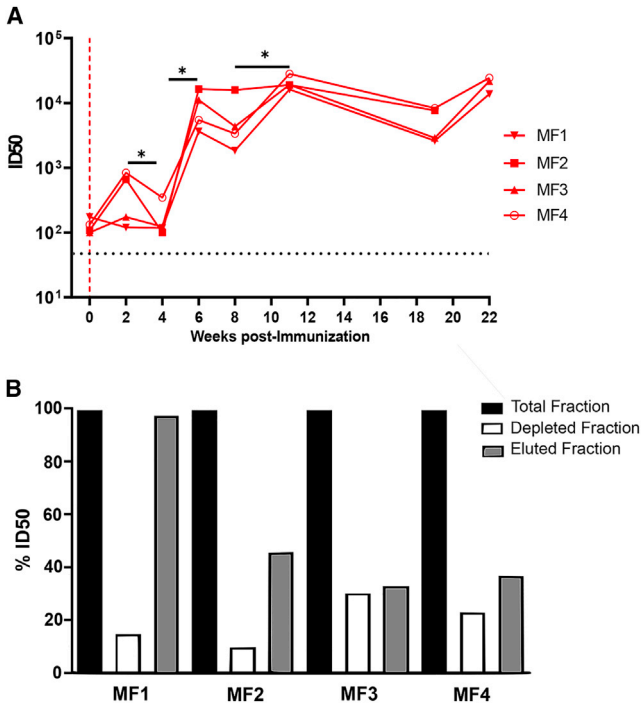

Figure 3. Serum neutralization of SARS-CoV-2 pseudovirus upon S-LV vaccination

(A) The evolution of SARS-CoV-2 neutralizing Ab titers is shown for sera collected at weeks 0, 2, 4, 6, 8, 10, 12, and 19. Bars indicate median titers of the four animals. Differences between matched groups were compared using the Wilcoxon signed-rank test ($p < 0.1$). Data presented are from technical duplicates.

(B) Serum from week 10 was depleted of RBD-specific Abs by affinity chromatography, and neutralization activity of the complete serum of each animal was set to 100% and compared with the RBD-depleted sera and the RBD-specific sera.

We conclude that S-LV vaccination can produce sterilizing immunity, indicating that such a vaccination scheme would be efficient to interrupt the chain of SARS-CoV-2 transmission.

S-LV vaccination generated robust neutralization of SARS-CoV-2 variants

Serum neutralization was further tested against variants B.1.1.7 (Alpha, UK), B.1.351 (Beta, South Africa [SA]), and P.1 (Gamma, Brazil [BR]). Comparing the sera of the vaccinated and non-vaccinated groups at weeks 24 and 28 showed high neutralization titers for all three variants, with median ID50s ranging from 10,000 to 20,000, comparable to WT pseudovirus neutralization (Figure S9). However, since the background of pre-exposure serum neutralization of the non-vaccinated challenge group was relatively high (median ID50s ranging from 400 to 1,100), we repeated the neutralization with purified IgG from serum samples of the vaccinated group from week 8 (after two immunizations), week 12 (3 immunizations) and weeks 24 and 28 (4 immunizations). This showed median ID50s of ~4,500 for WT and Alpha on week 8 (Figure 7), comparable to WT serum neutralization (Figure 3A). Lower ID50s were observed against Beta and Gamma at week 8. Neutralization potency was increased after the third immunization (week 12), with median ID50s of ~5,000 (WT), ~8,000 (Alpha), ~800 (Beta), and 1,000 (Gamma). Neutralization titers did not increase after the fourth immunization at week 24 and started to decrease at week 28 (Figure 7). We conclude that three immunizations provided robust protection against the variants, although neutralization titers may have already been within the protective range after two immunizations for the three variants tested.

DISCUSSION

Many vaccines are under development in pre-clinical and clinical testing,[60] and eight have been approved by regulatory agencies around the world. Here, we developed a two-component system employing the SARS-CoV-2 S glycoprotein coupled to liposomes. Since the stability of the WT SARS-CoV-2 S glycoprotein is low due to its tendency to spontaneously switch into its post-fusion conformation,[14] SARS-CoV-2 S was stabilized by two proline mutations that enhanced stability.[8] However, this S 2P version still showed limited stability over time, as reported,[8] which may be due to cold sensitivity.[77] We overcame the problem of stability by using FA cross-linking that increased the thermostability to 65°C, preserving the native S conformation over extended storage time periods. Furthermore, we detected two cross-linking sites by cryoelectron microscopy (cryo-EM), which showed that cross-linking locked the native S trimer in the closed, RBD-down conformation via covalent inter-protomer interactions, which prevent conformational changes leading to the post-fusion conformation. Notably, FA cross-linking is widely used in vaccine formulations.[78] S stability has since been improved by engineering six proline mutations (S 6P), which increased the thermostability to 50°C,[79] and by disulfide-bond engineering.[80] Moreover, ligand binding renders S more stable.[81,82]

Many previous studies have shown that immunogen multimerization strategies are highly beneficial for B cell activation, including the use of synthetic liposomes[71,72] such as HIV-1 Env-decorated liposome vaccination strategies.[76] We linked SARS-CoV-2 S to liposomes producing synthetic virus-like particles with controlled diameters. Our data show that the S-LVs show similar immunogenic properties as a number of reported self-assembling particles of SARS-CoV-2 RBDs and S.[66,67,69,70,83,84] Our S-LVs induce robust and potent neutralizing responses in cynomolgus macaques, which completely protected the animals from infection by sterilizing immunity. Notably, no signs of virus replication could be detected in the upper and lower respiratory tracts, consistent with the absence of clinical signs of infection such as lymphopenia and lung damage characteristics for COVID-19. The important correlate of protection against SARS-CoV-2 is provided by neutralizing antibodies.[51,85,86] The S-LV approach induces high titers already after two immunizations, with a median ID50 of ~8,000 2 weeks after the second immunization, which is substantially higher than neutralizing Ab responses reported for vaccines tested in non-human primate (NHP) studies, including licensed ones. Adenovirus-based vaccines (AstraZeneca ChAdOx1; Janssen AD26COV2SPP°),[56,57] inactivated virus vaccines (Sinovac PiCoVacc; Sinopharm/BIBP BBIP-CorV),[58,59] a DNA vaccine,[85]

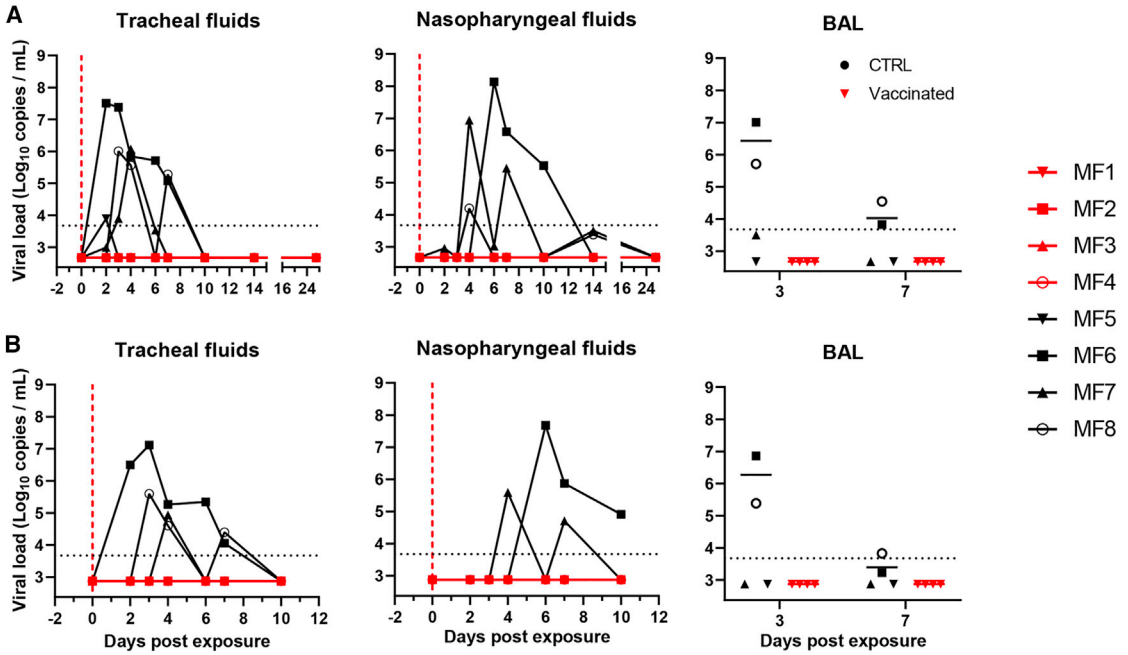

Figure 4. S-LV immunization protects cynomolgus macaques from SARS-CoV-2 infection

Genomic (A) and subgenomic (sg)RNA viral loads (B) in tracheal swabs (left) and nasopharyngeal swabs (middle) of control (black) and vaccinated (red) macaques after challenge. Viral loads in control and vaccinated macaques after challenge in BAL are shown (right). Bars indicate median viral loads. Vertical red dotted lines indicate the day of challenge. Horizontal dotted lines indicate the limit of quantification. Data presented are from technical duplicates.

and an mRNA vaccine (Pfizer/BionTech BNT162b2)[55] showed 10–20 times lower titers compared with the S-LVs in macaques studies. Further, the Moderna mRNA-1273 (Moderna),[54] S trimers (Clover Biopharmaceutical),[64] and NVX-CoV2373 (Novavax)[69] induced similar or higher titers in macaque studies. Median ID50 titers increased by a factor of ~4 after the third immunization but did not amplify after the fourth immunization. The T cell response in the vaccinated group was biased toward Th1 $CD4^+$ T cells, consistent with licensed or other experimental vaccines.[54,87–90]

Serum neutralization was already significant after the first immunization but increased by a factor of ~20 after the second immunization and by a factor of 3 after the third immunization, indicating that two immunizations with S-LVs may suffice to confer protection. Neutralizing antibody (nAb) titers decline within 10 weeks after the third immunization to the levels of week 8

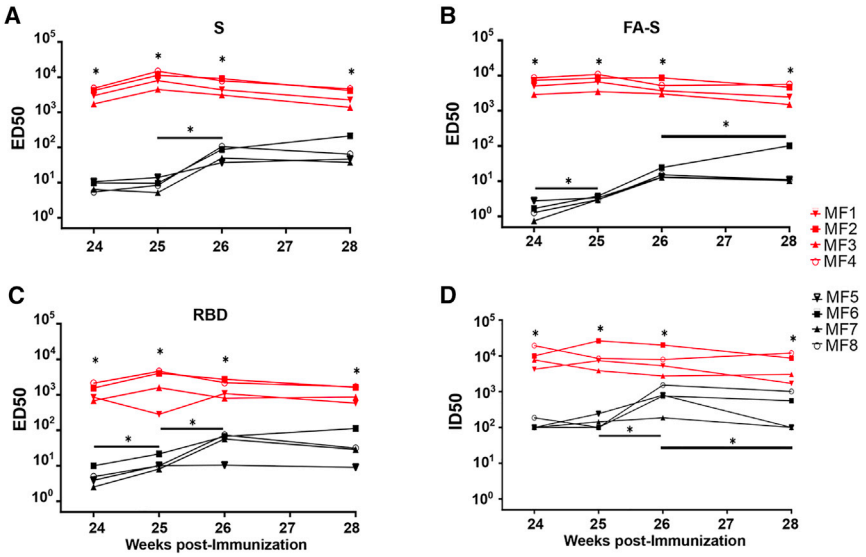

Figure 5. Serum antibody titers and neutralization of vaccinated and control group cynomolgus macaques after SARS-CoV-2 challenge

(A–C) Antibody IgG titers were determined by ELISA at weeks 24 (challenge), 25, 26, 27, and 28 against (A) SARS-CoV-2 S, (B) SARS-CoV-2 FA-S, and (C) SARS-CoV-2 S RBD. Vaccinated animals are shown with red symbols and control animals with black symbols.

(D) SARS-CoV-2 pseudovirus neutralization titers at week 24 (challenge) and 1, 2, and 4 weeks post-exposure (weeks 25, 26, and 28). The bars show the median titers.

Differences between matched groups were compared using the Wilcoxon signed-rank test ($p < 0.1$). Neutralization data presented are from technical triplicates.

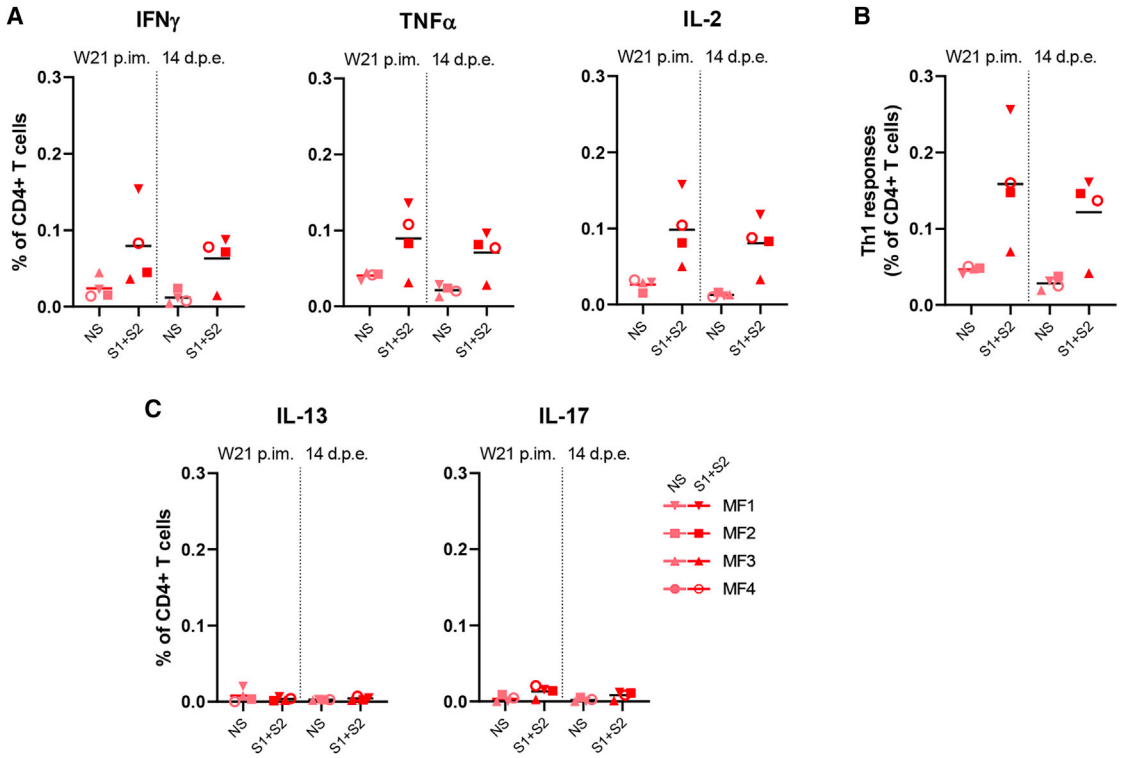

Figure 6. Antigen-specific CD4 T cell responses in S-LV-immunized cynomolgus macaques

Frequency of (A) interferon gamma (IFNγ)+, tumor necrosis factor alpha (TFNα)+, and interleukin (IL)-2+, (B) Th1 (IFNγ+/–, IL-2+/–, TNFα+), and (C) IL-13+ and IL-17+ antigen-specific CD4$^+$ T cells (CD154+) in the total CD4$^+$ T cell population, respectively, for each immunized macaque (n = 4) at week 21 (W21) post-immunization (p.im.) (i.e., 2 weeks after the fourth immunization, pre-exposure) and 14 days post-exposure (dpe). PBMCs were stimulated overnight with medium (pink symbols) or SARS-CoV-2 S overlapping peptide pools (red symbols). Bars indicate means. Time points in each experimental group were compared using the Wilcoxon signed rank test.

(prior to the third immunization) and increase slightly after the fourth immunization to the median ID50 level attained after the third immunization.

Vaccination prevented lymphopenia and lung damage in animals infected with SARS-CoV-2 at a dose comparable[54,56,57,69,85] or lower[70] than in previous studies. Protection was sterilizing since no replication could be detected in the upper and lower respiratory tracts, suggesting that vaccination with S-LVs will prevent virus shedding and transmission. Sterilizing immunity likely correlates with mucosal antibody responses that protect the upper respiratory tract from infection.[43,91] Since we detected significant IgG and IgA in nasopharyngeal fluids at the time of viral challenge, we propose that S-LV vaccination induces sterilizing protection by eliciting mucosal immune responses.

SARS-CoV-2 infection generates nAbs, with up to 90% targeting the RBD, which is immunodominant.[20,33,92] Similarly, mRNA vaccination elicits predominately RBD-specific nAbs.[93] RBD antibodies can be grouped into three classes[94,95] and seem to be easily induced by immunization, as many of them are generated by a few cycles of affinity maturation, indicating that extensive GC reactions are not required.[96] Consistent with these findings, we show that RBD-specific antibodies are predominant after the first and second immunizations as indicated by similar S- and RBD-specific titers. However, after the third immunization, median S-specific ED50s are 3 times higher than RBD-specific ED50s 4 weeks after the third immunization. This trend is continued after the fourth immunization, which revealed a 3.5 times higher median ID50 for S than for RBD 5 weeks post-immunization. This thus suggests that more than two immunizations expand the reactive B cell repertoire that targets non-RBD S epitopes.

Current variants carry the B.1D614G mutation and have been reported to be more infectious.[97–103] Although the D614G mutation alone was reported to increase neutralization susceptibility,[104] further mutations present in Beta (B1.351, SA) and Gamma (P1, BR) reduce neutralization potencies of natural and vaccine-induced sera,[105–112] while Alpha (B.1.1.7, UK) neutralization seems to be less affected.[113] The reduction in neutralization potency of polyclonal plasma Abs is mainly affected by mutations within the three main epitopes in the RBD. In particular, the E484K mutation present in Beta and Gamma was reported to reduce neutralization by a factor of 10.[114] Here, we show that S-LV vaccination produces robust neutralization of Alpha, Beta, and Gamma, although the median ID50s of Beta and Gamma neutralization are reduced 20- and 5-fold, respectively, after the second immunization compared with WT and Alpha. The third immunization boosted neutralization of Beta and Gamma, albeit with 6- and 3-fold reductions in potency,

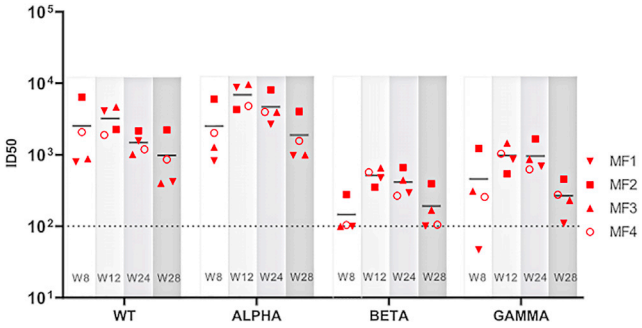

Figure 7. S-vaccination induces robust neutralization of SARS-CoV-2 variants

B.1.1.7 (Alpha, UK), B.1.351 (Beta, SA), and P.1 (Gamma, BR) pseudovirus neutralization titers were compared with the Wuhan vaccine strain. Titers were determined using total IgG purified from sera at weeks 8 (2 immunizations), 12 (3 immunizations), and 24 and 28 (4 immunizations). Background neutralization by IgG isolated from naive animals was <100 for all variants and is indicated by the dashed line. Data presented are from technical triplicates.

respectively, compared with WT, which is slightly more potent than the median ID50 of vaccinated and hospitalized patient cohorts using the same assay setup.[115]

In summary, S-LV vaccination represents an efficient strategy that protects macaques from high-dose challenge. Although the animals have been challenged only after the fourth immunization, which did not boost Ab or neutralization titers significantly, our neutralization data suggest that the animals might have been protected after two immunizations. Furthermore, our data suggest that the third immunization increases S-protein Ab titers more significantly than RBD-specific Ab titers. This points to an increase of non-RBD antibodies, which may be beneficial for the neutralization of different variants. Although other regions within S, most notably NTD, are targets for mutation within new variants, S2 or other epitopes may be less prone to mutations due to conformational constraints. Therefore, future vaccination strategies should consider boosting non-RBD antibodies to compensate for the loss of neutralization activity targeting RBD in variants. Notably, SARS-CoV-2 memory B cells are present over a long time period in convalescent[116,117] and mRNA-vaccinated individuals,[118] which is in line with potential boosting strategies.

Limitations of study

We provide data that the immunization of macaques with synthetic S-glycoprotein-coated liposomes induced robust antibody and neutralization titers after two immunizations. SARS-CoV-2 challenge after four immunizations revealed complete protection by sterilizing immunity. First, a limitation of the study is that the challenge was performed only after the fourth immunization. Secondly, although the SARS-CoV-2 challenge infection was performed 5 weeks after the last immunization, we cannot predict the efficacy of protection months post-immunization. The third limitation of the study is the small number of animals used, which prevents robust statistical analyses of the results. Fourth, although we observe robust pseudovirus neutralization of Alpha, Beta, and Gamma variants, we cannot predict the efficacy of protection upon infection, which will require further studies.

STAR★METHODS

Detailed methods are provided in the online version of this paper and include the following:

- KEY RESOURCES TABLE
- RESOURCE AVAILABILITY
  - Lead contact
  - Materials availability
  - Data and code availability
- EXPERIMENTAL MODEL AND SUBJECT DETAILS
  - Cell lines
  - Viruses
  - Ethics and biosafety statement
  - Animals and study design
- METHODS DETAILS
  - Protein expression and purification
  - SARS-CoV-2 S crosslinking
  - S protein coupling to liposomes
  - S protein thermostability
  - Negative stain electron microscopy
  - Cryo-electron microscopy
  - Virus quantification in NHP samples
  - Chest CT and image analysis
  - ELISA
  - Protein coupling to luminex beads
  - Luminex assay
  - Pseudovirus neutralization assay
  - Antigen specific T cell assays using non-human primate cells
  - Statistical analysis

SUPPLEMENTAL INFORMATION

Supplemental information can be found online at https://doi.org/10.1016/j.xcrm.2022.100528.

ACKNOWLEDGMENTS

This work acknowledges support by the European Union's Horizon 2020 research and innovation program under grant agreement no. 681032, H2020 EHVA (W.W.), the ANR, RA-Covid-19 (W.W. and R.I.G.), and the CNRS (W.W.). W.W. acknowledges access to the platforms of the Grenoble Instruct-ERIC center (IBS and ISBG; UMS 3518 CNRS-CEA-UGA-EMBL) within the Grenoble Partnership for Structural Biology (PSB), with support from FRISBI (ANR-10-INBS-05-02) and GRAL, a project of the University Grenoble Alpes graduate school (Ecoles Universitaires de Recherche) CBH-EUR-GS (ANR-17-EURE-0003). The IBS acknowledges integration into the Interdisciplinary Research Institute of Grenoble (IRIG, CEA) and financial support from CEA, CNRS, and UGA. The Infectious Disease Models and Innovative Therapies (IDMIT) research infrastructure is supported by the Program Investissements d'Avenir, managed by the National Research Agency (ANR) under reference ANR-11-INBS-0008. The Fondation Bettencourt Schueller and the Region Ile-de-France contributed to the implementation of IDMIT's facilities and imaging technologies. The NHP study received financial support from REACTing, the Fondation pour la Recherche Médicale (AM-CoV-Path), and the European Infrastructure TRANSVAC2 (730964). We acknowledge support from CoVIC, supported by the Bill and Melinda Gates Foundation. The virus stock was obtained through the EVAg platform (https://www.european-virus-archive.com/), funded by H2020 (653316). The funders had no role in study design, data collection, data analysis, data interpretation, or data reporting.

We thank J. McLellan for providing the S expression vector; B. Delache, E. Burban, J. Demilly, N. Dhooge, S. Langlois, P. Le Calvez, Q. Sconosciuti, V. Magneron, M. Rimlinger, A. Berriche, J.H. Qiu, M. Potier, J.M. Robert, and C. Dodan for help with animal studies and R. Ho Tsong Fang for his supervision; L. Bossevot, M. Leonec, L. Moenne-Loccoz, and J. Morin for the qRT-PCR and preparation of reagents; M. Gomez-Pacheco and J. van Wassenhove for cellular assays; N. Kahlaoui, B. Fert, and C. Mayet for help with the CT scans and C. Chapon for her supervision; M. Barendji, J. Dinh, and E. Guyon for the NHP sample processing; S. Keyser for the transports organization; F. Ducancel and Y. Gorin for their help with the logistics and safety management; and I. Mangeot for her help with resource management. We thank Antoine Nougairede for sharing the plasmid used for the sgRNA assay standardization. Finally, we thank Dietmar Katinger and Philipp Mundsperger (Polymun) for providing MPLA liposomes. Images in Figures 2A and S1F and the graphical abstract were created with BioRender.com.

AUTHOR CONTRIBUTIONS

Conceptualization, W.W., G.S., R.L.G., and P.M.; funding acquisition, W.W., R.L.G., and R.W.S.; investigation, G.S., P.M., A.A., G.E., D.G., J.A.B., M.P., M.G., M.B., S.D.D., T.N., J.L., W.G., A.-S.G., R.M., C.B., V.C., F.R., and D.F.; methodology, G.S., W.W., P.M., M.J.v.G., R.W.S., P.P., and R.L.G.; formal analyses, G.S., P.M., A.A., N.D.-B., S.D.D., T.N., and A.-S.G.; resources, M.T., I.B., N.T., F.F., N.D.-B., and S.v.d.W.; visualization: G.S., P.M., and G.E.; supervision, W.W., R.L.G., N.D.-B., G.S., M.J.v.G., R.W.S, and P.P.; writing – original draft, W.W., P.M., G.S., and R.L.G.; writing – review & editing, all authors.

DECLARATION OF INTERESTS

The authors declare no competing interests.

Received: July 27, 2021
Revised: November 26, 2021
Accepted: January 19, 2022
Published: January 24, 2022

REFERENCES

1. Zhou, P., Yang, X.L., Wang, X.G., Hu, B., Zhang, L., Zhang, W., Si, H.R., Zhu, Y., Li, B., Huang, C.L., et al. (2020). A pneumonia outbreak associated with a new coronavirus of probable bat origin. Nature *579*, 270–273.
2. Coronaviridae Study Group of the International Committee on Taxonomy of, V (2020). The species Severe acute respiratory syndrome-related coronavirus: classifying 2019-nCoV and naming it SARS-CoV-2. Nat. Microbiol. *5*, 536–544.
3. Plotkin, S.A. (2020). Updates on immunologic correlates of vaccine-induced protection. Vaccine *38*, 2250–2257.
4. Khoury, D.S., Cromer, D., Reynaldi, A., Schlub, T.E., Wheatley, A.K., Juno, J.A., Subbarao, K., Kent, S.J., Triccas, J.A., and Davenport, M.P. (2021). Neutralizing antibody levels are highly predictive of immune protection from symptomatic SARS-CoV-2 infection. Nat. Med. *27*, 1205–1211.
5. Earle, K.A., Ambrosino, D.M., Fiore-Gartland, A., Goldblatt, D., Gilbert, P.B., Siber, G.R., Dull, P., and Plotkin, S.A. (2021). Evidence for antibody as a protective correlate for COVID-19 vaccines. Vaccine *39*, 4423–4428.
6. Dagotto, G., Yu, J., and Barouch, D.H. (2020). Approaches and challenges in SARS-CoV-2 vaccine development. Cell Host Microbe *28*, 364–370.
7. Tortorici, M.A., and Veesler, D. (2019). Structural insights into coronavirus entry. Adv. Virus Res. *105*, 93–116.
8. Wrapp, D., Wang, N., Corbett, K.S., Goldsmith, J.A., Hsieh, C.L., Abiona, O., Graham, B.S., and McLellan, J.S. (2020). Cryo-EM structure of the 2019-nCoV spike in the prefusion conformation. Science *367*, 1260–1263.
9. Letko, M., Marzi, A., and Munster, V. (2020). Functional assessment of cell entry and receptor usage for SARS-CoV-2 and other lineage B betacoronaviruses. Nat. Microbiol. *5*, 562–569.
10. Hoffmann, M., Kleine-Weber, H., and Pohlmann, S. (2020). A multibasic cleavage site in the spike protein of SARS-CoV-2 is essential for infection of human lung cells. Mol. Cell *78*, 779–784.
11. Walls, A.C., Park, Y.J., Tortorici, M.A., Wall, A., McGuire, A.T., and Veesler, D. (2020). Structure, function, and antigenicity of the SARS-CoV-2 spike glycoprotein. Cell *181*, 281–292.
12. Ke, Z., Oton, J., Qu, K., Cortese, M., Zila, V., McKeane, L., Nakane, T., Zivanov, J., Neufeldt, C.J., Cerikan, B., et al. (2020). Structures and distributions of SARS-CoV-2 spike proteins on intact virions. Nature *588*, 498–502.
13. Turonova, B., Sikora, M., Schurmann, C., Hagen, W.J.H., Welsch, S., Blanc, F.E.C., von Bulow, S., Gecht, M., Bagola, K., Horner, C., et al. (2020). In situ structural analysis of SARS-CoV-2 spike reveals flexibility mediated by three hinges. Science *370*, 203–208.
14. Cai, Y., Zhang, J., Xiao, T., Peng, H., Sterling, S.M., Walsh, R.M., Jr., Rawson, S., Rits-Volloch, S., and Chen, B. (2020). Distinct conformational states of SARS-CoV-2 spike protein. Science *369*, 1586–1592.
15. Yan, R., Zhang, Y., Li, Y., Xia, L., Guo, Y., and Zhou, Q. (2020). Structural basis for the recognition of SARS-CoV-2 by full-length human ACE2. Science *367*, 1444–1448.
16. Lan, J., Ge, J., Yu, J., Shan, S., Zhou, H., Fan, S., Zhang, Q., Shi, X., Wang, Q., Zhang, L., et al. (2020). Structure of the SARS-CoV-2 spike receptor-binding domain bound to the ACE2 receptor. Nature *581*, 215–220.
17. Thépaut, M., Luczkowiak, J., Vivès, C., Labiod, N., Bally, I., Lasala, F., Grimoire, Y., Fenel, D., Sattin, S., Thielens, N., et al. (2021). DC/L-SIGN recognition of spike glycoprotein promotes SARS-CoV-2 trans-infection and can be inhibited by a glycomimetic antagonist. PLoS Pathog. *17*, e1009576.
18. Watanabe, Y., Allen, J.D., Wrapp, D., McLellan, J.S., and Crispin, M. (2020). Site-specific glycan analysis of the SARS-CoV-2 spike. Science *369*, 330–333.
19. Amanat, F., Stadlbauer, D., Strohmeier, S., Nguyen, T.H.O., Chromikova, V., McMahon, M., Jiang, K., Arunkumar, G.A., Jurczyszak, D., Polanco, J., et al. (2020). A serological assay to detect SARS-CoV-2 seroconversion in humans. Nat. Med. *26*, 1033–1036.
20. Piccoli, L., Park, Y.J., Tortorici, M.A., Czudnochowski, N., Walls, A.C., Beltramello, M., Silacci-Fregni, C., Pinto, D., Rosen, L.E., Bowen, J.E., et al. (2020). Mapping neutralizing and immunodominant sites on the SARS-CoV-2 spike receptor-binding domain by structure-guided high-resolution serology. Cell *183*, 1024–1042.
21. Premkumar, L., Segovia-Chumbez, B., Jadi, R., Martinez, D.R., Raut, R., Markmann, A., Cornaby, C., Bartelt, L., Weiss, S., Park, Y., et al. (2020). The receptor binding domain of the viral spike protein is an immunodominant and highly specific target of antibodies in SARS-CoV-2 patients. Sci. Immunol. *5*, eabc8413.
22. Liu, L., Wang, P., Nair, M.S., Yu, J., Rapp, M., Wang, Q., Luo, Y., Chan, J.F., Sahi, V., Figueroa, A., et al. (2020). Potent neutralizing antibodies against multiple epitopes on SARS-CoV-2 spike. Nature *584*, 450–456.
23. Wec, A.Z., Wrapp, D., Herbert, A.S., Maurer, D.P., Haslwanter, D., Sakharkar, M., Jangra, R.K., Dieterle, M.E., Lilov, A., Huang, D., et al. (2020). Broad neutralization of SARS-related viruses by human monoclonal antibodies. Science *369*, 731–736.
24. Rogers, T.F., Zhao, F., Huang, D., Beutler, N., Burns, A., He, W.T., Limbo, O., Smith, C., Song, G., Woehl, J., et al. (2020). Isolation of potent SARS-CoV-2 neutralizing antibodies and protection from disease in a small animal model. Science *369*, 956–963.
25. Yuan, M., Liu, H., Wu, N.C., Lee, C.D., Zhu, X., Zhao, F., Huang, D., Yu, W., Hua, Y., Tien, H., et al. (2020). Structural basis of a shared antibody response to SARS-CoV-2. Science *369*, 1119–1123.

26. Wang, C., Li, W., Drabek, D., Okba, N.M.A., van Haperen, R., Osterhaus, A., van Kuppeveld, F.J.M., Haagmans, B.L., Grosveld, F., and Bosch, B.J. (2020). A human monoclonal antibody blocking SARS-CoV-2 infection. Nat. Commun. *11*, 2251.

27. Pinto, D., Park, Y.J., Beltramello, M., Walls, A.C., Tortorici, M.A., Bianchi, S., Jaconi, S., Culap, K., Zatta, F., De Marco, A., et al. (2020). Cross-neutralization of SARS-CoV-2 by a human monoclonal SARS-CoV antibody. Nature *583*, 290–295.

28. Zost, S.J., Gilchuk, P., Case, J.B., Binshtein, E., Chen, R.E., Nkolola, J.P., Schafer, A., Reidy, J.X., Trivette, A., Nargi, R.S., et al. (2020). Potently neutralizing and protective human antibodies against SARS-CoV-2. Nature *584*, 443–449.

29. Kreer, C., Zehner, M., Weber, T., Ercanoglu, M.S., Gieselmann, L., Rohde, C., Halwe, S., Korenkov, M., Schommers, P., Vanshylla, K., et al. (2020). Longitudinal isolation of potent near-germline SARS-CoV-2-neutralizing antibodies from COVID-19 patients. Cell *182*, 1663–1673.

30. Baum, A., Ajithdoss, D., Copin, R., Zhou, A., Lanza, K., Negron, N., Ni, M., Wei, Y., Mohammadi, K., Musser, B., et al. (2020). REGN-COV2 antibodies prevent and treat SARS-CoV-2 infection in rhesus macaques and hamsters. Science *370*, 1110–1115.

31. Hansen, J., Baum, A., Pascal, K.E., Russo, V., Giordano, S., Wloga, E., Fulton, B.O., Yan, Y., Koon, K., Patel, K., et al. (2020). Studies in humanized mice and convalescent humans yield a SARS-CoV-2 antibody cocktail. Science *369*, 1010–1014.

32. Brouwer, P.J.M., Caniels, T.G., van der Straten, K., Snitselaar, J.L., Aldon, Y., Bangaru, S., Torres, J.L., Okba, N.M.A., Claireaux, M., Kerster, G., et al. (2020). Potent neutralizing antibodies from COVID-19 patients define multiple targets of vulnerability. Science *369*, 643–650.

33. Robbiani, D.F., Gaebler, C., Muecksch, F., Lorenzi, J.C.C., Wang, Z., Cho, A., Agudelo, M., Barnes, C.O., Gazumyan, A., Finkin, S., et al. (2020). Convergent antibody responses to SARS-CoV-2 in convalescent individuals. Nature *584*, 437–442.

34. Seydoux, E., Homad, L.J., MacCamy, A.J., Parks, K.R., Hurlburt, N.K., Jennewein, M.F., Akins, N.R., Stuart, A.B., Wan, Y.H., Feng, J., et al. (2020). Characterization of neutralizing antibodies from a SARS-CoV-2 infected individual. Immunity *53*, 98–105.

35. Seydoux, E., Homad, L.J., MacCamy, A.J., Parks, K.R., Hurlburt, N.K., Jennewein, M.F., Akins, N.R., Stuart, A.B., Wan, Y.H., Feng, J., et al. (2020). Analysis of a SARS-CoV-2-infected individual reveals development of potent neutralizing antibodies with limited somatic mutation. Immunity *53*, 98–105.

36. Wu, Y., Wang, F., Shen, C., Peng, W., Li, D., Zhao, C., Li, Z., Li, S., Bi, Y., Yang, Y., et al. (2020). A noncompeting pair of human neutralizing antibodies block COVID-19 virus binding to its receptor ACE2. Science *368*, 1274–1278.

37. Tortorici, M.A., Beltramello, M., Lempp, F.A., Pinto, D., Dang, H.V., Rosen, L.E., McCallum, M., Bowen, J., Minola, A., Jaconi, S., et al. (2020). Ultrapotent human antibodies protect against SARS-CoV-2 challenge via multiple mechanisms. Science *370*, 950–957.

38. Hassan, A.O., Case, J.B., Winkler, E.S., Thackray, L.B., Kafai, N.M., Bailey, A.L., McCune, B.T., Fox, J.M., Chen, R.E., Alsoussi, W.B., et al. (2020). A SARS-CoV-2 infection model in mice demonstrates protection by neutralizing antibodies. Cell *182*, 744–753.

39. Alsoussi, W.B., Turner, J.S., Case, J.B., Zhao, H., Schmitz, A.J., Zhou, J.Q., Chen, R.E., Lei, T., Rizk, A.A., McIntire, K.M., et al. (2020). A potently neutralizing antibody protects mice against SARS-CoV-2 infection. J. Immunol. *205*, 915–922.

40. Weinreich, D.M., Sivapalasingam, S., Norton, T., Ali, S., Gao, H., Bhore, R., Musser, B.J., Soo, Y., Rofail, D., Im, J., et al. (2021). REGN-COV2, a neutralizing antibody cocktail, in outpatients with Covid-19. N. Engl. J. Med. *384*, 238–251.

41. Seow, J., Graham, C., Merrick, B., Acors, S., Pickering, S., Steel, K.J.A., Hemmings, O., O'Byrne, A., Kouphou, N., Galao, R.P., et al. (2020). Longitudinal observation and decline of neutralizing antibody responses in the three months following SARS-CoV-2 infection in humans. Nat. Microbiol. *5*, 1598–1607.

42. Chen, Y., Zuiani, A., Fischinger, S., Mullur, J., Atyeo, C., Travers, M., Lelis, F.J.N., Pullen, K.M., Martin, H., Tong, P., et al. (2020). Quick COVID-19 healers sustain anti-SARS-CoV-2 antibody production. Cell *183*, 1496–1507.

43. Isho, B., Abe, K.T., Zuo, M., Jamal, A.J., Rathod, B., Wang, J.H., Li, Z., Chao, G., Rojas, O.L., Bang, Y.M., et al. (2020). Persistence of serum and saliva antibody responses to SARS-CoV-2 spike antigens in COVID-19 patients. Sci. Immunol. *5*, eabe5511.

44. Rodda, L.B., Netland, J., Shehata, L., Pruner, K.B., Morawski, P.A., Thouvenel, C.D., Takehara, K.K., Eggenberger, J., Hemann, E.A., Waterman, H.R., et al. (2021). Functional SARS-CoV-2-specific immune memory persists after mild COVID-19. Cell *184*, 169–183.

45. Iyer, A.S., Jones, F.K., Nodoushani, A., Kelly, M., Becker, M., Slater, D., Mills, R., Teng, E., Kamruzzaman, M., Garcia-Beltran, W.F., et al. (2020). Persistence and decay of human antibody responses to the receptor binding domain of SARS-CoV-2 spike protein in COVID-19 patients. Sci. Immunol *52*, eabe0367.

46. Long, Q.X., Tang, X.J., Shi, Q.L., Li, Q., Deng, H.J., Yuan, J., Hu, J.L., Xu, W., Zhang, Y., Lv, F.J., et al. (2020). Clinical and immunological assessment of asymptomatic SARS-CoV-2 infections. Nat. Med. *26*, 1200–1204.

47. Grifoni, A., Weiskopf, D., Ramirez, S.I., Mateus, J., Dan, J.M., Moderbacher, C.R., Rawlings, S.A., Sutherland, A., Premkumar, L., Jadi, R.S., et al. (2020). Targets of T Cell responses to SARS-CoV-2 coronavirus in humans with COVID-19 disease and unexposed individuals. Cell *181*, 1489–1501.

48. Munster, V.J., Feldmann, F., Williamson, B.N., van Doremalen, N., Perez-Perez, L., Schulz, J., Meade-White, K., Okumura, A., Callison, J., Brumbaugh, B., et al. (2020). Respiratory disease in rhesus macaques inoculated with SARS-CoV-2. Nature *585*, 268–272.

49. Rockx, B., Kuiken, T., Herfst, S., Bestebroer, T., Lamers, M.M., Oude Munnink, B.B., de Meulder, D., van Amerongen, G., van den Brand, J., Okba, N.M.A., et al. (2020). Comparative pathogenesis of COVID-19, MERS, and SARS in a nonhuman primate model. Science *368*, 1012–1015.

50. Maisonnasse, P., Guedj, J., Contreras, V., Behillil, S., Solas, C., Marlin, R., Naninck, T., Pizzorno, A., Lemaitre, J., Goncalves, A., et al. (2020). Hydroxychloroquine use against SARS-CoV-2 infection in non-human primates. Nature *585*, 584–587.

51. McMahan, K., Yu, J., Mercado, N.B., Loos, C., Tostanoski, L.H., Chandrashekar, A., Liu, J., Peter, L., Atyeo, C., Zhu, A., et al. (2021). Correlates of protection against SARS-CoV-2 in rhesus macaques. Nature *590*, 630–634.

52. Deng, W., Bao, L., Liu, J., Xiao, C., Liu, J., Xue, J., Lv, Q., Qi, F., Gao, H., Yu, P., et al. (2020). Primary exposure to SARS-CoV-2 protects against reinfection in rhesus macaques. Science *369*, 818–823.

53. Marlin, R., Godot, V., Cardinaud, S., Galhaut, M., Coleon, S., Zurawski, S., Dereuddre-Bosquet, N., Cavarelli, M., Gallouet, A.S., Maisonnasse, P., et al. (2021). Targeting SARS-CoV-2 receptor-binding domain to cells expressing CD40 improves protection to infection in convalescent macaques. Nat. Commun. *12*, 5215.

54. Corbett, K.S., Flynn, B., Foulds, K.E., Francica, J.R., Boyoglu-Barnum, S., Werner, A.P., Flach, B., O'Connell, S., Bock, K.W., Minai, M., et al. (2020). Evaluation of the mRNA-1273 vaccine against SARS-CoV-2 in nonhuman primates. N. Engl. J. Med. *383*, 1544–1555.

55. Vogel, A.B., Kanevsky, I., Che, Y., Swanson, K.A., Muik, A., Vormehr, M., Kranz, L.M., Walzer, K.C., Hein, S., Guler, A., et al. (2021). BNT162b vaccines protect rhesus macaques from SARS-CoV-2. Nature *592*, 283–289.

56. van Doremalen, N., Lambe, T., Spencer, A., Belij-Rammerstorfer, S., Purushotham, J.N., Port, J.R., Avanzato, V.A., Bushmaker, T., Flaxman, A., Ulaszewska, M., et al. (2020). ChAdOx1 nCoV-19 vaccine prevents SARS-CoV-2 pneumonia in rhesus macaques. Nature *586*, 578–582.

57. Mercado, N.B., Zahn, R., Wegmann, F., Loos, C., Chandrashekar, A., Yu, J., Liu, J., Peter, L., McMahan, K., Tostanoski, L.H., et al. (2020). Single-shot Ad26 vaccine protects against SARS-CoV-2 in rhesus macaques. Nature *586*, 583–588.

58. Gao, Q., Bao, L., Mao, H., Wang, L., Xu, K., Yang, M., Li, Y., Zhu, L., Wang, N., Lv, Z., et al. (2020). Development of an inactivated vaccine candidate for SARS-CoV-2. Science *369*, 77–81.

59. Wang, H., Zhang, Y., Huang, B., Deng, W., Quan, Y., Wang, W., Xu, W., Zhao, Y., Li, N., Zhang, J., et al. (2020). Development of an inactivated vaccine candidate, BBIBP-CorV, with potent protection against SARS-CoV-2. Cell *182*, 713–721.

60. Klasse, P.J., Nixon, D.F., and Moore, J.P. (2021). Immunogenicity of clinically relevant SARS-CoV-2 vaccines in nonhuman primates and humans. Sci. Adv. *7*, eabe8065.

61. Liu, X., Drelich, A., Li, W., Chen, C., Sun, Z., Shi, M., Adams, C., Mellors, J.W., Tseng, C.T., and Dimitrov, D.S. (2020). Enhanced elicitation of potent neutralizing antibodies by the SARS-CoV-2 spike receptor binding domain Fc fusion protein in mice. Vaccine *38*, 7205–7212.

62. Zang, J., Gu, C., Zhou, B., Zhang, C., Yang, Y., Xu, S., Zhang, X., Zhou, Y., Bai, L., Wu, Y., et al. (2020). Immunization with the receptor–binding domain of SARS-CoV-2 elicits antibodies cross-neutralizing SARS-CoV-2 and SARS-CoV without antibody-dependent enhancement. Cell Discov. *6*, 61.

63. Tan, H.X., Juno, J.A., Lee, W.S., Barber-Axthelm, I., Kelly, H.G., Wragg, K.M., Esterbauer, R., Amarasena, T., Mordant, F.L., Subbarao, K., et al. (2021). Immunogenicity of prime-boost protein subunit vaccine strategies against SARS-CoV-2 in mice and macaques. Nat. Commun. *12*, 1403.

64. Liang, J.G., Su, D., Song, T.Z., Zeng, Y., Huang, W., Wu, J., Xu, R., Luo, P., Yang, X., Zhang, X., et al. (2021). S-Trimer, a COVID-19 subunit vaccine candidate, induces protective immunity in nonhuman primates. Nat. Commun. *12*, 1346.

65. Mandolesi, M., Sheward, D.J., Hanke, L., Ma, J., Pushparaj, P., Perez Vidakovics, L., Kim, C., Adori, M., Lenart, K., Lore, K., et al. (2021). SARS-CoV-2 protein subunit vaccination of mice and rhesus macaques elicits potent and durable neutralizing antibody responses. Cell Rep. Med. *2*, 100252.

66. Zhang, B., Chao, C.W., Tsybovsky, Y., Abiona, O.M., Hutchinson, G.B., Moliva, J.I., Olia, A.S., Pegu, A., Phung, E., Stewart-Jones, G.B.E., et al. (2020). A platform incorporating trimeric antigens into self-assembling nanoparticles reveals SARS-CoV-2-spike nanoparticles to elicit substantially higher neutralizing responses than spike alone. Sci. Rep. *10*, 18149.

67. Walls, A.C., Fiala, B., Schafer, A., Wrenn, S., Pham, M.N., Murphy, M., Tse, L.V., Shehata, L., O'Connor, M.A., Chen, C., et al. (2020). Elicitation of potent neutralizing antibody responses by designed protein nanoparticle vaccines for SARS-CoV-2. Cell *183*, 1367–1382.

68. Arunachalam, P.S., Walls, A.C., Golden, N., Atyeo, C., Fischinger, S., Li, C., Aye, P., Navarro, M.J., Lai, L., Edara, V.V., et al. (2021). Adjuvanting a subunit COVID-19 vaccine to induce protective immunity. Nature *594*, 253–258.

69. Guebre-Xabier, M., Patel, N., Tian, J.H., Zhou, B., Maciejewski, S., Lam, K., Portnoff, A.D., Massare, M.J., Frieman, M.B., Piedra, P.A., et al. (2020). NVX-CoV2373 vaccine protects cynomolgus macaque upper and lower airways against SARS-CoV-2 challenge. Vaccine *38*, 7892–7896.

70. Brouwer, P.J.M., Brinkkemper, M., Maisonnasse, P., Dereuddre-Bosquet, N., Grobben, M., Claireaux, M., de Gast, M., Marlin, R., Chesnais, V., Diry, S., et al. (2021). Two-component spike nanoparticle vaccine protects macaques from SARS-CoV-2 infection. Cell *184*, 1188–1200.

71. Alving, C.R., Beck, Z., Matyas, G.R., and Rao, M. (2016). Liposomal adjuvants for human vaccines. Expert Opin. Drug Deliv. *13*, 807–816.

72. Nisini, R., Poerio, N., Mariotti, S., De Santis, F., and Fraziano, M. (2018). The multirole of liposomes in therapy and prevention of infectious diseases. Front. Immunol. *9*, 155.

73. Ingale, J., Stano, A., Guenaga, J., Sharma, S.K., Nemazee, D., Zwick, M.B., and Wyatt, R.T. (2016). High-density array of well-ordered HIV-1 spikes on synthetic liposomal nanoparticles efficiently activate B cells. Cell Rep. *15*, 1986–1999.

74. Bale, S., Goebrecht, G., Stano, A., Wilson, R., Ota, T., Tran, K., Ingale, J., Zwick, M.B., and Wyatt, R.T. (2017). Covalent linkage of HIV-1 trimers to synthetic liposomes elicits improved B cell and antibody responses. J. Virol. *91*, e00443–17.

75. Martinez-Murillo, P., Tran, K., Guenaga, J., Lindgren, G., Adori, M., Feng, Y., Phad, G.E., Vazquez Bernat, N., Bale, S., Ingale, J., et al. (2017). Particulate array of well-ordered HIV clade C Env trimers elicits neutralizing antibodies that display a unique V2 cap approach. Immunity *46*, 804–817.

76. Dubrovskaya, V., Tran, K., Ozorowski, G., Guenaga, J., Wilson, R., Bale, S., Cottrell, C.A., Turner, H.L., Seabright, G., O'Dell, S., et al. (2019). Vaccination with glycan-modified HIV NFL envelope trimer-liposomes elicits broadly neutralizing antibodies to multiple sites of vulnerability. Immunity *51*, 915–929.

77. Edwards, R.J., Mansouri, K., Stalls, V., Manne, K., Watts, B., Parks, R., Janowska, K., Gobeil, S.M.C., Kopp, M., Li, D., et al. (2021). Cold sensitivity of the SARS-CoV-2 spike ectodomain. Nat. Struct. Mol. Biol. *28*, 128–131.

78. Eldred, B.E., Dean, A.J., McGuire, T.M., and Nash, A.L. (2006). Vaccine components and constituents: responding to consumer concerns. Med. J. Aust. *184*, 170–175.

79. Hsieh, C.L., Goldsmith, J.A., Schaub, J.M., DiVenere, A.M., Kuo, H.C., Javanmardi, K., Le, K.C., Wrapp, D., Lee, A.G., Liu, Y., et al. (2020). Structure-based design of prefusion-stabilized SARS-CoV-2 spikes. Science *369*, 1501–1505.

80. Xiong, X., Qu, K., Ciazynska, K.A., Hosmillo, M., Carter, A.P., Ebrahimi, S., Ke, Z., Scheres, S.H.W., Bergamaschi, L., Grice, G.L., et al. (2020). A thermostable, closed SARS-CoV-2 spike protein trimer. Nat. Struct. Mol. Biol. *27*, 934–941.

81. Toelzer, C., Gupta, K., Yadav, S.K.N., Borucu, U., Davidson, A.D., Kavanagh Williamson, M., Shoemark, D.K., Garzoni, F., Staufer, O., Milligan, R., et al. (2020). Free fatty acid binding pocket in the locked structure of SARS-CoV-2 spike protein. Science *370*, 725–730.

82. Rosa, A., Pye, V.E., Graham, C., Muir, L., Seow, J., Ng, K.W., Cook, N.J., Rees-Spear, C., Parker, E., Dos Santos, M.S., et al. (2021). SARS-CoV-2 can recruit a heme metabolite to evade antibody immunity. Sci. Adv. *7*, eabg7607.

83. Cohen, A.A., Gnanapragasam, P.N.P., Lee, Y.E., Hoffman, P.R., Ou, S., Kakutani, L.M., Keeffe, J.R., Wu, H.J., Howarth, M., West, A.P., et al. (2021). Mosaic nanoparticles elicit cross-reactive immune responses to zoonotic coronaviruses in mice. Science *371*, 735–741.

84. Tan, T.K., Rijal, P., Rahikainen, R., Keeble, A.H., Schimanski, L., Hussain, S., Harvey, R., Hayes, J.W.P., Edwards, J.C., McLean, R.K., et al. (2021). A COVID-19 vaccine candidate using SpyCatcher multimerization of the SARS-CoV-2 spike protein receptor-binding domain induces potent neutralising antibody responses. Nat. Commun. *12*, 542.

85. Yu, J., Tostanoski, L.H., Peter, L., Mercado, N.B., McMahan, K., Mahrokhian, S.H., Nkolola, J.P., Liu, J., Li, Z., Chandrashekar, A., et al. (2020). DNA vaccine protection against SARS-CoV-2 in rhesus macaques. Science *369*, 806–811.

86. Addetia, A., Crawford, K.H.D., Dingens, A., Zhu, H., Roychoudhury, P., Huang, M.L., Jerome, K.R., Bloom, J.D., and Greninger, A.L. (2020).

Neutralizing antibodies correlate with protection from SARS-CoV-2 in humans during a fishery vessel outbreak with a high attack rate. J. Clin. Microbiol. *58*, e02107–e02120.

87. Keech, C., Albert, G., Cho, I., Robertson, A., Reed, P., Neal, S., Plested, J.S., Zhu, M., Cloney-Clark, S., Zhou, H., et al. (2020). Phase 1-2 trial of a SARS-CoV-2 recombinant spike protein nanoparticle vaccine. N. Engl. J. Med. *383*, 2320–2332.
88. Sahin, U., Muik, A., Derhovanessian, E., Vogler, I., Kranz, L.M., Vormehr, M., Baum, A., Pascal, K., Quandt, J., Maurus, D., et al. (2020). COVID-19 vaccine BNT162b1 elicits human antibody and TH1 T cell responses. Nature *586*, 594–599.
89. Ewer, K.J., Barrett, J.R., Belij-Rammerstorfer, S., Sharpe, H., Makinson, R., Morter, R., Flaxman, A., Wright, D., Bellamy, D., Bittaye, M., et al. (2021). T cell and antibody responses induced by a single dose of ChAdOx1 nCoV-19 (AZD1222) vaccine in a phase 1/2 clinical trial. Nat. Med. *27*, 270–278.
90. Ganneru, B., Jogdand, H., Daram, V.K., Das, D., Molugu, N.R., Prasad, S.D., Kannappa, S.V., Ella, K.M., Ravikrishnan, R., Awasthi, A., et al. (2021). Th1 skewed immune response of whole virion inactivated SARS CoV 2 vaccine and its safety evaluation. iScience *24*, 102298.
91. Pisanic, N., Randad, P.R., Kruczynski, K., Manabe, Y.C., Thomas, D., Pekosz, A., Klein, S., Betenbaugh, M.J., Clarke, W.A., Laeyendecker, O., et al. (2020). COVID-19 serology at population scale: SARS-CoV-2-specific antibody responses in saliva. J. Clin. Microbiol. *59*, e02204–e02220.
92. Suthar, M.S., Zimmerman, M.G., Kauffman, R.C., Mantus, G., Linderman, S.L., Hudson, W.H., Vanderheiden, A., Nyhoff, L., Davis, C.W., Adekunle, O., et al. (2020). Rapid generation of neutralizing antibody responses in COVID-19 patients. Cell Rep. Med. *1*, 100040.
93. Stamatatos, L., Czartoski, J., Wan, Y.H., Homad, L.J., Rubin, V., Glantz, H., Neradilek, M., Seydoux, E., Jennewein, M.F., MacCamy, A.J., et al. (2021). mRNA vaccination boosts cross-variant neutralizing antibodies elicited by SARS-CoV-2 infection. Science *372*, 1413–1418.
94. Barnes, C.O., Jette, C.A., Abernathy, M.E., Dam, K.A., Esswein, S.R., Gristick, H.B., Malyutin, A.G., Sharaf, N.G., Huey-Tubman, K.E., Lee, Y.E., et al. (2020). SARS-CoV-2 neutralizing antibody structures inform therapeutic strategies. Nature *588*, 682–687.
95. Barnes, C.O., West, A.P., Jr., Huey-Tubman, K.E., Hoffmann, M.A.G., Sharaf, N.G., Hoffman, P.R., Koranda, N., Gristick, H.B., Gaebler, C., Muecksch, F., et al. (2020). Structures of human antibodies bound to SARS-CoV-2 spike reveal common epitopes and recurrent features of antibodies. Cell *182*, 828–842.
96. Kreye, J., Reincke, S.M., Kornau, H.C., Sanchez-Sendin, E., Corman, V.M., Liu, H., Yuan, M., Wu, N.C., Zhu, X., Lee, C.D., et al. (2020). A therapeutic non-self-reactive SARS-CoV-2 antibody protects from lung pathology in a COVID-19 Hamster model. Cell *183*, 1058–1069.
97. Korber, B., Fischer, W.M., Gnanakaran, S., Yoon, H., Theiler, J., Abfalterer, W., Hengartner, N., Giorgi, E.E., Bhattacharya, T., Foley, B., et al. (2020). Tracking changes in SARS-CoV-2 spike: evidence that D614G increases infectivity of the COVID-19 virus. Cell *182*, 812–827.
98. Zhang, J., Cai, Y., Xiao, T., Lu, J., Peng, H., Sterling, S.M., Walsh, R.M., Jr., Rits-Volloch, S., Zhu, H., Woosley, A.N., et al. (2021). Structural impact on SARS-CoV-2 spike protein by D614G substitution. Science *372*, 525–530.
99. Ozono, S., Zhang, Y., Ode, H., Sano, K., Tan, T.S., Imai, K., Miyoshi, K., Kishigami, S., Ueno, T., Iwatani, Y., et al. (2021). SARS-CoV-2 D614G spike mutation increases entry efficiency with enhanced ACE2-binding affinity. Nat. Commun. *12*, 848.
100. Zhang, L., Jackson, C.B., Mou, H., Ojha, A., Peng, H., Quinlan, B.D., Rangarajan, E.S., Pan, A., Vanderheiden, A., Suthar, M.S., et al. (2020). SARS-CoV-2 spike-protein D614G mutation increases virion spike density and infectivity. Nat. Commun. *11*, 6013.
101. Gobeil, S.M., Janowska, K., McDowell, S., Mansouri, K., Parks, R., Stalls, V., Kopp, M.F., Manne, K., Li, D., Wiehe, K., et al. (2021). Effect of natural mutations of SARS-CoV-2 on spike structure, conformation, and antigenicity. Science *373*, eabi6226.
102. Cai, Y., Zhang, J., Xiao, T., Lavine, C.L., Rawson, S., Peng, H., Zhu, H., Anand, K., Tong, P., Gautam, A., et al. (2021). Structural basis for enhanced infectivity and immune evasion of SARS-CoV-2 variants. Science *373*, 642–648.
103. Yuan, M., Huang, D., Lee, C.D., Wu, N.C., Jackson, A.M., Zhu, X., Liu, H., Peng, L., van Gils, M.J., Sanders, R.W., et al. (2021). Structural and functional ramifications of antigenic drift in recent SARS-CoV-2 variants. Science *373*, 818–823.
104. Weissman, D., Alameh, M.G., de Silva, T., Collini, P., Hornsby, H., Brown, R., LaBranche, C.C., Edwards, R.J., Sutherland, L., Santra, S., et al. (2021). D614G spike mutation increases SARS CoV-2 susceptibility to neutralization. Cell Host Microbe *29*, 23–31.
105. Zhou, D., Dejnirattisai, W., Supasa, P., Liu, C., Mentzer, A.J., Ginn, H.M., Zhao, Y., Duyvesteyn, H.M.E., Tuekprakhon, A., Nutalai, R., et al. (2021). Evidence of escape of SARS-CoV-2 variant B.1.351 from natural and vaccine-induced sera. Cell *184*, 2348–2361.
106. Dejnirattisai, W., Zhou, D., Supasa, P., Liu, C., Mentzer, A.J., Ginn, H.M., Zhao, Y., Duyvesteyn, H.M.E., Tuekprakhon, A., Nutalai, R., et al. (2021). Antibody evasion by the P.1 strain of SARS-CoV-2. Cell *184*, 2939–2954.
107. Hoffmann, M., Arora, P., Gross, R., Seidel, A., Hornich, B.F., Hahn, A.S., Kruger, N., Graichen, L., Hofmann-Winkler, H., Kempf, A., et al. (2021). SARS-CoV-2 variants B.1.351 and P.1 escape from neutralizing antibodies. Cell *184*, 2384–2393.
108. Edara, V.V., Norwood, C., Floyd, K., Lai, L., Davis-Gardner, M.E., Hudson, W.H., Mantus, G., Nyhoff, L.E., Adelman, M.W., Fineman, R., et al. (2021). Infection- and vaccine-induced antibody binding and neutralization of the B.1.351 SARS-CoV-2 variant. Cell Host Microbe *29*, 516–521.
109. Garcia-Beltran, W.F., Lam, E.C., St Denis, K., Nitido, A.D., Garcia, Z.H., Hauser, B.M., Feldman, J., Pavlovic, M.N., Gregory, D.J., Poznansky, M.C., et al. (2021). Multiple SARS-CoV-2 variants escape neutralization by vaccine-induced humoral immunity. Cell *184*, 2372–2383.
110. Kuzmina, A., Khalaila, Y., Voloshin, O., Keren-Naus, A., Boehm-Cohen, L., Raviv, Y., Shemer-Avni, Y., Rosenberg, E., and Taube, R. (2021). SARS-CoV-2 spike variants exhibit differential infectivity and neutralization resistance to convalescent or post-vaccination sera. Cell Host Microbe *29*, 522–528.
111. Geers, D., Shamier, M.C., Bogers, S., den Hartog, G., Gommers, L., Nieuwkoop, N.N., Schmitz, K.S., Rijsbergen, L.C., van Osch, J.A.T., Dijkhuizen, E., et al. (2021). SARS-CoV-2 variants of concern partially escape humoral but not T-cell responses in COVID-19 convalescent donors and vaccinees. Sci. Immunol. *6*, eabj1750.
112. Rees-Spear, C., Muir, L., Griffith, S.A., Heaney, J., Aldon, Y., Snitselaar, J.L., Thomas, P., Graham, C., Seow, J., Lee, N., et al. (2021). The effect of spike mutations on SARS-CoV-2 neutralization. Cell Rep. *34*, 108890.
113. Supasa, P., Zhou, D., Dejnirattisai, W., Liu, C., Mentzer, A.J., Ginn, H.M., Zhao, Y., Duyvesteyn, H.M.E., Nutalai, R., Tuekprakhon, A., et al. (2021). Reduced neutralization of SARS-CoV-2 B.1.1.7 variant by convalescent and vaccine sera. Cell *184*, 2201–2211.e7.
114. Greaney, A.J., Loes, A.N., Crawford, K.H.D., Starr, T.N., Malone, K.D., Chu, H.Y., and Bloom, J.D. (2021). Comprehensive mapping of mutations in the SARS-CoV-2 receptor-binding domain that affect recognition by polyclonal human plasma antibodies. Cell Host Microbe *29*, 463–476.
115. Caniels, T.G., Bontjer, I., van der Straten, K., Poniman, M., Burger, J.A., Appelman, B., Lavell, H.A.A., Oomen, M., Godeke, G.J., Valle, C., et al. (2021). Emerging SARS-CoV-2 variants of concern evade humoral immune responses from infection and vaccination. Sci. Adv. *7*, eabj5365.
116. Sokal, A., Chappert, P., Barba-Spaeth, G., Roeser, A., Fourati, S., Azzaoui, I., Vandenberghe, A., Fernandez, I., Meola, A., Bouvier-Alias, M., et al. (2021). Maturation and persistence of the anti-SARS-CoV-2 memory B cell response. Cell *184*, 1201–1213.

117. Gaebler, C., Wang, Z., Lorenzi, J.C.C., Muecksch, F., Finkin, S., Tokuyama, M., Cho, A., Jankovic, M., Schaefer-Babajew, D., Oliveira, T.Y., et al. (2021). Evolution of antibody immunity to SARS-CoV-2. Nature *591*, 639–644.

118. Goel, R.R., Painter, M.M., Apostolidis, S.A., Mathew, D., Meng, W., Rosenfeld, A.M., Lundgreen, K.A., Reynaldi, A., Khoury, D.S., Pattekar, A., et al. (2021). mRNA vaccination induces durable immune memory to SARS-CoV-2 with continued evolution to variants of concern. Science *374*, eabm0829.

119. Schmidt, F., Weisblum, Y., Muecksch, F., Hoffmann, H.H., Michailidis, E., Lorenzi, J.C.C., Mendoza, P., Rutkowska, M., Bednarski, E., Gaebler, C., et al. (2020). Measuring SARS-CoV-2 neutralizing antibody activity using pseudotyped and chimeric viruses. J. Exp. Med. *217*, e20201181.

120. Lescure, F.X., Bouadma, L., Nguyen, D., Parisey, M., Wicky, P.H., Behillil, S., Gaymard, A., Bouscambert-Duchamp, M., Donati, F., Le Hingrat, Q., et al. (2020). Clinical and virological data of the first cases of COVID-19 in Europe: a case series. Lancet Infect. Dis. *20*, 697–706.

121. Lai, R.P.J., Hock, M., Radzimanowski, J., Tonks, P., Lutje Hulsik, D., Effantin, G., et al. (2014). A fusion intermediate gp41 immunogen elicits neutralizing antibodies to HIV-1. J. Biol. Chem. *289*, 29912–29926.

122. Scheres, S.H. (2012). RELION: implementation of a Bayesian approach to cryo-EM structure determination. J. Struct. Biol. *180*, 519–530.

123. Mastronarde, D.N. (2005). Automated electron microscope tomography using robust prediction of specimen movements. J. Struct. Biol. *152*, 36–51.

124. Zheng, S.Q., Palovcak, E., Armache, J.P., Verba, K.A., Cheng, Y., and Agard, D.A. (2017). MotionCor2: anisotropic correction of beam-induced motion for improved cryo-electron microscopy. Nat. Methods *14*, 331–332.

125. Zivanov, J., Nakane, T., Forsberg, B.O., Kimanius, D., Hagen, W.J., Lindahl, E., and Scheres, S.H. (2018). New tools for automated high-resolution cryo-EM structure determination in RELION-3. Elife *7*, e42166.

126. Zhang, K. (2016). Gctf: real-time CTF determination and correction. J. Struct. Biol. *193*, 1–12.

127. Cardone, G., Heymann, J.B., and Steven, A.C. (2013). One number does not fit all: mapping local variations in resolution in cryo-EM reconstructions. J. Struct. Biol. *184*, 226–236.

128. Sanchez-Garcia, R., Gomez-Blanco, J., Cuervo, A., Carazo, J.M., Sorzano, C.O.S., and Vargas, J. (2021). DeepEMhancer: a deep learning solution for cryo-EM volume post-processing. Commun. Biol. *4*, 874.

129. Pettersen, E.F., Goddard, T.D., Huang, C.C., Couch, G.S., Greenblatt, D.M., Meng, E.C., and Ferrin, T.E. (2004). UCSF Chimera–a visualization system for exploratory research and analysis. J. Comput. Chem. *25*, 1605–1612.

130. Adams, P.D., Afonine, P.V., Bunkoczi, G., Chen, V.B., Davis, I.W., Echols, N., Headd, J.J., Hung, L.W., Kapral, G.J., Grosse-Kunstleve, R.W., et al. (2010). PHENIX: a comprehensive Python-based system for macromolecular structure solution. Acta Crystallogr. D Biol. Crystallogr. *66*, 213–221.

131. Emsley, P., Lohkamp, B., Scott, W.G., and Cowtan, K. (2010). Features and development of coot. Acta Crystallogr. D Biol. Crystallogr. *66*, 486–501.

132. Williams, C.J., Headd, J.J., Moriarty, N.W., Prisant, M.G., Videau, L.L., Deis, L.N., Verma, V., Keedy, D.A., Hintze, B.J., Chen, V.B., et al. (2018). MolProbity: more and better reference data for improved all-atom structure validation. Protein Sci. *27*, 293–315.

133. Goddard, T.D., Huang, C.C., Meng, E.C., Pettersen, E.F., Couch, G.S., Morris, J.H., and Ferrin, T.E. (2018). UCSF ChimeraX: meeting modern challenges in visualization and analysis. Protein Sci. *27*, 14–25.

134. Corman, V.M., Landt, O., Kaiser, M., Molenkamp, R., Meijer, A., Chu, D.K., Bleicker, T., Brunink, S., Schneider, J., Schmidt, M.L., et al. (2020). Detection of 2019 novel coronavirus (2019-nCoV) by real-time RT-PCR. Euro Surveill. *25*, 2000045.

135. Wolfel, R., Corman, V.M., Guggemos, W., Seilmaier, M., Zange, S., Muller, M.A., Niemeyer, D., Jones, T.C., Vollmar, P., Rothe, C., et al. (2020). Virological assessment of hospitalized patients with COVID-2019. Nature *581*, 465–469.

136. Shi, R., Shan, C., Duan, X., Chen, Z., Liu, P., Song, J., Song, T., Bi, X., Han, C., Wu, L., et al. (2020). A human neutralizing antibody targets the receptor-binding site of SARS-CoV-2. Nature *584*, 120–124.

137. Pan, F., Ye, T., Sun, P., Gui, S., Liang, B., Li, L., Zheng, D., Wang, J., Hesketh, R.L., Yang, L., et al. (2020). Time course of lung changes at chest CT during recovery from coronavirus disease 2019 (COVID-19). Radiology *295*, 715–721.

STAR★METHODS

KEY RESOURCES TABLE

REAGENT or RESOURCE	SOURCE	IDENTIFIER
Antibodies		
Horsedish peroxidase conjugated goat anti-monkey H+L	Invitrogen	Cat# PA1-84631
Anti-IL2 PerCP5.5 (MQ1-17H12)	BD Bioscience	Cat# 560708
Anti-IL17a Alexa700 (N49-653)	BD Bioscience	Cat# 560613
Anti-IFN-γ V450 (B27)	BD Bioscience	Cat# 560371
Anti-TNF-α BV605 (Mab11)	Biolegend	Cat# 502936
Anti-IL-13 BV711 (JES10-5A2)	BD Bioscience	Cat# 564288
Anti-CD137 APC (4B4)	BD Bioscience	Cat# 550890; RRID:AB_2848292
Anti-CD154 FITC (TRAP1)	BD Bioscience	Cat# 555699; RRID:AB_396049
CD3 APC-Cy7 (SP34-2)	BD Bioscience	Cat# 557757; RRID:AB_396863
CD4 BV510 (L200)	BD Bioscience	Cat# 563094
CD8 PE-Vio770 (BW135/80)	Miltenyi Biotec	Cat# 130-113-721
FastImmune ™ CD28/CD49d	BD Bioscience	Cat# 130-113-159
Live/Dead Fixable Blue Dead Cell	Thermofisher	Cat# L34962
Anti-Monkey IgG (γ-chain specific)-Biotin antibody produced in goat	Sigma Aldrich	Cat# SAB3700768
Anti-Monkey IgA (α-chain specific)-Biotin antibody produced in goat	Sigma Aldrich	Cat# SAB3700761
Bacterial and virus strains		
SARS-CoV-2 (hCoV-19/France/IDF0372/2020 strain)	Lescure et al.[119]	EPI_ISL_410720 (GISAID ID)
TOP10 Chemically Competent *E. coli*	Thermofisher	C404010
Chemicals, peptides, and recombinant proteins		
Formaldehyde solution 36.5%	Sigma-Aldrich	Cat# F8775-25ML
Dithiothreitol	Sigma-Aldrich	Cat# 43819
Streptavidin-PE	ThermoFisher Scientific	Cat# 12-4317-87
EDC	ThermoFisher Scientific	Cat# A35391
Sulfo-NHS	ThermoFisher Scientific	Cat# A39269
Ampiciline	Euromedex	Cat# EU0400-D
Polyethylemine (PEI-25K)	Polyscience	Cat# 23966-1
L-α-phosphatidylcholine (PC)	Avanti Polar Lipids	840051
DGS-NTA(Ni)	Avanti Polar Lipids	790404
Cholesterol	Avanti Polar Lipids	700000
Bradford Protein Assay Reactive	BioRad	Cat# 5000006
Excel purification resin	Cytiva	Cat# 17-3712-01
PBS 10X	EuroMedex	Cat# ET330-A
Penicillin	Sigma-Aldrich	Cat# P3032-10MI
Streptomycin	VWR	Cat# 382-EU-100G
MPLA liposomes	Polymun Scientific	https://www.polymun.com/liposomes/reference-projects/
Bovine Serum Albumin	Sigma-Aldrich	Cat# A2153-1000
GlutaMax	Gibco	Cat# 35050061
PepMix™ SARS-CoV-2 (Spike Glycoprotein)	JPT peptide Technologies	Cat# PM-WCPV-S
Poly-L-Lysine Hydrobromide	Sigma-Aldrich	Cat# P1399

(*Continued on next page*)

Continued

REAGENT or RESOURCE	SOURCE	IDENTIFIER
Critical commercial assays		
SSIV Reverse Transcriptase	Thermo Fisher scientific	Cat# 18090050
Ligation Sequencing Kit	Nanopore	Cat# SQK-LSK109
Q5 Hot Start DNA Polymerase	NEB	Cat# M0494
Expi293™ Expression System Kit	Thermo Fisher scientific	Cat# A14635
Nano-Glo Luciferase Assay System	Promega	Cat# N1130
Nucleospin 96 Virus Core	Macharey-Nagel	Cat# 740452.4
Experimental models: Cell lines		
FreeStyle™ 293-F Cells	Thermo Fisher scientific	Cat# R79007
Expi293F™ Cells	Thermo Fisher scientific	Cat# A14527
VeroE6	ATCC	ATTC®CRL 1586TM
HEK293T/ACE2 cells	Schmidt et al.[120]	N/A
Desposited data		
PDB	7Q1Z	https://www.rcsb.org/
EMBD	EMD-13776	https://www.ebi.ac.uk/emdb/
Experimental models: Organisms/strains		
Cynomolgus macaques	Cynologics	N/A
Oligonucleotides		
Primers covid19 V3	ARTIC network	http://artic.network/resources/ncov-amplicon-v3.pdf
RdRp-IP4 primer, forward – GGTAACTGGTATGATTTCG	https://www.who.int/docs/default-source/coronaviruse/real-time-rt-pcr-assays-for-the-detection-of-sars-cov-2-institut-pasteur-paris.pdf?sfvrsn=3662fcb6_2	N/A
RdRp-IP4 primer, reverse - CTGGTCAAGGTTAATATAGG	https://www.who.int/docs/default-source/coronaviruse/real-time-rt-pcr-assays-for-the-detection-of-sars-cov-2-institut-pasteur-paris.pdf?sfvrsn=3662fcb6_2	N/A
RdRp-IP4 primer probe P - TCATACAAACCACGCCAG G	https://www.who.int/docs/default-source/coronaviruse/real-time-rt-pcr-assays-for-the-detection-of-sars-cov-2-institut-pasteur-paris.pdf?sfvrsn=3662fcb6_2	N/A
sgLead SARSCoV2-forward - CGATCTCTTGTAGATCTGTTCTC	Corman[121]	N/A
E-Sarbeco-reverse primer - ATATTGCAGCAGTACGCACACA	Corman[121]	N/A
E-Sarbeco probe HEX-ACACTAGCCATCCTTACTGCGCTTCG-BHQ1	Corman[121]	N/A
Recombinant DNA		
Plasmid: Protein S	Wrapp et al.[8]	N/A
Plasmid: RBD	NR-52309, BEI resources, NIAID, NIH	N/A
pHIV-1NL43ΔENV-NanoLuc plasmid	Schmidt et al.[120]	N/A
SARS-CoV-2-SΔ19 plasmid	Schmidt et al.[120]	N/A
gBlock B.1.1.7, B.1.351, and P.1	Integrated DNA Technologies	N /A
Variants : B.1.1.7, B.1.351, and P.1 cloned in pCR3 plasmid	Caniels et al.[115]	N/A

(*Continued on next page*)

Continued

REAGENT or RESOURCE	SOURCE	IDENTIFIER
Software and algorithms		
GraphPad Prism v7	GraphPad	N/A
GraphPad Prism v8	GraphPad	N/A
ProtParam		http://web.expasy.org/
Prometheus MT	Nanotemper	https://nanotempertech.com/prometheus/
Flowjo v10	Flowjo	N/A
INTELLISPACE PORTAL 8 software	Philips Healthcare	https://www.philips.fr/healthcare/product/HC881062/intellispace-portal-80-all-your-advanced-analysis-needs-one-comprehensive-solution
SerialEM	Mastronarde et al.[122]	N/A
motioncor2	Zheng et al.[123]	N/A
RELION 3.1.2	Zivanov et al.[124]	N/A
GCTF	Zhang et al.[125]	N/A
Blocres	Cardone et al.[126]	N/A
DeepEMhancer	Sanchez-Garcia et al.[127]	N/A
CHIMERA	Pettersen et al.[128]	N/A
COOT	Emsley et al.[129]	N/A
MOLPROBITY	Williams et al.[130]	N/A
PHENIX	Adams et al.[131]	N/A
CHIMERAX	Goddard et al.[132]	N/A
Others		
Superose 6 increase	GE Healthcare	28-9909-44
Superdex 75	GE Healthcare	N/A
Whatman® Nuclepore™ Track-Etched Membranes	Merck	**WHA111105**
FreeStyle Expression Medium	Thermo Scientific	Cat# 12338018
Opti-MEM™ I Reduced Serum Medium	Thermo Scientific	Cat#31985062
RPMI Medium 1640	GIBCO	Cat# 21875-034
DMEM	Sigma-Aldrich	Cat# D6429-500ML
Grilles Cu 400 mesh	Oxford Instruments	G2400C
NucleoBond PC 2000 EF	Macherey Nagel	Cat# 740549
NucleoBond Xtra Midi EF	Macherey Nagel	Cat# 740420
Nucleobond Xtra Mini Kit	Macherey-Nagel	N/A
ELISA microplates	Thermo Scientific	10547781
Protein A Sepharose ®	Abcam	Cat# ab193256
Protein G Sepharose ™	Abcam	Cat# ab17061801
Instant Blue Coomassie Protein Stain	Abcam	Cat# ab119211
Amicon® Ultra-15	Sigma-Aldrich	UFC903096
Amicon® Ultra-30	Sigma-Aldrich	UFC901096
Capillars		N/A
AKTA system	GE Healthcare	https://www.cytivalifesciences.com/en/us/shop/chromatography/chromatography-systems/akta-pure-p-05844
TMB	Interchim	UP 664781
Glomax	Turner BioSystems	Model# 9101-002
Microplate 96 well half area white	Greiner bio-one	Cat# 675074

(*Continued on next page*)

Continued

REAGENT or RESOURCE	SOURCE	IDENTIFIER
Greiner CELLSTAR® 96 well plates, round bottom clear wells	Merck	Cat# M9436
Greiner CELLSTAR® 96 well plates, flat bottom clear wells	Merck	Cat# M0812
MagPlex-C Microspheres 1 mL	Luminex	Cat# MC100XX-01
MAGPIX	Luminex	Cat# MAGPIX-XPON4.1-RUO

RESOURCE AVAILABILITY

Lead contact

Further information and requests for resources and reagents should be directed to and will be fulfilled by the Lead Contact, Winfried Weissenhorn (winfried.weissenhorn@ibs.fr).

Materials availability

All reagents will be made available from the Lead Contact on request and after completion of a Materials Transfer Agreement.

Data and code availability

Data: The raw data supporting the findings of the study are available from the lead contact upon request. Structural data have been deposited at https://www.rcsb.org/ and https://www.ebi.ac.uk/emdb/. They are publicly available as of the date of publication. Accession codes are listed in the key resources table.

Code: This paper does not report original code

General statement: Any additional information required to reanalyze the data reported in this paper is available from the Lead Contact upon request.

EXPERIMENTAL MODEL AND SUBJECT DETAILS

Cell lines

HEK293T (ATCC CRL-11268)[115] and HEK293F (Thermo Fisher Scientific) and are human embryonic kidney cell lines. HEK293F cells are adapted to grow in suspension. HEK293F cells were cultured at 37°C with 8% CO_2 and shaking at 125 rpm in 293FreeStyle expression medium (Life Technologies). HEK293T cells were cultured at 37°C with 5% CO_2 in flasks with DMEM supplemented with 10% fetal bovine serum (FBS), streptomycin (100 μg/mL) and penicillin (100 U/mL). HEK293T/ACE2 cells[119] are a human embryonic kidney cell line expressing human angiotensin-converting enzyme 2. HEK293T/ACE2 cells were cultured at 37°C with 5% CO_2 in flasks with DMEM supplemented with 10% FBS, streptomycin (100 μg/mL) and penicillin (100 U/mL). VeroE6 cells (ATCC CRL-1586) are a kidney epithelial cells from African green monkeys. VeroE6 cells were cultured at 37°C with 5% CO_2 in DMEM supplemented with or without streptomycin (100 μg/mL) and penicillin (100 U/mL) and with or without 5 or 10% FBS, and with or without TPCK-trypsin. PBMC were isolated from macaque sera and cultured in RPMI1640 Glutamax+ medium (Gibco) supplemented with 10 % FBS.

Viruses

SARS-CoV-2 virus (hCoV-19/France/ IDF0372/2020 strain) was isolated by the National Reference Center for Respiratory Viruses (Institut Pasteur, Paris, France) as previously described[120] and produced by two passages on Vero E6 cells in DMEM (Dulbecco's Modified Eagles Medium) without FBS, supplemented with 1% P/S (penicillin at 10,000 U ml^{-1} and streptomycin at 10,000 μg ml^{-1}) and 1 μg ml^{-1} TPCK-trypsin at 37 °C in a humidified CO_2 incubator and titrated on Vero E6 cells. Whole genome sequencing was performed as described[120] with no modifications observed compared with the initial specimen and sequences were deposited after assembly on the GISAID EpiCoV platform under accession number ID EPI_ISL_410720.

Ethics and biosafety statement

Cynomolgus macaques (*Macaca fascicularis*) originating from Mauritian AAALAC certified breeding centers were used in this study. MF1-MF4, vaccinated group and MF5-MF8, control group.

	Gender	Date of birth	Age (years)	Weight at Day 0 post exposure (kg)	Developmental stage
MF1	M	04/04/2017	3,68	3,96	Young adult
MF2	M	05/04/2017	3,68	4,52	Young adult
MF3	M	10/04/2017	3,67	4,98	Young adult

(*Continued on next page*)

Continued

	Gender	Date of birth	Age (years)	Weight at Day 0 post exposure (kg)	Developmental stage
MF4	M	12/04/2017	3,66	6,39	Young adult
MF5	M	27/04/2017	3,62	3,64	Young adult
MF6	M	27/04/2017	3,62	4,29	Young adult
MF7	M	12/05/2017	3,58	3,14	Young adult
MF8	M	15/05/2017	3,57	3,91	Young adult

All animals were housed in IDMIT infrastructure facilities (CEA, Fontenay-aux-roses), under BSL-2 and BSL-3 containment when necessary (Animal facility authorization #D92-032-02, Préfecture des Hauts de Seine, France) and in compliance with European Directive 2010/63/EU, the French regulations and the Standards for Human Care and Use of Laboratory Animals, of the Office for Laboratory Animal Welfare (OLAW, assurance number #A5826-01, US). The protocols were approved by the institutional ethical committee ''Comité d'Ethique en Expérimentation Animale du Commissariat à l'Energie Atomique et aux Energies Alternatives'' (CE-tEA #44) under statement number A20-011. The study was authorized by the ''Research, Innovation and Education Ministry'' under registration number APAFIS#24434-2020030216532863.

Animals and study design

Cynomolgus macaques were randomly assigned in two experimental groups. The vaccinated group (n = 4) received 50 μg of SARS CoV-2 S-LV adjuvanted with 500 μg of MPLA liposomes (Polymun Scientific, Klosterneuburg, Austria) diluted in PBS at weeks 0, 4, 8 and 19, while control animals (n = 4) received no vaccination. Vaccinated animals were sampled in blood at weeks 0, 2, 4, 6, 8, 10, 12, 14, 19, 21 and 22. At week 24, all animals were exposed to a total dose of 10^5 pfu of SARS-CoV-2 virus (hCoV-19/France/ IDF0372/ 2020 strain; GISAID EpiCoV platform under accession number EPI_ISL_410720) via the combination of intranasal and intra-tracheal routes (0,25 mL in each nostril and 4,5 mL in the trachea, i.e., a total of 5 mL; day 0), using atropine (0.04 mg/kg) for pre-medication and ketamine (5 mg/kg) with medetomidine (0.042 mg/kg) for anesthesia. Nasopharyngeal, tracheal and rectal swabs, were collected at days 2, 3, 4, 6, 7, 10, 14 and 27 days past exposure (dpe) while blood was taken at days 2, 4, 7, 10, 14 and 27 dpe. Bronchoalveolar lavages (BAL) were performed using 50 mL sterile saline on 3 and 7 dpe. Chest CT was performed at 3, 7, 10 and 14 dpe in anesthetized animals using tiletamine (4 mg kg^{-1}) and zolazepam (4 mg kg^{-1}). Blood cell counts, haemoglobin, and haematocrit, were determined from EDTA blood using a DHX800 analyzer (Beckman Coulter).

METHODS DETAILS

Protein expression and purification

The SARS-CoV-2 S gene encoding residues 1-1208 with proline substitutions at residues 986 and 987 (''2P''), a ''GSAS'' substitution at the furin cleavage site (residues 682-685) a C-terminal T4 fibritin trimerization motif, an HRV3C protease cleavage site, a TwinStrepTag and Hexa-His-tag[8] was transiently expressed in FreeStyle293F cells (Thermo Fisher scientific) using polyethylenimine (PEI) 1 μg/μl for transfection. Supernatants were harvested five days post-transfection, centrifuged for 30 min at 5000 rpm and filtered using 0.20 μm filters (ClearLine®). SARS-CoV-2 S protein was purified from the supernatant by Ni^{2+}-Sepharose chromatography (Excel purification resin, Cytiva) in buffer A (50 mM HEPES pH 7.4, 200 mM NaCl) and eluted in buffer B (50 mM HEPES pH 7.4, 200 mM NaCl, 500 mM imidazole). Eluted SARS-CoV-2 S containing fractions were concentrated using Amicon Ultra (cut-off: 30 KDa) (Millipore) and further purified by size-exclusion chromatography (SEC) on a Superose 6 column (GE Healthcare) in buffer A or in PBS.

For RBD expression, the following reagent was produced under HHSN272201400008C and obtained through BEI Resources, NIAID, NIH: Vector pCAGGS containing the SARS-Related Coronavirus 2, Wuhan-Hu-1 Spike Glycoprotein Receptor Binding Domain (RBD), NR-52309. The SARS-CoV-2 S RBD domain (residues 319 to 541) was expressed in EXPI293 cells by transient transfection according to the manufacturer's protocol (Thermo Fisher Scientific). Supernatants were harvested five days after transfection and cleared by centrifugation. The supernatant was passed through a 0.45 μm filter and RBD was purified using Ni^{2+}-chromatography (HisTrap HP column, GE Healthcare) in buffer C (20 mM Tris pH 7.5 and 150 mM NaCl buffer) followed by a washing step with buffer D (20 mM Tris pH 7.5 and 150 mM NaCl buffer, 75 mM imidazole) and elution with buffer E (20 mM Tris pH 7.5 and 150 mM NaCl buffer, 500 mM imidazole). Eluted RBD was further purified by SEC on a Superdex 75 column (GE Healthcare) in buffer C. Protein concentrations were determined using absorption coefficients at 280 nm calculated with ProtParam (https://web.expasy.org/).

SARS-CoV-2 S crosslinking

S protein at 1 mg/ml in PBS was cross-linked with 4% formaldehyde (FA) (Sigma) overnight at room temperature. The reaction was stopped with 1 M Tris HCl pH 7.4 adjusting the sample buffer to 7.5 mM Tris/HCl pH 7.4. FA was removed by PBS buffer exchange using 30 KDa cut-off concentrators (Amicon). FA crosslinking was confirmed by separating SARS-CoV-2 FA-S on a 10% SDS-PAGE under reducing conditions.

S protein coupling to liposomes

Liposomes for conjugating S protein were prepared as described previously[121] with modifications. Briefly, liposomes were composed of 60% of L-α-phosphatidylcholine, 4% His tag-conjugating lipid, DGS-NTA-(Ni^{2+}) and 36% cholesterol (Avanti Polar Lipids). Lipid components were dissolved in chloroform, mixed and placed for two hours in a desiccator under vacuum at room temperature to obtain a lipid film. The film was hydrated in filtered (0.22 μm) PBS and liposomes were prepared by extrusion using membrane filters with a pore size of 0.1 μm (Whatman Nuclepore Track-Etch membranes). The integrity and size of the liposomes was analyzed by negative staining-EM. For protein coupling, the liposomes were incubated overnight with FA-S or S protein in a 3:1 ratio (w/w). Free FA-S protein was separated from the FA-S-proteoliposomes (S-LVs) by sucrose gradient (5-40%) centrifugation in a SW55 rotor at 40,000 rpm for 2 h. The amount of protein conjugated to the liposomes was determined by Bradford assay and SDS-PAGE densitometry analysis comparing S-LV bands with standard S protein concentrations.

S protein thermostability

Thermal denaturation of SARS-CoV-2 S, native or FA-cross-linked was analyzed by differential scanning fluorimetry coupled to back scattering using a Prometheus NT.48 instrument (Nanotemper Technologies, Munich, DE). Protein samples were first extensively dialyzed against PBS pH 7.4, and the protein concentration was adjusted to 0.3 mg/ml. 10 μL of sample were loaded into the capillary and intrinsic fluorescence was measured at a ramp rate of 1°C/min with an excitation power of 30 %. Protein unfolding was monitored by the changes in fluorescence emission at 350 and 330 nm. The thermal unfolding midpoint (Tm) of the proteins was determined using the Prometheus NT software.

Negative stain electron microscopy

Protein samples were visualized by negative-stain electron microscopy (EM) using 3-4 μL aliquots containing 0.1-0.2 mg/ml of protein. Samples were applied for 10 s onto a mica carbon film and transferred to 400-mesh Cu grids that had been glow discharged at 20 mA for 30 s and then negatively stained with 2% (wt/vol) Uranyl Acetate (UAc) for 30 s. Data were collected on a FEI Tecnai T12 LaB6-EM operating at 120 kV accelerating voltage at 23k magnification (pixel size of 2.8 Å) using a Gatan Orius 1000 CCD Camera. Two-dimensional (2D) class averaging was performed with the software Relion[122] using on average 30–40 micrographs per sample. The 5 best obtained classes were calculated from around 6000 particles each.

Cryo-electron microscopy

Data collection

3.5 μL of sample were applied to 1.2/1.3 C-Flat (Protochips Inc) holey carbon grids and plunged frozen in liquid ethane with a Vitrobot Mark IV (Thermo Fisher Scientific) (6 s blot time, blot force 0). The sample was observed with a Glacios electron microscope (Thermo Fischer Scientific) at 200 kV. Images were recorded automatically on a K2 summit direct electron detector (Gatan Inc., USA) in counting mode with SerialEM.[123] Movies were recorded for a total exposure of 4.5 s with 40 frames per movie and a total dose of 40 $e^{-}/Å^2$. The magnification was 36,000x (1.15 Å/pixel at the camera level). The defocus of the images was changed between −1.0 and −2.5 μm. Two different datasets have been acquired on the same grid. First, 1040 movies were recorded with stage movement between each hole and then 7518 more movies were recorded with image shifts on a 3x3 hole pattern.

3D reconstruction

The movies were first drift-corrected with motioncor2.[124] The remaining image processing was performed with RELION 3.1.2 [125] and CTF estimation with GCTF.[126] An initial set of particles (box size of 200 pixels, sampling of 2.3 Å/pixel) was obtained by auto-picking with a Gaussian blob. After 2D classification, the best looking 2D class averages were used for a second round of auto picking. Following another 2D classification step, the particles belonging to the best looking 2D class averages were used to create an *ab-initio* starting 3D model which was then used to calculate a first 3D reconstruction with C3 symmetry. The 2D projections from that 3D model were then used for one last auto picking which resulted in a total of 2,582,857 particles. Following another 2D classification and a 3D classification (C1 symmetry, 5 classes) steps, a 3D map at 4.6 Å resolution was obtained from 240,777 particles. The particles were re-extracted (box size of 400 pixels, sampling of 1.15 Å/pixel). After further 3D refinement (C3 symmetry) and 3D classification (C1 symmetry, no alignment, 3 classes) steps, a final set of 126,719 particles was identified which resulted in a 3D reconstruction at 3.6 Å resolution. Refinement of CTF parameters, particle polishing and a second round of CTF parameter's refinement further improved the resolution to 3.4 Å. The resolution was determined by Fourier Shell Correlation (FSC) at 0.143 between two independent 3D maps. The local resolution was calculated with blocres[127] and found to be between 3 and 5 Å. The final 3D map was sharpened with DeepEMhancer.[128]

Model refinement

The atomic model of the S protein in the closed conformation (PDB 6VXX)[11] was rigid-body fitted inside the cryo-EM density map in CHIMERA.[129] The atomic coordinates were then refined with PHENIX.[130] The refined atomic models were visually checked and adjusted (if necessary) in COOT.[131] The final model was validated with MOLPROBITY.[132]

The figures were prepared with CHIMERA and CHIMERAX.[129,133] The data collection and atomic model statistics are summarized in Table S1. The atomic coordinates and the cryo-EM map have been deposited in the Protein Data Bank and in the Electron Microscopy Data Bank under the accession codes 7QIZ and EMD-13776, respectively.

Virus quantification in NHP samples

Upper respiratory (nasopharyngeal and tracheal) and rectal specimens were collected with swabs (Viral Transport Medium, CDC, DSR-052-01). Tracheal swabs were performed by insertion of the swab above the tip of the epiglottis into the upper trachea at approximately 1.5 cm of the epiglottis. All specimens were stored between 2°C and 8°C until analysis by RT-qPCR with a plasmid standard concentration range containing an RdRp gene fragment including the RdRp-IP4 RT-PCR target sequence. SARS-CoV-2 E gene subgenomic mRNA (sgRNA) levels were assessed by RT-qPCR using primers and probes previously described[134,135]: leader-specific primer sgLeadSARSCoV2-F CGATCTCTTGTAGATCTGTTCTC, E-Sarbeco-R primer ATATTGCA GCAGTACGCACACA and E-Sarbeco probe HEX-ACACTAGCCATCCTTACTGCGCTTCG-BHQ1. The protocol describing this procedure for the detection of SARS-CoV-2 is available on the WHO website (https://www.who.int/docs/default-source/coronaviruse/whoinhouseassays.pdf)

Chest CT and image analysis

Lung images were acquired using a computed tomography (CT) system (Vereos-Ingenuity, Philips) as previously described,[50,70] and analyzed using INTELLISPACE PORTAL 8 software (Philips Healthcare). All images had the same window level of −300 and window width of 1,600. Lesions were defined as ground glass opacity, crazy-paving pattern, consolidation or pleural thickening as previously described.[136,137] Lesions and scoring were assessed in each lung lobe blindly and independently by two persons and the final results were established by consensus. Overall CT scores include the lesion type (scored from 0 to 3) and lesion volume (scored from 0 to 4) summed for each lobe as previously described.[50,70]

ELISA

Serum antibody titers specific for soluble native S glycoprotein, FA-cross-linked S (FA-S) and for RBD were determined using an enzyme-linked immunosorbent assay (ELISA). Briefly, 96-well micro titer plates were coated with 1 μg of S, FA-S or RBD proteins at 4°C overnight in PBS and blocked with 3% BSA for 1 h at room temperature after 3 washes with 150 μL PBS Tween-20 0.05%. Serum dilutions were added to each well for 2h at 37°C and plates were washed 5 times with PBS Tween. A horseradish peroxidase (HRP) conjugated goat anti-monkey H+L antibody (Invitrogen) was then added and incubated for 1h before excess Ab was washed out and HRP substrate added. Absorbance was determined at 450 nm. Antibody titers were expressed as ED50 (effective Dilution 50-values) and were determined as the serum dilution at which IgG binding was reduced by 50%. ED50 were calculated from crude data (O.D) after normalization using GraphPad Prism (version 6) "log(inhibitor) vs normalized response" function. ELISA were performed in duplicates.

Protein coupling to luminex beads

Proteins were covalently coupled to Magplex beads (Luminex Corporation) via a two-step carbodiimide reaction using a ratio of 75 μg SARS-CoV-2 S to 12,5 million beads. Magplex beads (Luminex Corporation) were washed with 100 mM mono-basic sodium phosphate pH 6.2 and activated for 30 min on a rotor at RT by addition of Sulfo-N-Hydroxysulfosuccinimide (Thermo Fisher Scientific) and 1-Ethyl-3-(3-dimethylaminopropyl) carbodiimide (Thermo Fisher Scientific). The activated beads were washed three times with 50 mM MES pH 5.0 and added to SARS-CoV-2 S protein, which was diluted in 50 mM MES pH 5.0. The coupling reaction was incubated for 3 h on a rotator at RT. The beads were subsequently washed with PBS and blocked with PBS containing 2% BSA, 3% FCS and 0.02% Tween-20 for 30 min on a rotator at RT. Finally, the beads were washed and stored in PBS containing 0.05% Sodium Azide at 4°C and used within 3 months.

Luminex assay

50 μL of a working bead mixture containing 20 beads per μL was incubated overnight at 4°C with 50 μL of diluted nasopharyngeal fluid. Nasopharyngeal fluids were diluted 1:20 for detection of S-specific IgG and IgA.[70] Plates were sealed and incubated on a plate shaker overnight at 4°C. Plates were washed with TBS containing 0.05% Tween-20 (TBST) using a hand-held magnetic separator. Beads were resuspended in 50 μL of Goat-anti-monkey IgG-Biotin or Goat-anti monkey IgA-Biotin (Sigma Aldrich) and incubated on a plate shaker at RT for 2 h. Afterwards, the beads were washed with TBST, resuspended in 50 μL of Streptavidin-PE (ThermoFisher Scientific) and incubated on a plate shaker at RT for 1 h. Finally, the beads were washed with TBST and resuspended in 70 μL Magpix drive fluid (Luminex Corporation). The beads were agitated for a few minutes on a plate shaker at RT and then readout was performed on the MAGPIX (Luminex Corporation). Reproducibility of the results was confirmed by performing replicate runs.

Pseudovirus neutralization assay

Pseudovirus was produced by co-transfecting the pCR3 SARS-CoV-2-SΔ19 expression plasmid (Wuhan Hu-1; GenBank: MN908947.3) with the pHIV-1NL43 ΔEnv-NanoLuc reporter virus plasmid in HEK293T cells (ATCC, CRL-11268).[115] The pCR3 SARS-CoV-2-SΔ19 expression plasmid contained the following mutations compared to the WT for the variants of concern: deletion (Δ) of H69, V70 and Y144, N501Y, A570D, D614G, P681H, T716I, S982A and D1118H in B.1.1.7 (Alpha, UK); L18F, D80A, D215G, L242H, R246I, K417N, E484K, N501Y, D614G and A701V in B.1.351 (Beta, SA); L18F, T20N, P26S, D138Y, R190S, K417T, E484K, N501Y, D614G, H655Y and T1027I in P.1 (Gamma, BR).[115]

HEK293T/ACE2 cells kindly provided by Dr. Paul Bieniasz[119] were seeded at a density of 20,000 cells/well in a 96-well plate coated with 50 μg/mL poly-L-lysine 1 day prior to the start of the neutralization assay. Heat-inactivated sera (1:100 dilution) were serial

diluted in 3-fold steps in cell culture medium (DMEM (Gibco), supplemented with 10% FBS, penicillin (100 U/mL), streptomycin (100 μg/mL) and GlutaMax (Gibco)), mixed in a 1:1 ratio with pseudovirus and incubated for 1 h at 37°C. These mixtures were then added to the cells in a 1:1 ratio and incubated for 48 h at 37°C, followed by a PBS wash and lysis buffer added. The luciferase activity in cell lysates was measured using the Nano-Glo Luciferase Assay System (Promega) and GloMax system (Turner BioSystems). Relative luminescence units (RLU) were normalized to the positive control wells where cells were infected with pseudovirus in the absence of sera. The neutralization titers (ID_{50}) were determined as the serum dilution at which infectivity was inhibited by 50%, respectively using a non-linear regression curve fit (GraphPad Prism software version 8.3). Notably, this pseudovirus neutralization assay revealed an excellent correlation with authentic virus neutralization on a panel of human convalescent sera.[115]

Antigen specific T cell assays using non-human primate cells

To analyze the SARS-CoV-2 protein-specific T cell, 15-mer peptides (n = 157 and n = 158) overlapping by 11 amino acids (aa) and covering the SARS-CoV-2 Spike sequence (aa 1 to 1273) were synthesized by JPT Peptide Technologies (Berlin, Germany) and used at a final concentration of 2 μg/mL.

T-cell responses were characterized by measurement of the frequency of PBMC expressing IL-2 (PerCP5.5, MQ1-17H12, BD), IL-17a (Alexa700, N49-653, BD), IFN-γ (V450, B27, BD), TNF-α (BV605, Mab11, BioLegend), IL-13 (BV711, JES10-5A2, BD), CD137 (APC, 4B4, BD) and CD154 (FITC, TRAP1, BD) upon stimulation with the two peptide pools. CD3 (APC-Cy7, SP34-2, BD), CD4 (BV510, L200, BD) and CD8 (PE-Vio770, BW135/80, Miltenyi Biotec) antibodies was used as lineage markers. One million of PBMC were cultured in complete medium (RPMI1640 Glutamax+, Gibco; supplemented with 10% FBS), supplemented with co-stimulatory antibodies (FastImmune CD28/CD49d, Becton Dickinson). The cells were stimulated with S sequence overlapping peptide pools at a final concentration of 2 μg/mL. Brefeldin A was added to each well at a final concentration of 10 μg/mL and the plate was incubated at 37°C, 5% CO2 during 18 h. Next, cells were washed, stained with a viability dye (LIVE/DEAD fixable Blue dead cell stain kit, ThermoFisher), and then fixed and permeabilized with the BD Cytofix/Cytoperm reagent. Permeabilized cell samples were stored at -80 °C before the staining procedure. Antibody staining was performed in a single step following permeabilization. After 30 min of incubation at 4°C, in the dark, cells were washed in BD Perm/Wash buffer then acquired on the LSRII cytometer (Beckton Dickinson). Analyses were performed with the FlowJo v.10 software. Data are presented as the sum of each peptide pool and the non-stimulated (NS) condition was multiplied by two.

Statistical analysis

Statistical significance between groups was performed using Graphpad Prism (v9.2.0). Differences between unmatched groups were compared using an unpaired Mann–Whitney U test (significance $p<0.05$), and differences between matched groups were compared using Wilcoxon signed-rank test ($p<0.1$). Statistical analysis of NHP gRNA and sgRNA were carried out using Mann-Whitney unpaired t-test in GraphPad Prism software (v8.3.0).

RESUME

Parmi les personnes naturellement exposées à *Plasmodium falciparum (Pf)* et vivant en zone d'endémie, certaines développent naturellement des anticorps capables d'inhiber le développement du parasite dans le moustique, réduisant ou bloquant ainsi la transmission à l'homme. Bien que quelques protéines du stade sexuel de *Pf* aient été identifiées comme cibles de ces anticorps, les travaux récents de Stone et al. ont démontré l'existence de protéines encore non décrites associées à l'activité de réduction de la transmission (ART). La découverte de nouvelles cibles antigéniques des anticorps réducteurs de transmission (AcART) pourrait contribuer au développement de vaccins bloquant la transmission, efficaces pour éradiquer le paludisme. L'objectif principal de mon projet de thèse était donc d'identifier de nouveaux antigènes en utilisant une approche de vaccinologie inverse 2.0, par l'isolement, à partir de donneurs sélectionnés, d'anticorps monoclonaux (Acm) ayant une forte activité de réduction de la transmission. Pour se faire, nous avons conçu un pipeline innovant pour l'isolement des AcART à partir des cellules B mémoires (CBM) d'individus sélectionnés infectés de façon chronique par *Pf*. Dans une première approche, nous avons choisi d'isoler les CBM en fonction de leur capacité à se lier au parasite entier, ici sous la forme de gamètes vivants. Comme deuxième méthode, nous avons choisi d'activer les CBM dans un milieu de culture adapté et de cribler les immunoglobulines contenues dans le surnageant de culture cellulaire pour leur liaison aux protéines des gamét(ocyt)es en ELISA. Dans les deux méthodes, après la première sélection, les Acm ont été clonés, produits et testés pour leur liaison aux gamètes en immunofluorescence de surface et pour leur activité fonctionnelle par Standard Membrane Feeding Assay (SFMA).

La première approche n'a été réalisée qu'à titre expérimental, en utilisant les cellules mononuclées sanguines d'un donneur possédant des anticorps contre les protéines du stade sexuel de *Pf*, mais sans ART sérique. Un Acm ciblant les gamètes a pu être isolé mais aucun AcART. Ces résultats limités suggèrent que l'approche pourrait produire des anticorps d'intérêt, mais des expériences supplémentaires seraient nécessaires. En revanche, les cellules mononucléaires du sang périphérique d'un donneur sélectionné pour sa forte ART sérique et pour lequel il avait été démontré la présence d'AcART dirigés contre de nouvelles cibles ont été utilisées pour la deuxième approche. Sept AcART ont été isolés ; parmi eux, 4 se sont avérés être dirigés contre des protéines connues pour être associées à l'ART: Pfs230 et Pfs48/45. Sur les trois autres Acm, l'un s'est avéré être polyréactif mais, fait intéressant, les deux autres semblaient reconnaître des antigènes non caractérisés jusqu'à présent. Dans l'ensemble, les résultats ont validé l'approche adoptée et des travaux supplémentaires sont en cours pour

identifier les antigènes potentiellement nouveaux associés à l'ART et reconnus par les deux derniers Acm.

Grâce à l'approche d'activation, nous avons également isolé des anticorps sans ART, l'un d'entre eux, l'Acm B1E11K, présentant un profil de liaison intéressant. Cet anticorps reconnaît des protéines de différents stades du parasite (notamment Pfs230, Pf11.1, RESA, RESA3 et LSA3), par la reconnaissance de motifs riches en glutamate. B1E11K se lie de manière préférentielle aux répétitions EENVEE de RESA et RESA3. Les expériences de cristallographie ont montré que lorsque 2 Fabs se lient à des motifs répétés adjacents, ils s'engagent dans des interactions homotypiques. Il est intéressant de noter que certains des résidus impliqués dans ces interactions homotypiques sont acquis par hypermutation somatique, ce qui démontre un avantage sélectif. Cette observation apporte un nouvel éclairage sur les réponses immunitaires aux motifs répétés que l'on trouve couramment dans les protéines de *Pf*.

ABSTRACT

Among people naturally exposed to *Plasmodium falciparum (Pf)* in endemic areas some naturally develop antibodies that are capable of inhibiting the development of the parasites in the mosquito, thus reducing or blocking further transmission to human. Although a few *Pf* sexual stage proteins have been identified as targets for these antibodies, recent work by Stone et al. demonstrated the existence of yet undescribed transmission reducing activity-associated proteins. The discovery of novel antigenic targets for transmission reducing antibodies (TRAbs) could help the development of effective transmission blocking vaccines to eradicate malaria. The main purpose of my Ph.D. thesis project was thus to identify such new antigens using a reverse vaccinology 2.0 approach, through the isolation, from selected donors, of monoclonal antibodies (mAbs) with strong transmission reducing activity (TRA). For this purpose, we designed an innovative pipeline for isolation of TRAbs from memory B cells (MBCs) of selected individuals chronically infected by *Pf*. As a first approach, we opted for isolating MBCs based on their ability to bind to the whole parasite, here in the form of live gametes. We reasoned that this would indicate specificity for gamete surface proteins, some of which being potentially involved in TRA. As a second method we chose to activate MBCs in a high throughput format and screen immunoglobulin-containing supernatants for binding to gamet(ocyt)e proteins in an ELISA format. In both methods, following the first selection, mAbs were cloned, produced and tested further for binding to gametes in surface immunofluorescence and for functional activity in Standard Membrane Feeding Assay (SFMA).

The first approach was only performed as a proof of concept experiment, using peripheral blood mononuclear cells (PBMCs) from a donor with antibodies to *Pf* sexual stage proteins but no serum TRA. One mAb targeting gametes was potentially isolated but no TRAb. The limited results suggested that the approach could yield antibodies of interest but we could not conclude on its effectiveness, and additional experiments would be necessary. In contrast, PBMCs from a selected donor with strong serum TRA and evidence of TRAbs directed at novel targets were used for the second approach. Seven TRAbs were isolated; among them, 4 were found to be directed against well-known TRA-associated proteins: Pfs230 and Pfs48/45. Of the 3 remaining Abs one was found to be polyreactive, but interestingly the two others appeared to recognise so far not characterised antigens. Overall, the results validated the approach taken and further work is needed to identify the potentially novel TRA-associated antigens recognized by the 2 latter mAbs.

Through the activation approach we also isolated antibodies with no TRA, one of those, the B1E11K mAb, having an interesting binding profile. This mAb, although not being able to reduce transmission, was shown to recognize proteins from various stages of the parasite

(notably Pfs230, Pf11.1, RESA, RESA3 and LSA3), through the recognition of glutamate-rich motifs. B1E11K was found to preferentially bind RESA and RESA3 EENVEE repeats and structural determination showed that when 2 Fabs bind to adjacent repeats they engage in homotypic interactions. Interestingly, some of the residues involved in these homotypic interactions are acquired through somatic hypermutation demonstrating a selective advantage. This observation brings new insights into immune responses to repeated motifs commonly found in *Pf* proteins.

qd